Peter Zach, BSc

New phosphorescent porphyrins with enhanced solubility & absorption in the NIR region for oxygen sensing materials

MASTERARBEIT

Zur Erlangung des akademischen Grades
Diplom-Ingenieur
des Masterstudiums „Technische Chemie“

eingereicht an der
Technischen Universität Graz

unter Betreuung von
Ass.Prof. kand. Sergey Borisov
(Institut für Analytische Chemie und Lebensmittelchemie, TU Graz)

Graz, November 2014

To my family

1. Abstract

In this thesis two different synthetic routes, the conventional Lindsey condensation and the Template method, were investigated in order to synthesize two different highly soluble and photostable benzoporphyrin dyes. The sulfonyl-substituted benzoporphyrin compound, obtained via Template method, represents a potential candidate for outstanding solubility but also photostability properties using a cheap and time-saving synthetic strategy and should therefore be focused in future synthetic work.

Furthermore different benzoporphyrin indicator dyes (TTolTBP, TPTBPdM_4 and TTolTBPmM_4) were synthesized via Template method and investigated for their ability to form bridged compounds by intramolecular fusion via Scholl-reaction. Intramolecular bridging was successfully performed with Pt-TPTBP as well as with Pt-TTolTBPtert-Butyl$_4$, whereas the resulting product of the latter was examined more closely for the use of an oxygen sensor. Hereby oxygen sensitivity in the physiological area was determined, enabling to monitor the process of oxygen production during photosynthesis, due the clearly distinguishable emission (870 nm) of the dye compared to chlorophyll a and b. Moreover the suitability of the bridged dye as sensitizer in triplet-triplet annihilation-based upconversion could be successfully shown, establishing further fields of possible application like photovoltaics optics.

2. Kurzfassung

Im Zuge dieser Arbeit wurde die Synthese zweier hoch löslicher, photostabiler Benzoporphyrin Farbstoffe auf zwei unterschiedlichen Synthesewegen, einerseits der konventionellen Lindsey Kondensation andererseits der Template Methode versucht. Hierbei erwies sich, der über die Template Methode hergestellte Sulfon-substituierte Benzoporphyrin Farbstoff als ein sehr viel versprechender Kandidat, der aufgrund seiner zu erwartenden herausragenden Löslichkeits- als auch Photostabilitäts-Eigenschaften und der billigen und zeitsparenden Synthesestrategie in Zukunft auf alle Fälle weiter untersucht werden sollte.

Des Weiteren wurden verschiedene Benzoporphyrin Indikatorfarbstoffe (TTolTBP, TPTBPdM_4 und TTolTBPmM_4) mit Hilfe der Template Methode hergestellt und in weiterer Folge auf ihre Eignung verbrückte Verbindungen durch intramolekulare Fusion mittels Scholl-Reaktion zu bilden, untersucht. Schlussendlich konnten erfolgreiche Verbrückungen mit Pt-TPTBP als auch mit Pt-TTolTBPtert-Butyl$_4$ erreicht werden, wobei in weiterer Folge das verbrückte Produkt des letzteren genauer auf seine Eignung als Sauerstoffsensor untersucht wurde. Hierbei konnte die Sauerstoffsensitivität im physiologischen Bereich gezeigt werden, was die Beobachtung der Sauerstoffproduktion während der Photosynthese, bedingt durch die klar unterscheidbare Emission (870 nm) des Farbstoffes von Chlorophyll a und b, ermöglicht. Abschließend konnte auch noch die Verwendung des verbrückten Farbstoffes als Sensibilisator für Triplet-Triplet Up-conversion gezeigt werden, was weitere Anwendungsgebiete wie z.B. in der Photovoltaik oder der Optik eröffnet.

3. Acknowledgement/Danksagung

Zu allererst möchte ich mich bei Prof. Ingo Klimant bedanken, der diese Arbeit nicht nur ermöglicht hat, sondern mir auch stets eine große Unterstützung war.

Danke auch an Ass. Prof. kand. Sergey Borisov, der mir nicht nur mit seinen lehrreichen Tipps und Anregungen, sowie seiner Geduld und praktischen Unterstützung im Labor eine große Hilfe war, sondern mich auch durch seine grenzenlose Motivation und Leidenschaft für Chemie mehr als nur einmal mitgerissen hat. Ohne deine Hilfe wäre diese Arbeit nicht in dieser Form möglich gewesen.

Ich möchte mich vor allem auch bei der Arbeitsgruppe für die gemeinsamen, stets angenehmen und vor allen lustigen, Mittags- und Kaffeepausen bedanken. Die spaßigen Aktivitäten, aber auch die große Hilfsbereitschaft bei etwaigen Problemen und vor allem aber das freundliche und angenehme Arbeitsklima haben mir so viel Motivation und Freude für die Arbeit geschenkt.
Insbesondere möchte ich mich bei meinem Büro- und teilweise auch Laborkollegen Tobi für die Unterstützung im Labor aber auch die für aufbauenden und motivierenden Gespräche bedanken. Weiters möchte ich noch speziell Berni, Christoph und Susi für ihre Hilfe danken.
Eveline möchte ich für ihre große Geduld und Unterstützung bei allen organisatorischen Abwicklungen, sowie auch der Chemikalien-Bestellung herzlich danken.

Prof. Jörg Weber und seiner Arbeitsgruppe danke ich für die Anfertigungen der NMR-Spektren und für die steten Bemühungen um Problemlösungen. Für die Aufnahme der Massenspektren gilt mein Dank, Ing. Karin Bartl, Prof. Saf und seiner Arbeitsgruppe.

Bedanken möchte ich mich auch bei meinen Studienkollegen für die gemeinsame Zeit des Lernens, Feierns aber auch für alle lustigen Unternehmungen, die ich nie vergessen werde.

Spezieller Dank gilt vor allem Carina, die mir mit ihren fröhlichen, aufmunternden und offenen Art immer unterstützend zur Seite gestanden ist und stets für mich da war. Danke für die aufregende, spannende aber vor allem auch schöne Zeit die ich bisher mit dir verbringen durfte.

Der vermutlich größte Dank gebührt aber meinen Eltern, die mich nicht nur finanziell stets unterstützt haben, sondern mir auch immer hilfreich zur Seite gestanden sind und mich in meinen Entscheidungen stets bestärkt haben, mich aber auch meinen eigenen Weg gehen ließen. Danke für all die Unterstützung die ihr mir in allen Lebenslagen entgegen gebracht habt, ohne euch wäre ich heute nicht da, wo ich jetzt bin.

Content

4. Introduction

Oxygen is undoubtedly one of the most important and often measured analytes on earth due to its essentiality for life. Determination and monitoring of its concentration are very important in various fields of research such as medicine chemistry, molecular biotechnology, environmental and marine analyses, bioprocess control, food packaging but also industrial production monitoring. [1] In most of the cases continuously monitoring of oxygen concentration would be optimal and this implies the use of an oxygen sensor. Although many different ways to measure oxygen exist, optical sensor technology has received much attention in the last decades due to the various advantages. [1]

Most optical sensing systems developed for the detection of oxygen rely on the process of luminescence quenching of the indicator dye by molecular oxygen. [2] Among all the commonly used indicators platinum(II) and palladium(II) porphyrins are the most popular luminophores due to their strong phosphorescence at room temperature, relatively high molar absorption coefficients and large Stocke's shifts. [1]

Especially benzoporphyrins have attracted large interest in the last three decades due to the fact that they possess excellent brightness upon excitation in both the blue and the red region of the spectrum, because of their extremely high absorption coefficients, quantum yields of about 50% (platinum complexes), emission in the NIR at 760 nm and moderate to high photostability [3]. Even though much research was done in this field leading to significant improvements, still some limitations could not be completely overcome yet. A common problem for various benzoporphyrin derivatives is the moderate solubility.

Bad solubility limits not only photophysical studies and often hampers purification of the compounds but also complicates their application in various fields of material science especially the scaled-up preparation and industry applications requiring solvent processing. [4]

Furthermore extension of the porphyrins π-system leading to a red-shift of the absorption, resulting in emission in the deep NIR presents another interesting aspect for various applications in biology or medicine, especially when measuring oxygen in live cells or tissue, due to of minimal absorption and autofluorescence of biological tissues at these wavelengths. [quaranta] However the reported extended porphyrins are either not luminescent, or possess poor photostability and solubility such as naphthoporphyrins.

In the course of this master thesis different synthetic strategies were tested in order to synthesize a highly soluble and photostable dye. Moreover extension of the porphyrins π-system by intramolecular bridging via Scholl-reaction of substituents in β- and meso-position, leading to a red-shift of absorption and emission was more closely examined.

5. Theoretical Background

5.1 Luminescence

This chapter and the following sub-chapters are based on reference [5]. Other references will be quoted independently. The term luminescence describes the process in which photons are emitted (electromagnetic radiation) from an organic or inorganic compound during the relaxation of an exited electronic state to the lower ground state. Due to its high sensitivity to environmental influences it is often used in sensors to monitor different parameters. In photoluminescence a luminophore or dye reaches the electronically excited state by absorption of photons.

5.1.1 Absorption

A source of energy, mostly irritation with light, raises an electron from the ground state (energetically most stable state with the lowest energy), where the electrons have an opposite spin and therefore a muplicity of 1, into an energetically higher excited state (unoccupied energy level), S_1 or S_2, depending on the supplied energy. This extremely fast process takes place in approximately 10^{-15} seconds. Of special importance in the case of absorption are the highest occupied (HOMO) and the lowest unoccupied molecular orbital (LUMO). If during the process of excitation neither the spin nor the multiplicity changes, the excited states are called singlet states (S_1, S_2 … S_n). However the spin changes to the parallel form, also the multiplicity changes to M = 3. The so achieved orbitals are called triplet states (T_1, T_2 … T_n). Since direct transition from S_0 to T_1 is spin-forbidden, T_1 can only be populated indirectly (S_0 → S_1 → T_1).

Before the dye relaxes to its ground state, the electron can go through different transitions, which can be seen in the Perrin-Jablonski diagram (Figure 1).

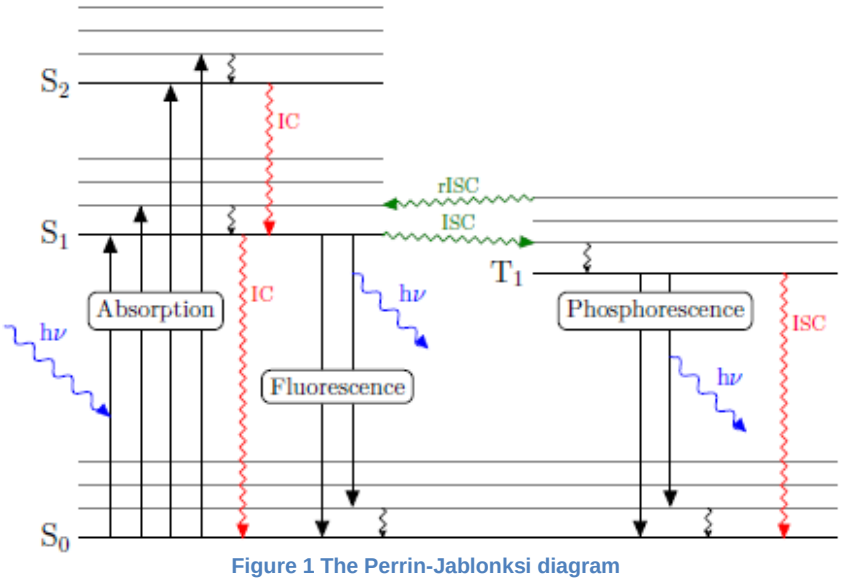

Figure 1 The Perrin-Jablonksi diagram

If visible light is absorbed the most observed transitions are the π → π* and the n → π*, because other transitions (like e.g. σ → σ* or n → σ*) take place at higher energies and therefore lower wavelengths. In general a greater conjugated π-system causes a decreased energy for π → π* transitions. However to reach an absorption in the Vis-region typically several conjugated bonds are required.

The efficiency of the absorption of a dye at a certain wavelength is given by the molar absorption coefficient in the Lambert-Beer law, in which the absorbance A of a sample is determined as the decadic logarithm of the light intensity ratio before (I_0) and after (I) the sample. Other parameters which influence the absorption are the optical path length (l) of the sample and the respective concentration (c) of the dye (Equation (1)).

$$A = \log \frac{I_0}{I} = \epsilon \cdot c \cdot l \qquad (1)$$

Within this fast excitation process the atoms can be regarded stationary according to the Born-Oppenheimer approximation, because the movements of the electrons are in comparison much faster than the movements of the heavy nuclei, resulting that the atoms have the same distance to each other in the ground state as well as in the excited state. The excited electrons are raised to an energetically higher vibrational level of the excited state, followed by a non-radiative vibrational relaxation to the lowest vibrational level of this state, in which the energy is passed to other molecules or is transformed to heat radiation. According to the Frank-Condon an electronic transition occurs usually without any changes of the nuclei position in the molecular unit.

5.1.2 Internal conversion (IC)

Internal conversion (IC) is a non-radiative transition (no photons are emitted) from a higher to a lower electronic state in a molecule or atom, which owns the same spin multiplicity. The energy of the electronically excited state is transferred over vibrational relaxation to the molecule or atom. Internal conversion can also occur between the even more excited singlet state S_2 and the lowest vibrational level of S_1. Important is to know that internal conversion (IC) from S_1 to S_0 can compete with the emission of photons (fluorescence) and the transition of the intersystem crossing (ISC) to the triplet state.

5.1.3 Fluorescence

The term Fluorescence describes a spontaneous process and the emission of photons accompanying the $S_1 \rightarrow S_0$ relaxation. Nevertheless $S_2 \rightarrow S_0$ relaxation with emission of photons is also possible, but not only in several dye classes e.g. porphyrins and can therefore be seen as exception. Due to the transition ($S_1 \rightarrow S_0$), the characteristics of fluorescence do not depend on the excitation wavelength. The average lifetime of the excited

state S_1 is 10^{-10} to 10^{-7} seconds and will take significantly longer than the absorption of a photon with about 10^{-15} seconds. The energy of the emitted light is however lower than the absorbed light due to the energy loss during IC and/or vibrational relaxation, which is called the Stokes shift. The radiative emission also follows, like the absorption, the Frank-Condon principle, finally leading to a mirroring of the absorption peaks at a higher wavelength due to similar spacing of the vibrational levels of the excited and the ground state.

During the fluorescence (or also phosphorescence) decay time (τ), it is possible to observe dynamic phenomena like quenching, which actually constitute the basic process of optical sensing. After the excitation of the molecules by means of a short pulse of light, the fluorescence intensity decreases exponentially within a characteristic time, through which it is possible to determine the average lifetime of the molecules in the excited state. The transition $S_1 \rightarrow S_0$ could be favored through the absence of heavy atoms, a large and pronounced π-electron system (shift to longer wavelength) and a rigid structure of the molecule.

5.1.4 Intersystem crossing (ISC)

ISC is a non-radiative transition between two isoenergetic vibrational levels (excited singlet state S_1 to excited triplet state T_1). In this case these levels belong to electronic states of different spin multiplicities. This process of intersystem crossing (ISC) lasts 10^{-10} to 10^{-8} seconds and therefore can also compete with other pathways of de-excitation from S_1, for example fluorescence and internal conversion from $S_1 \rightarrow S_0$.

Since this is a transition between two states of different multiplicity, the crossing is in principle forbidden, but can be bypassed in the presence of spin-orbit coupling. The lowest vibrational state of the excited triplet state can be reached by collision with other molecules. The transition of intersystem crossing could be favored in different ways.

One possibility is the presence of heavy atoms with a large atomic number. Another possibility is the prevention of vibrations or collisions with the solvent molecules, which could be reached through freezing and application on a solid or rigid matrix (e.g. polymer).

5.1.5 Phosphorescence

Phosphorescence is a metastable state, which has a lifetime of the excited state from 10^{-6} to about 1 second and shows high temperature dependence. In solution, room temperature tends to favor non-radiative de-excitation from the triplet state than radiative de-excitation. In case of the forbidden transition ($T_1 \rightarrow S_0$) the radiative rate constant is very low and so the numerous collisions with the solvent molecules favor vibrational relaxation and ISC in S_0. As mentioned before phosphorescence has high temperature dependence, meaning that phosphorescence or the lifetime of the triplet state at low temperatures or rigid medium can

be observed for minutes or sometimes even hours. The energy of the lowest vibrational level of the triplet state T_1 is lower than that of the single state S_1 in accordance to Hund´s rule, which implies a shift to higher wavelengths of phosphorescence in comparison to fluorescence.

5.1.6 Delayed fluorescence

The last possible transition of ISC is the reverse intersystem crossing from $T_1 \rightarrow S_1$, which further leads to delayed fluorescence. Hereby three different types of delayed fluorescence are known. The E-type delayed fluorescence occurs more likely at higher temperatures or can happen if there is a small energy difference between S_1 and T_1 and if the lifetime of the T_1 triplet state is long enough. The emission of photons (fluorescence) is hereby delayed by a stay (and therefore shows longer decay time constant) in the T_1 state but still has the same spectral distribution as normal fluorescence. The P-type (first observed with pyrene) delayed fluorescence describes a process in which the first excited singlet state is populated. The energy required for this process comes from the collision of two molecules in the triplet state (triple-triplet annihilation). In this process involving two photons the decay time constant of the delayed fluorescence process is only half the lifetime of the triplet state. The last known type of delayed fluorescence is known as recombination fluorescence. In this case excited singlet state becomes populated by recombination of radical ions with electrons on one hand or by recombination of radical ions of opposite charge. [6]

5.1.7 Lifetime

The measurement of lifetime gives an insight into the time scale of processes in the excited state and determines the time course of fluorescence intensity after pulse excitation, meaning that the resulting statistical values refer to the average time the molecules stay in its excited state before emitting a photon and are therefore only true for a large number of molecules. After the promotion of a molecule to the excited state S_1 (or actually T_1) there are generally two different pathways of de-excitation, the radiative (fluorescence and phosphorescence) and the non-radiative (IC and ISC) de-excitation, which can both (except for triplet-triplet-annihilation) be described by first order kinetics (see equation (2)). [A*] is the concentration of species A in the excited state and k the sum of possible de-activation rates that can occur.

$$-\frac{d[A^*]}{dt} = k \cdot [A^*] \tag{2}$$

Integration of this equation with the following definition of the lifetime of the excited state τ:

$$k = \tau \cdot t \tag{3}$$

yields in:

$$[A^*]_t = [A^*]_0 \cdot e^{\left(\frac{-t}{\tau}\right)} \quad (4)$$

According to this equation (see equation (4)) the fluorescence intensity decreases exponentially if excitation of species A does not occur any longer. Since the molecules remain a certain time in the excited state the fluorescence decay time defines the time window for the different possible dynamic phenomena. For an excited singlet-state the lifetimes are in the range of 10^{-11} to 10^{-7} seconds, while phosphorescence lifetimes are actually much longer and can last from 10^{-6} to sometimes even seconds.

5.1.8 Quantum yield

The quantum yield shows the efficiency of a performed fluorescence/phosphorescence process through observation of the fraction of the excited molecules that undergo the transition $S_1 \rightarrow S_0$ or rather $T_1 \rightarrow S_0$ back to the ground state with emission of photons (fluorescence or phosphorescence) and is therefore an important parameter for the sensors brightness.

$$\phi_F = \frac{k_r^S}{k_r^S + k_{nr}^S} = k_r^S * \tau_S \quad (5)$$

Hereby k_r^S is the rate constant for radiative deactivation ($S_1 \rightarrow S_0$) with emission of fluorescence, whereas k_{nr}^S presents the overall non-radiative rate constant and τ_S the fluorescence decay time. The quantum yield is defined as the ratio of the number of emitted photons (over the whole duration of the decay) to the number of the absorbed photons. Therefore the maximum achievable quantum yield is one (100%). In general of course not every absorbed photon is then emitted via radiation which is due to the faster non-radiative de-excitation. Using the radiative lifetime τ_r, it is also possible to define the quantum yield as follows according to equation (6).

$$\phi_F = \frac{emitted\ photons}{absorbed\ photons} = \frac{\tau_S}{\tau_r} \quad (6)$$

This equation is valid as long as the de-excitation pathways do not change from the in Figure 1 shown processes, otherwise both, the excited state lifetime and the fluorescence quantum yield will be affected. Furthermore, a higher temperature results in a decrease in the fluorescence quantum yield and lifetime, because the non-radiative processes (collisions with solvent molecules, intramolecular vibrations ant rotations etc.) are more efficient and occur faster.

5.1.9 Luminescence quenching

Luminescence quenching is a process, in which a decrease of intensity of the luminescence is observed due to e.g. collisions, electron transfer, energy transfer, excimer formation and many more without destroying the luminophore itself, in contrast to photobleaching. Luminescence quenching is therefore a reversible radiation-less de-excitation of a luminophore caused by intermolecular interactions. The process of luminescence quenching means either the prevention of the transition to the excited state (static quenching) or the non-radiative transition of the luminophore from the excited state to the ground state (dynamic quenching).

Both types of luminescence quenching can be described and illustrated through the Stern-Volmer equation, which simply describes the change of the luminescence intensity (I) as well as the lifetime (τ) according to the concentration of the quencher ([Q]) and in case of the dynamic quenching the quenching constant (k_q).

$$\frac{I_0}{I} = \frac{\tau_0}{\tau} = 1 + K_{SV} \cdot [Q] = 1 + k_q \cdot \tau_0 \cdot [Q] \quad (7)$$

The unquenched lifetime (τ_0) and the quenching constant k_q, which depends on the immediate environment of the dye, temperature and sterical factors can be furthermore combined to Stern-Volmer-constant K_{SV}, which is the key parameter for the measurement of the sensors sensitivity. Generally within a Stern-Volmer-diagramm the ratio of $\frac{I_0}{I}$ or $\frac{\tau_0}{\tau}$ is plotted against the quencher concentration [Q]. If the resulting graph (called a Stern-Volmer plot) is found to be linear and has an intercept of 1, the Stern-Volmer constant K_{sv} can be read off from its slope.

Static quenching (figure 2) occurs if the quencher is present in a very high concentration and has therefore a high probability to react with the luminophore due to the close distance. This results either in the formation of a ground state non-fluorescent complex or, if they cannot change their positions, in space during the excited-state lifetime this complex is formed via a sphere of effective quenching.

Hereby the concentration of free luminophores is obviously reduced, which reduces further only the luminescence intensity, due to induced changes in its properties, whereas the luminescence lifetime remains constant (ratio of $\frac{I_0}{I}$ is not proportional to $\frac{\tau_0}{\tau}$), because unassociated luminophores are still free and thereby not affected by the quencher.

$$\frac{I_0}{I} = 1 + K_s * [Q] \quad (8)$$

I_0 and I are the luminescence intensities (emission intensity can be said to be proportional to concentration) without and with quencher Q, and K is the quenching constant.

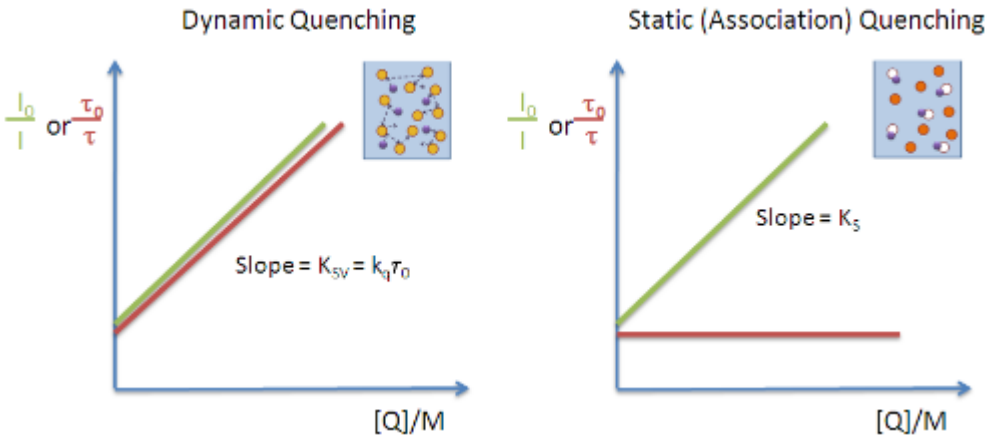

Figure 2 Illustration of the dynamic and static quenching process in comparison [7]

In dynamic quenching (figure 2) a collision of the excited luminophores and the quencher is required (e.g. low concentration of the quencher), which occurs more specifically via diffusion (rate limiting step) of the quencher through the solution and interacting with luminophore or vice versa, resulting in a radiation-less deactivation of the excited state (a return to the ground state). The emission intensity is reduced and a new deactivation pathway through the presence of the quencher is created, which is diffusion-controlled (and therefore also time dependant) and in competition with luminescence.

The energy of the excited luminophores is transferred to the quencher, representing a normal energy transfer reaction. This happens for example in the dynamic deletion of phosphorescent metal complexes by heavy atoms or paramagnetic molecules (e.g. oxygen). In this case the energy donor deactivates to in the ground state while the triplet oxygen gets promoted and excited highly active singlet oxygen is formed, which can easily influence the result of a measurement and therefore affect the sensor through interactions with nearby molecules.

Here the decrease in luminescence intensity and luminescence lifetime is equal, because the quenching process affects all luminophores and therefore it is likely that they will all collide with a quencher over the duration of their excited state lifetime. The quenching is even more effective the longer the luminescence lifetime (τ_0) of the luminophore is.

5.2 Chemical sensors

According to the Cambridge definition :"Chemical sensors are miniaturized devices that can deliver real time and on-line information on the presence of specific compounds or ions in even complex samples." [8]

This chapter and the following sub-chapter are based on [2] and [9] A chemical sensor therefore enables the production of the analyte signal without decomposing or changing the analyte itself, which makes them not only suitable for long term measurements, real-time monitoring but also in noninvasive in-vivo analysis. A major advantage of this sort of sensors

to various other analytical instruments is the broad range of applications also due to the fact that chemical sensors can not only be used to monitor chemical reactions but also to measure physical properties like the absorbance, refractive index, temperature, conductivity and some more.

Generally a chemical sensor (figure 3) is characterized by a recognition element (receptor), a transduction element (transducer) and a signal processor, which are intended to indicate a chemical concentration continuously and reversibly. The aim of the receptor is the transformation of the chemical information in a form of energy, which the transducer is then able to measure. The receptor is often immobilized on a certain platform, which interacts as a linkage between the receptor and the transducer. The transducer should then transform the energy, which is carrying the chemical information about the sample into an exploitable analytical signal.

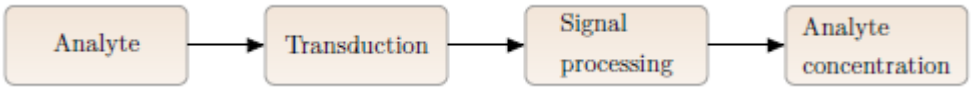

Figure 3 Functional principle of a sensor [2]

The transducer itself does not show any selectivity and therefore the receptor part of a sensor is even more important and could be based upon different principles. The above described build-up of the sensor (figure 3) can certainly be modified to eliminate disturbing signals and prevent the binding of certain compounds to the receptor or to receive a better immobilization on the respective platform. These effects are often achieved through the introduction of a polymer matrix with the desired properties.

Important in the use of all sensors is particularly the reversibility, great accuracy and of course ease of use. Furthermore, also a low detection limit, a broad dynamic range, fast response time, a long operating time and high sensitivity at low concentration values, specificity and selectivity are desired. Of course, the sensor should be small and cheap, which actually requires as further consequence a mass production, in which the other parameters mentioned should not be negatively influenced.

5.2.1 Optical oxygen sensors

The aim of an optical chemical sensor is to yield information of the analyte through using optical transduction techniques. The functional principle is mostly based on fluorescence or phosphorescence quenching (and is therefore a diffusion limited process) by molecular oxygen, which is present in a triplet state (ground state). The measurement relies hereby on the above described dynamic quenching of a luminophore indicator (dye) and the following generation of the highly reactive singlet state of oxygen generated by an energy transfer from

the excited indicator dye. Due to the higher efficiency of the quenching process with longer lifetimes of the indicator, phosphorescent dyes are more appropriate in use.

Commonly the luminescent indicator dye is physically (or even chemically) embedded in a matrix that is actually permeable for oxygen [10]. The matrix is not only responsible to maintain the desired concentration of the dye and to prevent the dye from aggregation but acts also as a barrier for various unwanted species that would disturb the measurement. Furthermore the chosen matrix is one of the two key parameters to fine-tune the sensitivity of the sensor. This tremendous effect is due to the fact that quenching is a diffusion limited process and an increased diffusion coefficient therefore leads, according to the Stern-Volmer-equation, to a higher quenching constant k_q and so to a tunable sensitivity of the sensor. The second parameter of great importance is of course the choice of the suitable luminophore, or in other words the lifetime of its excited state for a measurement on the desired oxygen level.

As mentioned previously the process of quenching or more precisely the concentration of the quencher (oxygen) leads to an analogous decrease in luminescent lifetime of the dye. The correlation is described by the Stern-Volmer-equation.

Due to various disadvantages of intensity measurements like signal fluctuations or photobleaching of the dye, which can be caused by intensity changes of the excitation source or a varying concentration of the dye in the sensor the lifetime-based measurement of the luminescent indicator are favored for the determination of the oxygen concentration within the sample. In the lifetime-based measurement the method of phase-fluorimetry is applied in which the sample is excited by the use of modulated light at a certain frequency (kHz).This leads in the following to a harmonic response of the sample, which is sinusoidally modulated at the same frequency but delayed in phase and also partially demodulated with respect to the excitation. Through the determined phase shift, which is related to the lifetime of the indicator dye according to the formula below, the lifetime of the excited state of the dye can be calculated.

$$\tan(\phi) = \omega \cdot \tau_\phi \tag{9}$$

$$\omega = 2 \cdot \pi \cdot f \tag{10}$$

ϕ … phase shift [°]

ω … angular frequency [rad/s]

τ_ϕ … phase shift lifetime [s]

f … excitation frequency [Hz]

5.3 Porphyrins-Introduction & historical development

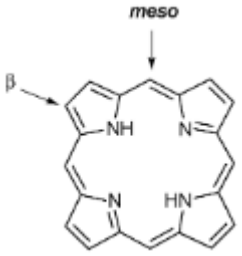

Figure 4 Structure of an un-substituted porphyrin[14]

Porphyrins, (figure 4) a class of naturally occurring macrocyclic compounds, are probably one of the most important pigments found in nature. They can be described as a square planar 18 π-aromatic macrocycles built up of four pyrroles and four methine carbons.[11] Porphyrins play a significant role in many different biological processes such as cell respiration, detoxification of xenobiotics, oxygen transport, fatty acid oxidation and also in light harvesting processes. [12], [13], [14] Due to many favorable properties like their structural robustness, chemical stability, intense absorption (in the visible region) and emission behavior, tunable optoelectronic properties, their versatile metal coordination possibilities and their outstanding strong aromaticity these macrocycles have been studied and successfully applied across an enormous range of research disciplines.[11] During the last decades it has been recognized that the electronic system of a porphyrin is susceptible to conjugative perturbation at its periphery [11], extension of the porphyrins core by fusion of external aromatic fragments [15] (leading to π-extended porphyrins) but also through manipulation of the porphyrins planarity [16] which pose the opportunity for rational electronic fine-tuning leading to systems showing completely different electronic but also optical properties. [14]

Among other changes within the structure of porphyrins, π-extension of a chromophore usually leads to a bathochromic shift of the absorption and emission spectrum and therefore offers a new field of potential applications in both medicine and technology for near-IR dyes, which is more closely examined in the following chapters.[1], [11], [17], [17]–[26] Nevertheless the understanding of structure-property relationships is very important for the development and the research of new porphyrin chromophores targeted for certain applications. [27]

The research in the field of porphyrins has gained particular interests in the last years due to many potential applications in various areas of research but also industry. These include catalysis [28], electronic devices [29], commercial dye industry [27], light emitting diodes [30], thin-film transistors [31], non-linear optical materials [32], supramolecular systems [33], photovoltaic cells [34], solar energy conversion [35], medicine recently especially in the field of photodynamic therapy [36]–[38] and of course optical sensors satisfying many different requirements. [14], [1] Due to this amount of diverse applications affording a large variety of porphyrins the next chapter will give a short overview of some selected and well applied metalloporphyrins in the field of optical oxygen sensing especially focusing on Pt(II) and Pd(II) porphyrins, which are one of the most popular luminophores for this application.

5.4 Metalloporphyrins and commonly used UV-Vis indicators

Since oxygen is essential for life it is definitively one of the most important chemical species on earth, wherefore the determination of this analyte is of great importance in various fields of science and technology. Even though several different approaches exist to measure the oxygen concentration in different environments, optical sensing of oxygen has become extremely popular in the last two decades due to a number of advantages in comparison to e.g. electrochemical or chemical principles of oxygen detection. [1], [39] Optical Sensing allows non- or minimally invasive routinely monitoring of oxygen without consumption of oxygen and is free from electrical interference. [1], [3] Furthermore the sensors are inexpensive, disposable and can be easily miniaturized. [3] Herein most optical sensing systems developed for the detection of oxygen rely on the process of luminescence quenching of the indicator dye by molecular oxygen. [2]

UV-Vis oxygen indicators are therefore quite well established and are most often represented by ruthenium(II) polypyridyl complexes [40], platinum(II) and palladium(II) porphyrins [41] and cyclometallated complexes of platinum(II) [42] and iridium(III) [43]. Among all the commonly used indicators platinum(II) and palladium(II) porphyrins are the most popular luminophores due to their strong phosphorescence at room temperature, relatively high molar absorption coefficients and large Stocke's shifts. [1] Moreover phosphorescent lifetime of these complexes is in a range of microseconds to milliseconds, which can be easily tuned by using different central atoms. Pd(II) porphyrins show for example much longer lifetimes in comparison to the Pt(II) analogs, which can be put in relation to the increase in spin-orbit coupling expected in the heavier metal [44] but only achieve two to three times lower emission quantum yields then the platinum(II) derivatives. Over the years many parameters of platinum(II) and palladium(II) porphyrins were improved or adjusted for the different requirements or various media, such as photophysical properties like brightness, lifetime and photostability or the modification of the suitable wavelength. Two prominent representatives of well-established indicators are platinum(II) and palladium(II) complexes with octaethylporphyrin (OEP) and the platinum(II) or palladium(II)tetrakis(pentafluorophenyl)porphyrin (PdTFPP). PtOEP and PdOEP possess quite strong room temperature phosphorescence with quantum yields of about 50% and 20%, long lifetime of approximately 91 µs and 990 µs under anoxic conditions [45]. Despite their rather low photostability these indicators were widely used as optical oxygen sensors and have often been immobilized in many different oxygen-permeable polymeric matrices like polystyrene [46], ethyl cellulose or polyvinylchloride [47]. PtTFPP, however has replaced the PtOEP and PdOEP in the most cases due to its higher photostability, which can be explained by electron withdrawing effect of the perfluorophenyl substituents, which decreases the electron density on the porphyrin ring leading to a reduced reactivity towards oxidation by singlet oxygen [48], the most dominant reason for photo bleaching of dyes. This

indicator shows nearly the same decay time (60 µs), quite good brightness after excitation in the visible range [48] and is widely used in various matrices but can also be covalently coupled to polymeric materials like polystyrene copolymers by nucleophilic substitution of the para-fluorine atoms of the pentafluorophenyl groups. [49]

All the indicators mentioned so far only show efficient absorption of light in the UV-Vis region and suffer therefore from several drawbacks obviously limiting their field of possible applications. Firstly excitation in the UV-Vis leads to the production of a high level of autofluorescence due to several natural fluorescent compounds like FAD, NAD or chlorophyll, which are present in biological samples or in fermentation media. Secondly these UV-Vis indicators are on one hand poorly suitable for oxygen measurements in scattering media, such as marine sediments or tissues and on the other hand are useless as implantable sensors due to the efficient absorption of blood in the visible region. [1] As a solution of this problem different red excitable and NIR emitting indicators were developed, which do not only overcome the drawbacks but even show much better compatibility with optical components leading to a field of research presented in the next chapter.

5.5 Near infrared indicators

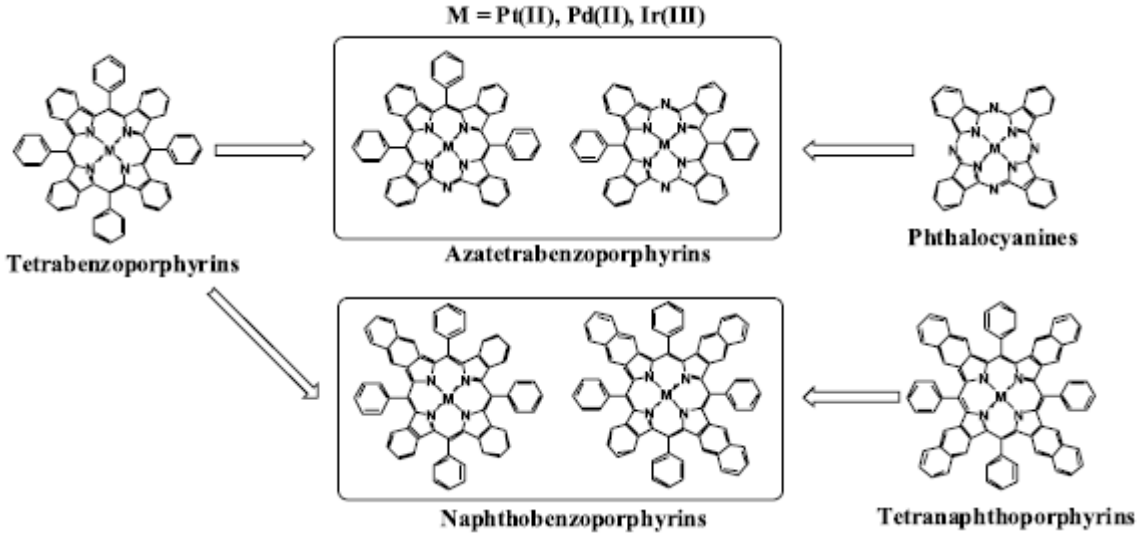

Figure 5 Chemical structures of the state-of-the-art and novel NIR emitting oxygen indicators [18]

Infrared (IR) light describes the electromagnetic radiation extending from the red edge (700 nm) of the Vis-spectrum to 1 mm at wavelength compared to those of visible light (400-700 nm). Furthermore this range of wavelengths can be subdivided into three parts, namely the near-infrared (NIR; 700-2500 nm), mid- and far-infrared regions. [23] The infrared region of the spectrum is not only an interesting and extensively studied field of research for applications concerning measurement of various parameters in biological samples but is also one of the key limiting factors in the area of organic solar cells or photovoltaic cells in

general, due to the fact that almost 50% of the energy from the sun reaching the earth is NIR radiation. [23] More efficient light collecting in this spectral region is therefore extremely important for improvement of organic solar cells in the future. [50], [24] Additionally the near-infrared region between 700 and 900 nm is well-known as the optical window for various therapeutic applications but also for real time *in vivo* biological imaging as previously described, because of minimal absorption and autofluorescence of biological tissues at these wavelengths, enabling deeper penetration of light compared to visible light. [23], [24] Another big advantage of red light excitable indicators is their compatibility with red laser diodes and Si photodiodes, which sensitivity increases at wavelengths higher than 600 nm. [39]

Bathochromic shift of the absorption and the emission bands of various porphyrinoids can now be achieved in different ways. In the last years quite a number of synthetic strategies were developed, including partial reduction of the tetrepyrolicmacrocycle (e.g. chlorins) [51] or oxidation of the porphyrin macrocycle (porphyrin lactones [52] and porphyrin ketones [45]), introduction of meso-alkynyl substituents [53], expansion of the conjugated core (e.g. sapphyrins) [54], linkage isomerization [55], by manipulation of the porphyrins planarity [22] or extension of the porphyrins core by fusion of external aromatic fragments [56]. The latter approach leading to π-extended porphyrins can again be achieved using different synthetic strategies such as oxidative aromatic coupling [57], construction of oligomers coupled through unsaturated bridges[58], by β-fusion of meso-linked oligomers (leading to porphyrin "tapes") or ring fusion of meso-bound polycyclic aromatic rings [14]. The most promising way to achieve bathochromic shifted phosphorescence is the extension of the π-conjugated system of the porphyrin core through fusion of various aromatic moieties at the β-pyrrole positions [20], [59], [60] creating for example tetrabezoporphyrins (TBP) or tetranaphthaloporphyrins (TNP) and many more.(figure 6) Extension of the meso-positions of the porphyrin core was also performed resulting in similar emission spectrum compared to not π-extended porphyrin due to the fact that the fused phenyl groups are almost out of plane to the porphyrin core and therefore show only little contribution to the extension of the π-conjugated system of the porphyrin. [23]

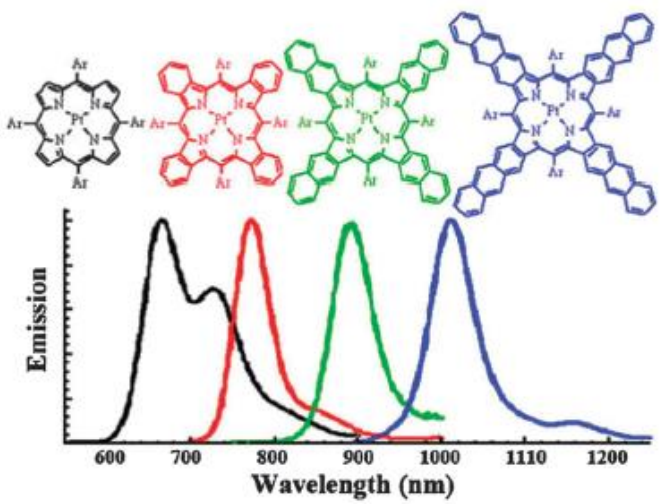

Figure 6 Emission spectra of different π-extended Pt(II) porphyrins in toluene at RT[23]

A negative aspect of the substitution with aromatic moieties at the β-pyrrole positions of the porphyrin core (e.g. TBP) is the strong tendency to π-π-stacking [26] and the aggregation due to their planar π-extended system leading to a lowered solubility. [23] However the substitution of these systems with for example four phenyl groups at the meso-positions results in a better soluble non-planar porphyrins with even slightly further red-shifted absorption and emission spectra.[23], [20] Generally it must be noted that laterally extended porphyrins as well as porphyrins with a larger π-conjugated system and especially TNP have considerable solubility problems due to the increased aggregation probability, which can be at least partially circumvented by introducing bulky groups (tert-butyl) to the meso-position of the porphyrin macrocycle resulting in the formation of a non-planar system.[22], [25] The substitution with fluorinated derivatives (e.g. trifluorophenyl-derivatives) in meso-position shows not only better solubility and photostability (due to their electron withdrawing effect) but also a shift to higher wavelengths of the emission bands. [3], [39]

For the development of new NIR indicators or rather the tuning of the emission in the NIR region it is very important to consider several design factors, which will be discussed in the following.[23] The key in the design of novel NIR emitters is the bathochromic shift in the absorption and the emission spectra, which is caused by narrowing of the energy gap between the HOMO and the LUMO. The HOMO-LUMO gap determines the optical as well as the electronic properties of organic molecules.[61] Moreover the effect of substituents in ligands plays a crucial role, depending on both the nature and the position of the substituent in the ligand. While electron-withdrawing substituents (-F, $-CF_3$) tend to stabilize the HOMO due to the removal of electron density from the metal leading to a blue shift of the emission, electron donating groups (-tBu or –OMe) show an inverse effect. [23], [62] Nevertheless the contribution of ligand substituents to the emission characteristics is much lower than the one of the parent ligand on the π-conjugated system of the porphyrin. [23] A red shift in the phosphorescence emission can also be achieved by extending π-conjugation length in the ligand, although this is a double-edged sword, which should be treated with caution.[23], [63] On the one hand the HOMO-LUMO energy gap can be lowered to a certain limit by increasing chain length but on the other hand this can lead to a decrease in the amount of the participating metal d-orbitals in the HOMO of phosphorescent transition metal complexes, resulting in an attenuated ISC effect and therefore to an increase of the $S_1 \rightarrow T_1$ energy gap and to a decreasing phosphorescent intensity. [64] The incorporation of more polarizable heteroatoms like sulfur and oxygen in the ring system of the ligand results in an easier achievable oxidation of the complex and therefore considerably lower transition energies and a red shift in the corresponding emission spectra. [65] Additional ways to lower the energy band gap would provide the introduction of a donor-acceptor system in the ligand [66] as well as intramolecular metal-metal interactions utilizing multinuclear d^8 Pt(II) complexes. [67]

Another important point is influence of the distortion (trough introduction of phenyl-ring at meso-position) on the photophysical properties of the extended π-system, which can of course only be revealed within studies on symmetrically extended porphyrins. A comparative photophysical study was therefore conducted comparing Ar_4TNPs with Ar_4TBPs, which displayed that the influence of the non-planar distortion on the red shifts of the optical transitions is much smaller than that of the π-conjugation.[27], [59] Furthermore another study revealed that the degrees of non-planarity of these two porphyrins are very similar, finally implying that the red shifts of the absorption of Ar_4TNPs is mainly caused by the different electronic effects of naphtho- and benzogroups.[68], [22]

Phosphorescent Pd(II) complexes are rare in comparison to their analogues Pt(II) complexes, because of their much weaker heavy atom effect exerted by the d^8 Pd(II) metal center. [69] Nevertheless many Pd(II) porphyrin complexes show intense NIR phosphorescence, but with significantly lower quantum yields, longer lifetimes and even more red shifted emission bands than usually Pt(II) porphyrin complexes. [70] Noteworthy is by all means that metallation step of Pd(II) ions into porphyrin ligands is usually far easier than that of Pt(II) ions. [23]

During the last decades many different successful examples of Pt(II) π-extended porphyrin complexes emitting in the NIR were synthesized showing outstanding thermal and chemical stability, sufficiently good solubility, various ways of chemical modification and high luminescence for different applications such as NIR OLEDs, PVCs, optical oxygen sensors and in the field of biomedicine for *in vivo* imaging. [23] Another very interesting purpose would illustrate the usage of oxygen optodes as “smart tattoos”. Hereby sensors are implanted into subcutaneous tissue and then used for continuous noninvasive monitoring of different vital analytes such as oxygen or glucose. They are excited through the skin and monitored with the aid of a photodiode or a CCD camera. (figure7) In the course of the next chapters some of the most prominent state-of-the-art porphyrin dyes are displayed.

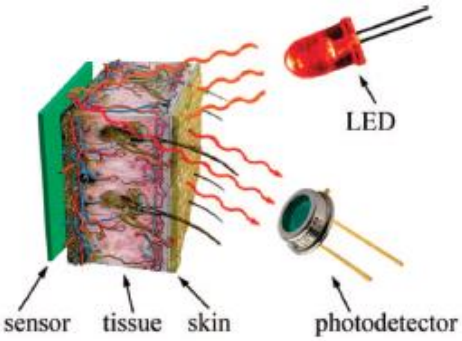

Figure 7 Schematic concept of sensing with the help of smart tattoos [3]

5.5.1 Benzoporphyrins

The first synthesis was reported by Helberger et al. in 1938 [71] and then later in 1940-1950 by Linstead et al. [72] Since that time benzoporphyrins have attracted worldwide remarkable attention, leading not only to the development of various new synthetic strategies but also to the discovery of wide field of application ranging from catalysis [28] over medicine [14] to material science and technology. Recently particularly porphyrins with fused benzene rings at the β-pyrrolic position have emerged as a hot topic of research.[14] These so called benzoporphyrins have generally a UV-Vis absorption spectrum similar to porphyrins depending now on the number of fused benzene rings the absorption of the Q band is red-shifted to 600-750 nm. These tetrabenzoporohyrins but especially tetraphenyltetrabenzoporphyrins (figure 9) (PtTPTBP, PdTPTBP), both members of the π-extended porphyrins family, possess excellent brightness upon excitation in both, the blue (200 000 M^{-1} cm^{-1}) and the red region (130 000 M^{-1} cm^{-1}) of the spectrum, because of their extremely high absorption coefficients, quantum yields of about 50% and 20% and emission at 760 nm. Furthermore these TPTBP complexes possess moderate to high photostability, [3] ,[73] a parameter that is from special interest for practical applications where high light densities are applied or long term measurements are performed. [74] Through substitution of the hydrogen atoms to fluorine (figure 8) in the meso-phenyl rings their photostability and also slightly their quantum yields can be further improved.[39] Since good solubility of the indicator is necessary for nearly all applications and is a well-known problem for benzoporphyrins due to their planar conjugated π-system, this drawback was overcome by introduction of phenyl rings like in TPTBPs or by bulky substituents in the meso-position of the porphyrin. [75] The increased solubility and the lowered tendency of self-aggregation are largely caused by the resulting non-planar structures, which are due to the steric crowding induced by the substituents.[16], [76]

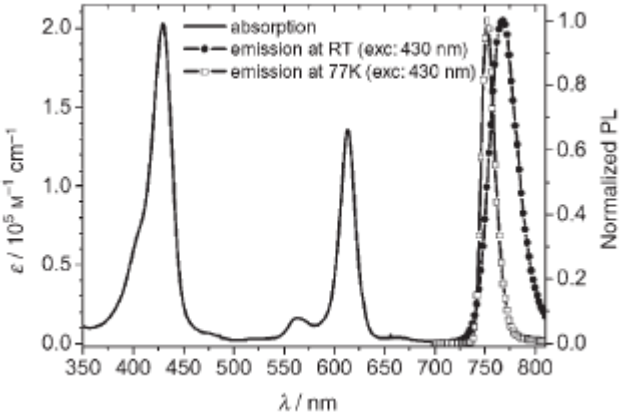

Figure 9 Absorption and emission spectra for Pt(II) TPTBP in 2-methyl-THF at RT or at 77K [20]

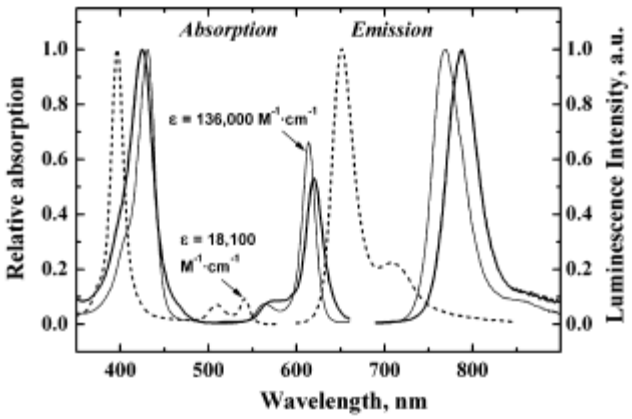

Figure 8 Absorption and emission spectra for PtTPTBP (thin lines), meso-tetra(3,4,5-trifluorophenyl)tetrabenzoporphyrin (thick lines) and PtTFPP (dotted lines) in anoxic toluene at RT[39]

Besides the increased solubility the resulting non-planar structure also affects the photophysical properties of porphyrins by shifting the absorption bands further into the red. [77] When dissolved in a suitable polymer matrix like polystyrene Pt(II) meso-substituted porphyrins can be perfectly used for measurements from 0 to 100% air saturation, whereas their analog Pd(II) dyes are more suitable for trace-oxygen measurements due to their higher sensitivity to oxygen with decay times about 300 µs. [1] Moreover the general structure of benzoporphyrins provides a range of possibilities to further tune the optical and photophysical properties of the resulting porphyrins in the future to broaden the already large field of application further.

The possibility of excitation in the red part of the spectrum and emission in the NIR, combined with the fact of being a good singlet oxygen generators puts benzoporphyrins and all their analogues in a privileged position for many medical and therapeutic applications, [14] which is already one of their major application fields. Unfortunately metalloporphyrins are in general hydrophobic and due to this not soluble in water and physiological fluids. Further modifications are necessary to enhance their interactions with the environment, when used to measure oxygenation of tumors in vivo [78] or generally in subcutaneous tissue. For the measurement of oxygen concentration in tissue the probe must also be impermeable to biological membranes to avoid penetration, they must further possess an absorption band in the near-infrared, because the excitation light needs to penetrate the depths of tissue [79] and of course they have to be not toxic or phototoxic. These requirements are reached by several kinds of sensing probes for extra- and intracellular microscopic imaging like dendrimers, dye conjugates and dyes covalently or not covalently entrapped in polymeric nanoparticles.

One often applied method is the encapsulation of metalloporphyrins into for example poly(arylglycine) dendrimers [79], which fold in aqueous environments and further generate diffusion barriers for oxygen, creating the possibility to regulate on the one hand the sensitivity but on the other hand also the dynamic range of the method. To further enhance the probes solubility, to reduce their toxicity and help to prevent interactions of the probe with biological environment PEG residues are used to modify dendrimers. [79], [1] Such dendritic phosphorescent probes are well-known in scientific society under the name Oxyphors and were already tested for high resolution microscopic in vivo microscopy of vascular pO_2 in rat's brain. [79] A famous representative of this class is the Pd(II)-meso-tetra (4-carboxyphenyl)-tetrabenzoporphyrin complex (Oxyphor G2; figure 10).

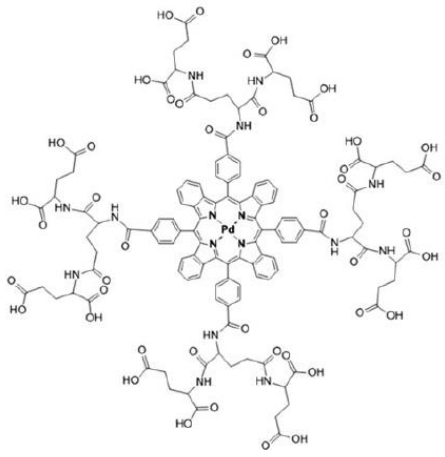

Figure10 Oxyphor G2[1]

This Oxyphor is perfectly suitable for the measurement of tissue oxygenation due to its absorption band near 632 nm. [1]

Another widespread method is the encapsulation of the indicator inside an inert nanoparticle often also named PEBBLE (probes encapsulated by biologically localized embedding). [80] Nanoparticles have the advantage of causing a rather negligible mechanical perturbation in mammalian cell's due to their small radii and are of course like all other optical oxygen sensors minimally invasive and can be used remotely. [1] So called nanosensors were already successfully applied in monitoring dissolved oxygen in human plasma [81] to monitor cellular respiration [82] and for the real-time measurement of oxygen concentration inside tumor cells under normal and also hypoxic conditions. [83] Other important biological applications for tetrabenzoporphyrins [14] in their use as oxygen sensors are for example life time imaging resolving the spatial-temporal dynamics of O_2 across the surface tissue of corals [39], or quantification of dissolved O_2 for the evaluation of complications from diabetes, peripheral vascular diseases, cerebrovascular and cardio-vascular events as well as the detection of tumors.[14], [84]

Probably one of the most promising applications of TBPs can be found in the area of medicine or more exactly in the detection and treatment of tumors namely the photodynamic therapy (figure 11).[37], [38] This method uses light irradiation, which is enhanced by a photosensitizer to reach therapeutic effects in cancer tissues. [36] Under radiation with light at a certain wavelength these photosensitizers promote the generation of cytotoxic free radicals (e.g. singlet oxygen)[85], which then affect tumor growth by destroying the neovasculature directly and by creating an inflammatory microenvironment that induces cancer cell death. [86] In 1993, Photofrin was first applied in PDT but even though some successes were achieved, wide clinical application of this compound is limited by many drawbacks, such as low deep-tissue penetration. Therefore it is essentially to develop new photosensitizers without these limitations such as TBPs to achieve better results. [36] Finally,

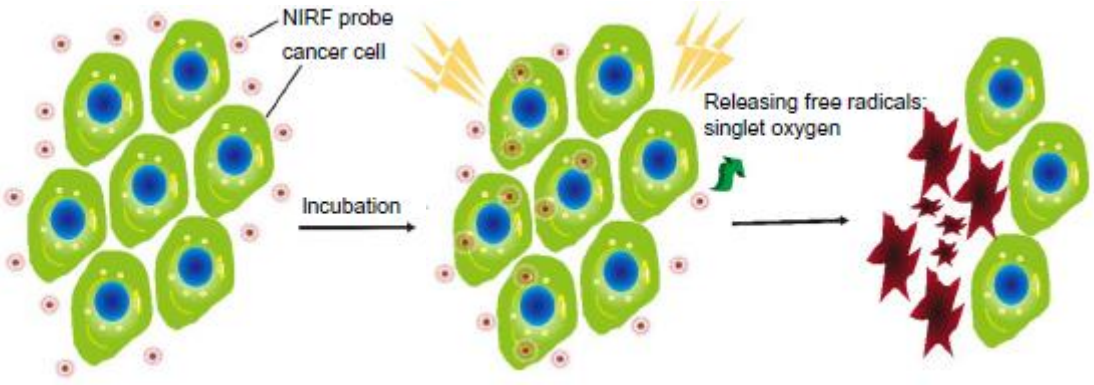

Figure 11 Schematic concept for NIR probes in photodynamic therapy [36]

there are also many possible applications for TBP in material science such as organic semiconductors, liquid crystals [87], optical limiters [88], non-linear optical materials [89] or sensitizers in photovoltaic cells [90] just to name some of them. As we can see on this large variety of applications the interest in the development of new analogues of TBPs in today's science community is not without cause.

5.5.1.1Highly soluble and stable benzoporphyrin dyes

In the last decades intensive research in the field of benzoporphyrins did not only lead to many new synthetic strategies but also to an improved understanding of the structure-property relationship and therefore an extension of their application area. Nevertheless some parameters such as the solubility as well as the photostability still display room for improvement in the future. Although problems of solubility and tendency towards aggregation of TBP due to their planar rigid structure are well known no completely satisfying solution achieving high solubility was found yet. Enhancements have been already achieved through the functionalization with solubilizing groups [91], the substitution of phenyl rings or bulky groups (e.g. tert-butyl) in the meso-position leading to non-planarity of the complex and therefore increased solubility [4] compared to the non-substituted analogue. Bad solubility not only limits their photophysical studies and often hampers synthesis and purification of the compounds but also complicates their application in various fields of material science especially the scaled-up preparation and industry applications requiring solvent processing. [4] Furthermore better solubility will also improve their use as oxygen sensors due to the possibility of higher dye concentration in polymer films without the problem of aggregation or leaching of the dye. Problems such as signal instability, inaccuracy of measurements and lower long term applicability could also be reduced. Similar problems were also observed with phthalocyanine complexes due to their usual tendency to form aggregates. Over time however many different strategies were found to improve solubility such as peripheral substitution with chloro ligands, with aryl substituents but also with tert-butyl groups and finally by axial substitution of aryl, alkyl and also alkyloxy groups. [92] The increased solubility is hereby not only reached through the inhibition of intermolecular interactions, but also through the effect of asymmetrical substitution due the resulting lower degree of order in the solid states which furthermore then facilitates dissolution. [92]

Photostability is as aforementioned a very important parameter and from special interest for practical applications where high light densities are applied or long term measurements are performed, and therefore also subject of extensive research. [74] In the majority of cases photo-degradation is due to the production of singlet oxygen produced upon quenching; Singlet oxygen further reacts with indicator molecules in the ground state resulting in products which are typically non luminescent. [39] Reason for the mostly moderate

photostability of benzoporphyrins is the destabilization of the third LUMO and the first HOMO of the porphyrin caused by the π-ring expansion. The fact that porphyrins became unstable against oxidation and reduction was predicted by Kobayashi et al. [93] As already mentioned in previous chapter electron withdrawing substituents [39] at the periphery (β-ormeso-position) of the porphyrinmacrocyle display increased photostability due to the lowered electron density of the porphyrin core. The suppression of the shown photooxidation is assumed to happen by lowering the HOMO level of the molecule. [4]

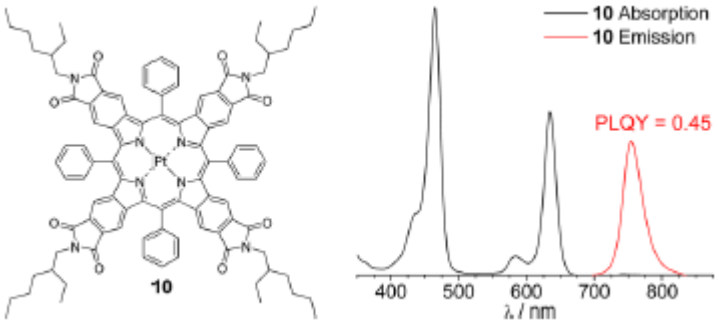

Figure 12 Structure, absorption and emission spectra of the highly soluble porphyrin-dye of Perepichka et al.[4]

Recently Perepichka et al. have prepared a new highly soluble platinum porphyrin (figure 12) with very good photostability, large Stokes shift, NIR emission at 755 nm with a quantum yield of 45% on a multigram scale. [4] Hereby the increased solubility is achieved by the cyclic imide moiety, the branched 2-ethylhexyl group but also the meso-phenyl substituents reducing the planarity of the porphyrin. The polarizable aromatic core and the aliphatic chains result in an enormously high solubility, for example 600 g/L in toluene. [4] Furthermore the dye possesses suppressed photobleaching due to the electron withdrawing imide substituents, resulting in a <30% degradation in an air saturated solution after six days of continuous irritation with a 500 W halogen/tungsten lamp at approximately 90°C. The combination of all these properties make the NIR emitting dye a potential candidate for various applications, including luminescent solar concentrators. [4] Nevertheless this synthetic strategy has also various disadvantages such as expensive and often not easy available chemicals and a high and time-consuming synthetic effort compared to other synthetic routes like the Template method. Here only three steps are necessary to obtain the desired platinum or palladium tetrabenzoporphyrin dye, beginning with cheap and easy available staring materials. [32] Although this dye displays a very promising future, modification and further development of new and different dyes as well as other synthetic strategies are necessary to widen the field of application in the future.

5.5.2 Naphthoporphyrins

Naphthoporphyrins present an interesting class of well-studied porphyrins in which the π-system is extended through fusion of naphtha moieties at the β-pyrrole positions showing a subsequent bathochromic shift of the emission spectrum. Herein every additional fused naphtha moiety leads to a red shift of the Q band by approximately 20 nm, resulting in an overall bathochromic shift of 80 nm when tetra-substituted. [1], [74] These tetranaphthoporphyrins show the highest order of molecular symmetry and therefore exhibit one of the strongest and most narrow spectral transitions. [22] Unfortunately the bathochromic shift is accompanied with a lowering of the phosphorescence quantum yield and a dramatically decrease of photostability, which correlates well with the number of naphtha moieties annealed to the porphyrin. [1], [27], [30] Notably in this case is that the extension of the conjugated system shifts the Q band significantly to higher wavelength, whereas the Soret band is only slightly affected. Although for Pt(II) and Pd(II) complexes the absorption coefficients are very high [74] the low solubility [93] and tendency to aggregation [60] of tetranaphthoporphyrins, due to their planar geometry, limits their potential application in oxygen sensing or within photovoltaics. [94] Nevertheless synthetic strategies exist to overcome solubility as well as photostability problems e.g. by halogenations of naphtho-porphyrins in meso-position, even though the multistep synthesis is not unchallenging. [95] Enhancement of the solubility can be also achieved on an easier way for example through meso-tetraarylation of the naphthoporphyrin (figure 13) resulting in complexes with a non-planar geometry. [59]

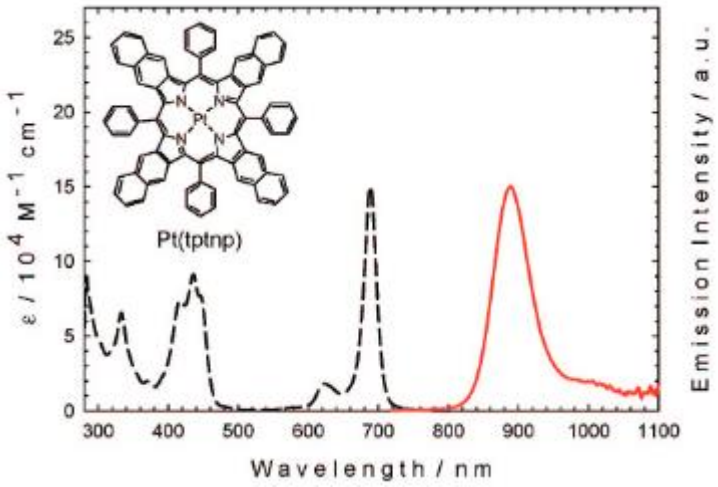

Figure 13 Absorption (black line) and emission spectra (red line)of Pt(II) tetraphenyltetranaphthoporphyrin in toluene at RT [30]

5.5.3 Hybrid benzo- and naphthoporphyrin complexes

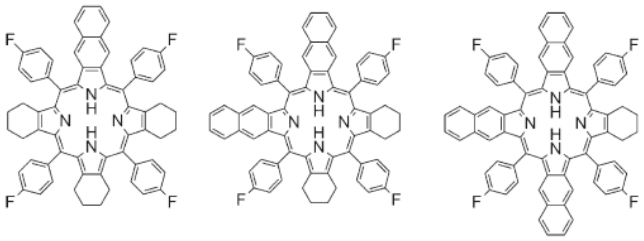

Figure15 Hybrid benzo- and naphthoporphyrin complexes [74]

The hybridization of benzo- and naphthoporphyrins attempts to combine the advantages of both to create a new functional chromophore with attractive photophysical properties. [74] This “tailor-made” near absorbing dye is achieved via systematic condensation of external aromatic fragments resulting in compounds with tunable absorption in the red part of the spectrum (628-691 nm) as well as controllable emission from 815 to 882 nm. (figure 15) [74] These strongly luminescent metalloporphyrins (figure 14) show quantum yields up to 53% in the case of Pt(II) complexes or up to 18% for palladium (II) complexes.[74] With systematic extension of the π-conjugated system with naphtha moieties a bathochromic shift of the Q band and the emission bands is observable whereas the position of the Soret band remains almost constant. Furthermore the enlargement of the aromatic system has a strong impact on the photophysical properties such as a decreased luminescent lifetime and quantum yields as well as a lowered sensitivity of the material to oxygen and increased photobleaching. [74] Nevertheless these chromophores are well-suitable for different multiplexing applications such as simultaneous measuring of oxygen and glucose in enzymatic sensors.[74] Synthetic efforts for the future aim at further improvement of photostability and solubility by introducing halogen atoms to the ligands although compared to tetranaphthoporphyrins these parameters were already significantly enhanced by the present benzo-moieties. [1]

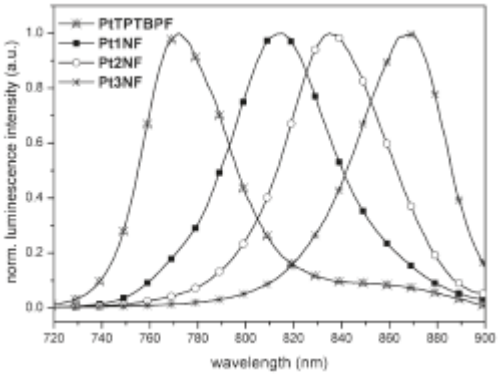

Figure 14 Emission spectra of Pt(II) porphyrins measured in toluene at RT [74]

5.5.4 Hybrid azatetrabenzoporphyrin complexes

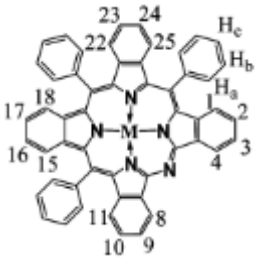

Figure17 Azatetrabenzo-porphyrin; M=Pt, Pd [75]

Hereby the synthesis of azatetrabezoporphyrin (Figure 17) was performed with the aim to generate a complex occupying the intermediate position between tetrabenzoporphyrins and phthalocyanines combining the advantages of both. Phthalocyanines on the one hand possess excellent chemical, thermal and photostability [1], [96] but on the other hand also very narrow absorption bands in the red part of the spectrum and poor phosphorescent quantum yields (<1%) [96] with Pt(II) and Pd(II) complexes and are therefore not really suitable for optical sensing and imaging of oxygen. [75] The hybrid complex shows in comparison to the TPTBP complexes a hypsochromic shift of the Soret band and a bathochromic shift of the Q band, whereas the emission of the azatetrabenzoporphyrin complex is approximately 80 nm shifted to the red. Furthermore the hybrid complexes possess strong phosphorescence emission at 842 nm for Pt(II) and 877 nm for Pd(II) complexes (Figure 16) at room temperature in anoxic solutions and polymers like polystyrene and sufficient brightness for practical applications. Unfortunately substitution of the meso-phenyl rings by nitrogens atoms and azasubstitution seems to shorten the luminescence decay time also the quantum yields.[96], [97] However the shorter decay times establish the possibility for the design of a less sensitive and faster responding sensor at higher oxygen partial pressure than 21 kPa. The photostability of the azatetrabenzoporphyrin sensors is higher than TPTBP and comparable to those of Pt(II) pentafluorophenylporphyrin which is commonly used as oxygen indicator. Despite the poor solubility of TBP and phthalocyanines [97], the solubility of the generated hybrid complex is already sufficiently good enough due to the phenyl substituents in meso-position but could be even further increased due the usage of bulky substituents (tert-butyl groups) at the meso-position. [98]

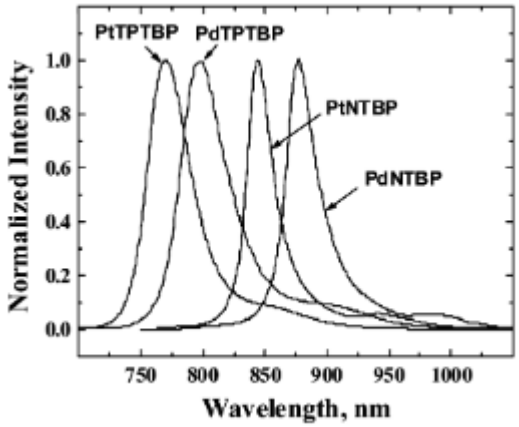

Figure 16 Emission spectra of Pt(II) and Pd(II) azatetrabenzoporphyrin and meso-tetraphenyltetra-benzoporphyrin complexes in anoxic toluene at RT [75]

5.5.6 Rigid porphyrins – alternative ways to NIR indicators

As shown in the previous chapters π-extension of porphyrins can be achieved through fusion of various aromatic rings at β-position of the tetrapyrolicmacrocycle. Using this strategy it was also possible to synthesize tetraacenaphthophorpyrin which shows a remarkable Soret band at 525 nm. [25] Despite bad solubility in all organic solvents, which limited further

investigations this represents one of the highest values observed for the Soret band of a non-expanded porphyrin structure. [25] Another noticeable bathochromic shift for a non-expanded porphyrin complex was shown for the Pb(II) chelate tetrakis(phenylethynyl)-tetraacenaphthoporphyrin where the Soret band was observed at 642 nm. [25] But porphyrins can of course also be extended by attaching other aromatic units via triple bonds, [99] by fusion with other porphyrins resulting in porphyrin dimers or even oligomers. [100] Due to the fact that porphyrins are electron rich and therefore easily undergo electrophilic aromatic substitution at both meso- and β-position the strategy of intramolecular oxidative coupling became really important to generate π-expanded porphyrins. [101], [102], [57] Examples for the fusion of porphyrins would be the synthesis of Osuka and co-workers leading to a diporphyrin with the lowest energy band 996 nm, [57] or the synthesis of the zinc porphyrin tape consisting of twelve porphyrin units causing a progressive red-shift reaching 2400 nm for a 12-mer array. [103] Whereas the diporphyrins possess a planar geometry resulting in a matchless delocalization of π-electrons, the porphyrin tapes show outstanding non-linear optical properties. Unfortunately mostly such fused porphyrin oligomers are fairly insoluble in commonly used organic solvent because of their rigid planar structure and the serious tendency of aggregation. [11] Furthermore porphyrin cores were also fused with naphthalene via oxidative ring closure reactions [104] or by oxidative aromatic coupling in presence of $FeCl_3$ displaying the lowest energy band at 682 nm for the Ni-porphyrin. [57] The idea to synthesize anthracene-fused porphyrins (figure 18) led to the formation of non-aggregating fully fused porphyrin, [105] without loss of planarity, a highly delocalized π-system and strong absorption in the NIR red-shifted at 1000 nm. [57] Moreover porphyrins were also fused with larger aromatic hydrocarbons, for example with pyrenes. Hereby doubly-fused pyrenyl compounds were synthesized via thermal fusion at 500-530°C under vacuum resulting in two region-isomers, displaying fluorescence in the NIR at 839 nm with 8% quantum yield and at 829 nm with 13% quantum yield. [57] Surprisingly the lack of alkoxy substituents as well as the potential distortion (out of plane) of this second isomer hindered disturbing aggregation via π-stacking and led to a product with an acceptable solubility according to the authors. [95] Another way to fuse porphyrins under oxidative conditions is the Scholl reaction, which has been especially studied extensively for

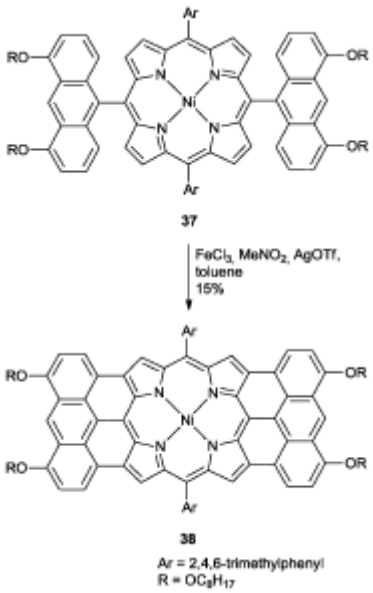

Figure 18 Reaction scheme for fusion of two anthracene units to the Ni-porphyrin ring system [57]

further ring closure of aromatic systems to the core of the porphyrin. [24] Notably however is that the ability of polycyclic aromatic hydrocarbons for fusion onto a porphyrin in a Scholl reaction (figure 20) is obviously dependent on the oxidation potential of the aromatic groups, with the upper limit located between perylene and pyrene rings. Thompson et al. showed that two perylene rings (without the need of an activation group) were fused onto a porphyrin leading to a Q-band that is red-shifted up to 900 nm. [24] This showed that the Scholl reaction outlines a really interesting and potential but unfortunately not well-studied possibility to achieve ring fusion onto a porphyrin core in the future.

The Scholl reaction describes the condensation of aromatics with the help of Lewis acids [106] (often $AlCl_3$) and is often used for dendritic oligo- and polyphenylene compounds. Hereby different Lewis acids ($FeCl_3$, $AlCl_3$, $CuCl_2$) show various product distributions, mostly because of the different coordination of the metals. [106] Furthermore Bronsted acids are

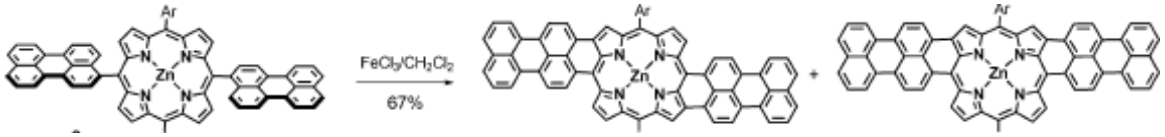

Figure 19 Scholl fusion of perylene-substituted pophyrin leading to β-meso annulated porphyrin with perylene rings[24]

often implicated as catalysts. Traces of HCl or even water accelerate the reaction and lead in the case of $AlCl_3$ to the $H[AlCl_3OH]$ complex and HCl. [106] Despite the common application of the Scholl reaction in literature the reaction mechanism is still not completely clarified. To date two possible reaction mechanisms (figure 19) were considered which are the radical cation and the arenium-cation mechanism, whereas the latter is energetically more feasible. [106], [107] While the Scholl-reaction is not common for fusion of different aromatic fragments to a metal-complex, it is very popular and also often successfully applied for the bridging of organic compounds such as shown in figure 21 and 22.

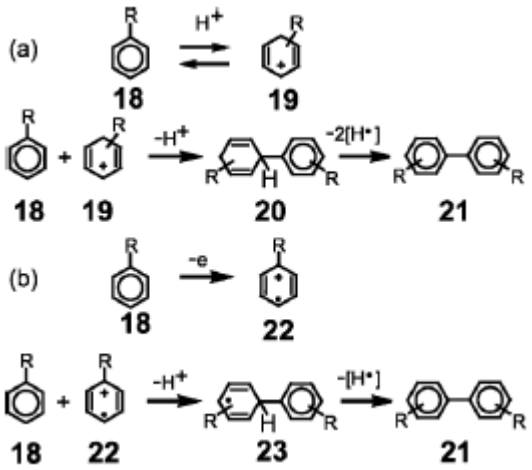

Figure 20 Proposed Mechanism of the Scholl-recation:(a) Arenium- (b) Radical-Cation Mechanism [106]

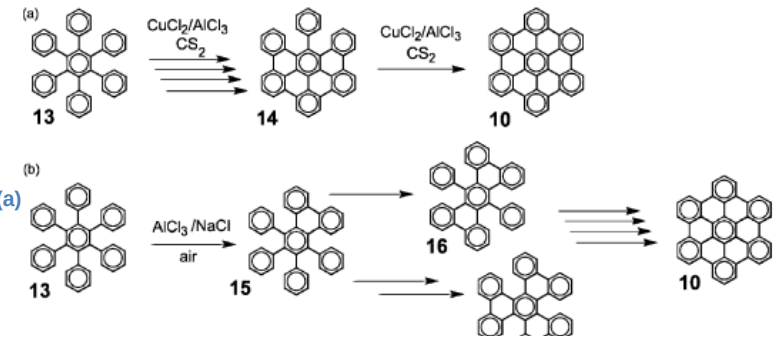

Figure 21 Different synthetic routes leading to Hexa-peri-hexabenzo-coronene [106]

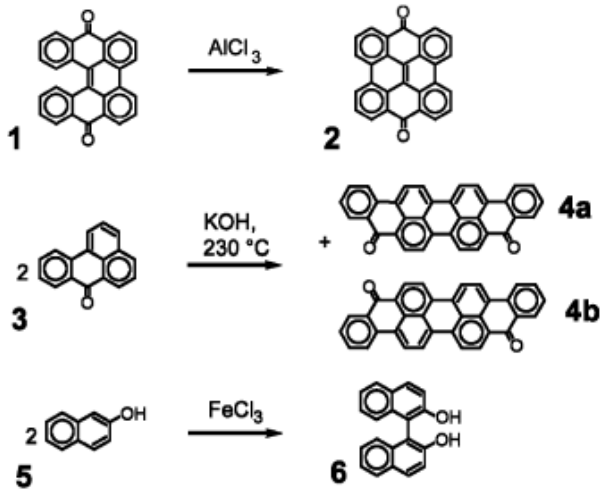

Figure 22 Examples of dehydrogenation coupling reactions of different aromatic compounds [106]

5.6 Triplet-Triplet based upconversion

The concept of upconversion can generally be described as the observation of photon emission after population of excited state at shorter wavelength (higher energy) through excitation at higher wavelength (lower energy). [108] Over time a few different techniques for upconversion were examined including upconversion with two photon absorption dyes (TPA), with inorganic crystals but also rare earth materials. [109], [110] Unfortunately all these concepts suffer from serious drawbacks like the need of high excitation power, poor absorption of visible light and also low upconversion quantum yields. Especially the necessary high excitation power constitute a serious problem since solar light has only low excitation power density. [108] Recently a new upconversion concept based on triplet-triplet annihilation (TTA) has attracted much attention in the science community. [111] TTA upconversion does not only overcome the drawbacks of the above techniques but shows furthermore many advantages such as a quite low requirement of excitation power density, which allows the use of solar light and not necessary a coherent excitation. [108] Moreover the excitation and emission wavelength of TTA upconversion (figure 23) can be varied, simply by a different selection of the two components (triplet sentiziser and triplet acceptor) of the upconversion system as long as their energy levels of the exited states still match. A clear disadvantage of the TTA upconversion however is the quenchability by oxygen. In comparison to other upconversion schemes, in TTA

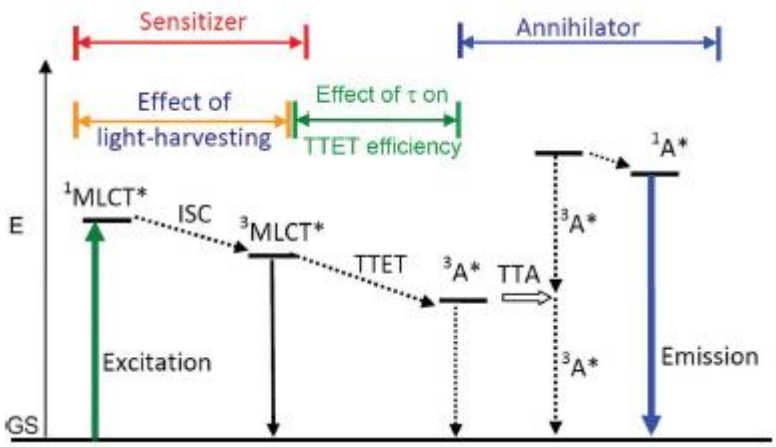

Figure 23 Qualitativ Jablonski diagram illustrating the TTA upconversion process between triplet sensitizer and acceptor [85]

upconversion the triplet sensitizer and triplet acceptor are mixed together. The excitation energy is first collected by the sensitizer before the energy is transferred to the acceptor via triplet-triplet energy transfer (TTET) leading to an emission at shorter wavelength than the excitation. [108] The photophysics of TTA upconversion can be shown in a qualitative Jablonski diagram. (figure 23) First the sensitizer is excited with photo-irradiation, leading to the population of the singlet excited state ($S_0 \rightarrow S_1$) followed by an intersystem crossing ($S_1 \rightarrow T_1$), which is enhanced through the presence of heavy atoms (transition metal) resulting in the population of the triplet excited state of the sensitizer. Due to the longer lifetime of the excited triplet state compared to the singlet excited state, the energy can be transferred from the triplet sensitizer to the triplet acceptor via TTET process, which is usually a Dexter process and therefore requires contact of the two components. [112] Further on, the collision of the acceptor molecules at the excited triplet state with each other will produce an acceptor molecule in the excited singlet state and an exceptor molecule in the ground state (following the spin statistic law), from where the radiative decay results in the upconverted fluorescence, whose energy is higher than the excitation light. [108] Hereby the maximal upconversion quantum yield will not be higher than 11.1% due to the spin statistic law, after which efficiency of TTA upconversion is limited, even though examples that exceed the limit have already been reported. [113] These results assume that triplets as well as possibly quintets are also leading to upconversion. On the supposition that quintet encounter complexes dissociate back into triplets and then follow the destiny of this channel higher quantum yields up to 40% maximum yield are possible. [114] Notably, several photophysical parameters concerning sensitizers and acceptors are crucial for efficient TTA upconversion. First the sensitizer should show strong absorption at the excitation wavelength to enable high concentration of the sensitizer in the excited triplet state. Furthermore the triplet excited state quantum yield of the sensitizer must be high, which requires an efficient ISC to produce the triplet excited state. [108] Moreover the lifetime of the triplet excited state of the sensitizer should be long and the relative energy levels of the triplet sensitizer and the triplet acceptor must be suitable to maximize the TTET efficiency. Finally, the radiative decay rate of the S_1 excited state should be powerful or in other words the fluorescence quantum yield of the acceptor should also be high. [108] To illustrate the so far described process a photographic image of a successfully performed upconversion is shown in figure 24.

Figure 24 Solution of sensitizer (Palladium(II) 2,3-bis(3,3,9,9-tetramethyl-2-hydroxyjulolidine) but-2-enedinitrile and annihilator (diisobutyl 3,9-perylenedicarboxylate) in deoxygenated toluene upon excitation with a 635 nm laser diode and LED[116]

During the last years different sensitizers were developed such as various Ru(II) polymine complexes, cyclometalated Pt(II)/Ir(III) complexes and Pt(II)/Pd(II) porphyrin complexes, which in comparison to Ru(II) complexes show more

intense absorption of visible light and longer triplet excited lifetimes. [108] Herein also an TBTBP platinum porphyrin complex as sensitizer mixed with a perylene acceptor was reported, which however showed only poor upconversion quantum yields of 0.65%. [115] The most promising sensitizers to date are Pt(II) acetylide complexes, that show tunable excitation and emission wavelength and very good upconversion quantum yields. [112] Unfortunately much less attention has been paid to the development of triplet acceptors so far, even though the development of new triplet acceptors with higher fluorescence quantum yields and better photostabilities would definitely contribute strongly to a better working upconversion system. [108]

Finally it can be concluded that TTA upconversion presents a promising upconversion concept, which is due to advantages compared to other upconversion techniques ideal for applications in the field photovoltaics, photocatalysis, artificial photosynthesis, optics [109], [110] and even suitable as optical oxygen sensors. [116] Nevertheless the development of new sensitizers with intense absorption especially in the NIR range and long lifetime of triplet excited states is highly desired in future.

.

6. Materials and Methods

6.1 Materials

6.1.1 Thin layer chromatography

The conversion of the reaction was predominantly checked via thin layer chromatography. For this purpose TLC plates from Sigma Aldrich Fluka Analytical (silica on TLC aluminum foils with fluorescent indicator 254 nm, H x W = 20 x 20 cm; Germany) were utilized. In exceptional cases, a TLC plate coated with ALOX (ALUGRAm, H x W = 20 x 20 cm, Macherey-Nagel, N/UV_{254} for TLC; Germany) was used to receive a good separation of the substances.The detection of the signals was done with UV light at a wavelength of λ = 254 nm or 366 nm.

6.1.2 Column chromatography (flash-chromatography)

Purification via flash chromatography was performed using silica gel 60 of ROTH or ALOX of Acros Organics. The particle size distribution was between 0.04 and 0.063 mm respectively 50-200 µm. In selecting the various columns attention was always paid to the separative amount of the product but also to the complexity of the separation process. The applied solvent compositions for the purification via flash chromatography are given in the experimental procedures.

6.2 Photophysical measurements

6.2.1 Absorption

All absorption spectra were recorded on a VARIAN CARY 50 conc; UV-Vis spectrophotometer by Varian (Palo Alto, United States) or on Agilent Cary 60UV-VIS by Agilent Technologies. Absorption measurements were performed between 800 and 300 nm at fast scan rate using the baseline correction setup with an adequate blank sample of the used solvent. Hellma 100-QS 10 mm precision cuvettes or Hellma101-OS 10 mm precision cuvettes were used for the measurements. The respective molar absorption coefficients were calculated using the Lambert-Beers law. For this purpose the sample was always measured in toluene and acetone, while a specific amount of the dye (in the range of 5 mg) was dissolved in DCM in a graduated flask (20 or 25 mL) on the ultrasonic bath for ten minutes, acting on the assumption that the dye dissolved completely.

6.2.2 Emission/excitation spectra and Quantum Yields

Emission and excitation spectra were recorded on a FluoroLog® 3 spectrofluorometer from Horiba Scientific equipped with a R2658 photomultiplier from Hamamazu.

6.2.3 Photostability

Dye solutions with known concentration were prepared in either toluene or DMF in a Hellma screw-cap fluorescence cuvette and illuminated with blue/green light emitting LEDs (458 nm) or (530 nm) at the following settings: 10.79 V, 0.689 A, 7.4 W or 5.85 V, 0.317 A, 1.9 W. The cuvette was placed in the focus of the LEDs. After shaking of the cuvette absorption spectra were recorded in defined time intervals (30 seconds to 2 minutes) in a wavelength range from 300 to 1000 nm. Depending on the intention of the measurement (oxygenated or deoxygenated atmosphere) the cuvette was unsealed shortly or not. (For the measurement of oxygenated dye solutions the cuvette was sometime unsealed for short time whereas deoxygenated probes remained closed during the photostability measurements). If the measurement took place in a deoxygenated atmosphere the dye solution was first de-oxygenated by bubbling Argon through the solution for 10 minutes. The final value for the degradation was determined by calculation of the average values of the three maximum absorption points in the respective band.

6.3 Structural and chemical measurements

6.3.1 Nuclear magnetic resonance spectroscopy (NMR spectroscopy)

All enclosed nuclear magnetic resonance spectra were recorded on a Bruker AVANCE III with an autosampler (300.36 MHz ^{1}H-NMR and and 75.5 MHz-^{13}C-NMR). In all ^{1}H spectra the residual signal of the deuterated solvent was used as internal standard for the interpretation of the chemical shifts δ. Furthermore it was often necessary to record an additional HH-COSY or a ^{13}C-ATP NMR. The chemical shift δ is indicated in ppm (parts per million) and the coupling constant J in Hz (Hertz). For the signal multiplicities following abbreviations were used: s (singlet), d (doublet), t (triplet), q (quartet), p (pentett), m (multiplet), bs (broad singlet) and dd (doublet of doublet). The chemical shifts δ were indicated in ppm (parts per million) whereas the coupling constants J was indicated in Hz (hertz). The analysis of the received data was done with MestraNova NMR software.

6.3.2 Gas chromatography with mass selective detection (GC-MS)

The analytical gas chromatography was performed on an Agilent Technologies 7890A GC-system equipped with a polar Agilent Technologies J&W HP-5MS capillary column (30 m x 0.25 mm, 0.25 µm film, (5%-phenyl)-methylpolysiloxane) in split mode with He 5.0 as carrier gas. The injection was carried out through an Agilent Technologies 7683 series autosampler. Electron impact (EI, E = 70 eV) was used for ionisation with the mass analyser 5975C inert MSD with triple-axis detector. GC-experiments and measurements were performed at the Institute of Organic Chemistry at the University of Technology in Graz.

6.3.3 High Resolution Mass spectroscopy (HR-MS)

The determination of high resolution mass was performed in a positive reflector on a MALDI-TOF/TOF (Bruker Ultraflex Extreme). The mass spectra were analyzed with FlexAnalysis 3.0 software (Bruker Daltonics) by Dr. Robert Saf's group at the Institute for Chemistry and Technology of Materials, Graz, University of Technology.

A list of all used chemicals and solvents can be found in the appendix.

7. Experimental

7.1 Well-soluble Porphyrins via Lindsey condensation

Lindsey Synthesis

Target compound : (3aR,8aS)-2-(2-ethylhexyl)-3a,4,8,8a-tetrahydropyrrolo[3,4-f]isoindole-1,3(2H,6H)-dione

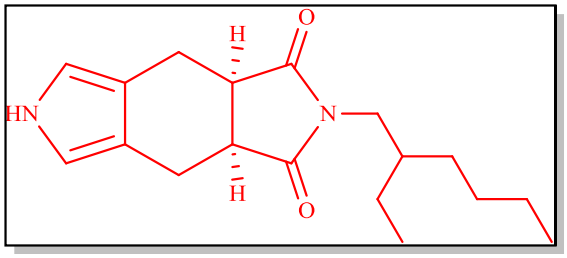

Figure 25 Target compound : (3aR,8aS)-2-(2-ethylhexyl)-3a,4,8,8a-tetrahydropyrrolo[3,4-f]isoindole-1,3(2H,6H)-dione

7.1.1 (3aR,7aS)-2-(2-ethylhexyl)-3a,4,7,7a-tetrahydro-1H-isoindole-1,3(2H)-dione

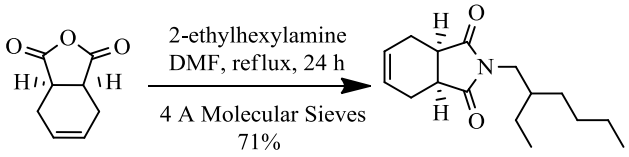

Figure 26 Reaction scheme for (3aR,7aS)-2-(2-ethylhexyl)-3a,4,7,7a-tetrahydro-1H-isoindole-1,3(2H)-dione

The reaction was conducted according to literature [4]. (3aR,7aS)-3a,4,7,7a-tetrahydroisobenzofuran-1,3-dione (35.00 g, 230.0 mmol, 1.00 eq) and 4 Å molecular sieves (50.00 g) were dissolved in 100 mL dry DMF, filled in a 2-neck-flask under argon counterflow followed by addition of 2-ethylhexylamine (32.70 g, 253.0 mmol, 1.10 eq), yielding a cloudy white solution. The reaction mixture was deoxygenated by bubbling N_2 through the solution for 10 minutes under vigorous stirring. The flask was closed and the reaction was refluxed for 24 hours under inert atmosphere. Reaction progress was controlled via TLC (CH:EE, 3:1). Finally DMF was removed using a rotary evaporator and the obtained product was distilled under reduced pressure (0.60 mbar, 180°C) to finally receive (3aR,7aS)-2-(2-ethylhexyl)-3a,4,7,7a-tetrahydro-1H-isoindole-1,3(2H)-dione as a yellow oil. NMR spectra can be seen in the appendix on the page 124.

Yield: Yellow oil, 43.22 g, 71%

R_f-value = 0.56 (silica, CH:EE, 3:1)

^{1}H NMR (300 MHz, Chloroform-d) δ 5.93-5.81 (m, 2H), 3.34 (d, J = 7.3 Hz, 2H), 3.10-2.98 (m, 2H), 2.60 (ddt, J = 14.0, 4.2, 2.2 Hz, 2H), 2.28-2.12 (m, 2H), 1.68 (p, J = 6.6 Hz, 1H), 1.33-1.09 (m, 8H), 0.85 (td, J = 7.1, 4.8 Hz, 6H).

7.1.2 (3aS,7aR)-5-chloro-2-(2-ethylhexyl)-6-(phenylthio)hexahydro-1H-isoindole-1,3(2H)-dione

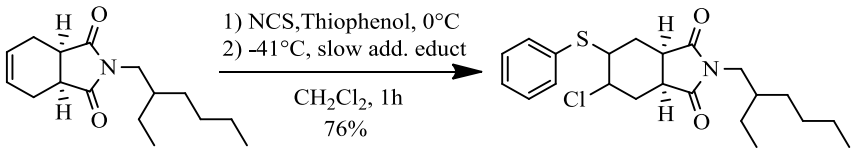

Figure 27 Reaction scheme for (3aS,7aR)-5-chloro-2-(2-ethylhexyl)-6-(phenylthio)hexahydro-1H-isoindole-1,3(2H)-dione

The reaction was conducted according to literature [4]. *N*-chlorosuccinimide (12.08 g, 90.5 mmol), 1.08 eq) was first completely dissolved (ultrasonic bath) in dry DCM (400 mL) under argon atmosphere in a 2-neck-flask. The flask was then immersed in an EtOH/liquid-N_2 bath at 0°C while N_2 was bubbled through the reaction mixture in argon counterflow for 30 minutes. Followed by dropwise addition (exothermic reaction) of thiophenol (9.969 g, 90.5 mmol, 1.08 eq, ρ=1.08 g/mL) dissolved in 12 mL dry DCM over 40 minutes, which gave rise to a color change from yellow to orange. The content was allowed to stir for 10 minutes at room temperature. Then the flask was cooled to -41°C with an EtOH/liquid-N_2-bath followed by slow addition (over 35 minutes) of (3aR,7aS)-2-(2-ethylhexyl)-3a,4,7,7a-tetrahydro-1H-isoindole-1,3(2H)-dione (22.00 g, 83.5 mmol, 1.00 eq) as a solution in 60 mL of dry DCM which was before deoxygenated by bubbling N_2 trough the solution for 10 minutes. The mixture was then brought to room temperature, by vigorous stirring for one hour before the by-product of succinimide was quickly filtered off. The solvent was removed under reduced pressure and the resulting orange oil was finally purified via column chromatography. The reaction progress was controlled via TLC (CH:EE, 4:1). NMR spectra can be seen in the appendix on the page 125.

Yield: Yellow oil, 25.75 g, 76 %

Rf: 0.48 (silica, CH : EE, 4:1)

^{1}H NMR (300 MHz, Chloroform-d) δ 7.48-7.39 (m, 2H), 7.39-7.28 (m, 3H), 4.21 (q, J = 4.4 Hz, 1H), 3.57 (q, J = 4.2 Hz, 1H), 3.48-3.32 (m, 2H), 3.10 (dt, J = 10.3, 7.7 Hz, 1H), 2.90 (td,

J = 8.1, 3.9 Hz, 1H), 2.58-2.49 (m, 2H), 2.34 (ddd, J = 13.8, 9.9, 4.1 Hz, 1H), 2.19 (ddd, J = 14.9, 7.6, 4.5 Hz, 1H), 1.76 (p, J = 6.3 Hz, 1H), 1.27 (tq, J = 11.8, 5.1, 4.1 Hz, 8H), 0.94-0.80 (m, 6H).

7.1.3 (3aS,7aR)-5-chloro-2-(2-ethylhexyl)-6-(phenylsulfonyl)hexahydro-1H-isoindole-1,3(2H)-dione

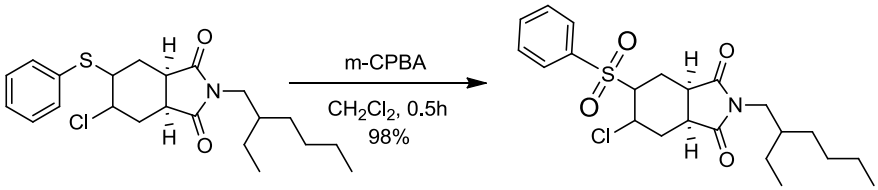

Figure 28 Reaction scheme for (3aS,7aR)-5-chloro-2-(2-ethylhexyl)-6-(phenylsulfonyl)hexahydro-1H-isoindole-1,3(2H)-dione

The reaction was conducted according to literature [4]. (3aS,7aR)-5-chloro-2-(2-ethylhexyl)-6-(phenylthio)hexahydro-1H-isoindole-1,3(2H)-dione (43.00 g, 105.4 mmol, 1.00 eq) was dissolved in 600 mL of dry DCM - while bubbling N_2 through the solution - in a 1 L round bottom flask. Then it was immersed into an EtOH/liquid-N_2 bath (0°C) and the solution was stirred vigorously for 30 minutes. The purified m-CPBA (47.61 g, 275.9 mmol, 2.62 eq) was added continuously every 15 seconds in small portions (exothermic reaction) with plastic spatulas over 30 minutes, resulting in a milky white hard to stir solution at the end of the addition. The reaction mixture was then brought to room temperature. After one hour vigorous stirring the by-product of m-chlorobenzoic acid was removed under vaccum filtration. The filtrate was washed with DCM (3 x 70 mL), whereas the combined organic solutions were concentrated under reduced pressure to an approximate volume of 450 mL and then washed with a 10% sodium carbonate solution (3 x 60 mL), followed by drying over Na_2SO_4 and the removal of the solvent under reduced pressure. The received yellow oil was directly used in the next reaction step without any further purification step. The reaction progress was controlled via TLC (CH:EE, 3:1). NMR spectra can be seen in the appendix on the page 125.

Yield: Yellow oil, 45.38 g, 98 %

R_f = 0.33 (silica, CH:EE, 3:1)

^{1}H NMR (300 MHz, Chloroform-d) δ 7.98-7.87 (m, 2H), 7.78-7.67 (m, 1H), 7.67-7.52 (m, 2H), 4.66 (dtd, J = 6.2, 4.3, 1.8 Hz, 1H), 3.55-3.44 (m, 1H), 3.44-3.29 (m, 3H), 3.09-2.97 (m, 1H), 2.60 (ddd, J = 15.1, 7.1, 4.5 Hz, 1H), 2.48-2.31 (m, 2H), 2.19 (ddd, J = 15.3, 9.6, 5.9 Hz, 1H), 1.72 (p, J = 6.1 Hz, 1H), 1.25 (dtd, J = 17.4, 9.7, 8.7, 4.3 Hz, 8H), 0.86 (dd, J = 7.9, 5.8 Hz, 6H).

7.1.4 (3aR,7aS)-2-(2-ethylhexyl)-5-(phenylsulfonyl)-3a,4,7,7a-tetrahydro-1H-isoindole-1,3(2H)-dione

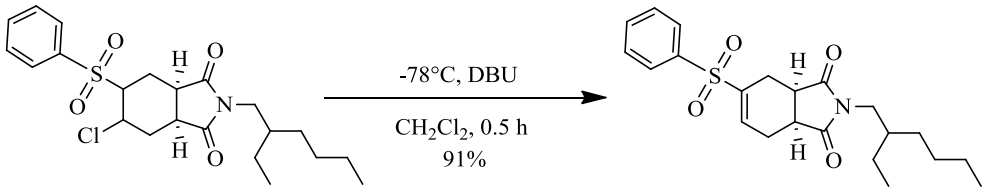

Figure 29 Reaction scheme for (3aR,7aS)-2-(2-ethylhexyl)-5-(phenylsulfonyl)-3a,4,7,7a-tetrahydro-1H-isoindole-1,3(2H)-dione

The reaction was conducted according to literature [4]. (3aS,7aR)-5-chloro-2-(2-ethylhexyl)-6-(phenylsulfonyl)hexahydro-1H-isoindole-1,3(2H)-dione (27.40 g, 62.3 mmol, 1.00eq) was dissolved in 250 mL of dry DCM in a 2-neck round bottom flask (yellow solution) and cooled down to -78°C in an EtOH/N_2 bath for 30 minutes while bubbling N_2 through the solution in argon counterflow. 1,8-Diaza-7-bicyclo[5.4.0]undecene (11.55 g, 75.9 mmol, 1.22 eq) was then added rapidly, after degassing the solution for 1 minute, via an addition funnel, which led to a dark brown-green solution. The flask was then immersed into an EtOH/liquid-N_2 bath (0°C), where the reaction mixture was allowed to stir for 10 minutes. Finally the mixture was washed with 5% HCl (3 x 60 mL) and dried over Na_2SO_4. The solvent was removed under reduced pressure to obtain a yellow oil. NMR spectra can be seen in the appendix on the page 126.

Yield: Yellow oil, 22.93 g, 91 %

1H NMR (300 MHz, Chloroform-d) δ 7.80 (dd, J = 7.4, 1.8 Hz, 2H), 7.67-7.58 (m, 1H), 7.54 (dd, J = 8.0, 1.9 Hz, 2H), 7.15 (dt, J = 6.3, 3.1 Hz, 1H), 3.24-2.98 (m, 4H), 2.84 (ddt, J = 19.1, 13.4, 2.5 Hz, 2H), 2.55-2.38 (m, 2H), 1.52 (ddd, J = 12.6, 7.9, 5.0 Hz, 1H), 1.32-1.02 (m, 8H), 0.84 (dtt, J = 11.4, 7.5, 3.9 Hz, 6H).

7.1.5 (4aS,7aR)-ethyl-6-(2-ethylhexyl)-5,7-dioxo-2,4,4a,5,6,7,7a,8-octahydropyrrolo[3,4-f]isoindole-1-carboxylate

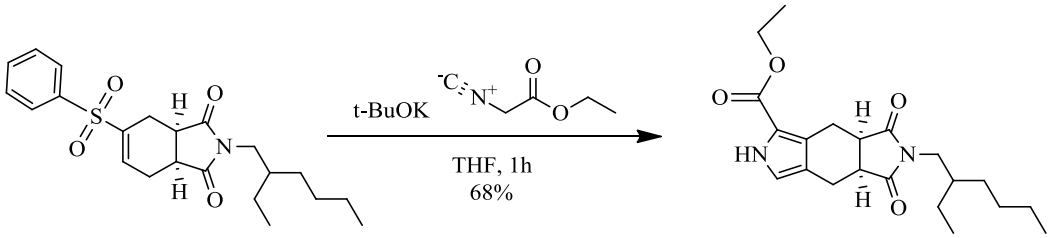

Figure 30 Reaction scheme for (4aS,7aR)-ethyl-6-(2-ethylhexyl)-5,7-dioxo-2,4,4a,5,6,7,7a,8-octahydropyrrolo[3,4-f]isoindole-1-carboxylate

The reaction was conducted according to literature [4]. Potassium t-butoxide (11.69 g, 104.2 mmol, 1.88 eq) was first dissolved in dry THF (1.2 L) in a 2-neck round bottom flask (vigorous stirring) under inert atmosphere. The solution was deoxygenated for ten minutes, producing a yellow solution. Afterwards the flask was subsequently immersed in an EtOH/liquid-N_2 bath (0°C) for 30 minutes and ethyl 2-isocyanoacetate (12.47 g, 110.2 mmol, 1.99 eq, ρ=1.035 g/mL) was added rapidly, yielding a bright brown/red transparent solution, which was furthermore stirred for 45 minutes at 0°C. (3aR,7aS)-2-(2-ethylhexyl)-5-(phenylsulfonyl)-3a,4,7,7a-tetrahydro-1H-isoindole-1,3(2H)-dione (22.35 g, 55.4 mmol, 1.00 eq) was dissolved in 100 mL dry THF and added dropwise over 40 minutes to the previous solution with the aid of an addition funnel. Then the reaction mixture was brought to room temperature and allowed to stir for one hour while the reaction progress was monitored via TLC (CH:EE, 3:1). Finally the solvent was removed under reduced pressure. The residue was re-dissolved in DCM (200 mL), subsequently washed with brine (3 x 50 mL) and the combined organic fractions were dried over sodium sulfate. The solvent was removed under reduced pressure to afford orange oil, which was further purified via flash chromatography. NMR spectra can be seen in the appendix on the page 126.

Yield: Yellow oil, 14.11 g, 68 %

R_f = 0.22 (silica, CH:EE, 3:1)

^{1}H NMR (300 MHz, Chloroform-d) δ 8.99 (s, 1H), 6.68 (d, J = 2.8 Hz, 1H), 4.36-4.21 (m, 2H), 3.81-3.70 (m, 1H), 3.27-3.09 (m, 5H), 2.84-2.62 (m, 2H), 1.44 (d, J = 10.5 Hz, 1H), 1.35 (t, J = 7.1 Hz, 3H), 1.14 (dtd, J = 10.9, 6.9, 6.4, 3.3 Hz, 3H), 0.84 (dtt, J = 12.9, 9.2, 4.3 Hz, 6H), 0.68 (dt, J = 11.2, 7.3 Hz, 3H).

*** m-CPBA purification ***

The reaction was conducted according to literature [4]. M-CPBA was purified, because it was commercially received as 70-75% mixture with water and m-chlorobenzoic acid. M-CPBA (90.00 g, 521.5 mmol) was dissolved in 450 mL DCM (5 mL/g of mixture) and washed (3 x 150 mL) with 500 mL pH 7.5 buffer (205 mL 0.1 M NaOH + 125 mL 0.2 M KH_2PO_4 diluted up to 500 mL). The resulting organic fractions were dried over sodium sulfate and evaporated at 30 °C under reduced pressure to give pure m-CPBA.
Like all peroxides, dry m-CPBA has a potential of spontaneous decomposition, therefore the removal of the solvent was done with a rotary evaporator placed in a hood. To avoid contamination with heavy metals only spatulas made of plastic were used in this experiment.

7.2 Well-soluble porphyrins via Template synthesis

Target compound: Platinum (II) meso-tetra(4-fluorophenyl)tetra(4,5-bis((2-ethylhexyl)sulfonyl)benzoporphyrin (Pt-TPTBPF$_4$bEHS$_4$)

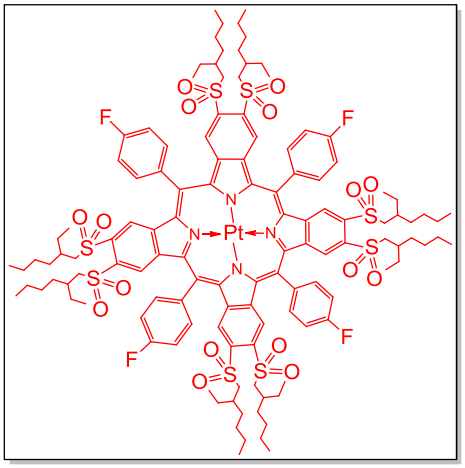

Figure 31 Target compound: Pt-TPTBPF$_4$bEHS$_4$

7.2.1 4,5-bis((2-ethylhexyl)thio)phthalonitrile

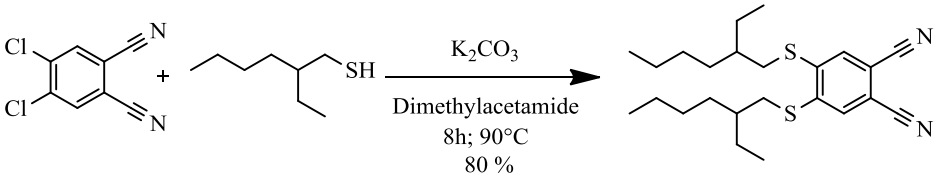

Figure 32 Reaction scheme for 4,5-bis((2-ethylhexyl)thio)phthalonitrile

The reaction was conducted according to literature [117]. 4,5-dichlorophthalonitrile (9.00 g, 45.7 mmol, 1.00 eq) was first dissolved in 100 mL dimethylacetamide (DMA) in a 2-neck round bottom flask and the solution was degassed in argon counterflow for 10 minutes. Then grinded, dry K_2CO_3 (18.00 g, 130.2 mmol, 2.85 eq) was added and the solution was again degassed for further 10 minutes. Then 2-ethylhexane-1-thiol (14.71 g, 100.5 mmol, 2.20 eq, ρ=0.8430 g/mL) was added and the resulting reaction mixture was heated to 90°C for 8 hours (vigorous stirring). Afterwards the reaction mixture was poured onto dest. H_2O and extracted with DCM (3 times) The organic fraction was washed with dest. H_2O (6 x 100 mL) to remove dimethylacetamide before the solvent was finally evaporated in vacuo to afford the product as yellow oil. NMR spectra can be seen in the appendix on the page 127.

Yield: Yellow oil, 14.85 g, 78 %

R_f = 0.80 (silica, CH : EE, 3:1)

^{1}H NMR (300 MHz, Chloroform-*d*) δ 7.41 (s, 2H), 2.97 (d, *J* = 6.2 Hz, 4H), 1.71 (p, *J* = 6.2 Hz, 2H), 1.58-1.40 (m, 8H), 1.36-1.26 (m, 8H), 0.94-0.84 (m, 12H).

7.2.2 4,5-bis((2-ethylhexyl)sulfonyl)phthalonitrile

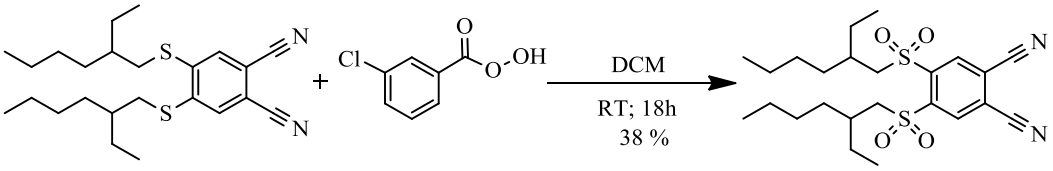

Figure 33 Reaction scheme for 4,5-bis((2-ethylhexyl)sulfonyl)phthalonitrile

The reaction was conducted according to literature [117]. 4,5-bis((2-ethylhexyl)thio)phthalonitrile (1.14 g, 2.7 mmol, 1.00eq) was dissolved in 25 mL of dry DCM at room temperature in a 2-neck round bottom flask, while bubbling N_2 through the solution in argon counterflow for 10 minutes. M-CPBA (3.00 g, 17.4 mmol, 6.44 eq, 70-75 % pure) was added with a plastic spatulas to the solution, which was again degassed for further 10 minutes, resulting in a color change of the reaction mixture from red to bright orange. It was kept stirring at room temperature for 19 hours. Then the reaction mixture was quenched with a saturated $NaHCO_3$ (40 mL) and extracted with Et_2O (3 x 60 mL). The reaction solution was finally dried over sodium sulfate and the solvent was removed under reduced pressure. The crude product was purified via column chromatography (silica, CH:EE, 5:1) to yield 4,5-bis((2-ethylhexyl)sulfonyl)phthalonitrile as yellow oil. NMR spectra can be seen in the appendix on the page 127.

Yield: Yellow oil, 0.570 g, 44 %

R_f = 0.70 (silica, CH : EE, 3:1)

^{1}H NMR (300 MHz, Chloroform-*d*) δ 8.69 (s, 2H), 3.65-3.47 (m, 4H), 2.16 (pd, *J* = 6.2, 1.8 Hz, 2H), 1.50 (ddd, *J* = 19.3, 10.5, 4.3 Hz, 8H), 1.27 (dq, *J* = 6.8, 3.9, 3.4 Hz, 8H), 0.89 (t, *J* = 7.2 Hz, 12H).

7.2.3 Zinc (II) -meso-tetra(4-fluorophenyl)tetra(4,5-bis((2-ethylhexyl)thio)benzo-porphyrin(Zn-TPTBPF$_4$bEHT$_4$)

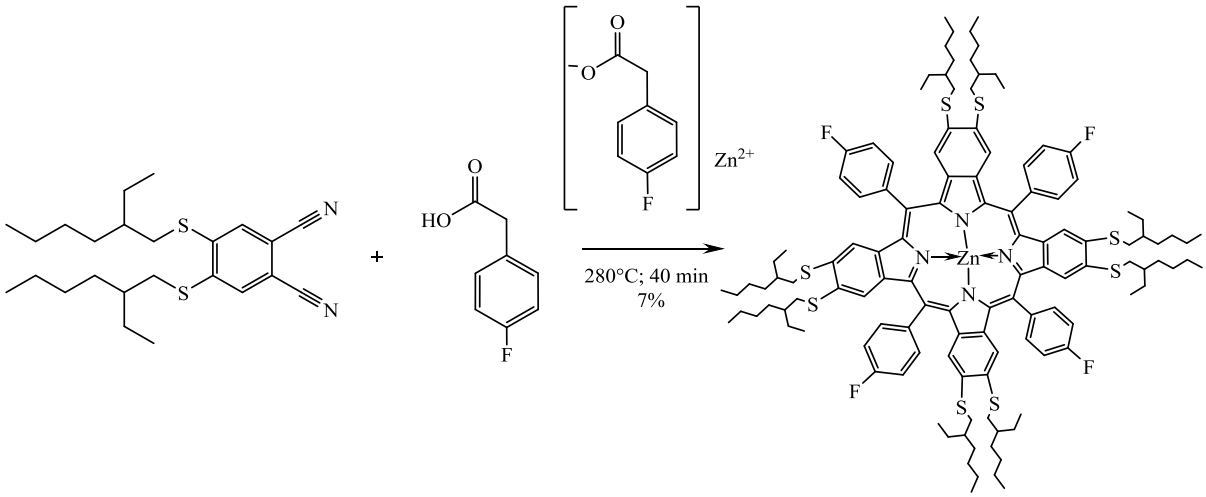

Figure 34 Reaction scheme for Zn-TPTBPF$_4$bEHT$_4$

4,5-bis((2-ethylhexyl)thio)phthalonitrile (12.94 g, 31.04 mmol, 4.00 eq), 2-(4-fluorophenyl)acetic acid (11.96 g, 77.61 mmol, 10.00 eq), zinc-4-fluorophenylacetate (2.90, 7.761 mmol, 1.00 eq) were mixed together and homogenized with a ceramic pestle in a mortar. Approximately 700 mg of the mixture were weighed in each 4 mL supelco-vial equipped with a stirring bar. The vials were sealed with a metal cap and put on a 160°C heating block and then heated up to 280°C. After reaching the 280°C the stirrer was started and the reaction mixture was kept at this temperature for 40 minutes. Then the vials were removed from the heating source and cooled down. Afterwards the vials were smashed with a hammer and the reaction mixture was dissolved in 800 mL acetone on the ultrasonic bath for ten minutes. The pieces of glass were separated through vacuum filtration and the solvent was removed under reduced pressure. The residue was re-dissolved in 800 mL cyclohexane/n-hexane (2:1) and washed with methanol (6 x 300 mL). The crude product was purified twice via column chromatography (silica, CH:DCM, 2:1). The product containing fractions were determined via absorption spectra and dried in the vacuum oven at 60°C. Mass spectrum can be seen in the appendix on page 131.

Yield: dark green solid, 0.92 g, 6%

Molar absorption coefficient, $\lambda_{max}/\varepsilon$ (nm, $M^{-1}cm^{-1}$) in toluene: 478/ 346500; 678/ 115200

λ_{max} (nm) in acetone: 479; 675

MALDI: m/z: [M+]; $C_{124}H_{160}F_4N_4S_8Zn$, calc. for 2103.966; found: 2103.964

7.2.4 Meso-tetra(4-fluorophenyl)tetra(4,5-bis((2-ethylhexyl)thio)benzoporphyrin (H_2-$PTBPF_4bEHT_4$)

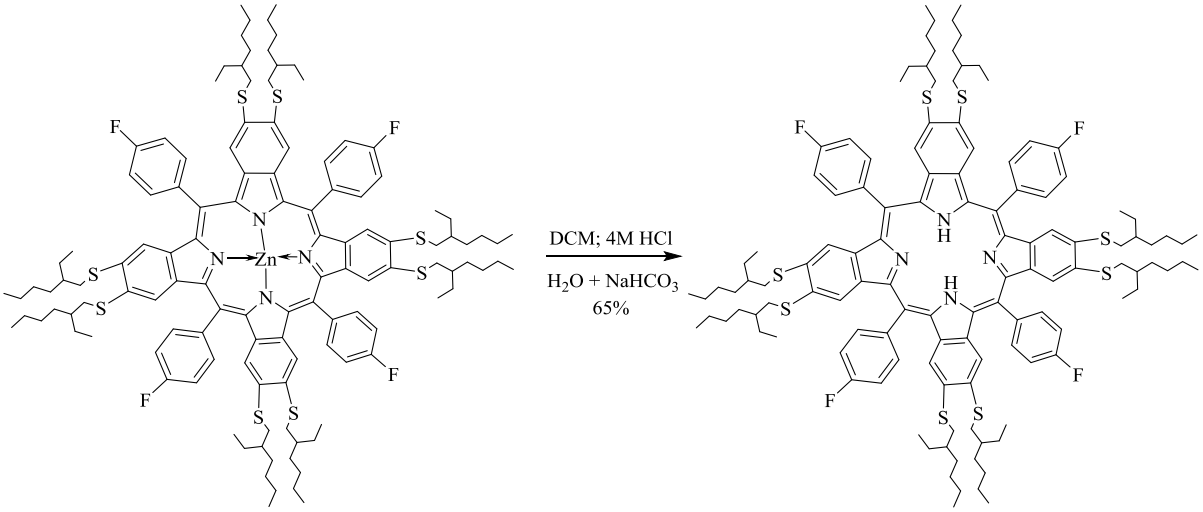

Figure 35 Reaction scheme for H_2-$TPTBPF_4bEHT_4$

Zn-$TPTBPF_4bEHT_4$ (20 mg, 9.5 µmol, 1.00 eq) was dissolved in 20 mL DCM and 5 mL of 4 M HCl were slowly added. The resulting protonated ligand could be determined via absorption spectra in acetone (λ_{max}: 524 nm). The reaction mixture was then extracted with dest. H_2O (2 x 25 mL) and with saturated $NaHCO_3$-solution (2 x 20 mL) until only free ligand was observed in the absorption spectra. Finally the organic layer was once more washed with dest. H_2O (20 mL), dried over Na_2SO_4 and the solvent was removed under reduced pressure. Mass spectrum can be seen in the appendix on page 132.

Yield: dark green solid, 12.7 mg, 65%

Molar absorption coefficient, $\lambda_{max}/\varepsilon$ (nm, $M^{-1}cm^{-1}$) in toluene: 475/ 155200

λ_{max} (nm) in acetone: 471

MALDI: m/z: [M+]; $C_{124}H_{162}F_4N_4S_8Zn$, calc. for 2040.053; found: 2040.038

7.2.5 Zn (II) -meso-tetra(4-fluorophenyl)tetra(4,5-bis((2-ethylhexyl)sulfonyl)benzo-porphyrin (Zn-TPTBPF$_4$bEHS$_4$)

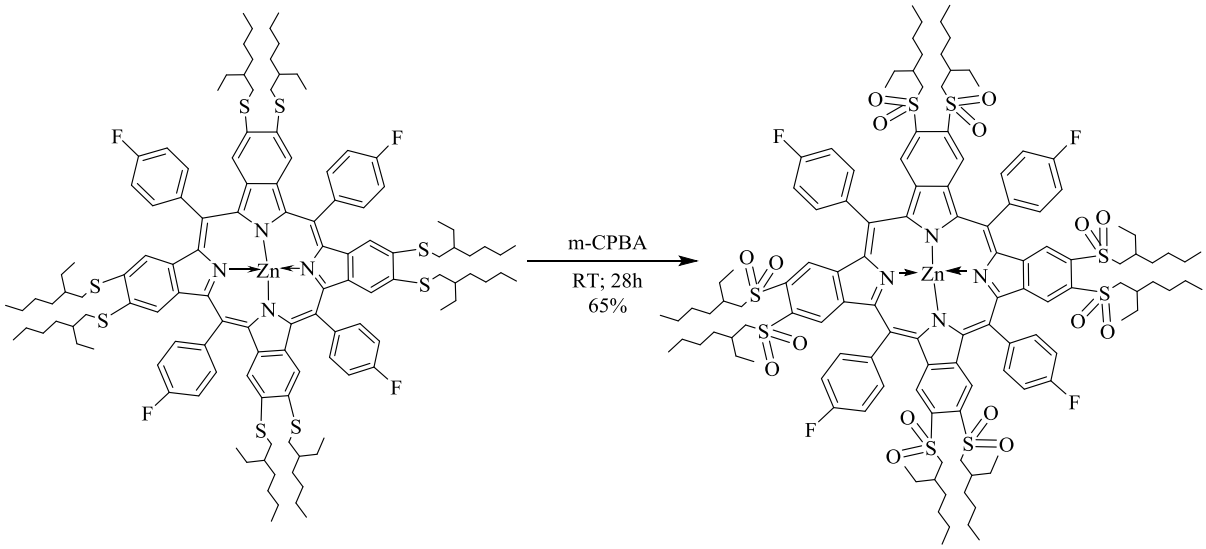

Figure 36Reaction scheme for Zn-TPTBPF$_4$bEHS$_4$

Zn-TPTBPF$_4$bEHT$_4$ (10 mg, 4.8 µmol, 1.00 eq) was dissolved in 1.5 mL DCM in a 2-neck round bottom flask. Then m-CPBA (16.40 mg, 95.0 µmol, 20.00 eq) was added slowly with plastic spatulas to the stirring solution. The reaction progress was monitored via absorption spectra (solvent: acetone). After complete conversion the reaction mixture was quenched with saturated $NaHCO_3$, extracted with DCM (3 x 25 mL) and dried over Na_2SO_4. The solvent was removed under reduced pressure. The crude product was finally purified via column chromatography (silica, CH:EE, 5:1) to yield Zn-TPTBPF$_4$bEHS$_4$ as dark green solid. The product containing fractions were determined via absorption spectra (solvent: acetone). Mass spectrum can be seen in the appendix on page 133.

Yield: dark green solid, 7.30 mg, 65%

λ_{max}/relative intensity (nm): 489/ 1.00; 629/ 0.0869; 673/ 0.1683

λ_{max} (nm) in acetone: 490; 675

7.2.6 Zn (II) -meso-tetra(4-fluorophenyl)tetra(4,5-bis((2-ethylhexyl)sulfonyl)benzo-porphyrin (Zn-TPTBPF$_4$bEHS$_4$)

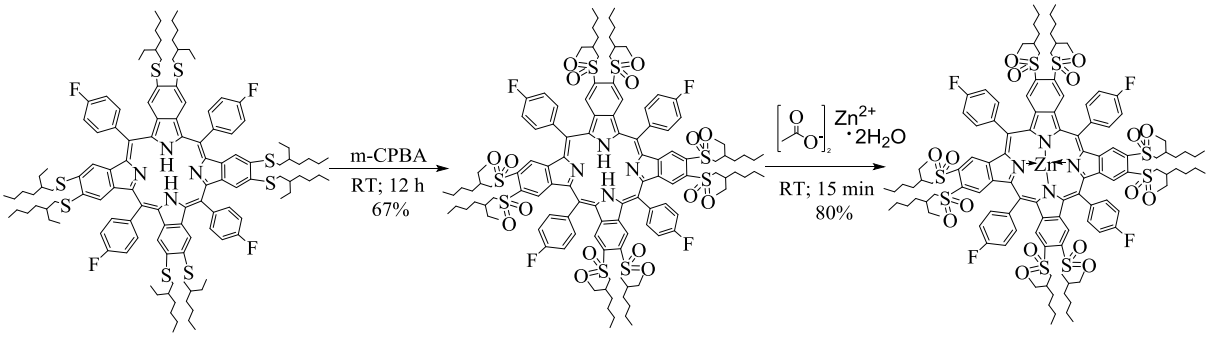

Figure 37 Reaction scheme for Zn-TPTBPF$_4$bEHS$_4$ via oxidation of the ligand

H_2-TPTBPF$_4$bEHT$_4$ (8.0 mg, 3.92 µmol, 1.00 eq) was dissolved in 1.2 mL DCM in a 2-neck round bottom flask and m-CPBA (13.5 mg, 78.4 µmol, 20.00 eq) was added slowly with plastic spatulas to the stirring solution. The reaction progress was monitored via absorption spectra (solvent: acetone). After complete conversion, the reaction mixture was quenched with saturated $NaHCO_3$-solution, extracted with DCM (3 x 60 mL) and dried over Na_2SO_4. The solvent was removed under reduced pressure. Finally the crude product was purified via column chromatography (silica, CH:EE, 5:1) to yield H_2-TPTBPF$_4$bEHS$_4$ as dark green solid. Afterwards the reaction product was re-dissolved in THF and zinc acetate dihydrate (800 µg, 3.92 µmol, 1.50 eq) was added. The reaction progress was monitored via absorption spectra (solvent: acetone). After complete conversion the solvent was removed in vacuo and the residue was purified via column chromatography (silica, CH:EE, 5:1) to yield Zn-TPTBPF$_4$bEHS$_4$ as dark green solid. The product containing fractions were determined via absorption spectra (solvent: acetone). Mass spectrum can be seen in the appendix on page 133.

Yield: dark green solid, 4.90 mg, overall 53%

λ_{max}/relative intensity (nm): 489/ 1.00; 629/ 0.0869; 673/ 0.1683

λ_{max} (nm) in acetone: 490; 675

MALDI: m/z: [M+]; $C_{124}H_{160}F_4N_4O_{16}S_8Zn$, calc. for 2358.884; found: 2358.905

7.3 Bridging of Porphyrins

Target compound: Platinum (II) meso-tetra(4-tolyl)tetrabenzoporphyrin (Pt-TTolTBP)

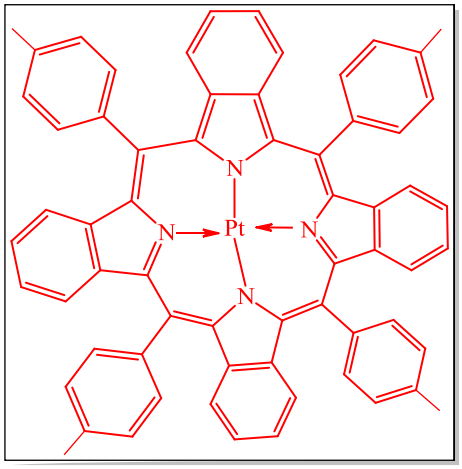

Figure 38 Target compound: Pt-TTolTBP

7.3.1 Zinc (II) meso-tetra(4-tolyl)tetrabenzoporphyrin (Zn-TTolTBP)

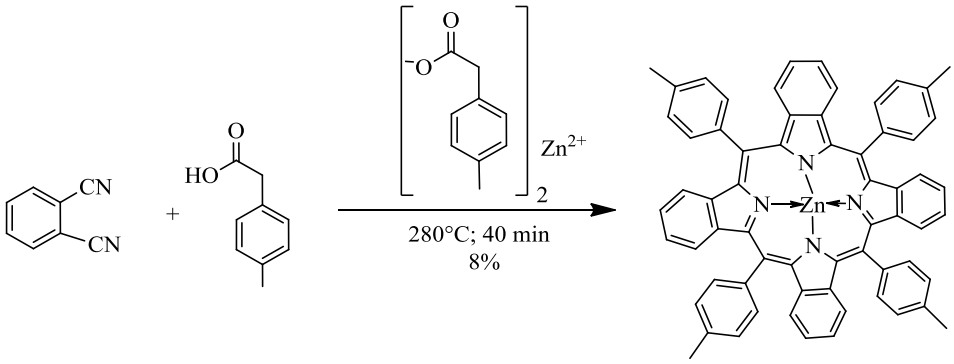

Figure 39 Reaction scheme for Zn-TTolTBP

Phthalonitrile (9.11 g, 71.10 mmol, 4.00 eq), 2-(p-tolyl)acetic acid (13.35 g, 88.87 mmol, 5.00 eq), zinc-4-tolylacetate (6.50 g, 17.77 mmol, 1.00 eq) were mixed together and homogenized with a ceramic pestle in a mortar and approximately 700 mg of the mixture were weighed in each 4 mL supelco-vial and equipped with a stirring bar. After sealing the vials with a metal cap they were placed on a preheated heating block at 160 °C and then further heated up to 280°C. After reaching 280°C the reaction mixture was stirred for 40 minutes. Afterwards the vials were removed from the heating block and cooled down. The vials were then smashed with a hammer, the oily residue was dissolved in 800 mL acetone and put on the ultrasonic bath for ten minutes. The pieces of glass were separated through vacuum filtration and the

solution was concentrated under reduced pressure to an approximate volume of 300 mL. The concentrated mixture was then added dropwise to 1.50 L ethanol/water (1:1 + 20 mL saturated $NaHCO_3$ + 20 mL brine) solution, producing a dark-green precipitate, which was then filtered off via vacuo filtration. Afterwards the residue was washed with an ethanol/water solution (1:2; 3 x 200 mL) and dried in the vaccum oven at 60°C. The crude product was purified via column chromatography first using silica (CH:EE, 4:1), then on ALOX (CH:EE, 6:1) as stationary phase. The product containing fractions were determined via absorption spectra and the product was finally dried in the vacuum oven at 60°C. 15 mg of Zn-TTolTBP were washed three times with cyclohexane on the ultrasonic bath for 10 minutes. The insoluble dark-green sediment was obtained via centrifugation after the removal of the light-green-brownish supernatant. NMR and mass spectra can be seen in the appendix on the pages 128 and 134.

Yield: dark green solid, 1.30 g, 8%

Molar absorption coefficient, $\lambda_{max}/\varepsilon$ (nm, $M^{-1}cm^{-1}$) in toluene: 463/ 185000; 653/ 44700

λ_{max} (nm) in acetone: 462; 651

^{1}H NMR (300 MHz, Benzene-d6) δ 8.26 (d, J = 7.8 Hz, 8H), 7.68 (dt, J = 6.5, 3.3 Hz, 8H), 7.48 (d, J = 7.6 Hz, 8H), 7.30 (dt, J = 6.3, 3.6 Hz, 8H), 2.47 (s, 12H).

MALDI: m/z: [M+]; $C_{64}H_{44}N_4Zn$, calc. for 932.2858; found: 932.2932

7.3.2 Bridged-Zinc (II) meso-tetra(4-tolyl)tetrabenzoporphyrin (bridged-Zn-TTolTBP)

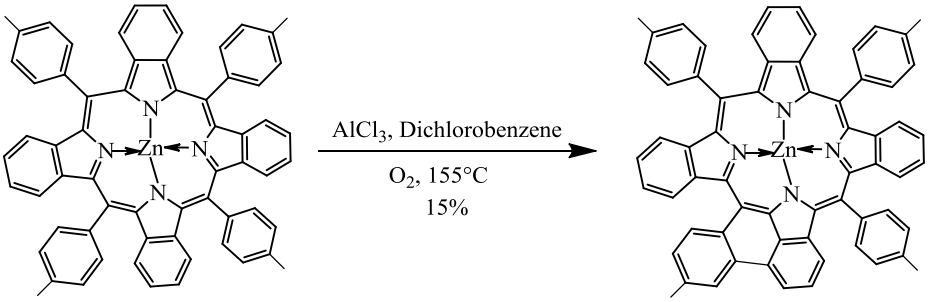

Figure 40 Reaction scheme for bridged-Zn-TTolTBP

Zn-TTolTBP (12.00 mg, 12.8 µmol, 1.00 eq) was dissolved in 12 mL dichlorobenzene for 5 minutes on the ultrasonic bath in a closed 25 mL round bottom flask. Then aluminum trichloride (222.6 mg, 1.669 mmol, 130 eq) was added to the solution and the reaction mixture was again sonicated again for 10 minutes, resulting in a color change from dark-green to a brownish-red solution. Afterwards the reaction mixture was quickly heated to 155°C, while moderate O_2 bubbling through the solution. The reaction progress was monitored via absorption spectra (solvent: DCM), the samples taken from the reaction mixture were neutralized with 2 drops of triethylamine, visible through a color change from dark-brown to bright green. After completion the reaction mixture was allowed to cool to room temperature while constant O_2 bubbling through the solution. During the work-up the reaction mixture was neutralized with a DCM:TEA solution (40:1). The precipitate was separated via centrifugation, and washed with DCM, whereas the diluted reaction mixture was washed with dest. H_2O (3 x 100 mL) and dried over sodium sulfate, before the solvent was removed under reduced pressure. Finally the resulting green solid was purified using column chromatography (silica, cond. CH, CH:EE, 3:1), yielding a green solid. The product was then re-dissolved in chloroform (10 mL), heated to 30°C and the produced complex was re-metalized through the addition of zinc acetate (3.00 mg, 16.4 µmol, 1.28 eq) under continuous stirring for 10 minutes. The solvent was removed in vacuo and the resulting green solid was purified via column chromatography (ALOX, DCM:EE, 7:1) yielding a dark-green solid. The product containing fractions were determined via absorption spectra. Mass spectrum can be seen in the appendix on page 135.

Yield: green solid, 1.8mg, 15%

λ_{max}/relative intensity (nm): 491/ 1.00; 641/ 0.0684; 697/ 0.1384

λ_{max} (nm) in acetone: 491; 697

MALDI: m/z: [M+]; $C_{64}H_{42}N_4Zn$, calc. for 930.2701; found: 930.2783

7.3.3 Meso-tetra(4-tolyl)tetrabenzoporphyrin (H_2-TTolTBP)

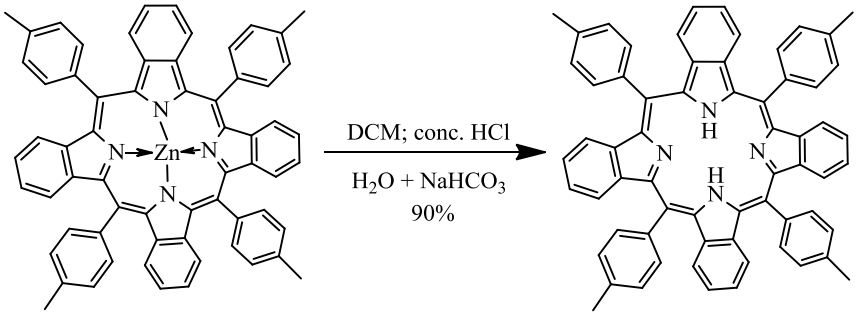

Figure 41 Reaction scheme for H_2-TTolTBP

Zn-TTolTBP (0.50 g, 535.1 µmol, 1.00 eq) was dissolved in 500 mL DCM and 50 mL of conc. HCl were slowly added. The resulting protonated ligand could be determined via absorption spectra in acetone (λ_{max}: 503 nm). The reaction mixture was then extracted with dest H_2O (2 x 300 mL) and with saturated $NaHCO_3$-solution (2 x 200 mL) until only free ligand was observed in the absorption spectra. Finally the organic layer was once more washed with dest H_2O (200 mL), dried over Na_2SO_4 and the solvent was removed under reduced pressure.

Yield: dark green solid, 0.42 g, 90%

Molar absorption coefficient, $\lambda_{max}/\varepsilon$ (nm, $M^{-1}cm^{-1}$) in toluene: 468/ 115800

λ_{max} (nm) in acetone: 462

7.3.4 Platinum (II) meso-tetra(4-tolyl)tetrabenzoporphyrin (Pt-TTolTBP)

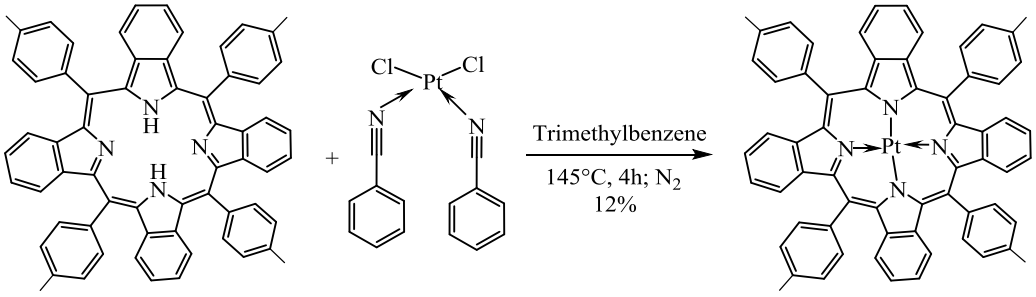

Figure 42 Reaction scheme for Pt-TTolTBP

H_2-TTolTBP (200.0 mg, 229.6 µmol, 1.00 eq) was dissolved in TMB (200 mL) in a 2-neck-round bottom flask and heated to 145°C, while bubbling N_2 through the reaction mixture. Then $Pt(C_6H_5CN)_2Cl_2$ (163.0 mg, 344.4 µmol, 1.50 eq) was added slowly in small portions (5 x 0.3 eq pre-dissolved in hot TMB) from a pre-heated addition funnel (100°C) over a period of 4 hours. The reaction progress was monitored via absorption spectra (solvent: acetone). After completion the reaction mixture was cooled down to room temperature, the by-products were removed via centrifugation and the solvent was removed under reduced pressure at 80 °C. The crude product was further purified via column chromatography (silica, CH:DCM, 2:1). The product containing fractions were determined via absorption spectra and the resulting viscous product was transferred into a 2-neck round bottom flask with a cold finger. Purification was carried out by heating to 350°C under high vacuo to remove side products, yielding a dark green solid. 15 mg of Pt-TTolTBP were washed with cyclohexane and sonicated for 10 minutes. This process was repeated three times. The insoluble dark-turquoise sediment could be received after the removal of the light-turquoise supernatant via centrifugation. NMR and mass spectra can be seen in the appendix on the pages 128 and 136.

Yield: dark green solid, 29.00mg, 12%

Molar absorption coefficient, $\lambda_{max}/\varepsilon$ (nm, $M^{-1}cm^{-1}$) in toluene: 433/ 146800; 615/ 94900

λ_{max} (nm) in acetone: 430; 612

^{1}H NMR (300 MHz, Chloroform-d) δ 8.11 (t, J = 6.7 Hz, 8H), 7.66 (d, J = 7.9 Hz, 8H), 7.21 (d, J = 3.4 Hz, 8H), 7.14 (dt, J = 6.4, 3.3 Hz, 7H), 2.79 (s, 12H).

MALDI: m/z: [M+]; $C_{64}H_{44}N_4Pt$, calc. for 1064.3235; found: 1064.3148

Target compound: Platinum (II) meso-tetraphenyltetra(di-methyl)benzoporphyrin (Pt-TPTBPdM$_4$)

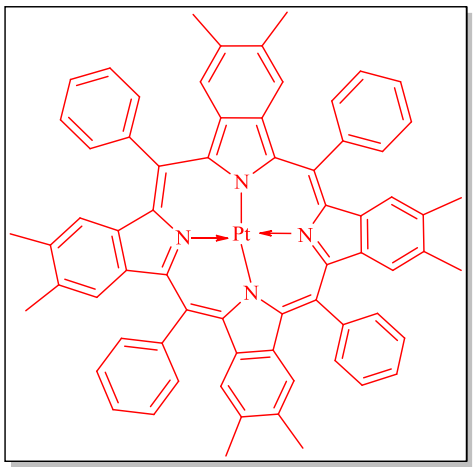

Figure 43 Reaction scheme for Pt-TPTBPdM$_4$

7.3.5 1,2-dibromo-4,5-dimethylbenzene

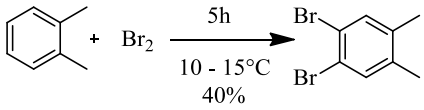

Figure 44 Reaction scheme for 1,2-dibromo-4,5-dimethylbenzene

The reaction was conducted according to literature [118]. Molecular bromine (132.56 g, 829.5 mmol, 2.00 eq, ρ=3.119 g/mL) was added to o-xylene (43.95 g, 414.0 mmol, 1.00 eq, ρ=0.8790 g/mL) over 5 hours (4 mL every 30 minutes) in a flask immersed in an ice/water bath (12°C). Afterwards the brown colored reaction mixture was stirred for 4 more hours at 15°C before diluting with 50 mL DCM and quenching with a $NaHSO_3$-solution (37.5% solution in water). The organic layer was washed with dest. H_2O (3 x 60 mL) and the solvent was removed under vacuo. The yellow residue was recrystallized from methanol, yielding white crystals. The reaction progress was controlled via GC-MS. NMR spectra can be seen in the appendix on the page 129.

Yield: White crystals, 7.50 g, 7 %; conversion detected via gc-ms: 40 %

GC-MS: retention time = 5.70; found mass = 263.9 g/mol

^{1}H NMR (300 MHz, Chloroform-*d*) δ 7.37 (s, 2H), 2.19 (s, 6H)

7.3.6 1,2-diethynyl-4,5-dimethylbenzene

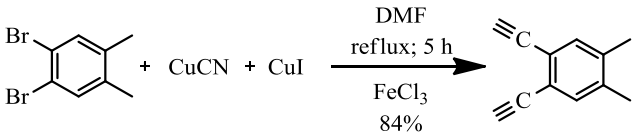

Figure 45 Reaction scheme for 1,2-diethynyl-4,5-dimethylbenzene

The reaction was conducted according to literature [118]. A mixture of 1,2-dibromo-4,5-dimethylbenzene (0.50 g, 1.894 mmol, 1.00 eq), copper(I)cyanide (967.0 mg, 10.80 mmol, 5.70 eq) and copper(I) iodide (36.10 mg, 189.4 µmol, 0.10 eq) was dissolved in dry DMF (7 mL) in a Schlenk-flask, producing a milky green solution. The reaction mixture was then refluxed for 5 hours. After cooling down to room temperature, the dark-green reaction mixture was poured into a stirred iron(III) chloride solution (1.751 g, 10.80 mmol, 5.70 eq) in 100 mL water. The resulting precipitate was filtered of via vacuum filtration, washed with dest. H_2O (5 x 50 mL) and extracted with DCM (150 mL). The combined organic phases were again washed with dest. H_2O (3 x 50 mL) to remove DMF, dried over Na_2SO_4 and finally the solvent was removed under reduced pressure, yielding a light yellow solid. The reaction progress was controlled via TLC (CH:EE, 5:1). NMR spectra can be seen in the appendix on the page 129.

Yield: Yellow solid, 248.5 mg, 84%

R_f = 0.28 (silica, CH:EE, 5:1)

^{1}H NMR (300 MHz, Chloroform-*d*) δ 7.55 (s, 2H), 2.38 (s, 6H).

7.3.7 Zinc (II) meso-tetraphenyltetra(di-methyl)benzoporphyrin (Zn-TPTBPdM$_4$)

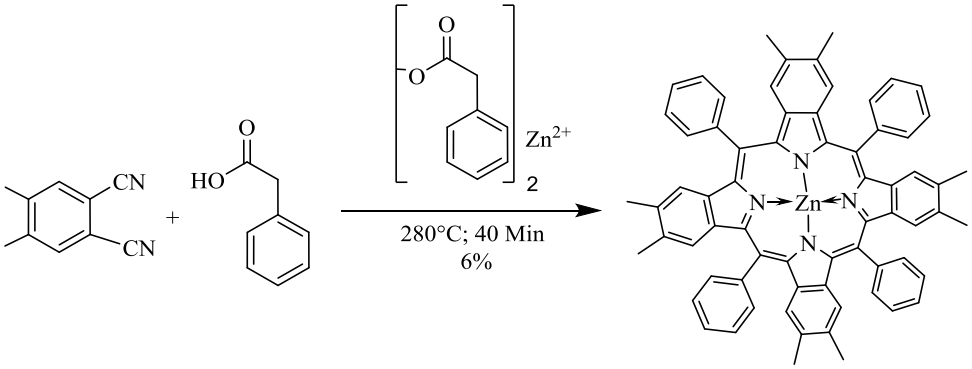

Figure 46Reaction scheme for Zn-TPTBPdM$_4$

4,5-dimethylphthalonitrile (1.110 g, 7.108 mmol, 4.00 eq), 2-phenylacetic acid (1.452 g, 10.66 mmol, 6.00 eq), phenylzincacetate (600.0 mg, 1.777 mmol, 1.00 eq) were mixed together and homogenized with a ceramic pestle in a mortar and approximately 700 mg of the reaction mixture were weighed in each 2.5 mL supelco-vial equipped with a stirring bar. After sealing the vials with a metal cap they were placed on a preheated heating block at 250°C under stirring and heated up to 280°C, where the reaction mixture was kept for 40 minutes. Afterwards the vials were cooled down to room temperature and then smashed with a hammer. The reaction mixture was dissolved in 200 mL acetone and put on the ultrasonic bath for ten minutes. The bits of glass were separated through vacuum filtration and the solution was concentrated under reduced pressure to an approximate volume of 60 mL. The concentrated reaction mixture was added dropwise to a 400 mL solution of ethanol/water (1:1 + 10 mL saturated $NaHCO_3$ + 10 mL brine), producing a dark-green precipitate, which was then filtered off under vacuum. Afterwards the residue was washed with an ethanol/water solution (1:2; 3 x 50 mL) and dried in the vaccum oven at 60°C.The crude product was purified via column chromatography first on silica (CH:EE, 10:1) and then on ALOX (CH:EE, 12:1) as stationary phase. The product containing fractions were determined via absorption spectra and the product was finally dried in the vacuum oven at 60°C. 15 mg of Zn-TPTBPdM$_4$ was then washed with cyclohexane on the ultrasonic bath for 10 minutes. This process was repeated three times. The insoluble dark-green was obtained after the removal of the light-green-brownish supernatant via centrifugation. NMR and mass spectra can be seen in the appendix on the pages 130 and 137.

Yield: dark green solid, 105.6mg, 6%

Molar absorption coefficient, $\lambda_{max}/\varepsilon$ (nm, $M^{-1}cm^{-1}$) in toluene: 457/ 219400; 654/ 71400

λ_{max} (nm) in acetone: 456; 651

^{1}H NMR (300 MHz, Benzene-d6) δ 8.41 – 8.28 (m, 8H), 7.78 – 7.59 (m, 12H), 7.31 (s, 8H), 2.27 (s, 24H).

MALDI: m/z: [M+]; $C_{68}H_{52}N_4Zn$, calc. for 988.3483; found: 988.3426

7.3.8 Meso-tetraphenyltetra(di-methyl)benzoporphyrin (H_2-TPTBPdM$_4$)

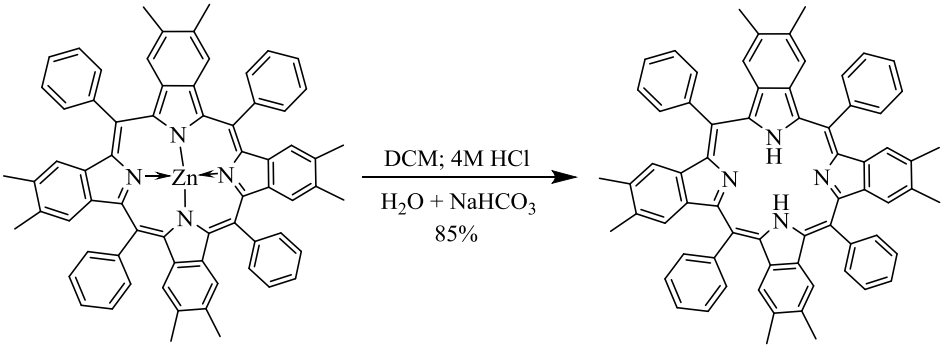

Figure 47 Reaction scheme for H_2-TPTBPdM$_4$

Zn-TPTBPdM$_4$ (50.00 mg, 50.48 µmol, 1.00 eq) was dissolved in 60 mL DCM, 10 mL of 4 M HCl were slowly added. The resulting protonated ligand could be determined via absorption spectra in acetone (λ_{max}: 499 nm). The reaction mixture was then extracted with dest H_2O (2 x 30 mL) and with saturated $NaHCO_3$-solution (2 x 30 mL) until only free ligand was observed in the absorption spectra. Finally the organic layer was once more washed with dest. H_2O (30 mL), dried over Na_2SO_4 and the solvent was removed under reduced pressure.

Yield: dark green solid, 39.8 mg, 85%

Molar absorption coefficient, $\lambda_{max}/\varepsilon$ (nm, $M^{-1}cm^{-1}$) in toluene: 467 nm, 145758 M^{-1} cm^{-1}

λ_{max} (nm) in acetone: 461 nm

7.3.9 Platinum (II) meso-tetraphenyltetra(di-methyl)benzoporphyrin (Pt-TPTBPdM$_4$)

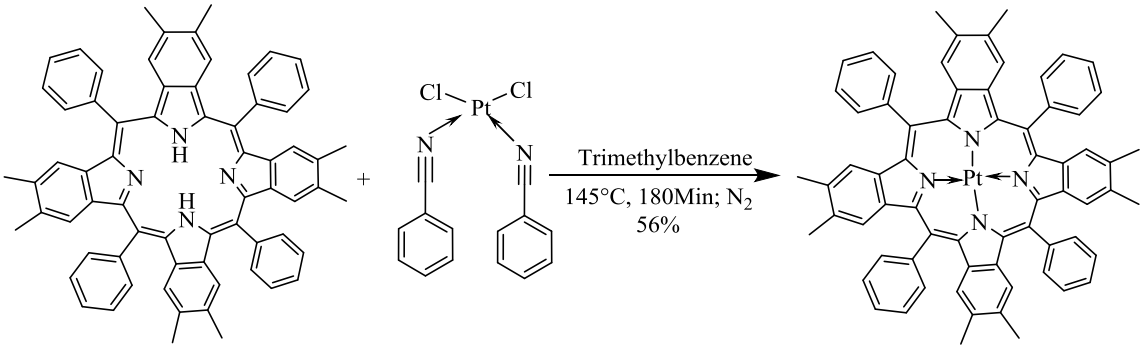

Figure 48 Reaction scheme for Pt-TPTBPdM$_4$

H_2-TPTBPdM$_4$ (20.0 mg, 21.57 µmol, 1.00eq) was dissolved in TMB (30 mL) in a 2-neck-round bottom flask and heated to 145°C, while bubbling N_2 through the reaction mixture. Then $Pt(C_6H_5CN)_2Cl_2$ (15.3 mg, 32.36 µmol, 1.50 eq) was added slowly in small portions (5 x 0.3 eq pre-dissolved in TMB) from a pre-heated addition funnel (100°C) over 3 hours. The reaction progress was monitored via absorption spectra (solvent: acetone). After complete conversion the reaction mixture was cooled down to room temperature, the by-products were removed via centrifugation and the solvent was removed under reduced pressure at 80 °C. The crude product was finally purified via column chromatography (silica, CH:DCM, 3:1). The product containing fractions were determined via absorption spectra, yielding a dark green solid. Mass spectrum can be seen in the appendix on page 138.

Yield: dark green solid, 13.5 mg, 56%

λ_{max}/relative intensity (nm) in toluene: 428/1.00; 619/ 0.7079

λ_{max} (nm) in acetone: 426; 616

MALDI: m/z: [M+]; $C_{68}H_{52}N_4Pt$, calc. for 1120.3861; found: 1120.3761

Target compound: Platinum (II) meso-tetraphenyltetra(mono-methyl)benzoporphyrin (Pt-TTolTBPmM$_4$)

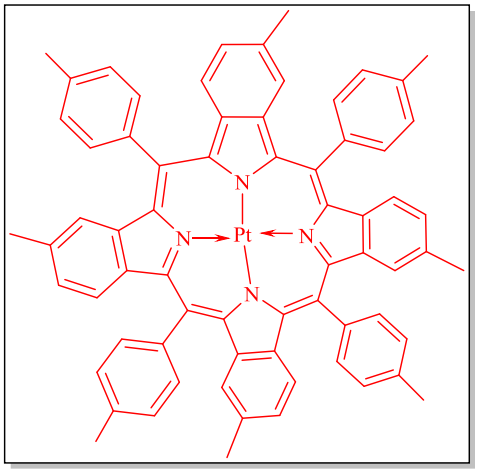

Figure 49 Reaction scheme for Pt-TTolTBPmM$_4$

7.3.10 Zinc (II) meso-tetratolyltetra(mono-methyl)benzoporphyrin (Zn-TTolTBPmM$_4$)

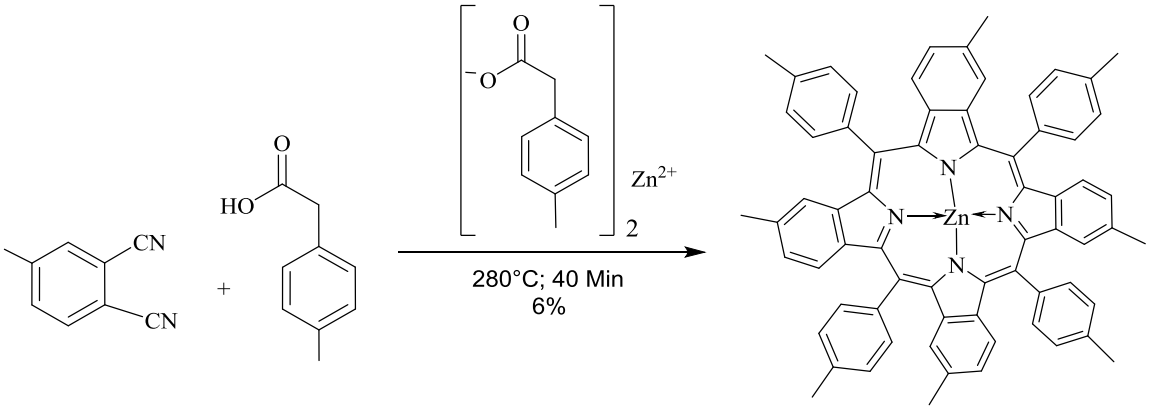

Figure 50 Reaction scheme for Zn-TTolTBPmM$_4$

Mono-methylphthalonitrile (6.722 g, 47.3 mmol, 4.00 eq), 2-(p-tolyl)acetic acid (15.98 g, 106.4 mmol, 9.00 eq), zinc-4-tolylacetate (4.30 g, 11.82 mmol, 1.00 eq) were mixed together and homogenized with a ceramic pestle in a mortar and approximately 700 mg of the reaction mixture were weighed in each 4 mL supelco-vial equipped with a stirring bar. After sealing the vials with a metal cap they were placed on a preheated heating block at 250°C under stirring and heated up to 280°C where the reaction mixture was kept for 40 minutes. Afterwards the vials were cooled down to room temperature and smashed with a hammer. The reaction mixture was dissolved in 800 mL acetone and sonicated for ten minutes. The pieces of glass were separated via vacuum filtration and the solution was concentrated under reduced pressure to an approximate volume of 300 mL. The concentrated reaction mixture was then added dropwise to 1.50 L ethanol/water (1:1 + 25 mL saturated $NaHCO_3$ + 25 mL

brine) solution, producing a dark-green precipitate, which was further filtered off in vacuo. Afterwards the residue was washed with an ethanol/water solution (1:2; 3 x 200 mL) and dried in the vaccum oven at 60°C. The crude product was purified via column chromatography, first on ALOX (DCM:EE, 10:1) and then on silica (DCM:EE, 5:1) as stationary phase. The product containing fractions were determined via absorption spectra. The product was finally dried in the vacuum oven at 60°C. 15 mg of Zn-TTolTBPmM_4 were then washed with cyclohexane on the ultrasonic bath for 10 minutes. This process was repeated for three times. The insoluble dark-green sediment was obtained after the removal of the light-green-brownish supernatant via centrifugation. NMR and mass spectra can be seen in the appendix on the pages 130 and 139.

Yield: dark green solid, 723.4 mg, 6%

Molar absorption coefficient, $\lambda_{max}/\varepsilon$ (nm, $M^{-1}cm^{-1}$) in toluene: 462/ 212000; 654/ 58030

λ_{max} (nm) in acetone: 460; 652

^{1}H NMR (300 MHz, Chloroform-d) δ 8.21 – 8.07 (m, 8H), 7.66 (q, J = 7.2 Hz, 8H), 7.23 – 7.04 (m, 8H), 7.01 (s, 2H), 6.90 (s, 2H), 2.81 (t, J = 3.3 Hz, 12H), 2.38 – 2.29 (m, 12H).

MALDI: m/z: [M+]; $C_{68}H_{52}N_4Zn$, calc. for 988.3483; found: 988.3405

7.3.11 Bridged zinc (II) meso-tetratolyltetra(mono-methyl)benzoporphyrin (bridged Zn-TTolTBPmM$_4$)

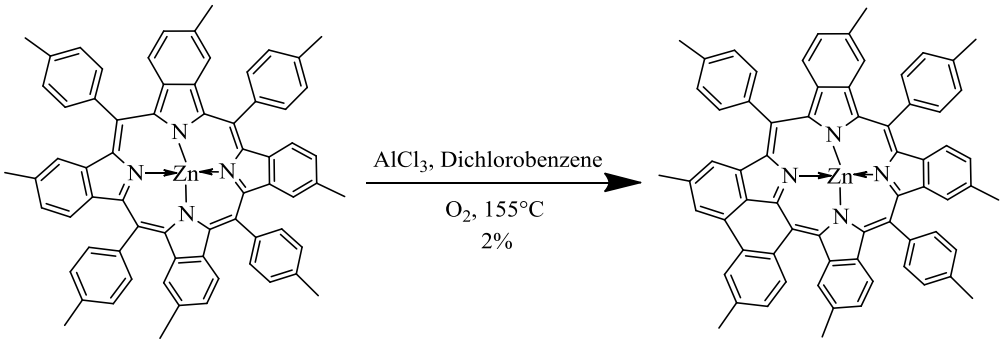

Figure 51 Reaction scheme for bridged Zn-TTolTBPmM$_4$

Zn-TTolTBPmM$_4$ (13.0 mg, 13.1 µmol, 1.00 eq) was dissolved in 13 mL dichlorobenzene for 5 minutes on the ultrasonic bath in a closed 25 mL round bottom flask. Then aluminum trichloride (437.5 mg, 3.281 mmol, 250 eq) was added to the solution and the reaction mixture was again put on the ultrasonic bath for 10 minutes, resulting in a color change from dark-green to a brownish-red solution. Afterwards the reaction mixture was quickly heated to 155°C, while moderate O_2-bubbling through the solution. The reaction progress was monitored via absorption spectra (solvent: DCM),the samples taken from the reaction mixture were neutralized with 2 drops of triethylamine, visualized through a color change from dark-brown to light-brownish-green. After completion of the reaction the reaction mixture was allowed to cool down to room temperature while continuous O_2-bubbling through the solution. During the work-up the reaction mixture was neutralized with a DCM:TEA solution (40:1) and the resulting precipitate was separated via centrifugation and washed with DCM. The reaction mixture was washed with dest. H_2O (3 x 100 mL) and then dried over Na_2SO_4, before removal of solvent under reduced pressure. Finally the resulting green solid was purified via column chromatography (silica, cond. CH, DCM:THF, 3:1), yielding a green solid. The solid was then re-dissolved in THF (10 mL), heated to 40°C and the produced complex re-metalized through the addition of zinc acetate (5.8 mg, 26.2 µmol, 2.00 eq) under continuous stirring for 10 minutes. The solvent was removed under reduced pressure and the resulting green solid was again purified via column chromatography (ALOX, DCM:EE, 10:1) yielding a dark-green solid. The product containing fractions were determined via absorption spectra. Mass spectrum can be seen in the appendix on page 140.

Yield: green solid, 0.2 mg, 2%

λ_{max}/relative intensity (nm): 492/ 1.00; 644/ 0.0849; 700/ 0.1632

λ_{max} (nm) in acetone: 492; 700

MALDI: m/z: [M+]; $C_{68}H_{50}N_4Zn$, calc. for 986.3327; found: 986.3288

7.3.12 Meso-tetratolyltetra(mono-methyl)benzoporphyrin (H_2-TTolTBPmM$_4$)

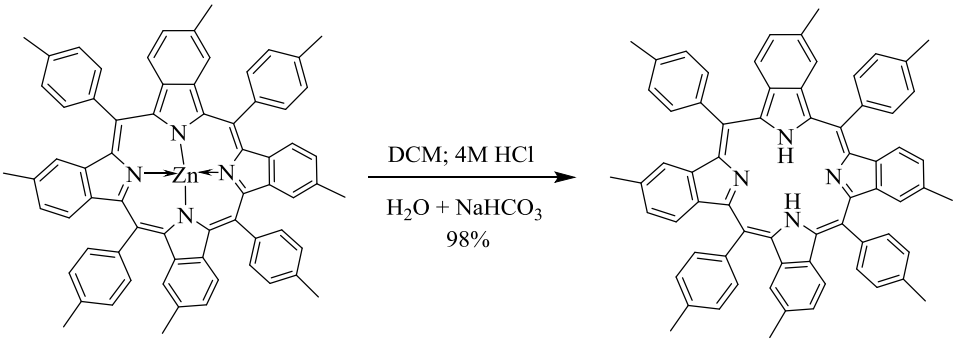

Figure 52 Reaction scheme for H_2-TTolTBPmM$_4$

Zn-TTolTBPmM$_4$ (50.0 mg, 50.5 mmol, 1.00 eq) was dissolved in 50 mL DCM and 10 mL of 4M HCl were slowly added. The resulting protonated ligand could be determined via absorption spectra in acetone (λ_{max}: 503 nm). The reaction mixture was then extracted with dest H_2O (2 x 25 mL) and with saturated $NaHCO_3$-solution (1 x 15 mL) until only free ligand was observed in the absorption spectra. Finally the organic layer was once more washed with dest. H_2O (25 mL), dried over Na_2SO_4 and the solvent was removed under reduced pressure.

Yield: dark green solid, 46.0 mg, 98%

Molar absorption coefficient, $\lambda_{max}/\varepsilon$ (nm, $M^{-1}cm^{-1}$) in toluene: 468 nm, 170604 M^{-1} cm^{-1}

λ_{max} (nm) in acetone: 461 nm

7.3.13 Platinum (II) meso-tetratolyltetra(mono-methyl)benzoporphyrin (Pt-TTolTBPmM$_4$)

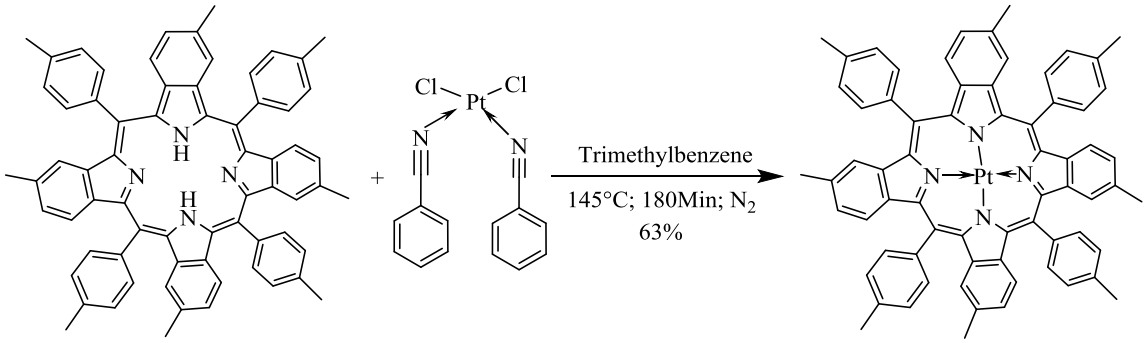

Figure 53 Reaction scheme for Pt-TTolTBPmM$_4$

H_2-TTolTBPmM$_4$ (35.0 mg, 37.7 µmol, 1.00 eq) was dissolved in TMB (40 mL) in a 2-neck-round bottom flask and heated to 145°C, while bubbling N_2 through the reaction mixture. Then Pt($C_6H_5CN)_2Cl_2$ (21.4 mg, 45.3 µmol, 1.20 eq) was added slowly to the solution in small portions (4 x 0.3 eq pre-dissolved in TMB) using a pre-heated Pasteur pipette (100°C) over the period of 3 hours. The reaction progress was monitored via absorption spectra (solvent: acetone). After complete conversion the reaction mixture was cooled down to room temperature, the by-products were removed via centrifugation and the solvent was removed under reduced pressure at 80 °C. The crude product was further purified via column chromatography (ALOX, CH:DCM, 3:1) yielding a dark green solid. The product containing fractions were determined via absorption spectra. Mass spectrum can be seen in the appendix on page 141.

Yield: dark green solid, 26.7 mg, 63%

Molar absorption coefficient, $\lambda_{max}/\varepsilon$ (nm, $M^{-1}cm^{-1}$) in toluene: 432/ 157300; 617/ 106500

λ_{max} (nm) in acetone: 429; 615

MALDI: m/z: [M+]; $C_{68}H_{52}N_4Pt$, calc. for 1120.3861; found: 1120.3890

7.3.14 Bridged-Platinum (II) meso-tetraphenyltetrabenzoporphyrin (bridged-Pt-TPTBP)

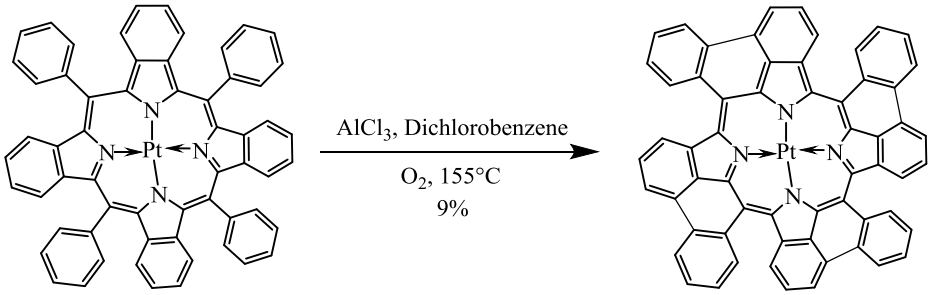

Figure 54 Reaction scheme for bridged-Pt-TPTBP

Pt-TPTBP (48.00 mg, 47.6 µmol, 1.00 eq) was dissolved in 12 mL dichlorobenzene for 5 minutes on the ultrasonic bath in a closed 25 mL round bottom flask. Then aluminum trichloride (825.4 mg, 6.190 mmol, 130 eq) was added to the solution and the reaction mixture was again sonicated for 10 minutes, resulting in a color change from dark-green to a brownish-red solution. Afterwards the reaction mixture was quickly heated to 155°C, by moderate O_2-bubbling through the solution. The reaction progress was monitored via absorption spectra (solvent: DCM), whereas the samples taken from the reaction mixture were neutralized with 2 drops of triethylamine, visualized in a color change from dark-brown to bright green. After completion the reaction mixture was allowed to cool to room temperature while continuous O_2-bubbling through the solution. During the work-up the reaction mixture was neutralized with a DCM:TEA solution (40:1). The precipitate was separated via centrifugation, and washed with DCM, whereas the reaction mixture was washed with dest. H_2O (3 x 100 mL) and dried over Na_2SO_4, before removal of solvent under reduced pressure. Finally the resulting green solid was purified via column chromatography (silica, cond. CH, DCM:THF, 3:1) and subsequently washed with cyclohexane (3 x 15 mL), yielding a green solid. Mass spectrum can be seen in the appendix on page 142.

Yield: green solid, 4.4mg, 9%

λ_{max}/relative intensity (nm): 438/ 0.4203; 452/ 0.4513; 479/ 1.00; 604/ 0.0722; 620/ 0.1004; 639/ 0.2077; 674/ 0.5656

λ_{max} (nm) in DCM: 479; 673

MALDI: m/z: [M+]; $C_{60}H_{28}N_4Pt$, calc. for 999.1967; found: 999.1927

7.3.15 Bridged platinum (II) meso-tetra(tolyl)benzoporphyrin (bridged Pt-TTolTBP)

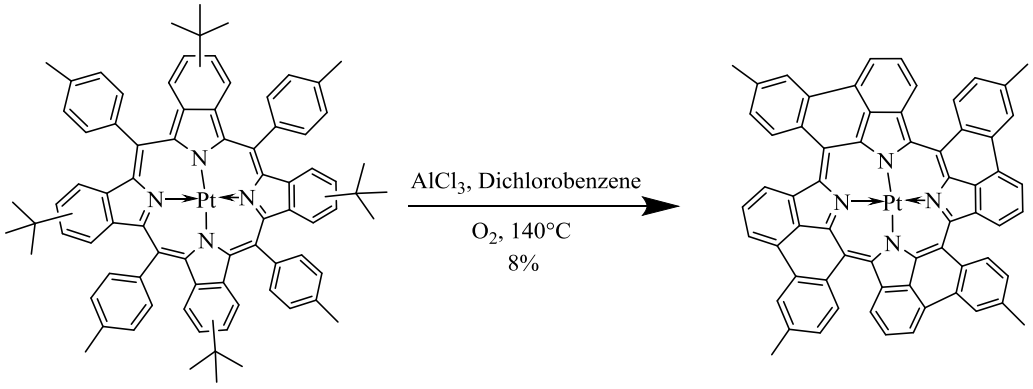

Figure 55 Reaction scheme for bridged Pt-TTolTBP

Pt-TTolTBPtert-butyl$_4$ (12.00 mg, 9.37 µmol, 1.00 eq) was dissolved in 12 mL dichlorobenzene via sonification for 5 minutes in a closed 25 mL round bottom flask. Then aluminum trichloride (162.5 mg, 1.22 mmol, 130 eq) was added to the solution and the reaction mixture was again sonicated for 10 minutes, resulting in a color change from dark-green to a brownish-red solution. The reaction mixture was quickly heated to 140°C, by moderately O_2-bubbling through the solution. The reaction progress was monitored via absorption spectra (solvent: DCM), whereas the samples taken from the reaction mixture were neutralized with 2 drops of triethylamine, which led to a color change from dark-brown to bright green. After completion of the reaction mixture was cooled down to room temperature while continuous O_2-bubbling through the solution. In the work-up the reaction mixture was neutralized with a DCM:TEA solution (40:1) and the precipitate separated via centrifugation, and washed with DCM, whereas the reaction mixture was washed with dest. H_2O (3 x 100 mL) and dried over Na_2SO_4, before removal of solvent under reduced pressure. Finally the resulting green solid was purified via column chromatography (silica, cond. CH, DCM:THF, 3:1) and subsequently washed with cyclohexane (3 x 15 mL), yielding a green solid. Mass spectra can be seen in the appendix on the pages 143 and 144.

Yield: green solid, 1.0 mg, 8%

Molar absorption coefficient, $\lambda_{max}/\varepsilon$ (nm, $M^{-1}cm^{-1}$) in toluene: 485/ 122600; 673/ 70100

λ_{max} (nm) in DMF: 484; 671

MALDI: m/z: [M+]; $C_{64}H_{36}N_4Pt$, calc. for 1056.26; found: 1056.26

7.3.16 Relative quantum yield:

For the measurement of relative quantum yield the respective dye (bridged Pt-TTolTBP Sample 1, Sample 2 and Sample 3) as well as the used standard (Pd-TPTBP for Sample 1; Pt-OEP for Sample 2 and 3) in diluted toluene solutions were adjusted to an absorption of approximately 0.12 (~$1*10^{-5}$ M) at the chosen excitation wavelength. The solutions were then deoxygenated for 10 minutes (argon bubbling through the solution). Afterwards the standard was excited at the respective wavelength (Pd-TPTBP at 443 nm; Pt-OEP at 533 nm) and the settings (EST and slit width) defined in order to achieve a value of the corrected emission below 2 000 000 [CPS]. Finally emission spectra of the bridged dyes (Sample 1-3) were recorded with the same settings. The calculation of the relative quantum yield was performed via integration of the area below the emission band using Origin, which were corrected for the amount of absorbed light for each dye.

Table 1 Photophysical properties and quantum yields of the used standards and bridged Pt-TTolTBP in toluene at room temperature

dye	absorption λ_{max} [nm]	emission λ_{max} [nm]	solvent	quantum yield [%]	reference
Pt-OEP	382, 536	647	toluene	41	[119]
Pd-TPTBP	444, 629	797	toluene	21	[74]
bridged Pt-TTolTBP S1	486, 640, 673	870	toluene	10.9	this work
bridged Pt-TTolTBP S2	521, 717	970	toluene	~0.03	this work
bridged Pt-TTolTBP S3	539, 730	995	toluene	~0.03	this work

8. Results and Discussion

8.1 Synthetic Considerations

The two aims of the thesis were on the one hand the synthesis of a highly soluble benzoporphyrin dye and on the other hand the examination of the effect of intramolecular bridging (fusion) on different benzoporphyrins and further characterization of the changed optical properties. Although the synthesis of benzoporphyrins can be performed in many different ways according to literature [14], two methods are well-known and widely used to synthesize tetrabenzoporphyrins. One of the first methods found is the conventional Lindsey-condensation. [120] This synthetic strategy usually allows the formation of very pure products and further the introduction of different functional groups due to the mild conditions. Though the starting materials are commercially available and mostly not very expensive, the number of the following reaction steps (figure 56, next page) until the porphyrin is synthesized make this method not only time consuming but also quite expensive compared to the later explained strategy.

The second often applied method is the so called template synthesis. [32] Here only three steps (formation of the zinc-complex, de-metalation and platination of the metal-free porphyrin) are necessary to obtain the desired platinum or palladium tetrabenzoporphyrin dye. Even though this method allows the use of cheap starting materials, it also suffers from several drawbacks such as low yields in the range of 5 to 10%, a complex product mixture due to the harsh conditions (250 to 300°C) and a limited possibility concerning the introduction of functional groups. The exchange of phthalimide to dicyanobenzene as starting material in the template synthesis led not only to an increased yield of the respective zinc-complex but also to the avoidance of previously often observed benzyl-substituted side products, which were extremely challenging to separate. [121], [88]

All in all the smaller synthetic effort of the Template method makes this synthetic strategy a good alternative to the conventional applied Lindsey method.

8.2 Lindsey method leading to highly soluble benzoporphyrin

Basically the synthetic steps for the synthesis of target compound 1 were all conducted according to literature presented in figure 56 [4]. Hereby the synthesis from step one to step four, the (3aR,7aS)-2-(2-ethylhexyl)-5-(phenylsulfonyl)-3a,4,7,7a-tetrahydro-1H-isoindole-1,3(2H)-di-one compound were all performed without any problems, even though the yields were basically slightly lower compared to literature.

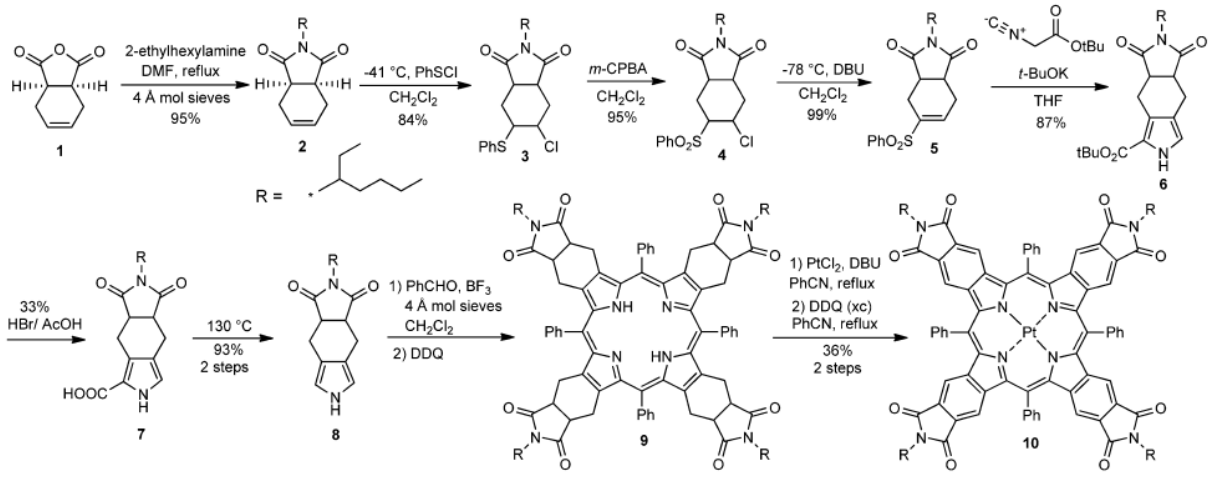

Figure 56 Synthetic strategy for the synthesis of imide-substituted platinum(II)benzoporphyrin dye [4]

Despite that the NMR of the phenyl-sulfonic compound showed traces of grease, the desired product could be clearly identified, therefore the synthesis was continued without further purification of this compound. In step five, the Barton-Zard condensation of phenylsulfone, the cheaper and readily available ethyl-2-isocyanoacetate was used instead tert-butyl isocyanoacetate. Even though this reaction was performed with moderate yield (68%) the following conversion to tetra-hydroisoindole failed.

The acidic treatment with 33% HBr as described by Perepichka et al. [4] did not lead to the ethylester-cleavage, which was already observable via TLC and could be proved by NMR. Hereby the product was partly destroyed, whereas the rest remained unchanged (figure 57). Notable is that ethyl esters are generally cleaved with bases and not with acids, due to the fact that the stabilization of an ethyl residue in solution is much lower than that of a tert-butyl ester.

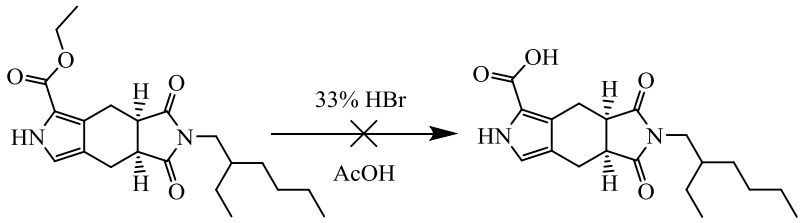

Figure 57 Synthetic strategy for the synthesis of 6-(2-ethylhexyl)-5,7-dioxo-2,4,4a,5,6,7,7a,8-octahydropyrrolo[3,4-f]isoindole-1-carboxylic acid by acidic treatment with HBr

The treatment with different bases, such as LiOH or NaOH in a solvent mixture of THF, MeOH and dest. H_2O (3:1:1 or 5:4:1) did not yield the desired product (figure 58). Hereby almost complete conversion to a different compound was visible on the TLC. Both NMR and

MS measurements showed the presence of a carboxylic acid group, amine functionality but also of an ester group, which led to the assumption of following two possibilities: either this reaction led to a mixture of the desired product and the un-cleaved ester or to a hydrolysis of the imide without an ester cleavage. The first possibility could be mainly excluded after an attempt with a more concentrated base, longer duration as well as smooth heating of the reaction. Therefore the formation of the following side product was assumed.

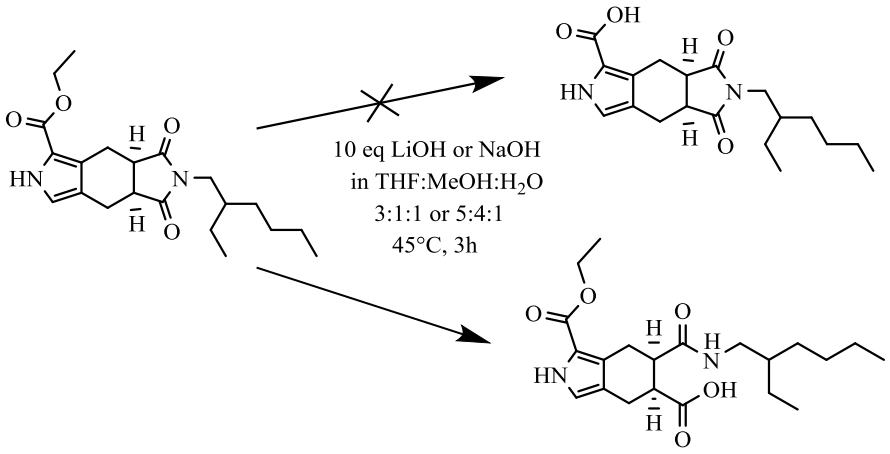

Figure 58 Synthetic strategy for the synthesis of 6-(2-ethylhexyl)-5,7-dioxo-2,4,4a,5,6,7,7a,8-octahydropyrrolo[3,4-f]isoindole-1-carboxylic acid by basic treatment with LiOH or NaOH

Furthermore, many different approaches were tested to hydrolyze the ethyl ester moiety to finally achieve the desired tetra-hydroisoindole. Since the ethyl ester cleavage was not possible neither under acidic nor under basic conditions a transesterification was attempted (figure 59). Hereby tert-butoxide was added to the ethyl ester compound dissolved in dry diethylether at room temperature. Unfortunately no formation of the trans-esterified product could be detected. [122]

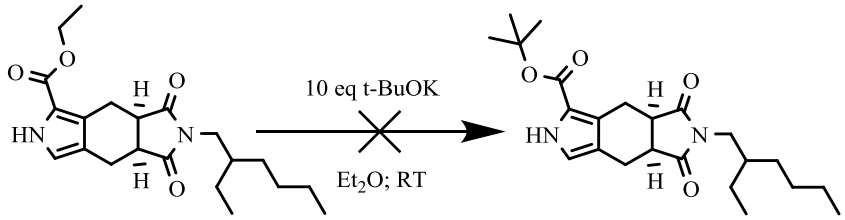

Figure 59 Synthetic strategy for the transesterifacation of (4aS,7aR)-ethyl-6-(2-ethylhexyl)-5,7-dioxo-2,4,4a,5,6,7,7a,8-octahydropyrrolo[3,4-f]isoindole-1-carboxylate to t-butyl-6-(2-ethylhexyl)-5,7-dioxo-2,4,4a,5,6,7,7a,8-octahydropyrrolo[3,4-f]isoindole-1-carboxylate

Moreover different attempts to cleave the ethyl ester. were performed, in which either $AlCl_3$ was added to the dissolved ethyl ester compound in DCM under reflux or boron trifluoride diethyl etherate was added to the dissolved ethyl ester compound in chloroform or toluene at room temperature. Also in this case no formation of the desired product was observed (figure 60).

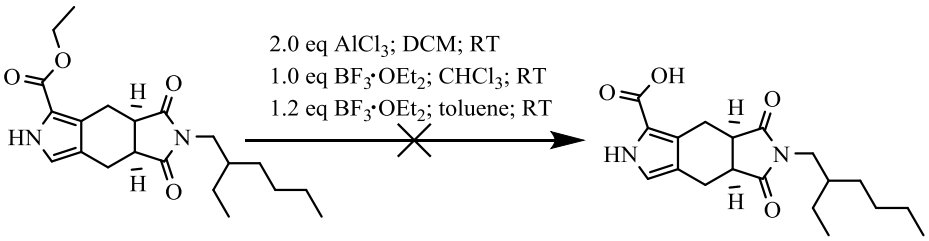

Figure 60 Synthetic strategy for the synthesis of 6-(2-ethylhexyl)-5,7-dioxo-2,4,4a,5,6,7,7a,8-octahydro-pyrrolo[3,4-f]isoindole-1-carboxylic acid by addition of $AlCl_3/BF_3$-OEt_2 in DCM/$CHCl_3$/toluene

After the unsuccessful attempts of the ethyl ester cleavage to form the carboxylic acid a completely different approach was finally started in which the ester-cleavage and the following decarboxylation should be performed in one single step (figure 61). In so called Krapcho-Decarboxylation the ethyl ester compound was dissolved in DMSO, then LiCl (previously dissolved in water) was added and the reaction mixture was heated to 150°C. Even though conversion was observed on the TLC-plate, the yielded purified compound after flash chromatography was not the desired product according to the NMR.

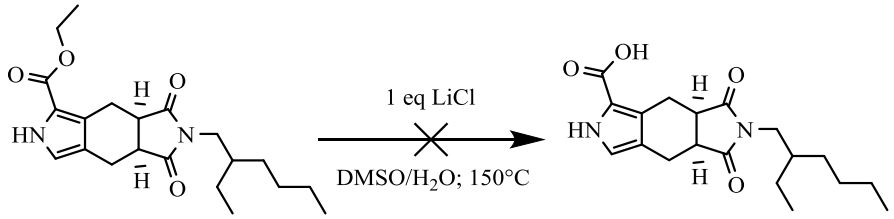

Figure 61 Synthetic strategy for the synthesis of 6-(2-ethylhexyl)-5,7-dioxo-2,4,4a,5,6,7,7a,8-octahydropyrrolo[3,4-f]isoindole-1-carboxylic acid by Krapcho-decarboxylation in DMSO

Therefore it was concluded to repeat the Barton-Zard condensation of the phenylsulfone compound using tert-butyl isocyanoacetate instead of ethyl-2-isocyanoacetate although this compound is much more expensive and definitely increases the price for the upscale of the synthesis seriously. Furthermore, the necessity of this compound makes the synthesis not only more expensive but also hardly feasible due to the limited accessibility of the compound on the market. Also the synthesis of tert-butyl isocyanoacetate compound itself is not unchallenging because of the multistage synthetic route. Due to the relatively high synthetic effort and the restricted availability of this chemical the synthesis of target compound 1 could not be finished within the master thesis. (figure 62).

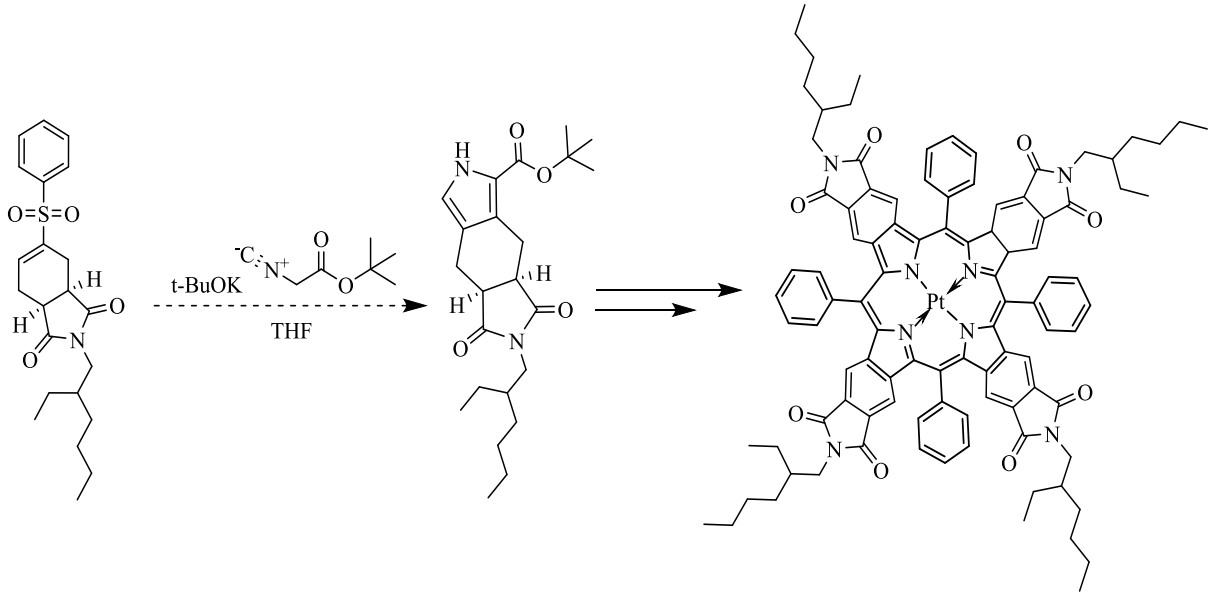

Figure 62 Synthetic strategy for the synthesis of t-butyl-6-(2-ethylhexyl)-5,7-dioxo-2,4,4a,5,6,7,7a,8-octahydropyrrolo[3,4-f]isoindole-1-carboxylate further leading to the platinum benzo-porphyrin dye substituted with imide functionalities according to Perepichka et al.

As mentioned in chapter 5.5.1.1 the final Pt(II) porphyrin dye displays very high solubility as well as photostability, a large Stockes shift and NIR emission at 755 nm with a quantum yield of 45%. Responsible for the great solubility in various organic solvents are especially the branched 2-ethylhexyl groups and also the meso-phenyl substituents, which reduce the planarity of the porphyrin. Furthermore the electron withdrawing imide substituents reduce the sensitivity towards oxidation resulting in a very high photostability of the dye. Beside the outstanding solubility, photostability and optical properties the synthesis of the dye nevertheless suffers from unchallenging and very time consuming Lindsey condensation (particularly the limited accessibility or the challenging synthesis of the educts) as preparation strategy.

Reason for this limitation is the complexity of the substituents in meso-position, which are not adequate for hard reaction conditions as used for example in the template synthesis method. The usage of this method would definitely enhance the synthesis of the dye by decreasing the preparation costs and working-time. To overcome these drawbacks an attempt was conducted to synthesize a dye with similar or even enhanced photophysical properties with a different, more easy to perform synthetic strategy. Due to all the advantages described at the beginning, the synthetic pathway of choice was the template method. Despite all advantages of the method it is nevertheless not trivial to find components, which are suitable for this strategy. These components must tolerate high temperatures, have to be relatively cheap and easily producible but must also be potential candidates to display the expected properties (high solubility and photostability) after a successful synthesis. These requirements were fulfilled by one compound, which is described in the next chapter.

8.3 Template method leading to highly soluble benzoporphyrin

The idea for the synthesis of the following compound was given by the literature of Ragoussi et al. [117], in which a phthalocyanine was substituted with 4,5-bis(2-ethylhexylsulfonyl)phthalonitrile substituents in a three step synthesis with little synthetic effort. Of particular interest from this synthetic pathway (figure 63) is step two in which 4,5-Bis(2-ethylhexylthio)phthalonitrile gets oxidized using m-CPBA (70-75% wet) resulting in 4,5-Bis(2-ethylhexylsulfonyl)phthalonitrile after quenching with $NaHCO_3$-solution.

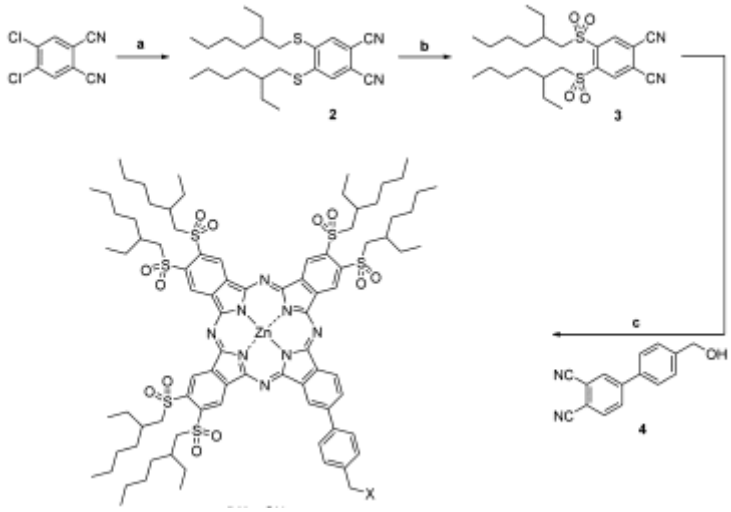

Figure 63 Synthetic strategy for the synthesis of 2-(Hydroxymethyl)phenyl-9,10,16,17,23,24-hexakis-(2-ethylhexylsulfonyl)-5,28:14,19-diimino-7,12:21,26-dinitrilotetrabenzo[c, h, m, r][1, 6, 11, 16]-tetraazacycloeicosinato-(2-)-N29, N30, N31, N32 zinc (II) compound of Ragoussi et al. [117]

The introduction of this compound via template method seems to show big potential for the accomplishment of similar or probably even better suppressed photobleaching properties and comparable solubility as the dye of Perepichka et al. [4]. While the long alkyl chains would provide good solubility, the already completely oxidized sulfur would definitely increase photostability due to its strong electron withdrawing effect. The two reactions leading to 4,5-bis(2-ethylhexylthio)phthalonitrile and 4,5-bis(2-ethylhexylsulfonyl)-phthalonitrile from cheap chemicals were successfully performed according to the literature [4], both compounds where tested for their usability within the template method. Hereby it could be revealed that the Template synthesis with 4,5-bis(2-ethylhexylthio)phthalonitrile led to the formation of a benzoporphyrin complex (figure 64), whereas Template synthesis with 4,5-bis(2-ethylhexylsulfonyl)phthalonitrile did not display the desired absorption spectra (figure 65) but a mixture of phathalocyanines and azaporphyrins. (figure 66).

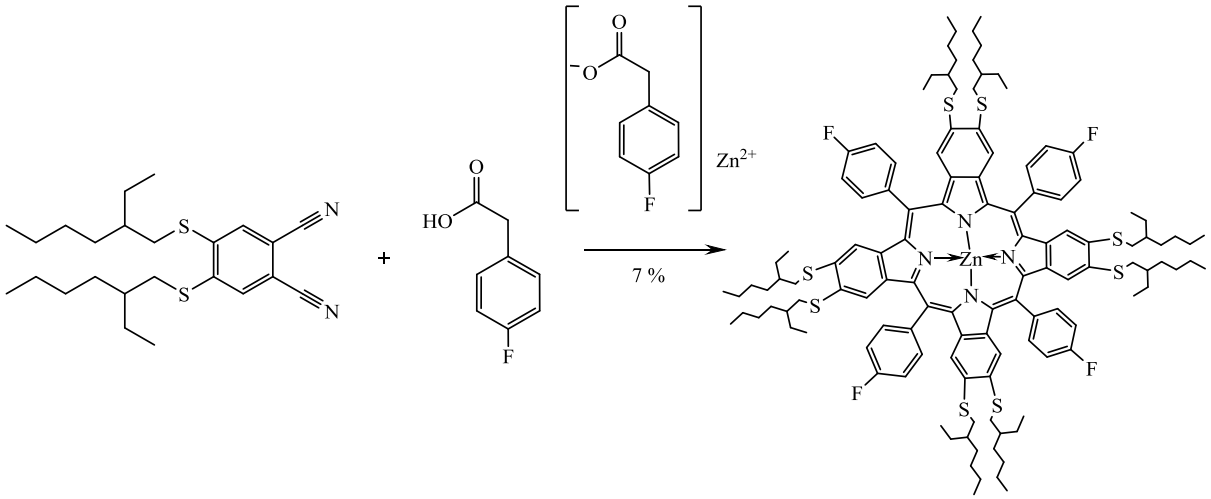

Figure 64 Reaction scheme for Zinc (II) -meso-tetra(4-fluorophenyl)tetra(4,5-bis((2-ethylhexyl)thio)benzoporphyrin

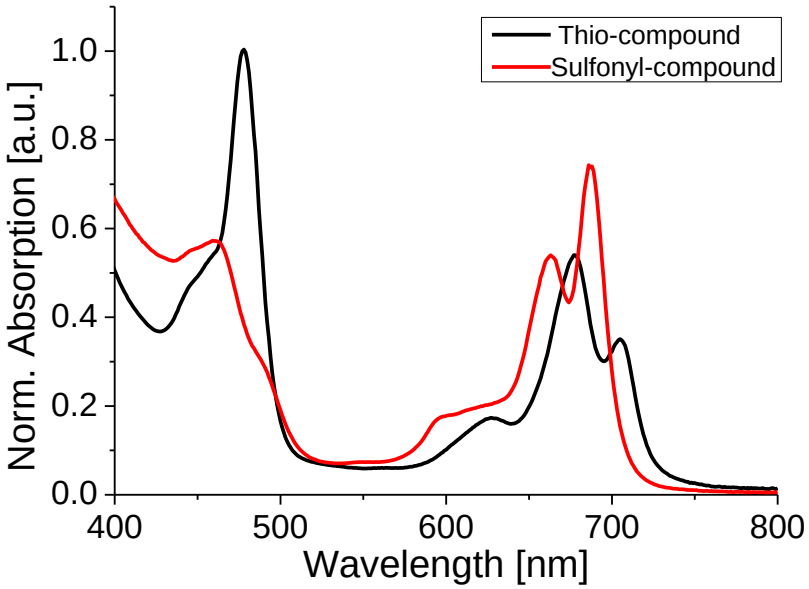

Figure 65 Normalized absorption Spectrum of the received zinc-benzoporphyrin complex with 4,5-Bis(2-ethylhexylthio)phthalonitrile or 4,5-Bis(2-ethylhexylsulfonyl)phthalonitrile after the Template synthesis in acetone

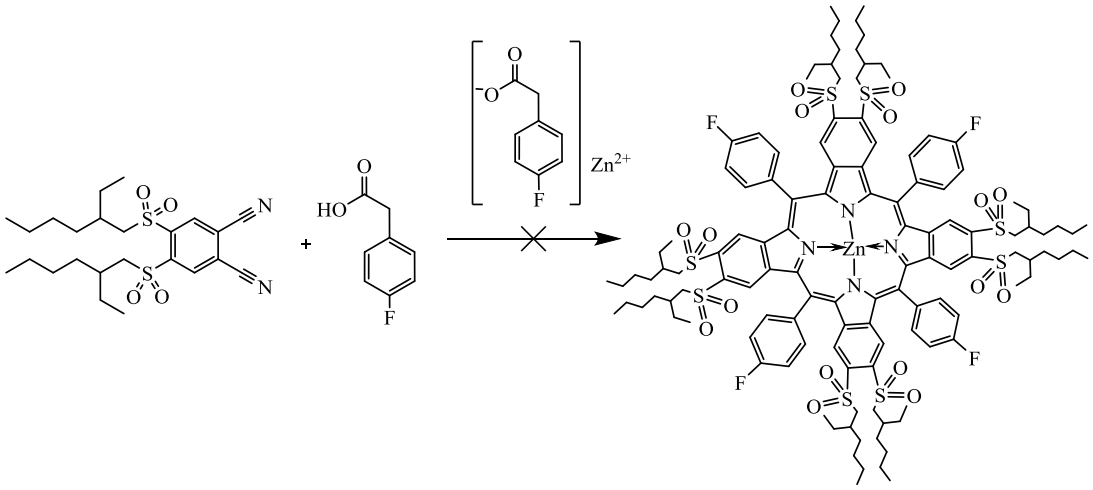

Figure 66Synthetic strategy for the synthesis of Zinc (II) -meso-tetra-(4-fluorophenyl)tetra(4,5-bis((2-ethylhexyl)sulfonyl)benzoporphyrin

This result showed that the influence of substituents, even if there are only relatively small differences can have a huge impact on the formation of the desired benzoporphyrin complex. Electron withdrawing groups (e.g. sulfones) appear not to favor the formation of benzoporphyrin via Template synthesis. Reason for the failed Template synthesis could certainly also be the two oxygen atoms at the sulfur probably leading to an increased efficiency of side reaction (e.g. formation of phthalocyanine) at these high temperatures.

Even after some attempts (other temperatures, different equivalents of 2-(4-fluorophenyl) acetic acid and varying reaction time) no formation of the desired product could be identified within the absorption spectra after Template synthesis. On the contrary Template synthesis with 4,5-Bis(2-ethylhexylthio)phthalonitrile produced the desired benzoporphyrin-complex. Here also different attempts to modify the reaction conditions and to increase the formation of the benzoporphyrin were tested, such as different starting temperatures (180-250°C), various equivalents of 2-(4-fluorophenyl)acetic acid (5-20 equivalents) in comparison to the zinc-4-fluorophenylacetate (1 equivalent) as well as reaction times between 40 to 60 minutes until the best method was found. The usage of a Mg-template instead of a Zn-template did not succeed. Furthermore an exchange from relatively volatile 2-(4-fluorophenyl)acetic acid to the higher melting phenylacetic sodium salt of the acid was attempted, which also did not work out. Optimal conditions were finally achieved with 10 equivalents of 2-(4-fluorophenyl)acetic acid, 4 equivalents of 4,5-bis((2-ethylhexyl)thio)phthalonitrile and 1 equivalent of zinc-4-fluorophenylacetate at 250°C starting temperature with 40 minutes reaction time at 280°C. To probably further increase the photostability and solubility the hydrogen at the para-position of the meso-phenyl rings were substituted with a fluorine atom to achieve also a small electron withdrawing effect at the meso-position of the porphyrin core.

The process of the Template synthesis itself due to the paste like consistence of the 4,5-bis(2-ethylhexylsulfonyl)phthalonitrile but also the precipitation of the prepared solution varied a lot from the usual procedure for the purification of benzoporphyrin complexes due to the sticky nature of the Zn-complex. Nevertheless after all a suitable separation method for the well soluble Zn-benzoporphyrin complex could be found by washing the dye dissolved in a cyclohexan/n-hexane mixture with methanol using a separation funnel. Thus many side products could be separated before purifying via flash chromatography. Finally after all purification steps the desired product could be isolated and proved via MS. It was assumed that the Zn-complex with the thio-substituents was not very photostable and also sensitive to oxygen, therefore it was stored in the dark under argon atmosphere. To examine how the dye (in an air saturated or deoxygenated toluene) behaves under irradiation a photostability test was started, revealing that as already supposed the dye is completely and irreversibly destroyed under irradiation after a relatively short time.

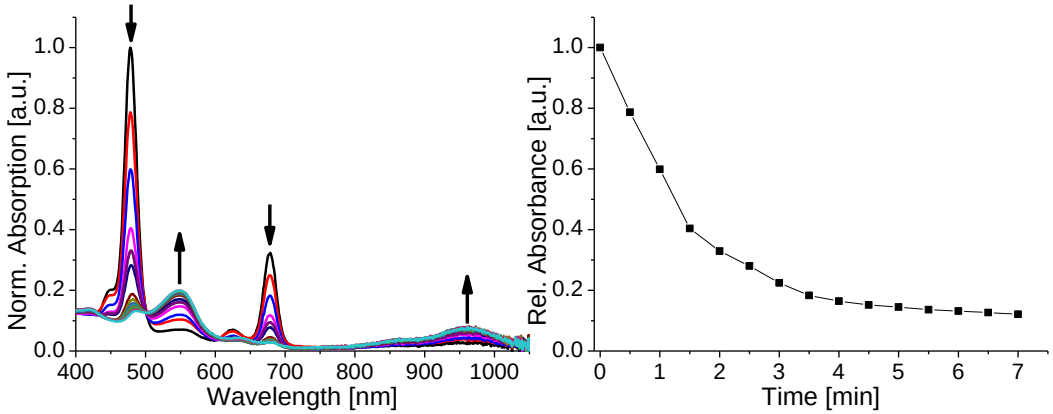

Figure 67 Photodegradation curves for Zn-TPTBPF$_4$bEHT$_4$ complex in air saturated toluene solution at room temperature. Irradiation is performed with a blue LED array (λ_{max}=458 nm; 10.79 V, 0.689 A, 7.4 W).

Moreover parallel to the degradation of the Zn-TPTBPF$_4$bEHT$_4$ the formation of a new compound at longer wavelengths in the air saturated solution of toluene can be observed (figure 67). In the deoxygenated (10 minutes via argon bubbling) dye solution in toluene, this effect was not so strong, as we can see here in figure 68. Also the degradation occurred slightly slower than in the air saturated toluene solution.

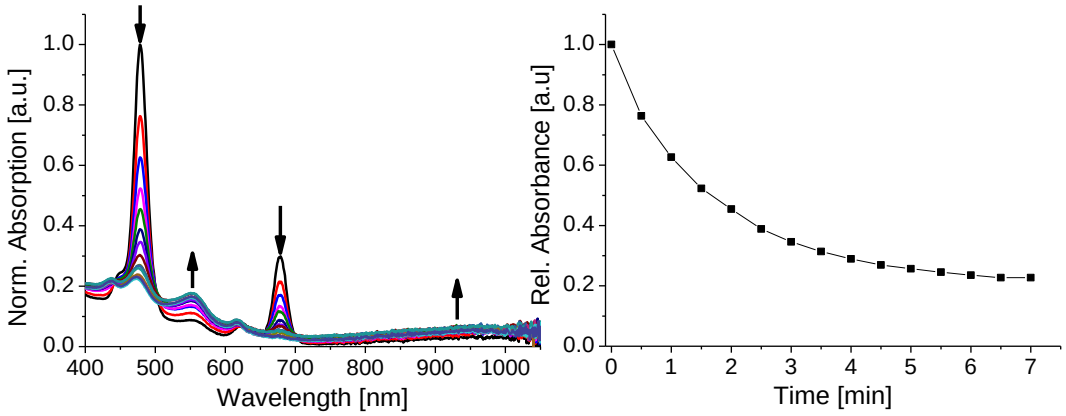

Figure 68 Photodegradation curves for Zn-TPTBPF$_4$bEHT$_4$ complex in deoxygenated toluene solution at room temperature. Irradiation is performed with a blue LED array (λ_{max}=458 nm; 10.79 V, 0.689 A, 7.4 W).

Therefore it was supposed that the formation of the new compound could be an oxidation product from the Zn-TPTBPF4bEHT$_4$ and created highly reactive singlet oxygen through the irradiation. Although the dye exhibits really interesting optical properties such as a Soret band at 478 nm and a Q band at 678 nm in toluene, which is red-shifted compared to the bands of Zn-TBP (Soret band 430 nm and Q band 628 nm) [32] it cannot be used in any sensor for optical measurement if the complex is not photostable. Due to the failed Template condensation of the 4,5-bis(2-ethylhexylsulfonyl)phthalonitrile substituent the only possibility to achieve useful photostability was to oxidize the Zn-complex. The resulting complex is expected to display outstanding photostability values due to the completely oxidized sulfur groups and thereby the increased electron withdrawing character of the porphyrin dye.

For the oxidation of the complex on the one hand m-CPBA and on the other hand DDQ were tested. To avoid partly de-metalation of the Zn-complex and therefore a product mixture because of the acid conditions with m-CPBA, similar to those in the de-metalation step, the Zn-complex was first specifically de-metalated according to experimental procedure. Hereby the yield was not as high compared as for de-metalation step of other benzoporphyrins. First it was assumed that probably the concentrated HCl partly degrades the complex but even after replacement with 4 M HCl the yield did not increase dramatically. Furthermore an interesting shape of the Soret band (Figure 69) was observed in the absorption spectrum, which could be not explained at this time.

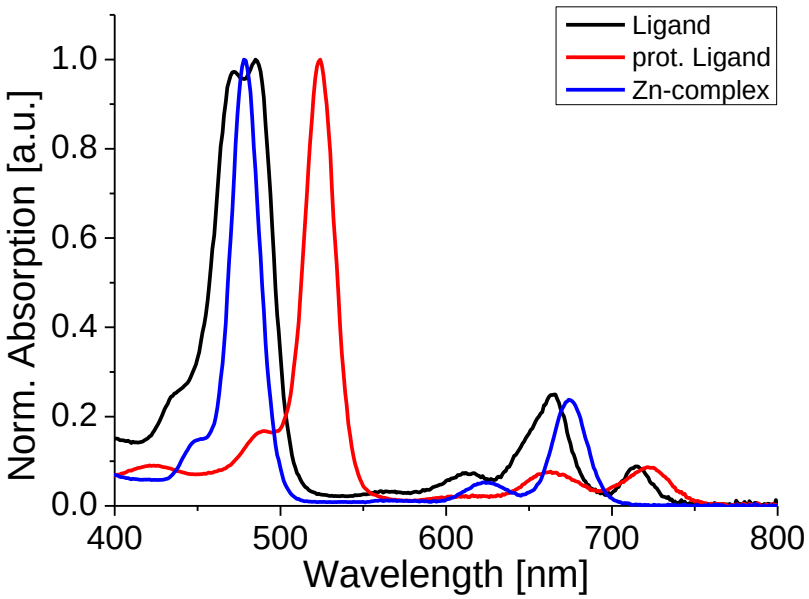

Figure 69 Normalized absorption spectrum of different products during the process of de-metalation of Zn-TPTBPF$_4$bEHT$_4$ complex in acetone solution at room temperature

Obviously a combination of acid and air contact during this procedure led partly to an irreversible degradation of the product. The following oxidation of the ligand with m-CPBA in the dark however led to change in the absorption spectrum, visible through a slight red-shift of the Soret band with increasing degree of oxidation. After addition of 20 equivalents of m-CPBA and approximately 24 hours reaction time no more shift of the Soret band was observed and therefore the reaction was terminated, worked-up and purified according to the experimental procedure. To facilitate purification but also characterization of the oxidized compound it was again metalated with zinc acetate di-hydrate. As can be seen, on the following spectra (figure 70) a clear difference and further also red-shift of the Soret band from the initial Zn-complex (Soret band: 479 nm; Q band: 675 nm), to the oxidized Zn-complex (Soret band: 489 nm; Q band: 673 nm) can be observed in the spectra, whereas the Q band shifts 2 nm to lower wavelengths. Unfortunately the determination of the extinction

coefficients of the oxidized compounds could not be performed, due to the small amount of isolated product, wherefore only the relative intensity is presented in the experimental part.

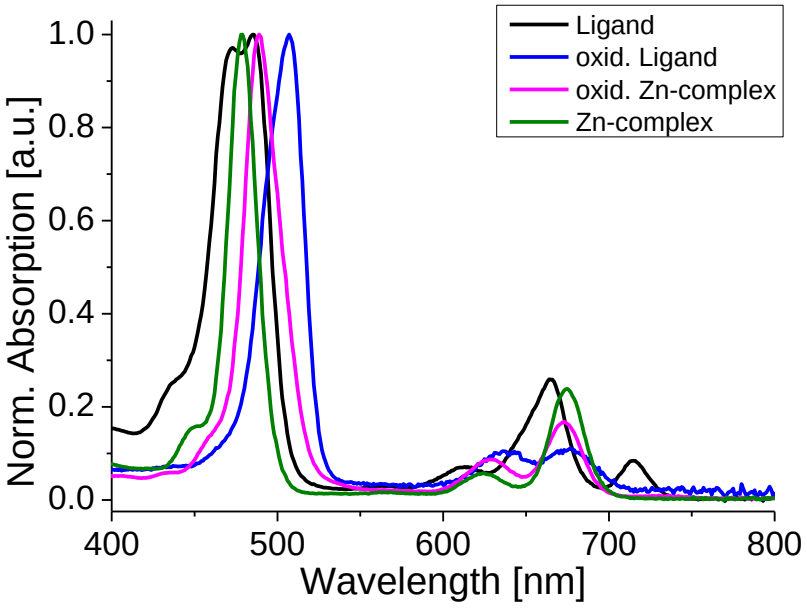

Figure 70 Normalized absorption spectrum of different products during the process of oxidation of TPTBPF$_4$bEHT$_4$-ligand to Zn-TPTBPF$_4$bEHS$_4$ complex in acetone solution at room temperature

The complete oxidation, with overall 16 oxygen atoms coordinated to the sulfurs could be proved with the help of a MS spectrum (figure 71).

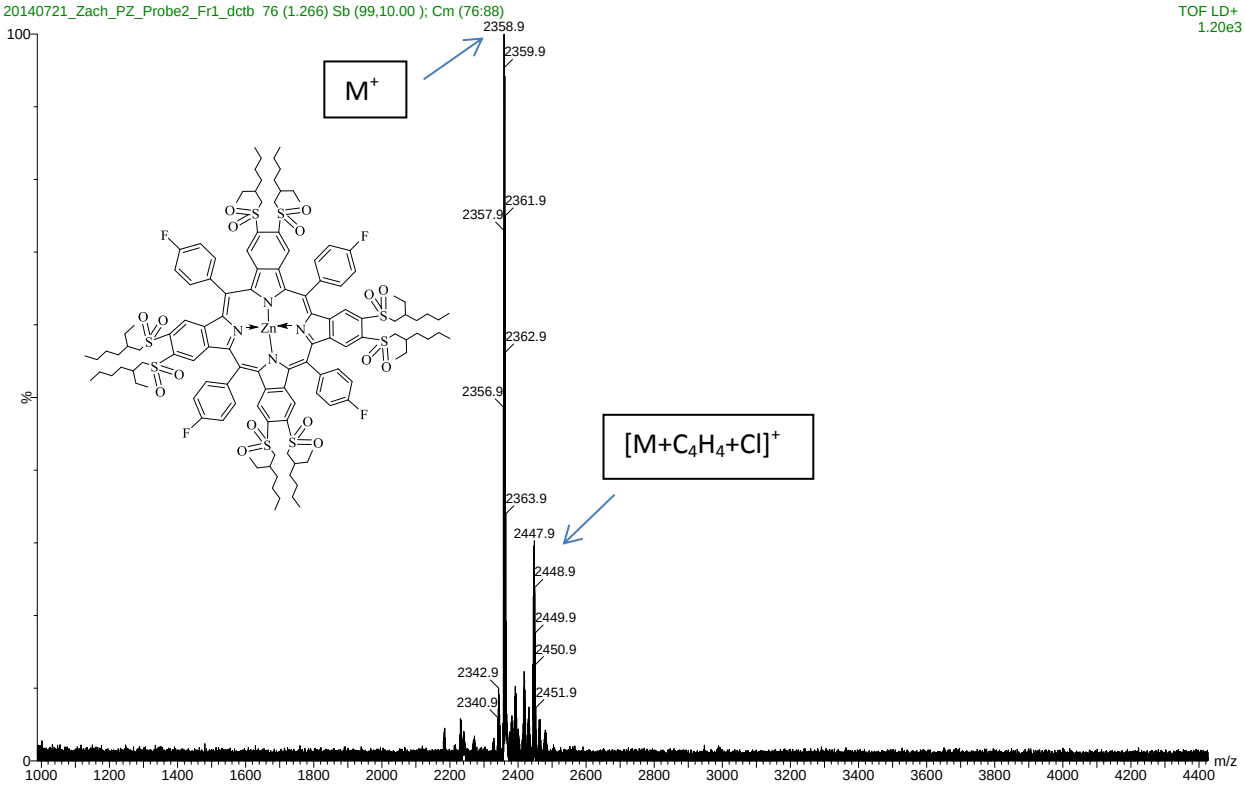

Figure 71 Mass spectra of Zn (II) -meso-tetra(4-fluorophenyl)tetra(4,5-bis((2-ethylhexyl)sulfonyl)benzoporphyrin

In further consequence it could be shown that direct oxidation of the Zn-complex with m-CPBA is also possible and results in the same product with little higher yields than the oxidation of the ligand with following re-metalation with zinc.
The oxidation with DDQ on the other hand did not work out with neither the Zn-complex nor the ligand. Due to time issues the successfully performed oxidation of both the ligand and the Zn-complex could not be up-scaled yet. Based on the shift of the Soret and Q band of the absorption spectrum of known zinc-benzopo phyrins to their respective platinum(II) complexes (TTolTBP, TPTBPdM_4 and TTolTBPmM_4; λ_{max} can be found in experimental part) the Soret band and the Q band of the platinum complex of meso-tetra(4-fluorophenyl)tetra(4,5-bis((2-ethylhexyl)sulfonyl)benzoporphyrin could be expected around 450 nm and 640 nm. This supposition would fit with the Soret and Q band of the imide-substituted dye of Perepichka et al., which is located at 464 and 634 nm in DCM. [4]
All things considered it could be shown that meso-tetra(4-fluorophenyl)tetra(4,5-bis((2-ethylhexyl)sulfonyl)benzoporphyrin received with the template method definitely possess great potential to achieve similar or even better properties (solubility, photostability and probably also red-shift of the Q-band) than then dye synthesized by Perepichka et al. Furthermore this method would provide the advantage of a cheap, not time-consuming and easy to perform synthetic strategy compared to the Lindsey method to yield a really promising new benzoporphyrin dye with outstanding properties and should therefore be focused in future synthetic work.

8.4 Bridging of benzoporphyrins

As previously reported in the theoretical background chapter several ways are already known to achieve absorption of porphyrins in the red part of the spectrum leading to emission of those NIR-dyes in the infrared region above 700 nm. These include fusion with other porphyrins resulting in porphyrin dimers or even oligomers [58], [14] extension of the porphyrins core by fusion of external aromatic fragments (leading to π-extended porphyrins) but also bridging of these fused aromatic fragments (perylenes, anthracenes, …) via thermal fusion [57] or as also shortly mentioned via Scholl-reaction. [24], [57] Until today however no literature is known in which the substituents in the β- and meso-position of a benzoporphyrin are bridged intramoleculary to extend the π-system of the porphyrin. The feasibility of this consideration and the impact on the changed structure properties on the respective benzoporphrin and their prospective field of application are main-part of the purpose of this thesis. To design as many different benzoporphyrin derivatives as possible, the template method was chosen, due to its advantages in cost and time issues versus the Lindsey condensation. While Pt-TPTBP and Pt-TTolBPtert-butyl$_4$ were received from Ass. Prof. kand.

Sergey Borisov, TTolTBP, TPTBPdM_4 and TTolTBPmM_4 were synthesized within this master thesis via the template method. In further consequence it was focused on the Scholl-reaction and the optimization of the conditions for the respective benzoporphyrin dye. Details concerning the Scholl-reaction, their relevancy, their supposed mechanism and their scope of application are presented in the theoretical part in chapter 5.5.6 In the course of the master thesis different zinc and platinum benzoporphyrin complexes were bridged and the resulting compounds examined regarding to their structure via MS and their optical properties via absorption spectrum, in which a bathochromic shift for each dye due to the extension of the π-system was observed. Furthermore, the most promising one was embedded in a polystyrene matrix, characterized and more closely examined (emission, ϕ and τ) for the applicability of an optical oxygen sensor and a sensitizer for triplet-triplet annihilation-based upconversion.

8.5 Scholl-reaction with TPTBP

The first compound which was chosen to proof the concept of extension of the π-system of a benzoporphyrin via intramolecular Scholl-reaction was TPTBP. Before the first test could be started a solvent suitable for the reaction at these high temperatures had to be found, which further does not easily react with the porphyrin itself. Due to the fact that porphyrins are generally electron rich and therefore easily undergo electrophilic aromatic substitution [101], [102] 1,2-dichlorobenzene was chosen as solvent. As Lewis-acid $FeCl_3$, $AlCl_3$ and $MoCl_5$ were screened. Another parameter influencing the reaction was the bubbling of oxygen through the solution during the reaction, to ensure an oxidative environment. Finally the parameters presented in the experimental part were chosen to be best and most reproducible ones to perform this reaction. Whereas the addition of $FeCl_3$ showed almost no effect, the addition of only small amounts of $MoCl_5$ led to a relatively fast decomposition of the platinum complex. Furthermore these studies revealed that the oxidative environment created by bubbling O_2 through the reaction mixture is necessary for the conversion of the reaction.

The Scholl-reaction has to be terminated after the desired absorption spectrum of the bridged complex is observed; otherwise the platinum complex is further bridged resulting in a shift to longer wavelengths and in the extreme case to a complete decomposition of the build complex due to the harsh conditions of the reaction. Another explanation would be that the formed bridged complex becomes insoluble and precipitates during the reaction, due to high degree of bridging (increased planarity) and therefore cannot be determined via absorption spectrum. Before the absorption spectra for the monitoring of the reactions conversion could be recorded a small amount of TEA was added to the dissolved sample to neutralize the formed complex.

With the help of the performed mass spectrum it could be shown that the isolated product is mainly four-fold bridged (figure 72). The spectrum also revealed that beside the main product, different four-fold bridged side-products were formed with substituted chlorine and/or chlorobenzene units, which obviously originates from the used solvent.

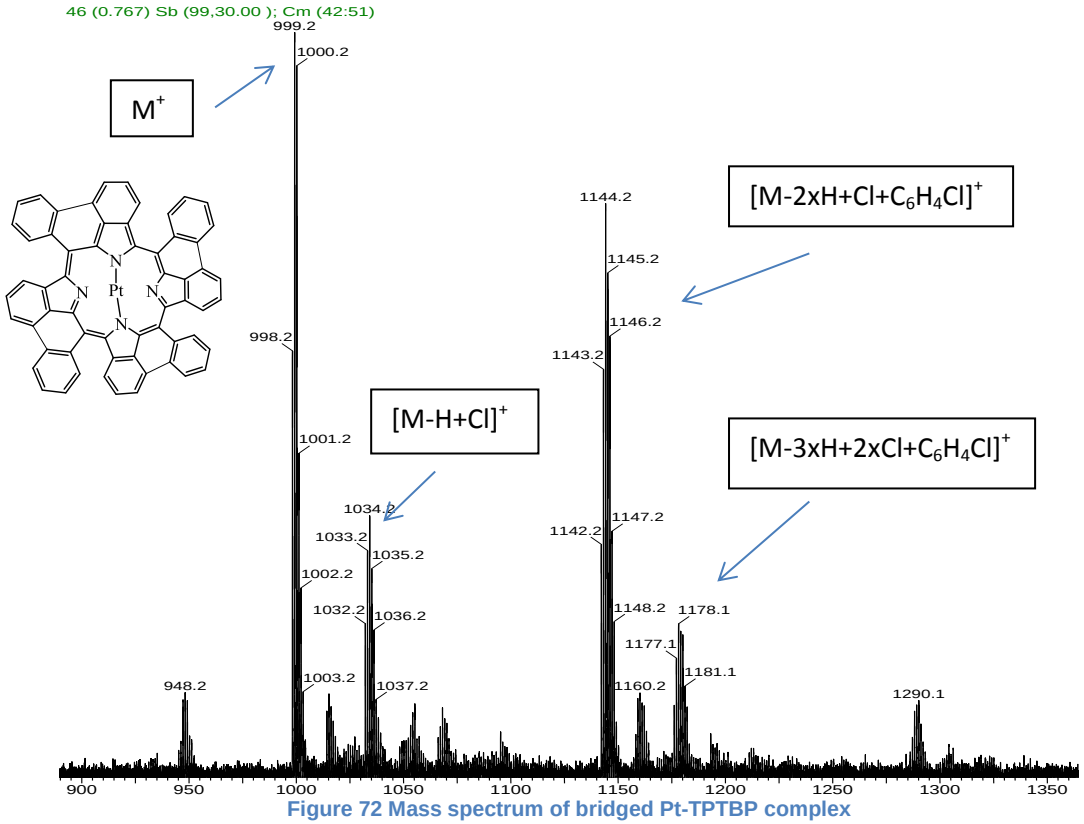

Figure 72 Mass spectrum of bridged Pt-TPTBP complex

Unfortunately it was not possible to separate these four-fold bridged impurities from the product by flash chromatography due to similar behavior on the column but also because of bad overall solubility of the compound. A purification of the compound via preparative HPLC could be performed in future. The solubility of benzoporphyrins is generally not very high [23] and is further significantly decreased by bridging. Through the bridging of the benzoporphyrin the planarity of the complex is even more enhanced than in other unbridged benzoporphyrins leading to an even higher tendency of aggregation due to the increased effect of π-π-stacking. [26] Furthermore the free rotation of the phenyl-groups in meso-position, which normally increase solubility, is completely hindered through the process of bridging. Due to the limited possibilities to remove the solvent-made impurities various other high boiling solvents (naphthalene, bi-phenyl, diphenyl-sulfone, diphenyl-ether and trimethylbenzene) were tested as potential solvents to enable a reaction under such high temperatures. Regrettably, none of these solvents led to the formation of a bridged TPTBP. Therefore it was concluded to design other benzoporphyrin compounds with increased solubility due to the substitution of methyl moieties on the β-position or at the meso-position substituted phenyl rings. This minor changes were not expected to have a tremendous effect on the process of bridging but should ideally increase solubility to a certain point that better

purification or at least better separation of the solvent substituted compounds becomes possible. Despite all the purification problems this experiment has also proved that the concept of intramolecular bridging of TPTBP works and that the desired product can also be isolated even though in relatively low yields. Unfortunately the determination of the molar absorption coefficient for this compound could not be performed, due to the small amount of isolated product, therefore the relative intensity is presented in the experimental part. Furthermore also the expectable and desired red shift compared to the educt could be observed in the absorption spectra (figure 73).

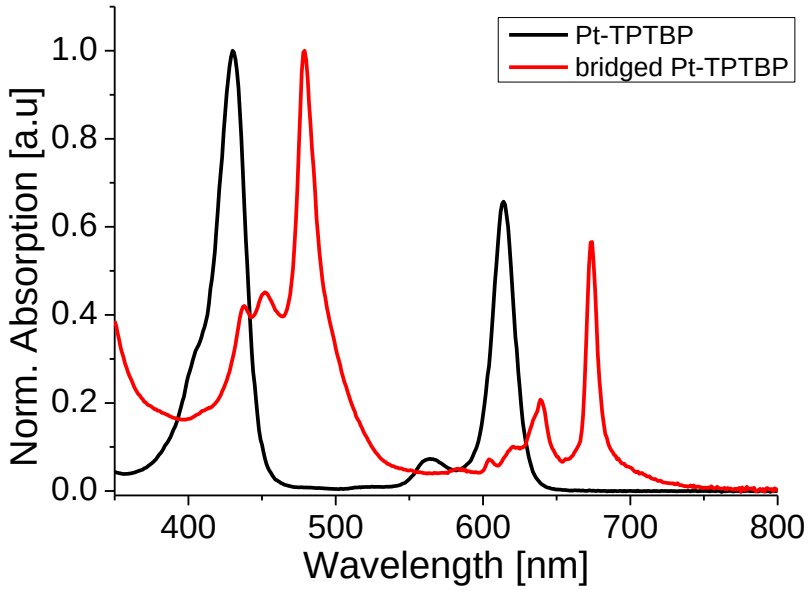

Figure 73 Normalized absorption spectrum of the educt (Pt-TPTBP) and the purified bridged Pt-TPTBP in DCM at room temperature

Hereby the Soret band and the Q band are shifted from 430 and 614 nm to 480 and 675 nm, which means an overall shift of 50 nm for the Soret band and 61 nm of the Q band due to the four-fold bridging of TPTBP. Moreover crude and purified product showed the same distribution of absorption bands, only distinguishable due to the reduced underground of the purified bridged Pt-TPTBP. This confirms that all absorption bands belong to the bridged compound or to the respective product mixture. The Soret band as well as the Q band shows very narrow and defined absorption bands compared to those of Pt-TPTBP before, which is often preferred in various applications to avoid excitation of other compounds. Nevertheless it has to be noted that this absorption spectrum belongs unfortunately not to a specific compound but to a mixture of the desirable product and some side products. Not only for the further research but also for different applications following better solubility remains the most important point to increase within the design of the next compounds.

8.6 Scholl-reaction withTTolTBP

TTolTBP was synthesized using the template method, starting with Phthalonitrile and 2-(p-tolyl)acetic acid, which can be both purchased in large quantities to a moderate price. Zinc-4-tolylacetate was received by an exchange reaction of ZnO and 2-(p-tolyl)acetic acid. The equivalents of the starting materials were optimized through a fast screening process with the aim to achieve Zn-TTolTBP as main product and only little amount of aza-porphyrin and phthalocyanine as side products. Unfortunately still relatively much aza-porphyrin was formed during this reaction, which can be probably explained by the lowered reaction time of 2-(p-tolyl)acetic acid compared with phenyl-acetic acid, due to the electron donating effect of the methyl moiety. The phenyl-acetic acid with the methyl-residue probably reacts slower with the phthalonitrile during the Template synthesis process, leading to a higher degree of aza-porphyrin formation compared to TTolTBP formation. Furthermore mass spectrum analysis of both the zinc and the platinum complex after purification revealed obviously the respective product, but also product with two and four condensed phenyl rings as side product (figure 74). Interestingly, such products were not observed for other porphyrins using the Template synthesis with dicyanobenzene, but are well-known for Template condensation using phthalimide. [121]

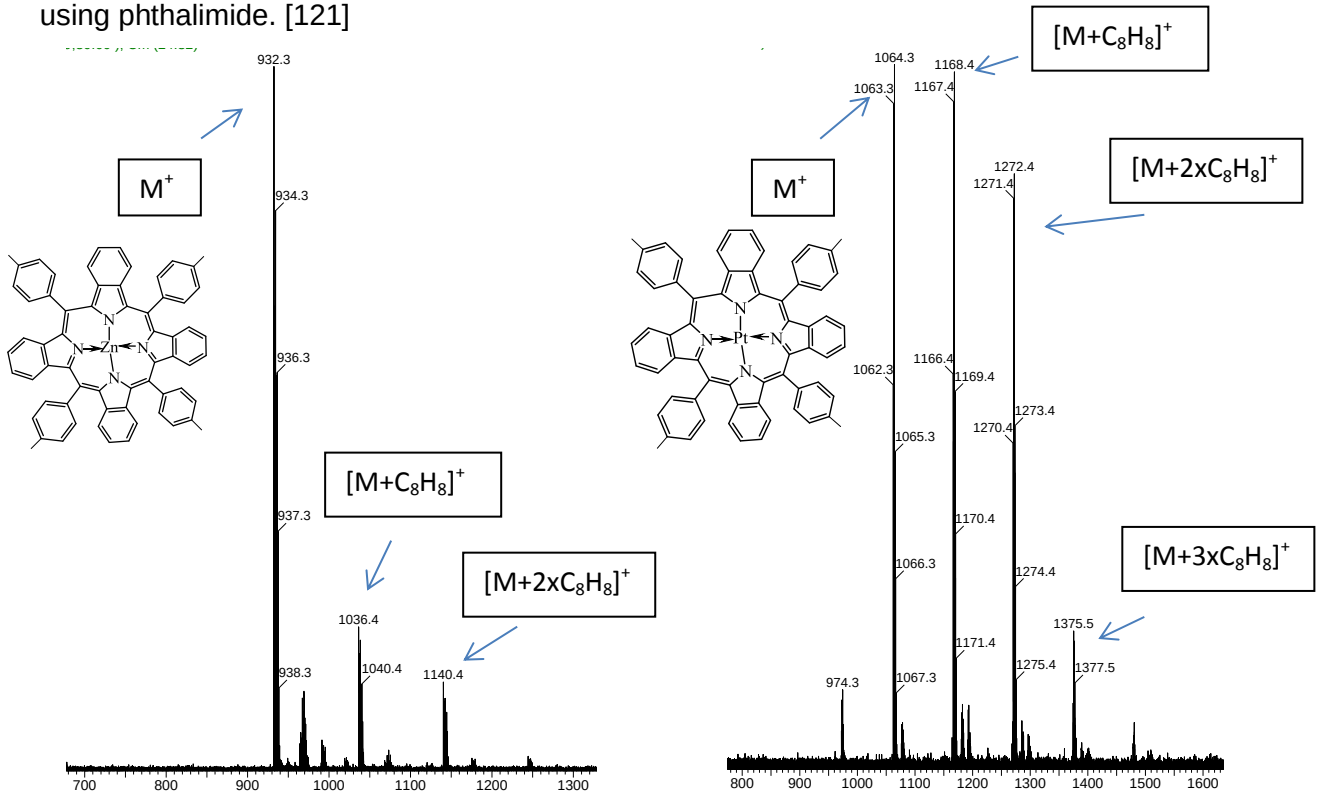

Figure 74 Mass spectra of Zn-TTolTBP (on the left) and Pt-TTolTBP (on the right) synthesized using the template method

The unwanted condensation of phenyl rings is a known problem of the template method and has been already observed several times within the synthesis of different other benzoporphyrin complexes. Also in this case the separation of those impurities via flash chromatography was not possible. Furthermore the MS spectrum of the platinum complex

shows an increased amount of condensed side-products, leading to the assumption that on either the condensed side-products were favorably collected or the main product (according to the MS spectrum of the zinc complex) was lost during the de-metalation or the platination step. The inseparable impurities could also be a reason for the problems within the course of the platination reaction and the resulting low yields of just 12%. The purification of the received platinum(II) complex was generally challenging due to the viscous consistency of the product. A similar problem was already once observed within the master thesis of Bernhard Müller, were he assumed an encapsulation of TMB (solvent for the platination reaction), between two dyes which are linked together by π-stacking effects. For this reason the purification of the Pt-TTolTBP was performed under high vaccum in a round flask with a cold finger by heating the product up to 350°C. Hereby the viscous film was deposited on the cold finger, whereas the pure and crystalline product remained on the bottom of the round flask. The de-metalation step however was performed without any problems.

Due to the higher amount of side-product (with condensed phenyl rings) in the platinum(II) complex compared to the zinc complex the bridging of the Pt-TTolTBP compound was quit. The Zn-TTolTBP was however bridged with 15% yield in a Scholl-reaction leading to an interesting insight. In contrast to the bridging of the platinum complex, the zinc complex was subsequently de-metalated in 1,2-dichlorobenzene after addition of $AlCl_3$. Since the resulting protonated ligand is not as electron rich as a platinum metal complex the process of bridging occurs much slower, yielding only a one bridged unit compared to the four-fold bridged platinum complex. If the reaction is continued and not stopped after the first bridging the ligand is rather decomposed than bridged a second time. The formation of the one-fold bridged ligand could also be proved by mass spectroscopy after work-up, purification and re-metalisation with zinc acetate di-hydrate. Unfortunately the determination of the molar absorption coefficients for both, the bridged Zn-TTolTBP as well as the later mentioned bridged Zn-TTolTBPmM_4 compound could not be performed, due to the small amount of isolated product, thus the relative intensity is presented in the experimental part. As it was the case with the bridged Pt-TPTBP, inseparable side products (with substituted chlorine of 1,2-dichlorobenzene) are also observed in the mass spectrum (figure 75). Although in the case of Zn-TTolTBP only one bridged unit was formed, a clear shift to the red part of the spectrum is observed (figure 76).

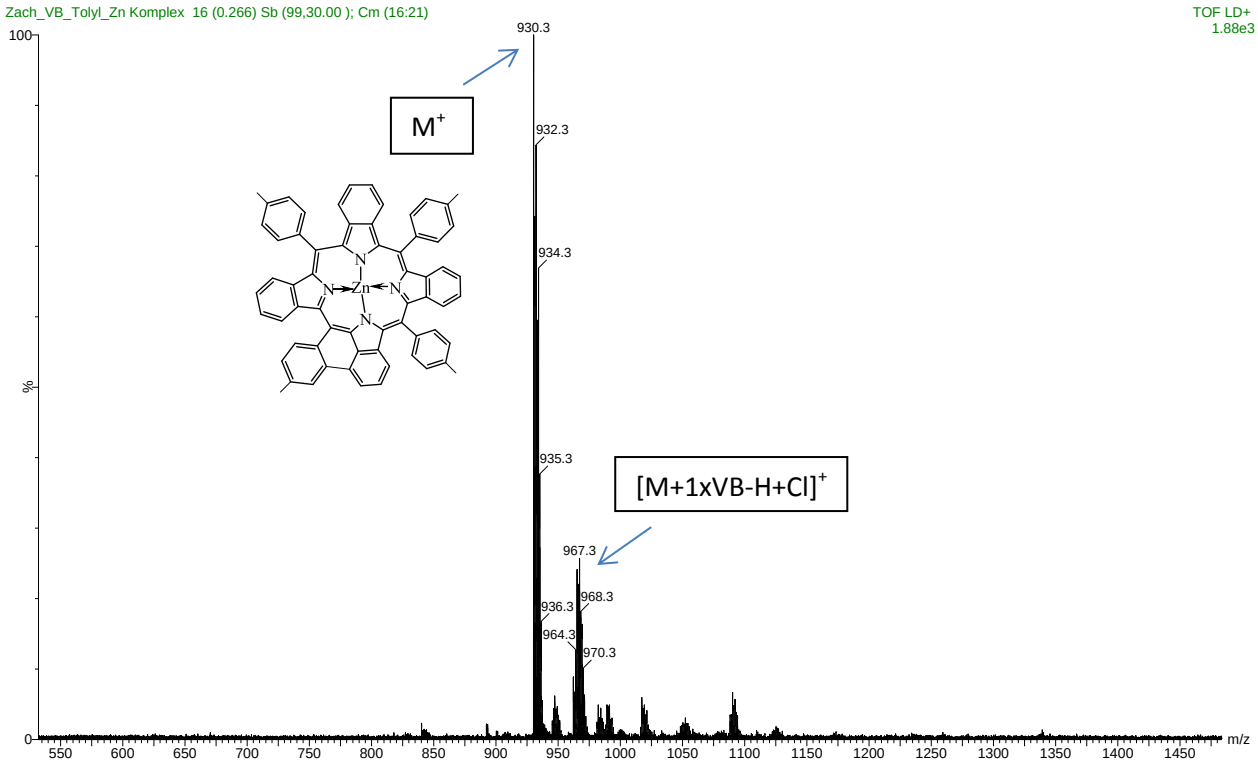

Figure 75 Mass spectrum of one-fold bridged Zn-TTolTBP

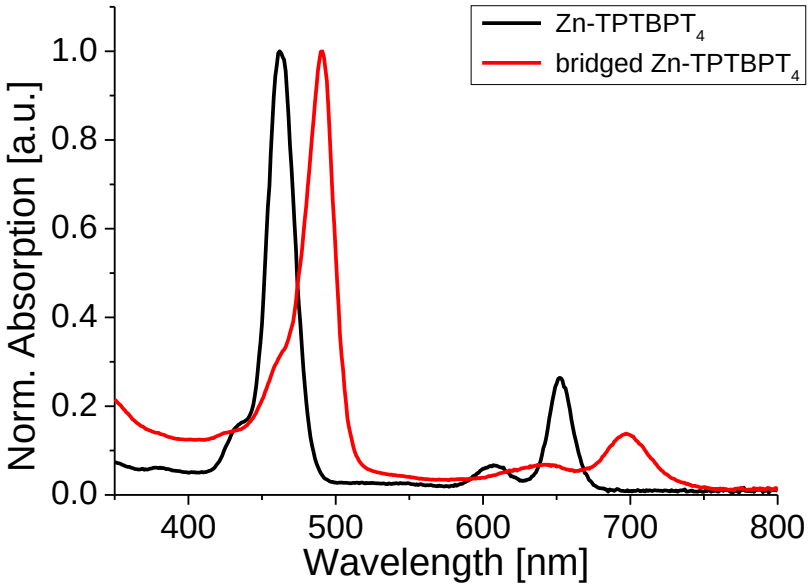

Figure 76 Normalized absorption spectrum of the educt (Zn-TTolTBP) before the reaction and the product (bridged Zn-TTolTBP) after the Scholl-reaction in DCM with small amounts of TEA at room temperature

It can be concluded, that the Pt-TTolTBP possesses on the one hand clearly increased solubility compared to the Pt-TPTBP but could on the other hand not be used for the examination of the Scholl-reaction due to inseparable side products. Therefore the aim for the design of the next benzoporphyrin compound is to regulate the solubility over substitution of the β-β-positions in the hope that this will not affect the formation of the respective zinc complex during the Template synthesis and will so avoid formation of unwanted phenyl ring substituted side products.

8.7 Scholl-reaction with TPTBPdM$_4$

The design of the new benzoporphyrin with additional four methyl moieties compared to TTolTBP and so in total eight methyl moieties was expected to improve the solubility and to prevent the formation of impurities (condensed phenyl rings) during the Template synthesis through modification at the β-β-positions of the porphyrin core. Furthermore, it should be noted that this dye despite the many methyl groups is still highly symmetrical. The starting materials were not commercially available and were synthesized. Due to the very small yield and the poor selectivity for the para position at the ring system despite many failed attempts to optimize the reaction, it was finally concluded to buy the 1,2-dibromo-4,5-dimethylbenzene compound. Beginning with this compound the Rosenmund von Braun reaction yielding 1,2-diethynyl-4,5-dimethylbenzene was performed. Nevertheless, the two methyl moieties in the para-position to the bromine atoms promote this reaction, the Rosenmund von Braun reaction is generally known in literature to receive low yields. [123] Also according to the literature [118] which served as model for this reaction the yield was relatively low with 48%. Significant increase (84%) of the yield was achieved by conducting the reaction under inert atmosphere in dry DMF. A repetition of the reaction using a round-bottom flask and a reflux condenser sealed with a dry tube filled with $CaCl_2$ led not only to very low yield (12%) but also to a mixture of mono- and di-substituted product, which could then be separated only in an elaborate process of recrystallization.

The synthesis of Zn-TPTBPdM$_4$ was this time performed without any problems, leading to the formation of the zinc complex in 6% yield. Furthermore the de-metalation step and the platination proceeded trouble-free and in good yields of 85% and 56%. The insertation of platinum in the metal-free porphyrin is a crucial step for the synthesis of a platinated dye following the Template reaction pathway. For a successful performance of the reaction HCl, which is released during the insertion of platinum in the porphyrin, has to be removed from the reaction via N_2 bubbling. Otherwise HCl leads to protonation of the ligand, which further reduces its solubility and so finally inhibits the process of metalation. This can be controlled on the one hand through the amount of nitrogen bubbled through the solution or on the other hand through the quantity of added Pt-precursor, which has to be dissolved in a preheated TMB. To avoid side-reactions it is important that the addition of the Pt-precursor is not too fast. Although reaction time should be kept as short as possible due to the relatively harsh reaction conditions (high temperatures) and the destructive role of the decomposed residues of the Pt-precursor. For a successful reaction the accomplishment of good and reproducible balance of all equilibriums (like in the experimental procedure) is very important. This has to be of course also adapted for each different benzoporphyrin dye according to its properties (solubility, etc.).

This time no condensation of phenyl rings as side product could be observed from the mass spectrum which is probably due to the higher solubility of the eight methyl moieties and the

following facilitation of the purification via flash chromatography. Another reason could be a better interaction between the 4,5-dimethylphthalonitrile and the zinc-phenylacetate during the Template synthesis, which may be due to similar reaction speed of these two compounds. Also the position for the condensation of the benzyl rings may be occupied by the methyl-groups at the β-β-positions of the porphyrin. Unexpectedly, the bridging of both the zinc and the platinum complex was not successfully (figure 77 and 78).

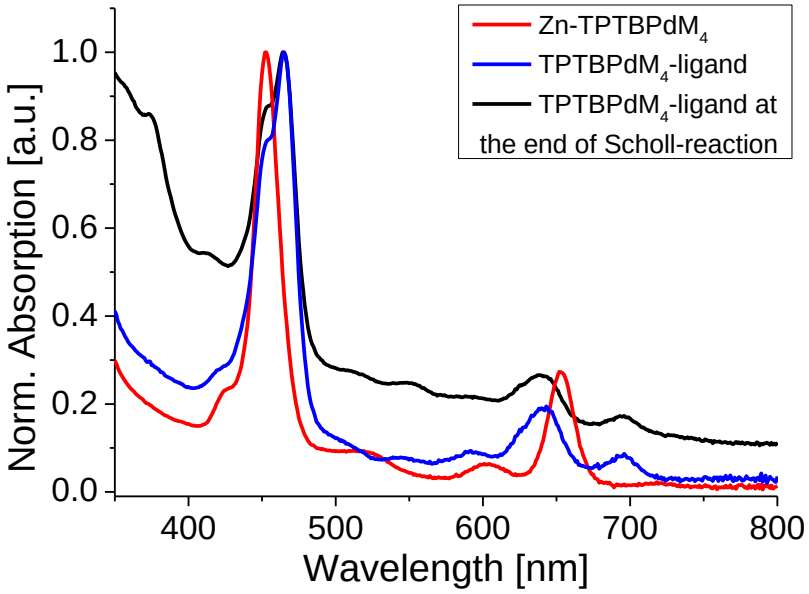

Figure 77 Normalized absorption spectrum of the educt (Zn-TPTBPdm$_4$) before the reaction and the un-bridged (TPTBPdm$_4$-ligand) after the Scholl-reaction in DCM with small amounts of TEA at room temperature

In the case of Zn-TPTBPdM$_4$ formation of the bridged complex was not observable even after addition of $MoCl_5$. The observed bathochromic shift in figure 77 shows only the neutral form of the ligand and not the bridged species as seen before with TTolTBP. In the case of Pt-TPTBPdM$_4$ the addition of 300 equivalents of $AlCl_3$ and 100 equivalents of $MoCl_5$ led to formation of a bridged compound, but at very low yield, before the Pt-TPTBPdM$_4$ complex was destroyed due to the harsh conditions (huge excess of $AlCl_3$ and $MoCl_5$). (figure 78)

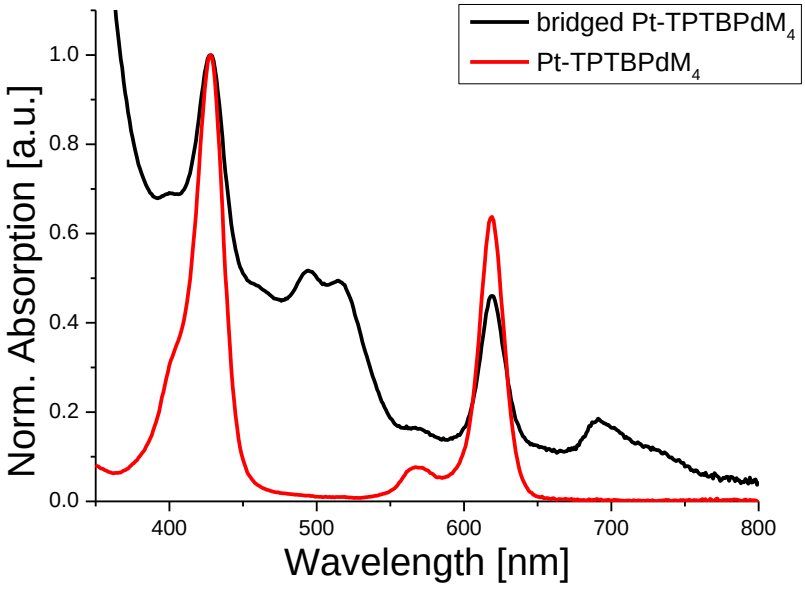

Figure 78 Normalized absorption spectrum of the educt (Pt-TPTBPdm$_4$) before the reaction and a mixture of educt and partly bridged product after the Scholl-reaction in DCM with small amounts of TEA at room temperature

One reason for the unsuccessful bridging reaction could be that the $AlCl_3$ could not undergo addition due to the steric effects caused by methyl moieties at the β-position. Another reason could be that the resulting arenium-cation (under the assumption of the areniumcation mechanism) or the radical-cation (under the assumption of the radical cation mechanism) is very good stabilized by the two methyl moieties so that the C-C bond formation is not achieved easily.

However, in order to exclude the argument of steric hindrance it was concluded to design another benzoporphyrin dye with similar solubility properties but with only one unsubstituted β-position at each side of the porphyrin.

8.8 Scholl-reaction with TTolTBPmM$_4$

The synthesis was aimed to investigate the possibility of tuning the degree of bridging through the introduction of only one methyl moiety at the β-position of the porphyrin and on the other hand by achieving simultaneously similar solubility properties compared to the TPTBPdM$_4$ due to the eight methyl moieties overall.

Two of the starting materials (mono-methylphthalonitrile and 2-(p-tolyl)acetic acid) for this synthesis were commercially available, whereas the zinc-4-tolylacetate was received by an exchange reaction of ZnO and 2-(p-tolyl)acetic acid. The synthesis of the Zn-TTolTBPmM4 complex was performed with moderate yield of 6% after optimization of the reaction conditions and equivalent ratio of the compounds. The following de-metalation step and the platination of the ligand occurred without any problems. According to the mass spectra both

the zinc and the platinum complex could be almost or completely purified via flash chromatography. The bridging reaction of the Zn-TTolTBPmM$_4$ compound could be performed more or less successfully according to the absorption spectra obtained during the reaction (figure 79).

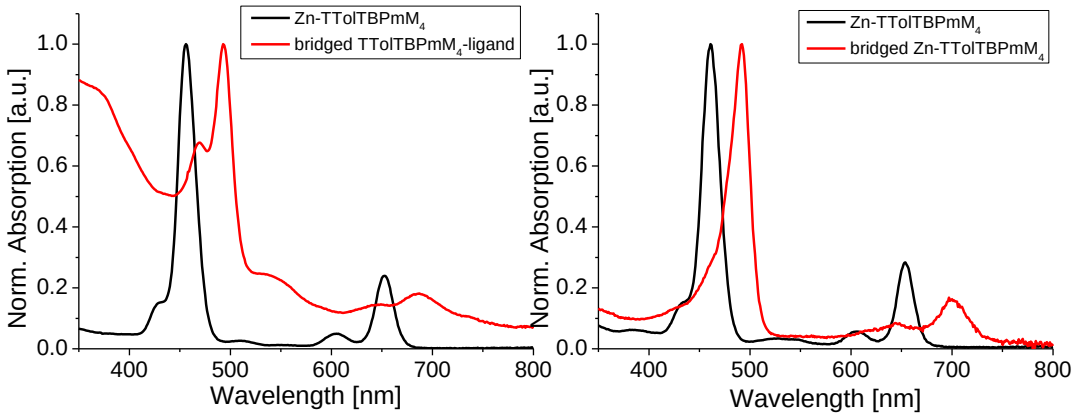

Figure 79 Normalized absorption spectrum of the educt (Zn-TPTBPmM$_4$) before the reaction and the product (bridged TPTBPmM$_4$-ligand) after the Scholl-reaction in DCM with small amounts of TEA at room temperature (left) and the Zn-TPTBPmM$_4$ and bridged Zn-TPTBPmM$_4$ after re-metalation of bridged TPTBPmM$_4$-ligand (right)

Unfortunately after workup, purification and re-metalation with zinc acetate di-hydrate the bridged product could be only isolated in very low yield. Notably at this point is also that the Scholl reaction of Zn-TTolTBPmM4 took approximately 2 hours with a yield of 2% compared to the Scholl reaction of Zn-TTolTBP which was completed within 30 minutes with a yield of 15%. Reason for this result could be that the un-substituted β-position of this benzoporphyrin is indeed accessible (or the resulting cation not that good stabilized) compared to the TPTBPdM$_4$ but provides no completely steric un-hindered access like in the case of TTolTBP. Scholl reaction in this compound is therefore possible, but proceeds with lower speed and lower overall yields due to the degradation of the ligand during the Scholl-reaction because of the harsh conditions. Therefore the β-positions of the porphyrin might play a very important role within intramolecular Scholl-reaction. Despite these differences during synthesis, the mass spectra of these two compounds look very similar. Also here only one fold bridging could be observed accompanied with other species as side-product in which one hydrogen atom was substituted by on chlorine atom (figure 80).

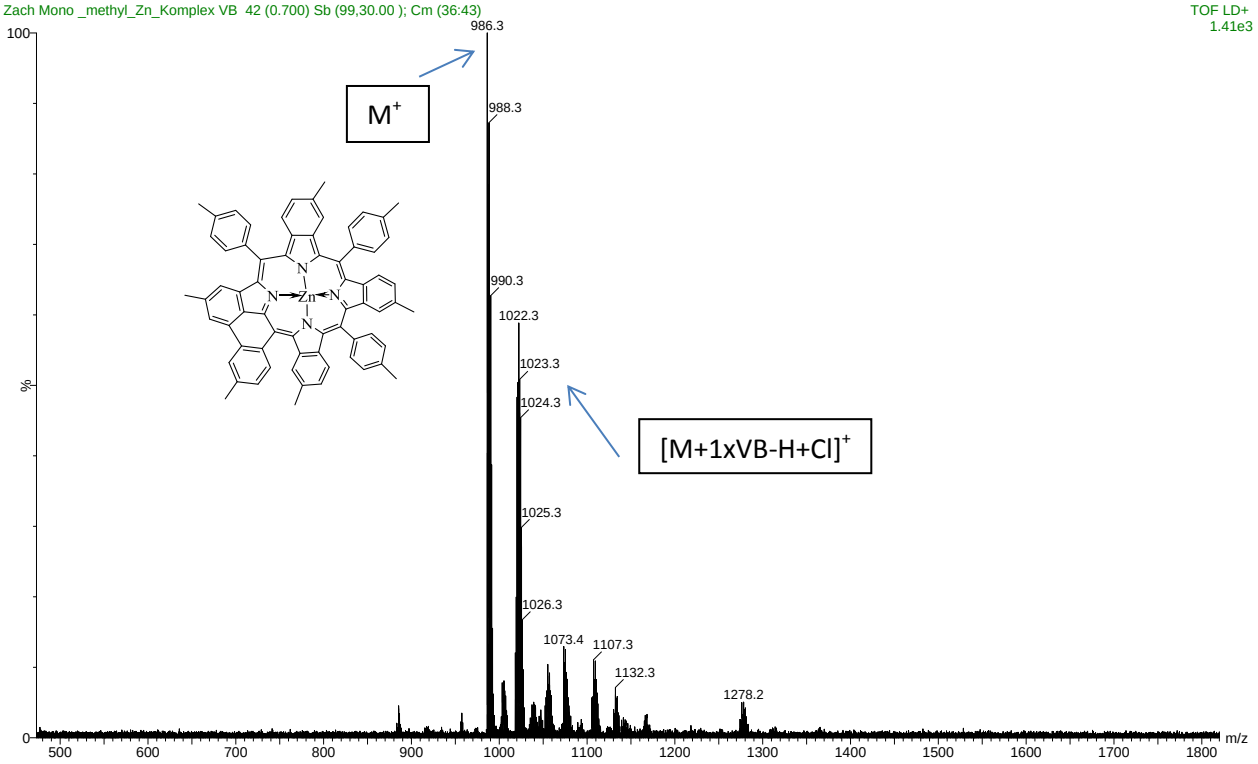

Figure 80 Mass spectrum of one-fold bridged Zn-TTolTBPmM$_4$

Next, the Scholl-reaction of the Pt-TTolTBPmM$_4$ was conducted, which led to unexpected results. The first attempt to bridge this complex following the standard experimental procedure used for all other benzoporphyrins so far failed, even though at the end of the reaction before the whole platinum complex was destroyed, little conversion to another species (red shifted in the absorption spectrum) could be observed (figure 81).

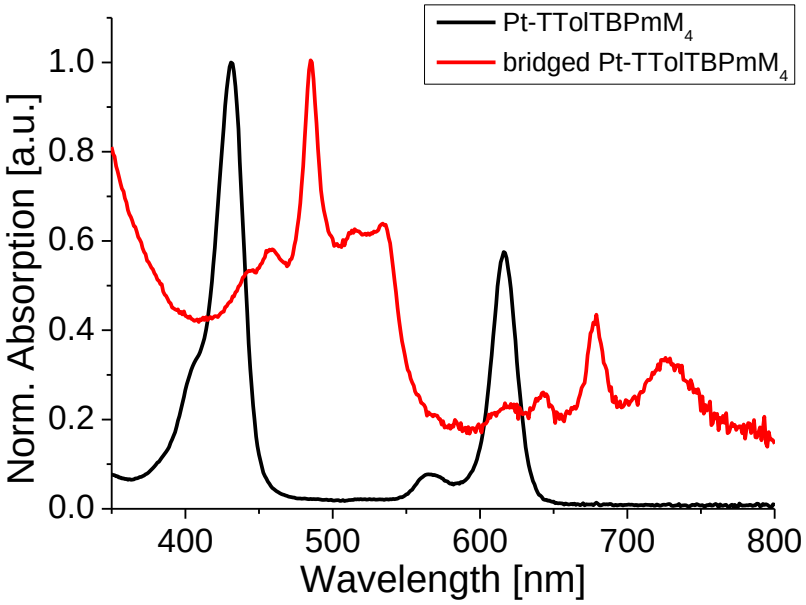

Figure 81 Normalized absorption spectrum of the educt (Pt-TPTBPmM$_4$) before the reaction and little amounts of bridged product after the Scholl-reaction in DCM with small amounts of TEA at room temperature

Based on this insight the second attempt was performed at a lower heating rate. Even though the temperatures were lower than the first time the degradation of the platinum complex occurred at same speed. This time almost no conversion to the species absorbing at higher wavelengths could be seen. This result is especially strange due to the usually higher stability of a platinum complex compared to a zinc complex. Up to that point, unfortunately, no reasons or suppositions for the behavior of the Pt-TTolTBPmM$_4$ complex in the Scholl-reaction could be found.

Due to the unsuccessful bridging of the unsymmetrically Pt-TTolTBPmM$_4$ it was concluded to design another dye with maximal solubility, since this was one important limitation of to date most successfully bridged Pt-TPTBP.

8.9 Bridging of TTolTBPtert-Butyl$_4$

Pt-TTolTBPtert-Butyl4 was received from Ass. Prof. kand. Sergey Borisov. The following conducted Scholl-reaction under the described optimized conditions was performed with 8% yield. The educt of the reaction and the crude product can be seen in figure 82.

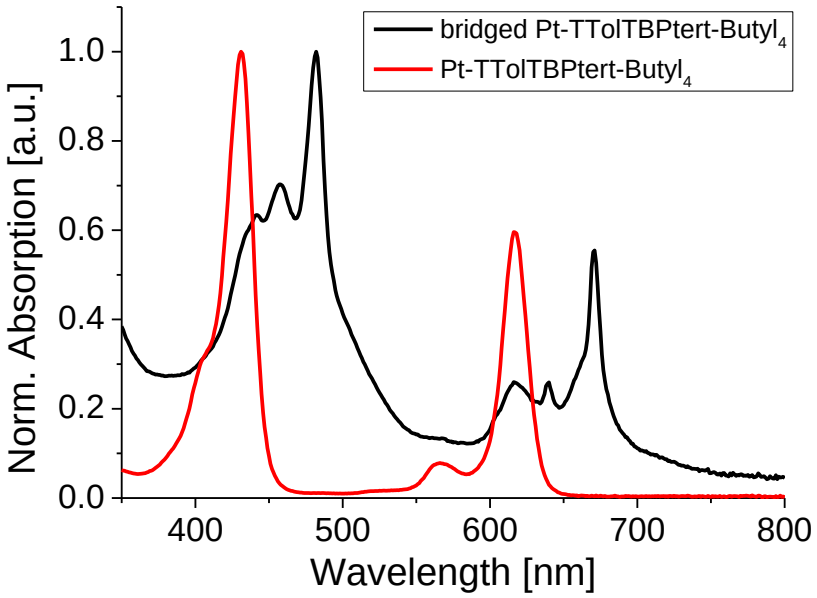

Figure 82 Normalized absorption spectrum of the educt (Pt-TTolTBP tert-Butyl$_4$) before the reaction and the product (bridged Pt-TTolTBP tert-Butyl$_4$) after the Scholl-reaction in DCM with small amounts of TEA at room temperature

After work-up and a challenging purification via flash chromatography due to the complex product mixture formed in this reaction; finally three compounds, showing different characteristic absorption spectra, could be isolated (figure 83).

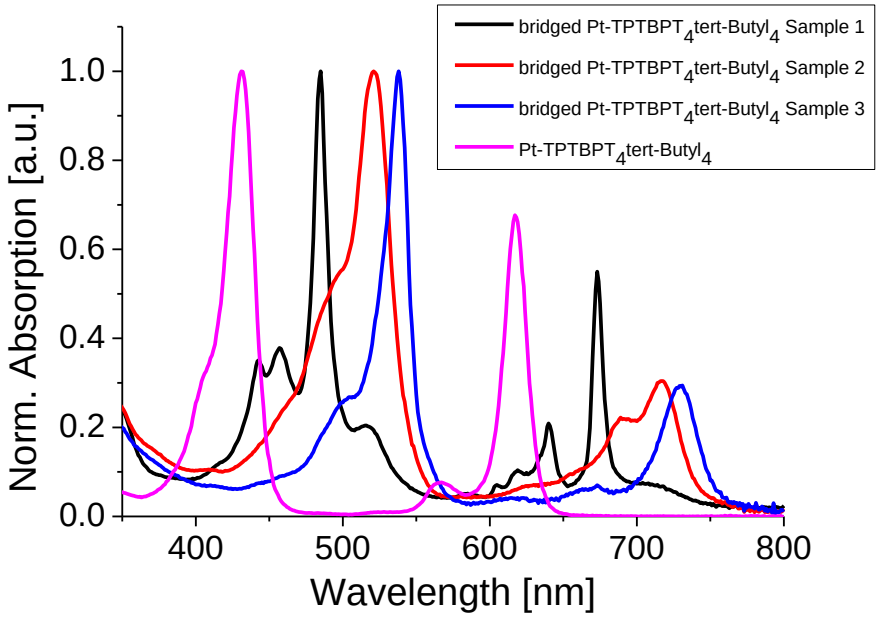

Figure 83 Normalized absorption spectrum of the educt (Pt-TTolTBP tert-Butyl$_4$) before the reaction and the three samples showing different characteristic absorption spectra after purification of the isolated product (bridged Pt-TTolTBP tert-Butyl$_4$) in toluene at room temperature

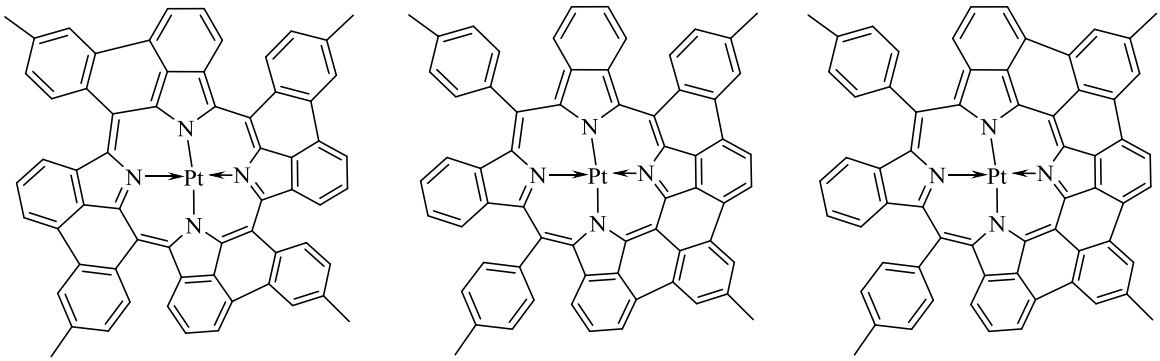

Figure 84 Assumption of the chemical scaffold of the four-fold bridged main product Pt-TTolTBP (Sample 1), the three-fold bridged Pt-TTolTBP (Sample 2) and the four-fold bridged Pt-TTolTBP (Sample 3) according to the mass and absorption spectra without illustration of substituted tert-butyl groups or chlorine atoms observable in respective mass spectra of the compounds

According to the mass spectra (figure 85-88) the above shown three structures (figure 84) ould be assigned to the three different absorption spectra. In the following the mass spectra of Sample 1 (proof-of-concecpt-synthesis and up-scale synthesis), Sample 2 (up-scale synthesis) and Sample 3 (up-scale synthesis) are presented.

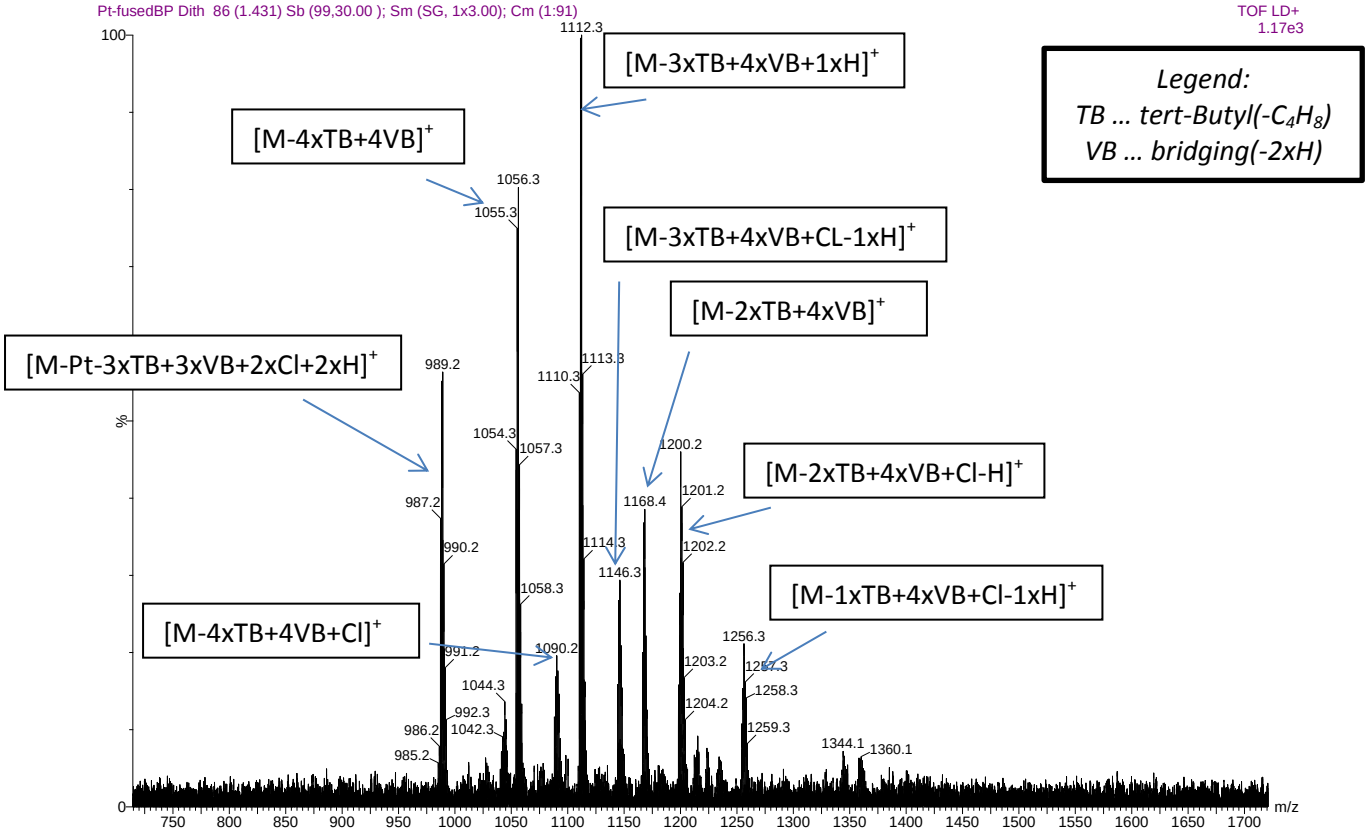

Figure 85 Mass spectrum of the four-fold bridged main product Pt-TTolTBP of the proof-of-concept-synthesis

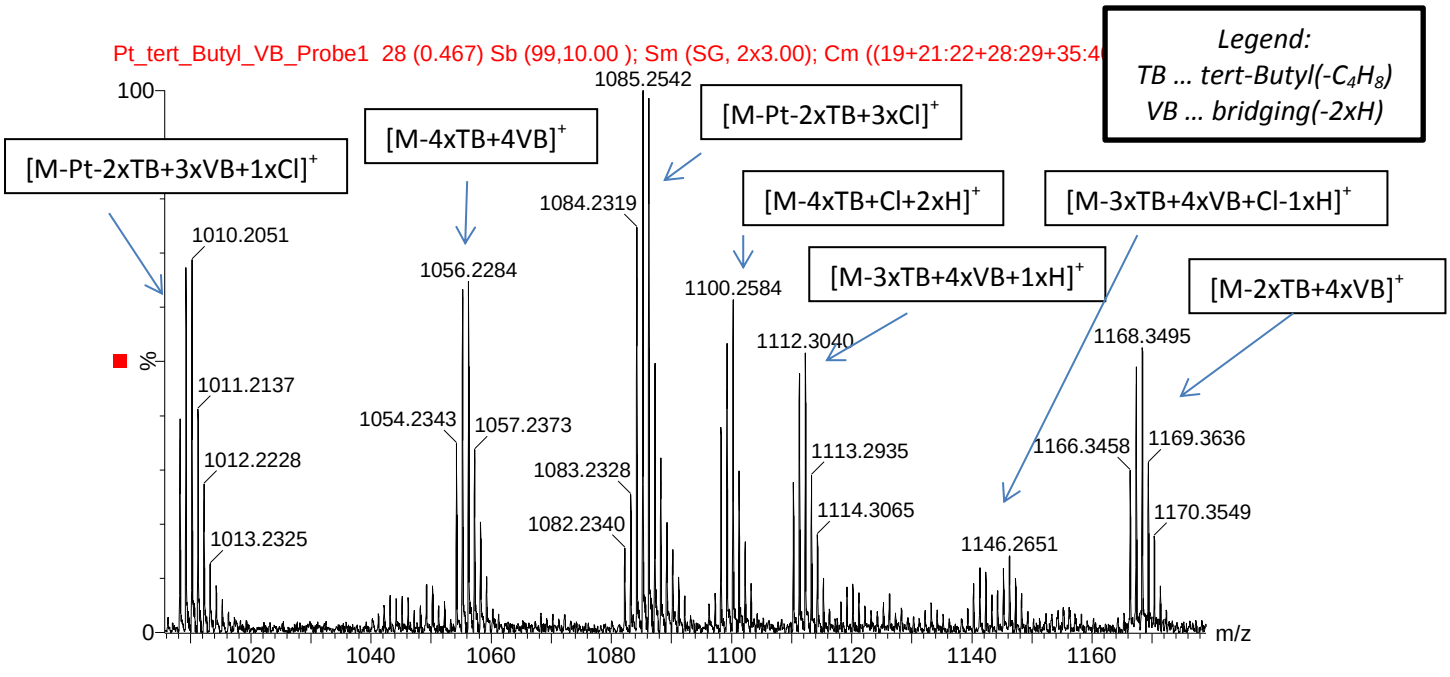

Figure 86 Mass spectrum of the four-fold bridged main product Pt-TTolTBP (Sample 1) of the up-scaled synthesis

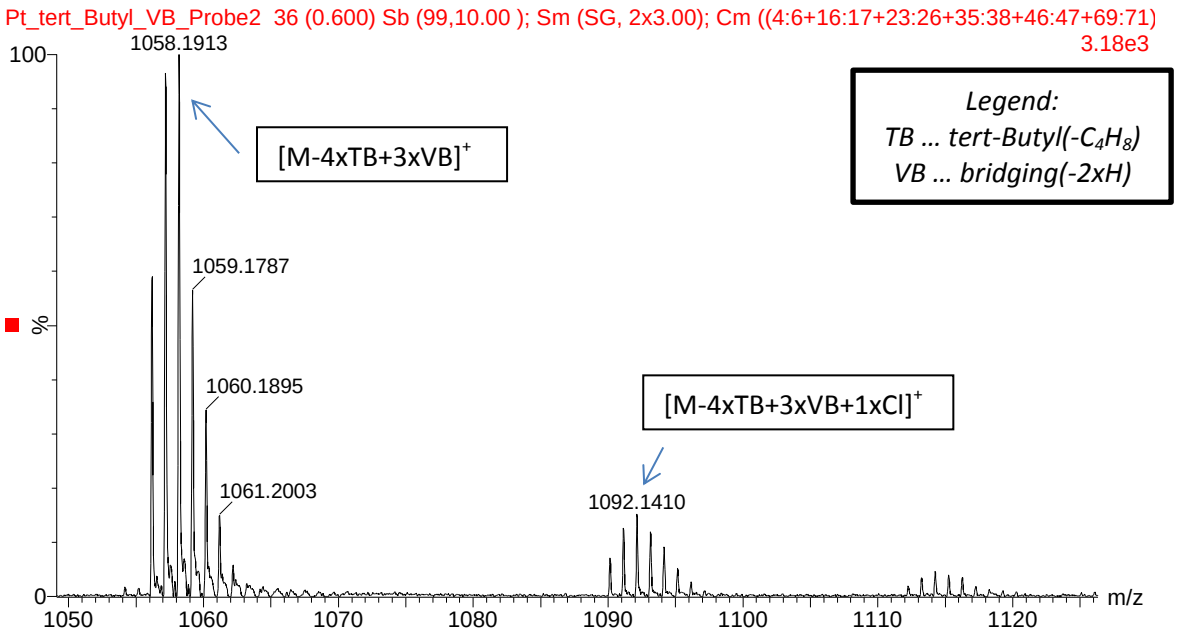

Figure 87 Mass spectrum of the three-fold bridged Pt-TTolTBP (Sample 2) of the up-scaled synthesis

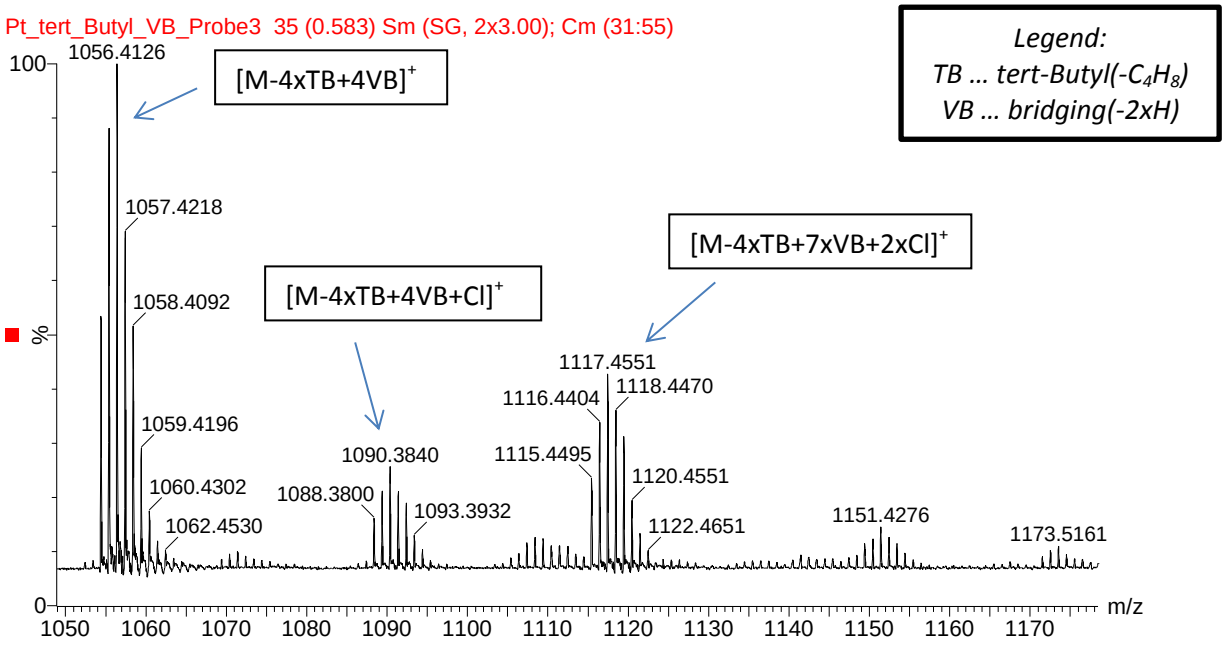

Figure 88 Mass spectrum of the four-fold bridged Pt-TTolTBP (Sample 3) of the up-scaled synthesis

It should be noted that the product mixture of the proof-of-concept-synthesis shown in figure 85 and the up-scaled synthesis (figure 86) resulted in the formation of a different product distribution concerning the mass spectrum, even though the absorption spectra look the same. This observation leads to the assumption that the product mixture of this synthesis will also vary in future, necessitating a characterization of each produced batch, making it more challenging even though the product is actually obtained in one single synthetic step. Moreover the inseparable (at least via flash chromatography) formed product mixture makes the determination of a single chemical structure for the four-fold bridged main product Pt-TTolTBP (Sample 1) via NMR or x-ray spectroscopy impossible. The position of e.g. the

Soret band (486 nm) in the absorption spectrum (figure 83) compared to the other two products (521 nm or 539 nm) induces however the assumption of the presented pattern of bridging. This assumption is supported by the shape of the absorption spectrum for the four-fold bridged main product Pt-TTolTBP (Sample 1) enabling also the presence of un-bridged or bridged ligands as well as un-bridged platinum complex. Also the occurrence of the four-fold bridged species without any tert-butyl groups, which seems to be main component of the bridged Pt-TTolTBP (Sample 3), confirms the assumption of the presented-bridging pattern. Or the four-fold bridged Pt-TTolTBP (Sample 3) is likely to ionize better than the supposed seven-fold-bridged species and is therefore more visible in the mass spectrum. But to confirm this assumption a purification of Pt-TTolTBP (Sample 3) using the preparative HPLC would be required.

The distribution of the peaks for the four-fold bridged main product Pt-TTolTBP (Sample 1) can be explained through different de-alkylation processes of tert-Butyl groups but also through addition of chlorine atoms of the used solvent to the platinum complex (figure 85 and 86) probably due to the harsh conditions of the reaction. Friedel-crafts de-alkylation of tert-butyl groups, catalyzed by the huge excess of $AlCl_3$ in the reaction, is easily achieved, since the tert-butyl groups, in contrast to methyl groups, are able to stabilize themselves. Nevertheless the mass spectrum shows that the formation of the four-fold bridged species is favored, since also nearly all side products show a four-fold bridged structure. Surprisingly such a variety of peaks is not observed in the mass spectra of the three-fold bridged Pt-TTolTBP (Sample 2) in figure 87 and the four-fold bridged Pt-TTolTBP (Sample 3) in figure 88, which possess the further red-shifted absorption spectra compared to absorption spectrum of Pt-TTolTBP (Sample 1) even though also here traces of side products could be found. Hereby sample 2 could be identified as three-fold bridged compound with no tert-butyl group left, whereas sample 3 is mostly four-fold bridged equally with no tert-butyl group left. The assumption of the chemical structures and the bridging pattern for the two products presented in figure 84 is supported by the observable red-shift in the absorption spectra presumably originating from an extension of the π-system and could be possibly clarified via quantum mechanics simulation.

The absorption spectrum of all three samples is clearly red-shifted compared to the educt. Furthermore they are excitable in the red part of the spectrum or even in the NIR region making them potential dyes for oxygen sensing and many other applications in the field of medicine. Notably, at this point is that the process of bridging significantly shifts both the Soret band as well as the Q band to longer wavelength. The comparison of the recorded absorption spectra and the excitation spectra for each bridged Pt-TTolTBP Sample (figure 89 and 90) showed that the respective compounds were relatively pure and no mixture of

different bridging patterns. Differently substituted compounds with e.g. tert-butyl groups or chlorine atoms however show no influence on the absorption. Therefore it can be noted that all major bands in the respective absorption spectra really belong to the isolated porphyrin-compounds. This information could not be obtained via mass spectroscopy, since all compounds contained in the samples show different ionization. The green arrows display some impurities in Sample 1 which could not be separated via flash chromatography. Most probably this impurity belongs to Sample 2. Due to the emission at different wavelengths of Sample 1 and 2, this band is only observable in the absorption spectrum but not in the excitation spectrum. The black arrows mark the band at half wavelength of the excitation light used.

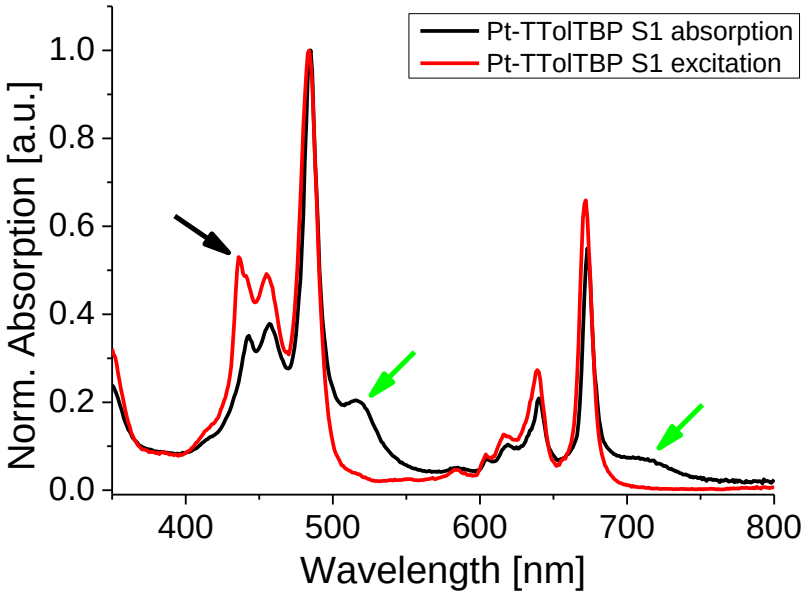

Figure 89 Normalized absorption and excitation spectra of Pt-TTolTBP Sample 1 (excitation at 872 nm)

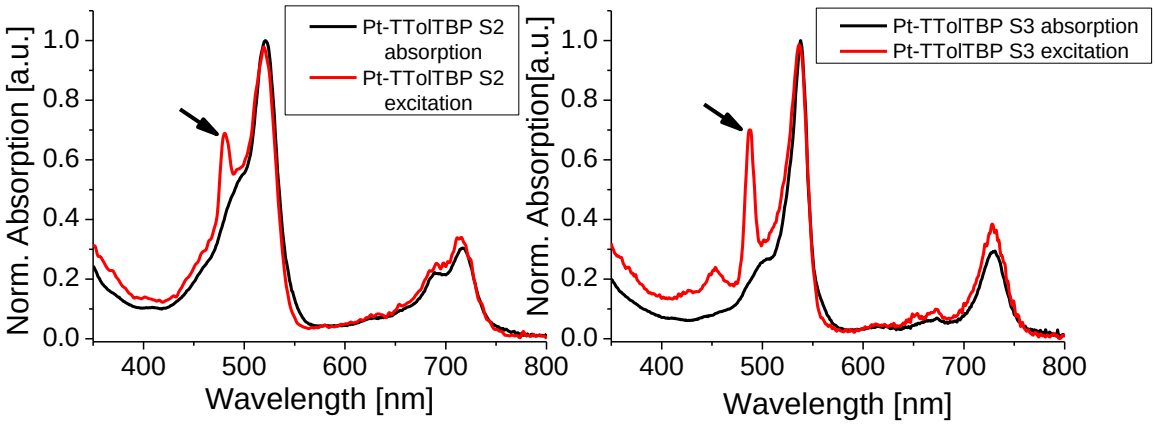

Figure 90 Normalized absorption and excitation spectra of Pt-TTolTBP Sample 2 (left; excitation at 960 nm)) and Pt-TTolTBP Sample 3 (right; excitation at 975 nm)

Moreover these three samples revealed emission maxima in toluene solutions under ambient conditions in the NIR range of 880-975 nm, showing that not only absorption but also

emission wavelengths are tunable by systematic intramolecular bridging of the porphyrin framework (figure 91).

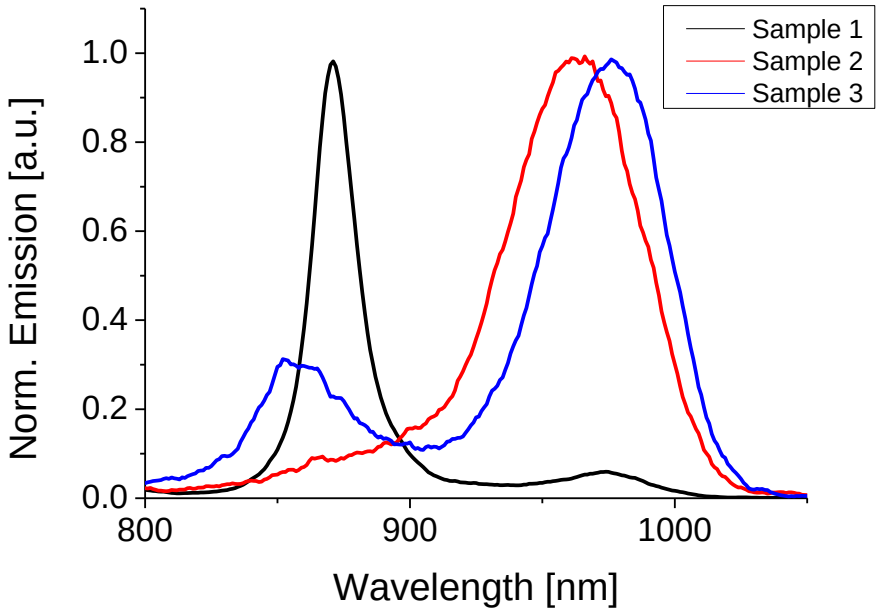

Figure 91 Normalized uncorrected emission spectra of the four-fold bridged main product (Sample 1), the three-fold bridged Pt-TTolTBP (Sample 2) and the four-fold bridged Pt-TTolTBP (Sample 3) of the Scholl-reaction in toluene solutions at room temperature

Notably here is the very narrow emission of the four-fold bridged Sample 1, which is similar the absorption. The band at 855 nm in Sample 3 shows supposably one- or two-fold bridged impurities, which are also luminescent. These optical properties shown so far make the dyes already potential candidates for enzymatic sensors or other biological applications such as O_2 or glucose probes for measurement in tissue, due to the minimal absorption and autofluorescence of biological tissues at these wavelengths. Quantum yields (ϕ) of the three samples were also measured in deoxygenated toluene solutions (10 minutes argon-bubbling through the solution), whereas Pt-OEP and Pd-TPTBP were used as standards. The observed luminescence quantum yields for the three samples are presented in table 1. Furthermore, the luminescence lifetimes of the three samples were obtained via phase fluorimetry. The received results are shown in table 1.

Table 2 Photophysical properties of the three samples of bridged Pt-TTolTBP complexes in diluted toluene solution at room temperatures

complex	abs, λ_{max}, λ [nm] (ε [10^{-3} cm^{-1} M^{-1}])	emission, λ_{max} [nm]	τ [µs]	ϕ [%]
4-fold- bridged-Pt-TTolTBP S1	486 (123), 640 (22), 673 (70)	870	11	10.9
3-fold- bridged Pt-TTolTBP S2	521 (128), 717 (37)	970	10	~0.03
4-fold- bridged Pt-TTolTBP S3	539 (157), 730 (40)	995	14	~0.03

Notably at this point is, that the quantum yields for the Samples 2 and 3 are just rough estimations, due to the aggravated evaluation at long wavelengths of the emission bands. The sensitivity of PMT at these wavelengths is poor and therefore no reliable correction for this region can be obtained, resulting in a graph like shown in figure 92 for Sample 2 and 3.

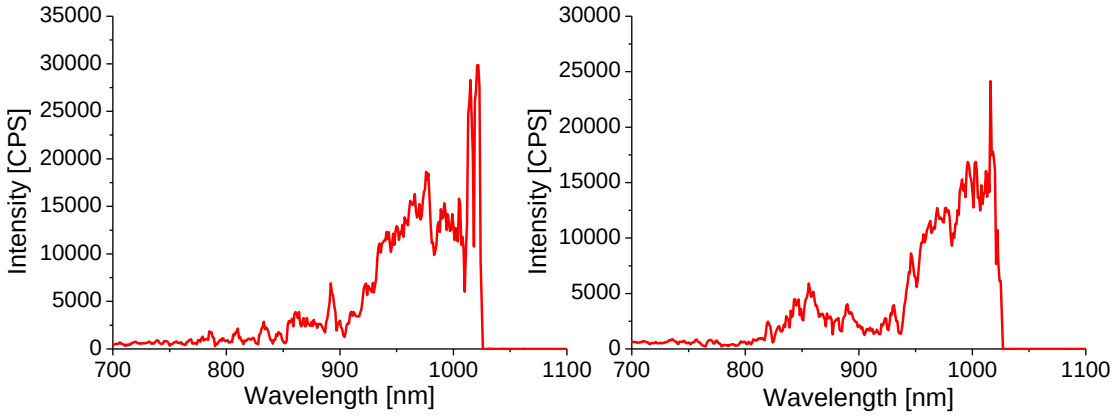

Figure 92 Emission spectra of Sample 2 and 3 for the calculation of the quantum yield in toluene at room temperatures

Therefore the quantum yield was calculated by integrating only the half of the respective emission band and by finally multiplying this value times 2. This process allows at least the estimation of the approximate value for the quantum yield of Sample 2 and 3. In contrast to this the quantum yield of Sample 1 could be calculated without any problems due to the capability of the PMT to correct the spectra at these wavelengths. Sample 2 and 3 showed only weak emission and can therefore be compared with Pt-phthalocyanines, which emit also in the same part of the spectrum with quantum yields about 1% [75].Sample 1 with quantum yield of more than 10% in the NIR can be seen as moderate emitter, almost comparable to platinum(II) tetraphenyltetranaphthoporphyrin with 22% quantum yield at 883 nm. [30].

Due to the low quantum yield of sample 2 and 3 only sample 1 was embedded in a polystyrene matrix (0.5 wt% of the indicator), resulting in a slight red shift of 6 nm for both the Soret and the Q band. Efficient phosphorescence quenching by oxygen was observed for sample 1 in polystyrene film. Hereby polystyrene was chosen as rigid polymer due to good

optical properties and the moderate permeability coefficient for oxygen. [10] Due to the widespread use of polystyrene it also serves as model matrix, enabling better comparison with literature data. [39] Notably here is that in heterogeneous luminescent oxygen-sensing films the Stern-Volmer plots are not linear in contrast to the behavior in solution. This nonlinear behavior is not only common for benzoporphyrins in polystyrene but also most other oxygen-sensing materials. [3], [73] In such cases the two-site model is applied to describe the quenching plots. [124] The assumption of this model is the localization of an oxygen-sensitive chromophore in two environments resulting from micro-inhomogenities in the respective polymeric film. Because these areas of the polymer possess different gas permeabilities, two Stern-Volmer constants K_{SV1} and K_{SV2} are received for the same chromophore following equation (11):

$$\frac{I_0}{I} = \frac{\tau_0}{\tau} = \frac{1}{\frac{P}{1+K_{SV1}*p_{O2}} + \frac{1-P}{1+K_{SV2}*p_{O2}}} \tag{11}$$

Herein P constitutes the partition coefficient for the fraction of the chromophore which is located in the first environment, while 1-P describes the second environment. In the simplified equation K_{SV2} is set as 0 which is found to excellently fit the nonlinear Stern-Volmer plot, also for the decay time if values are obtained in the frequency domain like shown in figure 93. [74] Furthermore figure 93 and 94 shows the lifetime and the Stern-Volmer plot for sample 1 in polystyrene at 25°C for different O_2 concentrations.

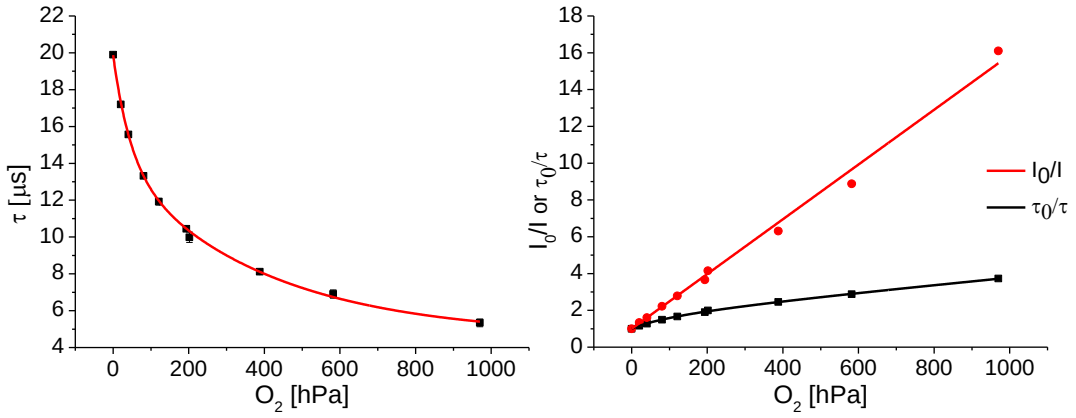

Figure 93 Response of sensor based on bridged Pt-TTolTBP sample 1 in polystyrene (0.5 w% of the indicator) to oxygen at 25°C: decay time plot (on the left) and Stern-Volmer plot (on the right)

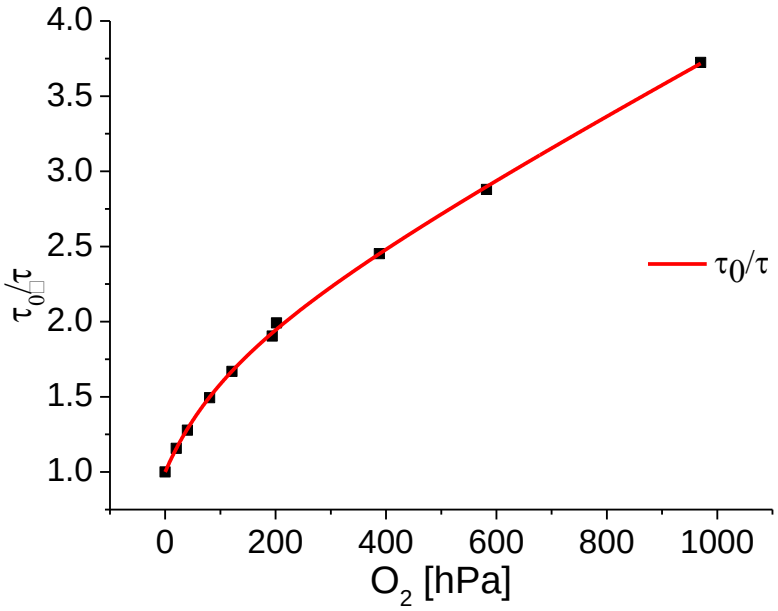

Figure 94 Response of sensor based on Pt-TTolTBP sample 1 in polystyrene (0.5 w% of the indicator) to oxygen at 25°C: Stern-Volmer plot (τ_0/τ)

The fit with the Two Site model resulted in a Stern-Volmer plot revealing P = 0.56 and K_{SV1} = 0.0145 hPa^{-1}. Notably here is the much more linear I_0/I plot compared to τ_0/τ, with nevertheless a similar K_{SV1} of 0.015 hPa^{-1}. The mass spectrum of Sample 1 shows indeed a mixture of different dyes but since nearly all of them are four-fold bridged no different quenching behaviors for oxygen were expected. Also the various substitutions (chlorine atoms and tert-butyl groups) of the dyes should not have an influence on the oxygen quenching ability. Therefore two possible approaches to explain the bending of τ_0/τ and the low partition coefficient were assumed. Probably the mixture of similar dyes is located in two different areas within the polystyrene matrix, whereas one is well quenched by oxygen and the other one not. Another approach assumes the formation of dimers in the matrix, which are only minimal or not quenched by oxygen, whereas the respective monomers are sensitive to oxygen quenching.

Furthermore it can be said, that the sensor is sensitive to oxygen over a wide area, although the sensitivity to oxygen is higher at lower oxygen concentrations and could therefore be applied as broadband sensor for oxygen measurements in physiological area. Regarding the sensitivity bridged Pt-TTolTBP sample 1 is suitable as optical oxygen sensor for most biological applications, e.g. to monitor the process of oxygen production during photosynthesis, due the clearly distinguishable emission (870 nm) of the dye compared to chlorophyll a and b as it can be seen in figure 95.

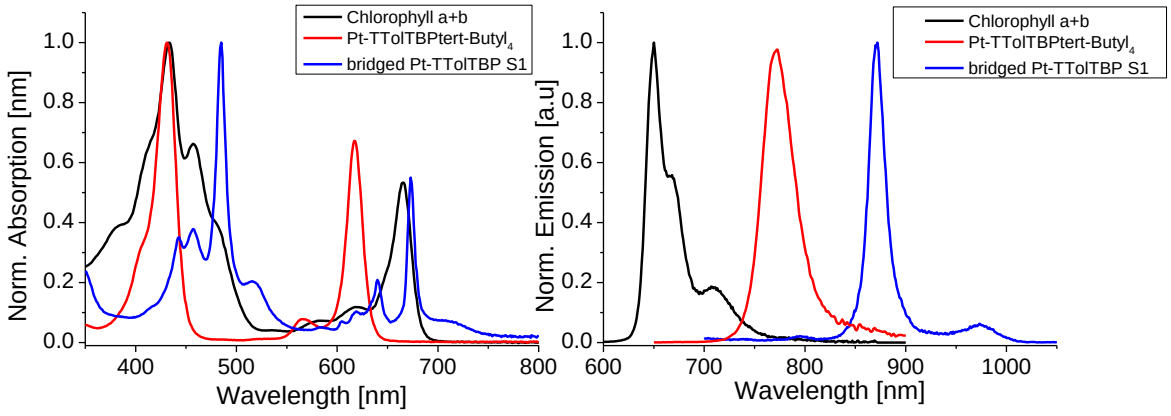

Figure 95 Normalized absorption spectra (left) and emission spectra (right) of chlorophyll a and b, Pt-TTolTBPtert-Butyl$_4$ and bridged Pt-TTolTBP Sample 1 in toluene (anoxic toluene for emission measurements) at room temperature

As it can be seen in figure 95 Pt-TTolTBPterrt-Butyl$_4$ allows excitation of mainly chlorophyll a in the Soret band and partly chlorophyll b in the Q band, whereas the bridged Pt-TTolTBP Sample 1 enables excitation of both, chlorophyll a and b in the Soret band as well as in the Q band (but mostly chlorophyll a). Furthermore the emission spectra of chlorophyll a and b and the bridged Pt-TTolTBP Sample 1 can be clearly distinguished, even if measured in frequency domain. Therefore this dye could be also applied in simultaneous measurements of oxygen and chlorophyll a and b. In comparison the emission of chlorophyll a and b and Pt-TTolTBPterrt-Butyl$_4$ (and other standard benzoporphyrins like TPTBP or TPTBP) cannot be separated exactly when measured in frequency domain. To achieve separation of these emission bands measurements in time domain would be necessary.

Since photostability of oxygen indicators is of particular interest for nearly all practical applications especially if usage of high light densities is necessary, long-term measurements were performed. The most abundant cause of photodegradation is the singlet oxygen production upon quenching. This highly reactive singlet oxygen further interacts with the dye in the ground state leading to the formation of products which are usually not luminescent. [125] According to the literature the substitution of both the β- as well as the meso-position affect the redox potential on the porphyrin ring due to electronic effects (withdrawing or donating) and non-planar deformations of the macrocycle initiated by crowding at the periphery of the porphyrin. [126] Therefore, examination of the photostability allows an insight into the relationship of the structure and the stability against photodegradation of the respective luminescent dye. The photostability was determined for the three samples in DMF solutions by continuously irradiating the three different bridged Pt-TTolTBP samples of the same concentrations with either a blue LED (λ_{max}=458 nm; 10.79 V, 0.689 A, 7.4 W) for sample 1 and Pd3NF as reference or with a green LED (λ_{max}=530 nm, 5.85 V, 0.317 A, 1.9 W) for sample 2 and 3 as well as Pd-TFPP and Pt-OEP which were used as reference materials. Within this measurement the irradiation intervals were adjusted to the behavior

and photodegradation of the respective dye. Due to the fact that not all the dyes could be excited exactly in their absorption maximum, the values were corrected for the amount of the absorbed light at the excitation wavelengths. In the following figures the process of photodegradation for the three different samples is illustrated (figure 96 and 97). An overview of the decrease of relative absorbance with the time of all dyes and measured standards is presented in figure 96 and 98.

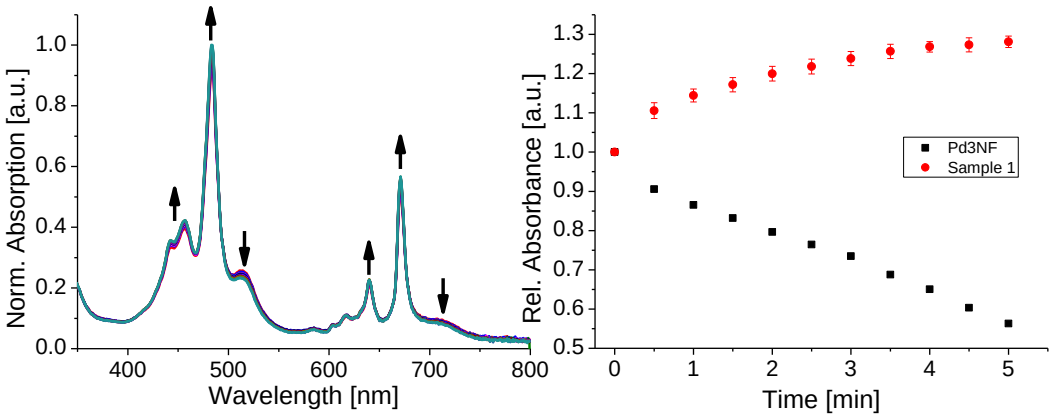

Figure 96 Photodegradation curves for Pt-TTolTBP sample 1 (on the left) and comparison (on the right) of Sample 1 to Pd3NF in air saturated DMF solution at room temperature. Irradiation is performed with a blue LED array (λmax=458 nm; 10.79 V, 0.689 A, 7.4 W).

This experiment revealed on the one that Sample 1 possess generally an excellent photostability compared with Pd3NF, whose Q band is also very far red-shifted to 681 nm but also showed an increase in the absorption under irradiation, which cannot be explained yet. Apparently the absorbance in the Soret and Q band of the dye increases during the 5 minutes of the measurement, whereas the band at 514 nm decreases continuously.

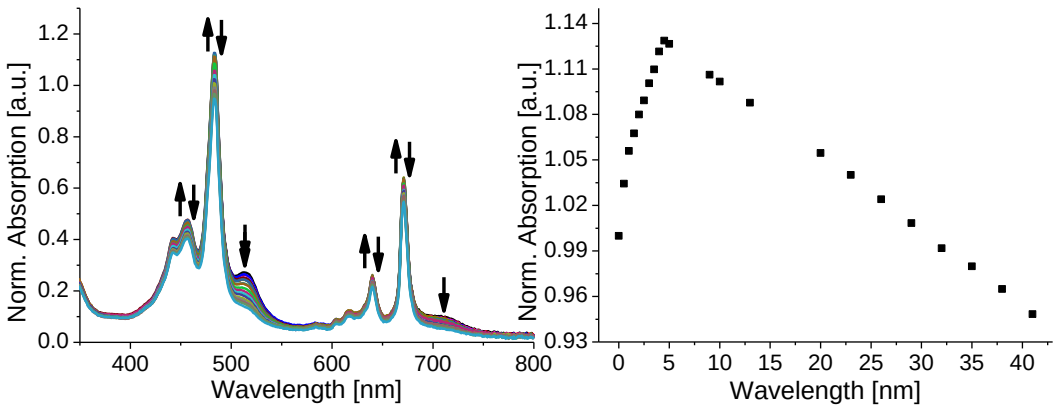

Figure 97 Photodegradation curves for Pt-TTolTBP sample 1 in air saturated DMF solution at room temperature. Irradiation is performed with a blue LED array (λmax=458 nm; 10.79 V, 0.689 A, 7.4 W).

Due to the inexplicable process of Sample 1 in the five minutes photostability test a second attempt was started in which photodegradation of the dye could be shown within 40 minutes. At the beginning the same inexplicable trend as in the last experiment was observed until

after five minutes photobleaching of the dye started. Although the second experiment could not clarify the trend at the beginning it revealed the excellent photostability of the bridged Pt-TTolTBP Sample 1 compared to Sample 2 and 3 but also to the reference Pd3NF used in the first photobleaching experiment. Despite the obtained values in figure 97 were not corrected for the amount of the absorbed light at the excitation wavelengths this experiment displayed the clearly higher photostability of Sample 1 compared to Pd3NF. In the case of Pd3NF 40% bleaching is observed after 5 minutes of irradiation, whereas Sample 1 of the bridged Pt-TTolTBP shows only a decrease of approximately 5% after 40 minutes.

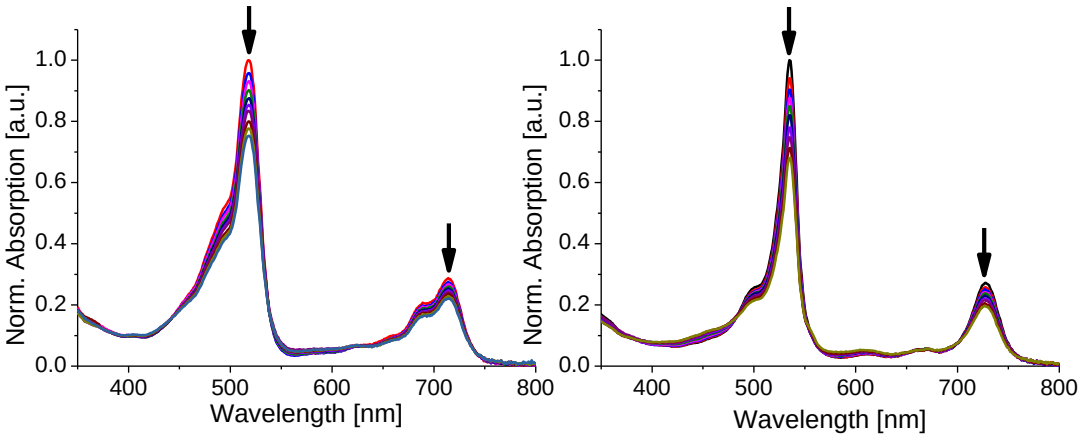

Figure 98 Photodegradation curves for Pt-TTolTBP sample 2 (on the left) and Pt-TTolTBPtert-Butyl$_4$ sample 3 in air saturated DMF solution at room temperature. Irradiation is performed with a green LED (λ_{max}=530 nm, 5.85 V, 0.317 A, 1.9 W).

In contrast to Sample 1 shown above, Sample 2 and Sample 3 show the expected decrease of absorption observable in the Soret as well as the Q band upon irradiation (figure 34).

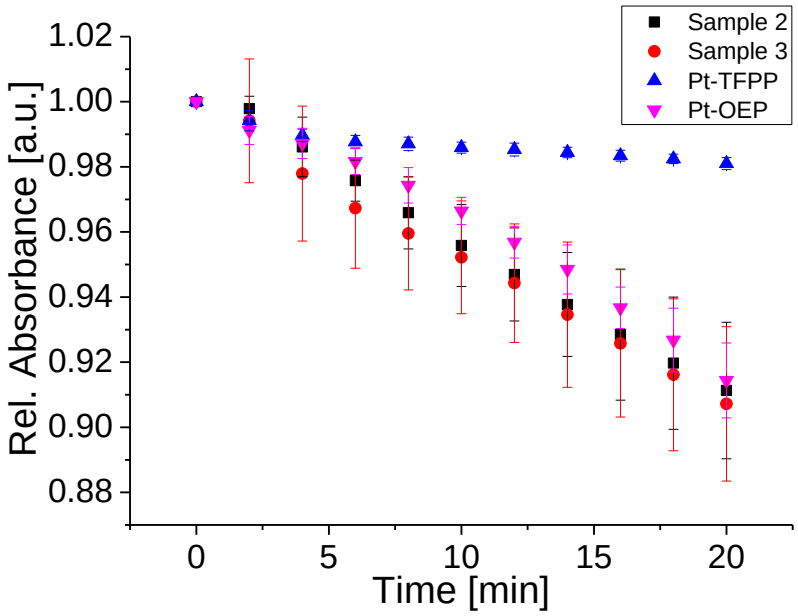

Figure 99 Photodegradation curves for Pt-TTolTBP sample 2 and 3 compared with other available and commercially used porphyrin dyes (Pt-OEP and Pt-TFPP) in air saturated DMF solution at room temperature. Irradiation is performed with a green LED (λ_{max}=530 nm, 5.85 V, 0.317 A, 1.9 W).

Here Sample 2 and 3 (figure 98) were compared with Pt-OEP and Pt-TFPP, which led to expectable results (figure 99). Pt-TFPP shows only minor photo bleaching, whereas Pt-OEP, Sample 2 and 3 lost about 9% of their initial absorption. Noticeable at this graph is relatively big standard deviation of Sample 2 and 3 after 20 minutes compared to Pt-OEP. One reason for the decreased photostability of Sample 2 and 3 could be the different bridging pattern from Sample 1. Maybe the adjacent bridging of these Samples, leading to further π-extension, shows an anthracene like character, which are known for their low photostability.

Moreover it is well known in literature that electron withdrawing substituents like chlorine or fluorine atoms have a positive influence on the photostability due to an increase of the reduction potential of the respective dyes. These of course leads to the conclusion that electron pushing substituents like methyl or tert-butyl moieties enhance the oxidative decomposition. [39] However benzoporhyrins dyes in general are highly photostable compared to other commercially available porphyrins. [127] Finally it should be anyhow mentioned that the nature of the solvent has tremendous influence on the photobleaching rates.

In conclusion, three different compounds of Pt-TTolTBPtert-Butyl$_4$ have been isolated after the Scholl-reaction. Under investigation sample 1 showed most suitable properties for different applications. The absorption of this product, the first known intramolecular-π-extended benzoporphyrin formed by a Scholl-reaction, displays a clear red-shift of both the Soret and the Q band compared with the educt and therefore allows excitation in the red part of the spectrum at 673 nm (Q band). Furthermore the Q band shows a very narrow and defined absorption band compared to those of other benzoporphyrins, which is often preferred in various applications to avoid excitation of other compounds. Moreover the compound shows emission in the NIR at 870 nm, which makes the compound a promising candidate for different multiplexing applications, e.g. simultaneous glucose and oxygen determination in enzymatic sensors. Unfortunately, the extension of the aromatic system has a significant impact on the photophysical properties. As already mentioned the emission bands are shifted to longer wavelengths, the luminescence lifetimes becomes shorter, the luminescence quantum yield decreases and the sensitivity to oxygen can also be affected and gradually reduced. Moreover the compound displays high photostability compared to other commercially available dyes like Pt-OEP. The observed sensitivity of the sensor ranging from low to very high oxygen concentrations make the dye suitable as indicator for use in optical oxygen sensors and various biological applications. Furthermore the sensitivity of the sensor can also be tuned using a different matrix with higher oxygen permeability.The future synthetic work concerning the intramolecular bridging of benzoporphyrins will essentially focus on the further improvement of solubility and the finer adjustment of the

location as well as the number of bridged units to have a better control over the optical properties of the resulting dye.

Due to the phosphorescence observed at 870 nm for Sample 1, it was expected that the dye can be a promising sensitizer for triplet-triplet annihilation-based upconversion. Annihilators 3,9-perylenedicarboxylate (known as Solvent Green 5), perylene (94710 fluorescent orange) and perylene (94720 fluorescent red) were used; all possess good solubility in most organic solvents and similarly to other perylene dyes excellent photostability. [128], [129]For the measurement four-fold bridged Pt-TTolTBP sample 1 ($5*10^{-4}$mol/L) and the respective annihilator ($1*10^{-4}$mol/L) were mixed in a toluene solution and deoxygenated for 10 minutes (argon bubbling trough the solution). Afterwards an emission spectrum of the reaction mixture was recorded on a Fluorolog 3 fluorescence spectrometer with an excitation at 670 nm (Q band of the sensitizer). Hereby up-converted fluorescence in the visible region of the spectrum was observed within all sensitizer-annihilator combinations. In the case of Solvent Green 5 (figure 100) and perylene orange (94710 fluorescent orange) (figure 101) the observed up-converted fluorescence was unfortunately really low, wherefore this part of the spectrum was zoomed out.

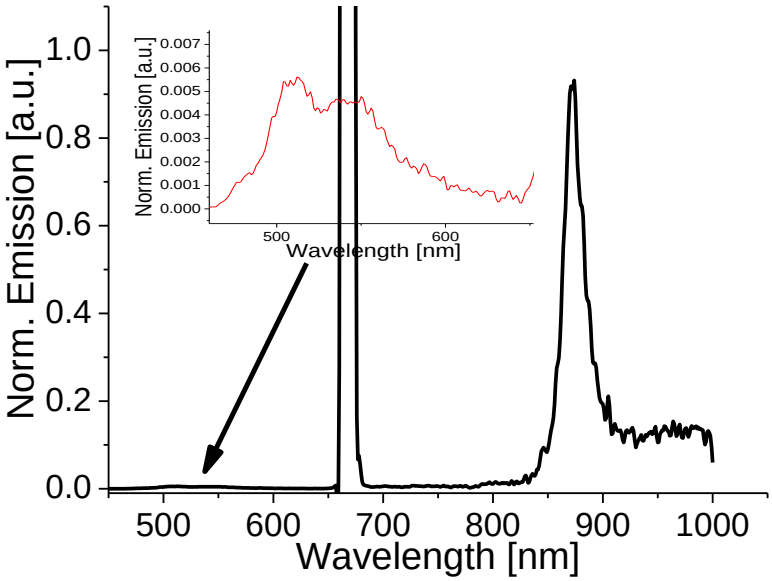

Figure 100 Normalized emission spectra of the sensitizer Pt-TTolTBP sample 1 ($5*10^{-4}$mol/L) and the annihilator ($1*10^{-4}$mol/L) Solvent Green 5 in deoxygenated toluene solution at room temperature excited at 670 nm

In the case of Solvent Green 5 (figure 100) emission was observed in the region of 490 to 570 nm, whereas the mixture with perylene orange showed emission bands from 490 to 580 nm. Hereby the insert shows the signals for the upconverted fluorescence. Nevertheless all three mixtures of sensitizer and annihilator have the same concentrations a clear difference concerning the intensity of the up-converted fluorescence can be observed. In the case of

the annihilator Solvent Green 5 the up-converted fluorescence is lowered by a factor of 200 compared to the phosphorescence at 880 nm, whereas with perylene orange it is just a factor of 40 lowered (figure 101). The up-converted fluorescence with the annihilator perylene red however shows already 40% of the phosphorescence intensity (figure 102), which is already an acceptable value.

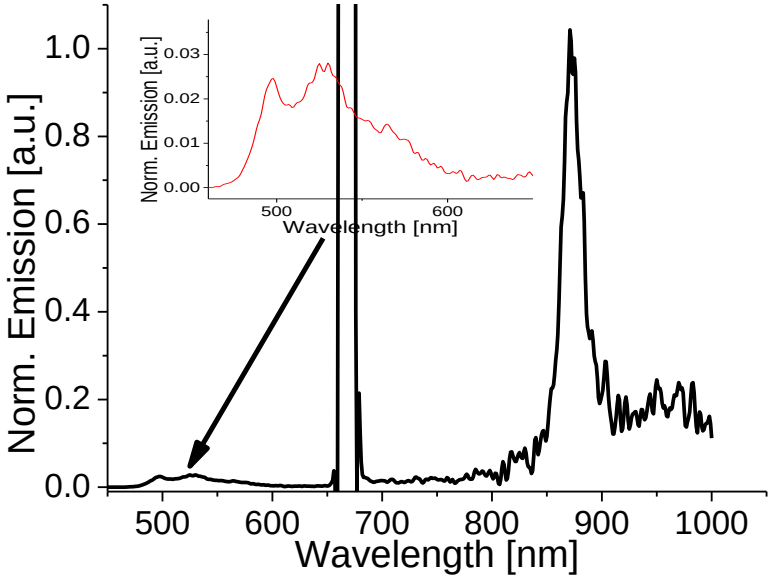

Figure 101 Normalized emission spectra of the sensitizer Pt-TTolTBP sample 1 ($5*10^{-4}$mol/L) and the annihilator ($1*10^{-4}$mol/L) perylene orange (94720 fluorescent red) in deoxygenated toluene solution at room temperature excited at 670 nm

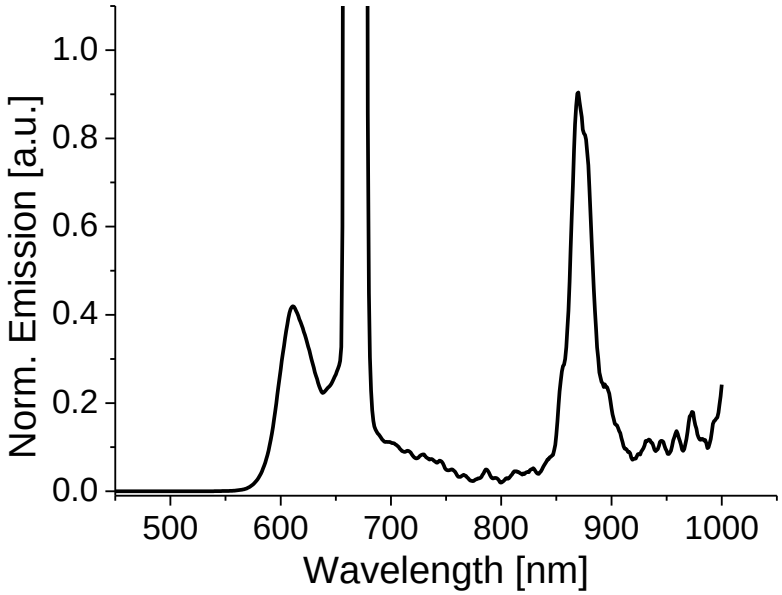

Figure 102 Normalized emission spectra of the sensitizer Pt-TTolTBP sample 1 ($5*10^{-4}$mol/L) and the annihilator ($1*10^{-4}$mol/L) perylene red (94720 fluorescent red) in deoxygenated toluene solution at room temperature excited at 670 nm

The mixture of the sensitizer and perylene red displayed up-converted fluorescence in the region of 580 to 640 nm. The other observable bands in the spectrum of figure 102 are the emission of the sensitizer at 880 nm and the scattered light at which the sensitizer has been excited (670 nm). It should be noted that the intensity of the upconverted fluorescence strongly depends on the intensity of the excitation light (quadratic dependence), so much better spectra are expected to be obtained at stronger excitation light, which was not possible with current set-up. Besides the mentioned facts in the theoretical background that must be kept in mind concerning the requirements of the sensitizer and the annihilator it should be noticed at this point that the energy levels of the excited states of both the sensitizer and the annihilator must be matched to enhance the TTET process and to ensure successful upconversion.

The best match of the energy levels with the tested sensitizer/ annihilator mixtures and therefore the most efficiently energy transfer was definitely obtained with perylene red, which could be seen at the higher intensity of the up-converted fluorescence in the emission spectrum.

Herby photos were taken of the sensitizer/annihilator solutions in deoxygenated toluene while excited with a 670-nm laser diode to illustrate the described process (figure 103).

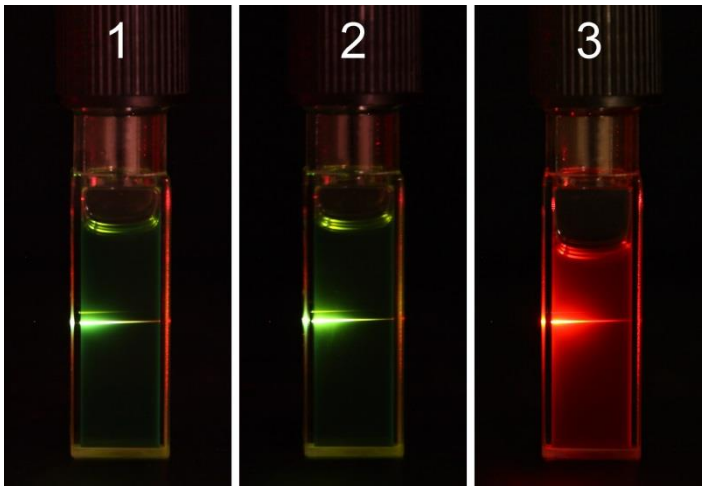

Figure 103 Photographic images of the solutions composed of $5*10^{-4}$mol/L of the sensitizer Pt-TTolTBP sample 1 and $1*10^{-4}$mol/L of the respective annihilator 3,9-perylenedicarboxylate (known as Solvent Green 5), perylene (94710 fluorescent orange) and perylene (94720 fluorescent red) in deoxygenated toluene solution at room temperature upon excitation with a 670-nm laser diode

The successful examination of the use of Pt-TTolTBP sample 1 as sensitizer for triplet-triplet upconversion establishes another field of possible application for the newly synthesized bridged Pt-TTolTBP sample 1 NIR emitting dye, such as photovoltaics, optics [109], [110] but also as optical oxygen sensor. [116]

In future also bridged palladium(II) porphyrin could be used as sensitizer, due to its longer decay time it is expected to be an even more promising candidate for TTA-based upconversion.

9. Conclusion and Outlook

The two aims of the thesis were on the one hand the synthesis of a highly soluble benzoporphyrin dye and on the other hand the examination of the effect of intramolecular bridging (fusion) on different benzoporphyrins and further characterization of the changed optical properties and their prospective field of application.

In case of the highly soluble benzoporphyrin dye two different synthetic strategies were followed. First of all the synthesis of the benzoporphyrin substituted with an imide functionality with alkyl chains was attempted according to the well-known conventional Lindsey-condensation method. Unfortunately this synthesis has to be aborted due to problems in the de-esterification step and to unavailability of the tert-butyl isocyanoacetate, one of the key substances for this strategy. Therefore the synthesis of another benzoporphyrin compound with similar or even enhanced solubility or photostability properties following a different synthesis pathway was performed.
Hereby the template method was chosen due to some advantages such as affordability of the educts and chemical simplicity compared to Lindsey condensation. Aim of this synthesis was a benzoporphyrin substituted with a sulfone functionality with alkyl chains. Although this compound could not be directly obtained through the melting step, the following oxidation of the zinc complex or the respective ligand with m-CPBA yielded the desired completely oxidized compound, which was proved via mass spectroscopy. Due to time issues the platination of the oxidized compound was not performed. Nevertheless the new compounds represent very promising candidates to achieve the targeted properties, which are very important for several fields of application, where a very economic and easy up-scalable process is required. Therefore it should be focused in future synthetic work.

In the second part of the thesis the feasibility of the concept of intermolecular bridging through Scholl-reaction and the impact on the changed structure properties on the respective benzoporphyrin dye was examined. In the proof of concept experiment Tetraphenyltetrabenzoporphyrin was successfully bridged and the resulting structure analyses via mass spectroscopy, displayed the formation of a four-fold bridged product. Unfortunately the synthesized compound suffered from low solubility, difficult purification as well as difficulties with characterization of the structure via NMR due to formation of side products. Since the side-products formed through substitution of the used solvent could not be separated and various other tested solvents did not lead to the formation of the bridged complex the synthesis of other benzoporphyrin derivatives with increased solubility was

concluded. The synthesis of Tetratolyltetrabenzoporphyrin did not contribute to further insight of the bridging via Scholl-reaction due to the unachievable purification of the platinum complex. Furthermore Tetraphenyltetra(di-methyl)benzoporphyrin, the better soluble derivative, could not be bridged probably due to the steric hindrance in the addition of $AlCl_3$ or maybe through the stabilization effect of the two methyl moieties in β-β-position on the formed cation. The next synthesized derivative, Tetraphenyltetra(mono-methyl)benzoporphyrin, could not be bridged either due to decomposition of the platinum complex at already low temperatures (120°C) during the Scholl-reaction. The synthesis of the zinc complexes of Tetratolyltetrabenzoporphyrin and Tetraphenyltetra(mono-methyl)benzoporphyrin revealed at least that Scholl-reaction of zinc complexes only leads to one-fold bridging due to the instant de-metalation of the metal-complex through $AlCl_3$ at the start of the reaction. The C-C bond formation of the metal-free porphyrin is considerably more difficult due to the lower electron density of the protonated ligand compared with metal-complexes.

Finally the Scholl-reaction of the platinum(II) tetra(tolyl)tetra(tert-butyl)benzoporphyrin led to the formation of a four-fold bridged compound with sufficient solubility despite the off splitting of tert-Butyl groups. Although tert-butyl groups are eliminated and chlorine atoms are substituted during the Scholl-reaction leading to a complex product mixture, definitive optical properties, which are especially important for practical applications are obtained for the four-fold bridged platinum(II) complex. Unfortunately it was not possible to get a definite mass spectrum of the structure even after repeated purification due to the different bridging patterns and the formation of several substitution products of dichlorobenzene. Nevertheless this and the other two isolated compounds were examined more closely in respect to their photophysical properties by recording of emission spectra and determination of the relative quantum yield and lifetime via phase fluorimetry. Due to the narrow, defined absorption bands at 673 nm, the emission in the NIR region at 870 nm, the good photostability and sufficient quantum yield (10.9%) and lifetime of 11 µs, it was embedded in a polystyrene matrix and tested for the use of an optical oxygen sensor for diverse biological and medical applications. Oxygen sensitivity over a physiological range make this compound a very promising candidate for different multiplexing applications, e.g. simultaneous glucose and oxygen determination in enzymatic sensors but also as optical oxygen sensor to monitor the oxygen production during photosynthesis due to the emission in the NIR (870 nm) which is easily distinguishable of the one from chlorophyll a and b. The demonstrated performance as sensitizer with different annihilators in the triplet-triplet-annihilation based upconversion process opens another field of various applications such as photovoltaics, optics as well as photocatalysis.

Nevertheless the future synthetic work, concerning the intramolecular bridging of benzoporphyrins should essentially focus on the further improvement of solubility and the finer adjustment of the location as well as the number of bridged units to have a better control over the optical properties of the resulting dye, leading to wider expansion of the field of possibly applications. Using different synthetic approaches in future may yield similar bridged compounds without the formation of side products, enabling the characterization of a defined structure.

10. References

[1] M. Quaranta, S. M. Borisov, und I. Klimant, „Indicators for optical oxygen sensors“, *Bioanal. Rev.*, Bd. 4, Nr. 2–4, S. 115–157, Dez. 2012.

[2] C. McDonagh, C. S. Burke, und B. D. MacCraith, „Optical Chemical Sensors“, *Chem. Rev.*, Bd. 108, Nr. 2, S. 400–422, Feb. 2008.

[3] S. M. Borisov, G. Nuss, und I. Klimant, „Red light-excitable oxygen sensing materials based on platinum(II) and palladium(II) benzoporphyrins“, *Anal. Chem.*, Bd. 80, Nr. 24, S. 9435–9442, Dez. 2008.

[4] Y. Zems, A. G. Moiseev, und D. F. Perepichka, „Convenient synthesis of a highly soluble and stable phosphorescent platinum porphyrin dye“, *Org. Lett.*, Bd. 15, Nr. 20, S. 5330–5333, Okt. 2013.

[5] Bernard Valeur, *Molecular Fluorescence: Principles and Applications*. .

[6] M. Nič, J. Jirát, B. Košata, A. Jenkins, und A. McNaught, Hrsg., „delayed fluorescence“, in *IUPAC Compendium of Chemical Terminology*, 2.1.0 Aufl., Research Triagle Park, NC: IUPAC, 2009.

[7] M. Seery, „Quenching Mechanisms“, *The Photochemistry Portal*. .

[8] O. S. Wolfbeis, „Fiber-Optic Chemical Sensors and Biosensors“, *Anal. Chem.*, Bd. 78, Nr. 12, S. 3859–3874, Juni 2006.

[9] P. Gründler, *Chemische Sensoren; Eine Einführung für Naturwissenschaftler und Ingenieure*. Springer, 2004.

[10] Y. Amao, „Probes and Polymers for Optical Sensing of Oxygen“, *Microchim. Acta*, Bd. 143, Nr. 1, S. 1–12, Sep. 2003.

[11] T. Tanaka und A. Osuka, „Conjugated porphyrin arrays: synthesis, properties and applications for functional materials“, *Chem. Soc. Rev.*, Jan. 2014.

[12] C. M. Drain, A. Varotto, und I. Radivojevic, „Self-Organized Porphyrinic Materials“, *Chem. Rev.*, Bd. 109, Nr. 5, S. 1630–1658, Mai 2009.

[13] D. Wohrle, „The colours of life. An introduction to the chemistry of porphyrins and related compounds. By L. R. Milgrom, Oxford university press, Oxford 1997, vi, 225 pp., softcover, £49.50, ISBN 019-855380-3“, *Adv. Mater.*, Bd. 9, Nr. 15, S. 1191–1192, Jan. 1997.

[14] C. M. B. Carvalho, T. J. Brocksom, und K. T. de Oliveira, „Tetrabenzoporphyrins: synthetic developments and applications“, *Chem. Soc. Rev.*, Bd. 42, Nr. 8, S. 3302–3317, März 2013.

[15] A. Mills und A. Lepre, „Controlling the Response Characteristics of Luminescent Porphyrin Plastic Film Sensors for Oxygen“, *Anal. Chem.*, Bd. 69, Nr. 22, S. 4653–4659, Nov. 1997.

[16] O. S. Finikova, A. V. Cheprakov, I. P. Beletskaya, P. J. Carroll, und S. A. Vinogradov, „Novel versatile synthesis of substituted tetrabenzoporphyrins“, *J. Org. Chem.*, Bd. 69, Nr. 2, S. 522–535, Jan. 2004.

[17] P. Chen, Y. Fang, K. M. Kadish, J. P. Lewtak, D. Koszelewski, A. Janiga, und D. T. Gryko, „Electrochemically driven intramolecular oxidative aromatic coupling as a pathway toward π-extended porphyrins“, *Inorg. Chem.*, Bd. 52, Nr. 16, S. 9532–9538, Aug. 2013.

[18] S. M. Borisov und I. Klimant, „Luminescent chemosensors - Advanced tools in analytical chemistry“, *Inf. MIDEM*, Bd. 40, Nr. 4, S. 291–297, 2010.

[19] V. V. Roznyatovskiy, C.-H. Lee, und J. L. Sessler, „π-Extended isomeric and expanded porphyrins“, *Chem. Soc. Rev.*, Bd. 42, Nr. 5, S. 1921, 2013.

[20] C. Borek, K. Hanson, P. I. Djurovich, M. E. Thompson, K. Aznavour, R. Bau, Y. Sun, S. R. Forrest, J. Brooks, L. Michalski, und J. Brown, „Highly Efficient, Near-Infrared Electrophosphorescence from a Pt–Metalloporphyrin Complex“, *Angew. Chem. Int. Ed.*, Bd. 46, Nr. 7, S. 1109–1112, Feb. 2007.

[21] S. A. Vinogradov, L. W. Lo, W. T. Jenkins, S. M. Evans, C. Koch, und D. F. Wilson, „Noninvasive imaging of the distribution in oxygen in tissue in vivo using near-infrared phosphors.“, *Biophys. J.*, Bd. 70, Nr. 4, S. 1609–1617, Apr. 1996.

[22] O. S. Finikova, S. E. Aleshchenkov, R. P. Briñas, A. V. Cheprakov, P. J. Carroll, und S. A. Vinogradov, „Synthesis of Symmetrical Tetraaryltetranaphtho[2,3]porphyrins“, *J. Org. Chem.*, Bd. 70, Nr. 12, S. 4617–4628, Mai 2005.

[23] H. Xiang, J. Cheng, X. Ma, X. Zhou, und J. J. Chruma, „Near-infrared phosphorescence: materials and applications“, *Chem. Soc. Rev.*, Bd. 42, Nr. 14, S. 6128–6185, Juni 2013.

[24] V. V. Diev, C. W. Schlenker, K. Hanson, Q. Zhong, J. D. Zimmerman, S. R. Forrest, und M. E. Thompson, „Porphyrins Fused with Unactivated Polycyclic Aromatic Hydrocarbons“, *J. Org. Chem.*, Bd. 77, Nr. 1, S. 143–159, Nov. 2011.

[25] J. D. Spence und T. D. Lash, „Porphyrins with Exocyclic Rings. 14.1 Synthesis of Tetraacenaphthoporphyrins, a New Family of Highly Conjugated Porphyrins with Record-Breaking Long-Wavelength Electronic Absorptions“, *J. Org. Chem.*, Bd. 65, Nr. 5, S. 1530–1539, Feb. 2000.

[26] T. Ishizuka, Y. Saegusa, Y. Shiota, K. Ohtake, K. Yoshizawa, und T. Kojima, „Multiply-fused porphyrins--effects of extended π-conjugation on the optical and electrochemical properties“, *Chem. Commun. Camb. Engl.*, Bd. 49, Nr. 53, S. 5939–5941, Juli 2013.

[27] J. E. Rogers, K. A. Nguyen, D. C. Hufnagle, D. G. McLean, W. Su, K. M. Gossett, A. R. Burke, S. A. Vinogradov, R. Pachter, und P. A. Fleitz, „Observation and Interpretation of Annulated Porphyrins: Studies on the Photophysical Properties of meso-Tetraphenylmetalloporphyrins“, *J. Phys. Chem. A*, Bd. 107, Nr. 51, S. 11331–11339, Dez. 2003.

[28] C.-M. Che, V. K.-Y. Lo, C.-Y. Zhou, und J.-S. Huang, „Selective functionalisation of saturated C–H bonds with metalloporphyrin catalysts“, *Chem. Soc. Rev.*, Bd. 40, Nr. 4, S. 1950–1975, März 2011.

[29] M. O. Senge, M. Fazekas, E. G. A. Notaras, W. J. Blau, M. Zawadzka, O. B. Locos, und E. M. Ni Mhuircheartaigh, „Nonlinear Optical Properties of Porphyrins“, *Adv. Mater.*, Bd. 19, Nr. 19, S. 2737–2774, Okt. 2007.

[30] J. R. Sommer, R. T. Farley, K. R. Graham, Y. Yang, J. R. Reynolds, J. Xue, und K. S. Schanze, „Efficient near-infrared polymer and organic light-emitting diodes based on electrophosphorescence from (tetraphenyltetranaphtho[2,3]porphyrin)platinum(II)“, *ACS Appl. Mater. Interfaces*, Bd. 1, Nr. 2, S. 274–278, Feb. 2009.

[31] A. R. Murphy und J. M. J. Fréchet, „Organic Semiconducting Oligomers for Use in Thin Film Transistors“, *Chem. Rev.*, Bd. 107, Nr. 4, S. 1066–1096, Apr. 2007.

[32] S. A. Vinogradov und D. F. Wilson, „Metallotetrabenzoporphyrins. New phosphorescent probes for oxygen measurements“, *J. Chem. Soc. Perkin Trans. 2*, Nr. 1, S. 103, 1995.

[33] C. M. Drain, K. C. Russell, und J.-M. Lehn, „Self-assembly of a multi-porphyrin supramolecular macrocycle by hydrogen bond molecular recognition“, *Chem. Commun.*, Nr. 3, S. 337, 1996.

[34] M. G. Walter, A. B. Rudine, und C. C. Wamser, „Porphyrins and phthalocyanines in solar photovoltaic cells“, *J. Porphyr. Phthalocyanines*, Bd. 14, Nr. 09, S. 759–792, Sep. 2010.

[35] D. M. Guldi, „Fullerene-porphyrin architectures; photosynthetic antenna and reaction center models“, *Chem. Soc. Rev.*, Bd. 31, Nr. 1, S. 22–36, Jan. 2002.

[36] X. Yi, F. Wang, W. Qin, X. Yang, und J. Yuan, „Near-infrared fluorescent probes in cancer imaging and therapy: an emerging field“, *Int. J. Nanomedicine*, Bd. 9, S. 1347–1365, März 2014.

[37] S. Pervaiz und M. Olivo, „Art and science of photodynamic therapy“, *Clin. Exp. Pharmacol. Physiol.*, Bd. 33, Nr. 5–6, S. 551–556, Juni 2006.

[38] R.-M. Szeimies, „Geschichte der Photodynamischen Therapie“, *Aktuelle Dermatol.*, Bd. 31, Nr. 5, S. 193–197, Mai 2005.

[39] G. N. S. M. Borisov, „New NIR-emitting complexes of platinum(II) and palladium(II) with fluorinated benzoporphyrins“, *J. Photochem. Photobiol. -Chem. - J PHOTOCHEM PHOTOBIOL -CHEM*, Bd. 201, Nr. 2, S. 128–135, 2009.

[40] P. Roche, R. Al-Jowder, R. Narayanaswamy, J. Young, und P. Scully, „A novel luminescent lifetime-based optrode for the detection of gaseous and dissolved oxygen utilising a mixed ormosil matrix containing ruthenium (4,7-diphenyl-1,10-phenanthroline)3Cl2 (Ru.dpp)“, *Anal. Bioanal. Chem.*, Bd. 386, Nr. 5, S. 1245–1257, Nov. 2006.

[41] S. M. Borisov, A. S. Vasylevska, C. Krause, und O. S. Wolfbeis, „Composite Luminescent Material for Dual Sensing of Oxygen and Temperature“, *Adv. Funct. Mater.*, Bd. 16, Nr. 12, S. 1536–1542, Aug. 2006.

[42] E. Vander Donckt, B. Camerman, R. Herne, und R. Vandeloise, „Fibre-optic oxygen sensor based on luminescence quenching of a Pt(II) complex embedded in polymer matrices“, *Sens. Actuators B Chem.*, Bd. 32, Nr. 2, S. 121–127, Mai 1996.

[43] M. C. DeRosa, P. J. Mosher, G. P. A. Yap, K.-S. Focsaneanu, R. J. Crutchley, und C. E. B. Evans, „Synthesis, Characterization, and Evaluation of [Ir(ppy)2(vpy)Cl] as a Polymer-Bound Oxygen Sensor“, *Inorg. Chem.*, Bd. 42, Nr. 16, S. 4864–4872, Juli 2003.

[44] D. Eastwood und M. Gouterman, „Porphyrins: XVIII. Luminescence of (Co), (Ni), Pd, Pt complexes“, *J. Mol. Spectrosc.*, Bd. 35, Nr. 3, S. 359–375, Sep. 1970.

[45] D. B. Papkovsky, „New oxygen sensors and their application to biosensing“, *Sens. Actuators B Chem.*, Bd. 29, Nr. 1–3, S. 213–218, Okt. 1995.

[46] I. Klimant, M. Kühl, R. N. Glud, und G. Holst, „Optical measurement of oxygen and temperature in microscale: strategies and biological applications“, *Sens. Actuators B Chem.*, Bd. 38, Nr. 1–3, S. 29–37, Jan. 1997.

[47] P. Douglas und K. Eaton, „Response characteristics of thin film oxygen sensors, Pt and Pd octaethylporphyrins in polymer films“, *Sens. Actuators B Chem.*, Bd. 82, Nr. 2–3, S. 200–208, Feb. 2002.

[48] S.-K. Lee und I. Okura, „Photostable Optical Oxygen Sensing Material: PlatinumTetrakis(pentafluorophenyl)porphyrin Immobilized in Polystyrene“, *Anal. Commun.*, Bd. 34, Nr. 6, S. 185–188, Jan. 1997.

[49] K. Koren, S. M. Borisov, und I. Klimant, „Stable optical oxygen sensing materials based on click-coupling of fluorinated platinum(II) and palladium(II) porphyrins--A convenient way to eliminate dye migration and leaching“, *Sens. Actuators B Chem.*, Bd. 169, Nr. 5, S. 173–181, Juli 2012.

[50] P. Peumans, A. Yakimov, und S. R. Forrest, „Small molecular weight organic thin-film photodetectors and solar cells“, *J. Appl. Phys.*, Bd. 93, Nr. 7, S. 3693–3723, Apr. 2003.

[51] F.-P. Montforts, B. Gerlach, und F. Hoeper, „Discovery and Synthesis of Less Common Natural Hydroporphyrins“, *Chem. Rev.*, Bd. 94, Nr. 2, S. 327–347, März 1994.

[52] G. Khalil, M. Gouterman, S. Ching, C. Costin, L. Coyle, S. Gouin, E. Green, M. Sadilek, R. Wan, J. Yearyean, und B. Zelelow, „Synthesis and spectroscopic characterization of Ni, Zn, Pd and Pt tetra(pentafluorophenyl)porpholactone with comparisons to Mg, Zn, Y, Pd and Pt metal complexes of tetra(pentafluorophenyl)porphine“, *J. Porphyr. Phthalocyanines*, Bd. 06, Nr. 02, S. 135–145, Feb. 2002.

[53] H. L. Anderson, A. P. Wylie, und K. Prout, „meso-Tetraalkynylporphyrins“, *J. Chem. Soc. [Perkin 1]*, Nr. 10, S. 1607–1612, Jan. 1998.

[54] A. Jasat und D. Dolphin, „Expanded Porphyrins and Their Heterologs“, *Chem. Rev.*, Bd. 97, Nr. 6, S. 2267–2340, Okt. 1997.

[55] E. Vogel, „Novel porphyrinoid macrocycles and their metal complexes“, *J. Heterocycl. Chem.*, Bd. 33, Nr. 5, S. 1461–1487, Sep. 1996.

[56] T. D. Lash, „Modification of the porphyrin chromophore by ring fusion: identifying trends due to annelation of the porphyrin nucleus“, *J. Porphyr. Phthalocyanines*, Bd. 5, Nr. 3, S. 267–288, März 2001.

[57] J. P. Lewtak und D. T. Gryko, „Synthesis of π-extended porphyrins via intramolecular oxidative coupling“, *Chem. Commun.*, Bd. 48, Nr. 81, S. 10069–10086, Sep. 2012.

[58] T. E. O. Screen, I. M. Blake, L. H. Rees, W. Clegg, S. J. Borwick, und H. L. Anderson, „Making conjugated connections to porphyrins: a comparison of alkyne, alkene, imine and azo links“, *J. Chem. Soc. [Perkin 1]*, Nr. 3, S. 320–329, Jan. 2002.

[59] V. V. Rozhkov, M. Khajehpour, und S. A. Vinogradov, „Luminescent Zn and Pd tetranaphthaloporphyrins“, *Inorg. Chem.*, Bd. 42, Nr. 14, S. 4253–4255, Juli 2003.

[60] O. S. Finikova, A. V. Cheprakov, und S. A. Vinogradov, „Synthesis and luminescence of soluble meso-unsubstituted tetrabenzo- and tetranaphtho[2,3]porphyrins“, *J. Org. Chem.*, Bd. 70, Nr. 23, S. 9562–9572, Nov. 2005.

[61] G. Qian und Z. Y. Wang, „Near-Infrared Organic Compounds and Emerging Applications“, *Chem. – Asian J.*, Bd. 5, Nr. 5, S. 1006–1029, Mai 2010.

[62] K. Dedeian, P. I. Djurovich, F. O. Garces, G. Carlson, und R. J. Watts, „A new synthetic route to the preparation of a series of strong photoreducing agents: fac-tris-ortho-metalated complexes of iridium(III) with substituted 2-phenylpyridines“, *Inorg. Chem.*, Bd. 30, Nr. 8, S. 1685–1687, Apr. 1991.

[63] M. S. Lowry und S. Bernhard, „Synthetically Tailored Excited States: Phosphorescent, Cyclometalated Iridium(III) Complexes and Their Applications“, *Chem. – Eur. J.*, Bd. 12, Nr. 31, S. 7970–7977, Okt. 2006.

[64] Y. Feng, J. Cheng, L. Zhou, X. Zhou, und H. Xiang, „Ratiometric optical oxygen sensing: a review in respect of material design“, *Analyst*, Bd. 137, Nr. 21, S. 4885–4901, Okt. 2012.

[65] W. Lu, B.-X. Mi, M. C. W. Chan, Z. Hui, C.-M. Che, N. Zhu, und S.-T. Lee, „Light-Emitting Tridentate Cyclometalated Platinum(II) Complexes Containing σ-Alkynyl Auxiliaries: Tuning of Photo- and Electrophosphorescence“, *J. Am. Chem. Soc.*, Bd. 126, Nr. 15, S. 4958–4971, Apr. 2004.

[66] A. Ajayaghosh, „Donor–acceptor type low band gap polymers: polysquaraines and related systems“, *Chem. Soc. Rev.*, Bd. 32, Nr. 4, S. 181–191, Juni 2003.

[67] H.-K. Yip, C.-M. Che, Z.-Y. Zhou, und T. C. W. Mak, „Photophysical properties and X-ray crystal structure of a luminescent platinum(II) dimer [Pt2(2,2′ : 6′,2″-terpyridine)2(Gua)](ClO4)3·H2O (Gua = guanidine anion)“, *J. Chem. Soc. Chem. Commun.*, Nr. 18, S. 1369–1371, Jan. 1992.

[68] O. S. Finikova, A. V. Cheprakov, P. J. Carroll, und S. A. Vinogradov, „Novel route to functionalized tetraaryltetra[2,3]naphthaloporphyrins via oxidative aromatization“, *J. Org. Chem.*, Bd. 68, Nr. 19, S. 7517–7520, Sep. 2003.

[69] R. C. Evans, P. Douglas, und C. J. Winscom, „Coordination complexes exhibiting room-temperature phosphorescence: Evaluation of their suitability as triplet emitters in organic light emitting diodes“, *Coord. Chem. Rev.*, Bd. 250, Nr. 15–16, S. 2093–2126, Aug. 2006.

[70] D. B. Papkovsky, G. V. Ponomarev, W. Trettnak, und P. O'Leary, „Phosphorescent Complexes of Porphyrin Ketones: Optical Properties and Application to Oxygen Sensing“, *Anal. Chem.*, Bd. 67, Nr. 22, S. 4112–4117, Nov. 1995.

[71] J. H. Helberger, A. von Rebay, und D. B. Hevér., „Über die Einwirkung von Metallen auf o-Cyanacetophenon sowie auf 3-Methylphtalimidin; Synthese des Tetrabenzoporphins. III. Mitteilung zur Kenntnis der Benzoporphine“, *Justus Liebigs Ann. Chem.*, Bd. 533, Nr. 1, S. 197–215, Jan. 1938.

[72] P. A. Barrett, R. P. Linstead, F. G. Rundall, und G. a. P. Tuey, „197. Phthalocyanines and related compounds. Part XIX. Tetrabenzporphin, tetrabenzmonazaporphin and their metallic derivatives“, *J. Chem. Soc. Resumed*, Nr. 0, S. 1079–1092, Jan. 1940.

[73] D. B. P. S. M. Borisov, „Photophysical properties of the new phosphorescent platinum(II) and palladium(II) complexes of benzoporphyrins and chlorins“, *J. Photochem. Photobiol. -Chem. - J PHOTOCHEM PHOTOBIOL -CHEM*, Bd. 206, Nr. 1, S. 87–92, 2009.

[74] F. Niedermair, S. M. Borisov, G. Zenkl, O. T. Hofmann, H. Weber, R. Saf, und I. Klimant, „Tunable Phosphorescent NIR Oxygen Indicators Based on Mixed Benzo- and Naphthoporphyrin Complexes“, *Inorg. Chem.*, Bd. 49, Nr. 20, S. 9333–9342, Sep. 2010.

[75] S. M. Borisov, G. Zenkl, und I. Klimant, „Phosphorescent Platinum(II) and Palladium(II) Complexes with Azatetrabenzoporphyrins--New Red Laser Diode-Compatible Indicators for Optical Oxygen Sensing“, *ACS Appl. Mater. Interfaces*, Bd. 2, Nr. 2, S. 366–374, Feb. 2010.

[76] R.-J. Cheng, Y.-R. Chen, S. L. Wang, und C. Y. Cheng, „Crystal and molecular structure of a five-coordinate zinc complex of meso-tetraphenyltetrabenzoprophyrin“, *Polyhedron*, Bd. 12, Nr. 11, S. 1353–1360, Juni 1993.

[77] R. E. Haddad, S. Gazeau, J. Pécaut, J.-C. Marchon, C. J. Medforth, und J. A. Shelnutt, „Origin of the Red Shifts in the Optical Absorption Bands of Nonplanar Tetraalkylporphyrins“, *J. Am. Chem. Soc.*, Bd. 125, Nr. 5, S. 1253–1268, Feb. 2003.

[78] I. Dunphy, S. A. Vinogradov, und D. F. Wilson, „Oxyphor R2 and G2: phosphors for measuring oxygen by oxygen-dependent quenching of phosphorescence“, *Anal. Biochem.*, Bd. 310, Nr. 2, S. 191–198, Nov. 2002.

[79] A. Y. Lebedev, A. V. Cheprakov, S. Sakadzić, D. A. Boas, D. F. Wilson, und S. A. Vinogradov, „Dendritic phosphorescent probes for oxygen imaging in biological systems“, *ACS Appl. Mater. Interfaces*, Bd. 1, Nr. 6, S. 1292–1304, Juni 2009.

[80] H. A. Clark, S. L. R. Barker, M. Brasuel, M. T. Miller, E. Monson, S. Parus, Z.-Y. Shi, A. Song, B. Thorsrud, R. Kopelman, A. Ade, W. Meixner, B. Athey, M. Hoyer, D. Hill, R. Lightle, und M. A. Philbert, „Subcellular optochemical nanobiosensors: probes encapsulated by biologically localised embedding (PEBBLEs)“, *Sens. Actuators B Chem.*, Bd. 51, Nr. 1–3, S. 12–16, Aug. 1998.

[81] Y. Cao, Y.-E. Lee Koo, und R. Kopelman, „Poly(decyl methacrylate)-based fluorescent PEBBLE swarm nanosensors for measuring dissolved oxygen in biosamples“, *The Analyst*, Bd. 129, Nr. 8, S. 745, 2004.

[82] Y.-E. L. Koo, Y. Cao, R. Kopelman, S. M. Koo, M. Brasuel, und M. A. Philbert, „Real-Time Measurements of Dissolved Oxygen Inside Live Cells by Organically Modified Silicate Fluorescent Nanosensors“, *Anal. Chem.*, Bd. 76, Nr. 9, S. 2498–2505, Mai 2004.

[83] Y.-E. K. Lee, E. E. Ulbrich, G. Kim, H. Hah, C. Strollo, W. Fan, R. Gurjar, S. Koo, und R. Kopelman, „NIR luminescent oxygen nanosensors with nanoparticle matrix tailored sensitivity“, *Anal. Chem.*, Bd. 82, Nr. 20, S. 8446–8455, Okt. 2010.

[84] K. Koren, S. M. Borisov, R. Saf, und I. Klimant, „Strongly Phosphorescent Iridium(III)-Porphyrins - New Oxygen Indicators with Tuneable Photophysical Properties and Functionalities“, *Eur. J. Inorg. Chem.*, Bd. 2011, Nr. 10, S. 1531–1534, Apr. 2011.

[85] A. Yuan, J. Wu, X. Tang, L. Zhao, F. Xu, und Y. Hu, „Application of near-infrared dyes for tumor imaging, photothermal, and photodynamic therapies“, *J. Pharm. Sci.*, Bd. 102, Nr. 1, S. 6–28, Jan. 2013.

[86] J. Qian, D. Wang, F. Cai, Q. Zhan, Y. Wang, und S. He, „Photosensitizer encapsulated organically modified silica nanoparticles for direct two-photon photodynamic therapy and In Vivo functional imaging“, *Biomaterials*, Bd. 33, Nr. 19, S. 4851–4860, Juni 2012.

[87] M.-H. Qi und G.-F. Liu, „Synthesis and properties of transition metal benzoporphyrin compound liquid crystals“, *J. Mater. Chem.*, Bd. 13, Nr. 10, S. 2479–2484, Sep. 2003.

[88] S. M. Borisov und I. Klimant, „Efficient metallation in diphenylether – A convenient route to luminescent platinum(II) complexes“, *Dyes Pigments*, Bd. 83, Nr. 3, S. 312–316, Dez. 2009.

[89] N. K. M. N. Srinivas, S. V. Rao, D. V. G. L. N. Rao, B. K. Kimball, M. Nakashima, B. S. DeCristofano, und D. N. Rao, „Wavelength dependent studies of nonlinear absorption in zinc meso-tetra(p-methoxyphenyl)tetrabenzoporphyrin (Znmp TBP) using Z-scan technique“, *J. Porphyr. Phthalocyanines*, Bd. 5, Nr. 7, S. 549–554, Juli 2001.

[90] K. Yamashita, „EFFECTS OF EXPANSION OF THE π-ELECTRON SYSTEM ON PHOTOCURRENT QUANTUM YIELDS FOR PORPHYRIN PHOTOCELLS: MAGNESIUM AND ZINC TETRABENZPORPHYRIN SENSITIZERS“, *Chem. Lett.*, Bd. 11, Nr. 7, S. 1085–1088, 1982.

[91] K. R. Graham, Y. Yang, J. R. Sommer, A. H. Shelton, K. S. Schanze, J. Xue, und J. R. Reynolds, „Extended Conjugation Platinum(II) Porphyrins for use in Near-Infrared Emitting Organic Light Emitting Diodes“, *Chem. Mater.*, Bd. 23, Nr. 24, S. 5305–5312, Dez. 2011.

[92] G. Bringmann, D. C. G. Götz, T. A. M. Gulder, T. H. Gehrke, T. Bruhn, T. Kupfer, K. Radacki, H. Braunschweig, A. Heckmann, und C. Lambert, „Axially chiral beta,beta'-bisporphyrins: synthesis and configurational stability tuned by the central metals“, *J. Am. Chem. Soc.*, Bd. 130, Nr. 52, S. 17812–17815, Dez. 2008.

[93] J. Mack, Y. Asano, N. Kobayashi, und M. J. Stillman, „Application of MCD spectroscopy and TD-DFT to a highly non-planar porphyrinoid ring system. New insights on red-shifted porphyrinoid spectral bands“, *J. Am. Chem. Soc.*, Bd. 127, Nr. 50, S. 17697–17711, Dez. 2005.

[94] M. J. Currie, J. K. Mapel, T. D. Heidel, S. Goffri, und M. A. Baldo, „High-Efficiency Organic Solar Concentrators for Photovoltaics“, *Science*, Bd. 321, Nr. 5886, S. 226–228, Nov. 2008.

[95] A. V. C. Mikhail A. Filatov, „The synthesis of new tetrabenzo- and tetranaphthoporphyrins via the addition reactions of 4,7-dihydroisoindole“, *Tetrahedron*, Bd. 67, Nr. 19, S. 3559–3566, 2011.

[96] T. C. Rosenow, K. Walzer, und K. Leo, „Near-infrared organic light emitting diodes based on heavy metal phthalocyanines“, *J. Appl. Phys.*, Bd. 103, Nr. 4, S. 043105, Feb. 2008.

[97] P. S. Vincett, E. M. Voigt, und K. E. Rieckhoff, „Phosphorescence and Fluorescence of Phthalocyanines“, *J. Chem. Phys.*, Bd. 55, Nr. 8, S. 4131–4140, Okt. 1971.

[98] B. Nacht, C. Larndorfer, S. Sax, S. M. Borisov, M. Hajnsek, F. Sinner, E. J. W. List-Kratochvil, und I. Klimant, „Integrated catheter system for continuous glucose measurement and simultaneous insulin infusion“, *Biosens. Bioelectron.*, Bd. 64, S. 102–110, Feb. 2015.

[99] S. M. LeCours, H.-W. Guan, S. G. DiMagno, C. H. Wang, und M. J. Therien, „Push−Pull Arylethynyl Porphyrins: New Chromophores That Exhibit Large Molecular First-Order Hyperpolarizabilities“, *J. Am. Chem. Soc.*, Bd. 118, Nr. 6, S. 1497–1503, Jan. 1996.

[100] P. N. Taylor, J. Huuskonen, R. T. Aplin, H. L. Anderson, J. Huuskonen, G. Rumbles, und E. Williams, „Conjugated porphyrin oligomers from monomer to hexamer“, *Chem. Commun.*, Nr. 8, S. 909–910, Jan. 1998.

[101] A. Wickramasinghe, L. Jaquinod, D. J. Nurco, und K. M. Smith, „Investigations on the directive effects of a single meso-substituent via nitration of 5,12,13,17,18-pentasubstituted porphyrins: syntheses of conjugated β-nitroporphyrins“, *Tetrahedron*, Bd. 57, Nr. 20, S. 4261–4269, Mai 2001.

[102] H. Fliegl und D. Sundholm, „Aromatic pathways of porphins, chlorins, and bacteriochlorins“, *J. Org. Chem.*, Bd. 77, Nr. 7, S. 3408–3414, Apr. 2012.

[103] T. K. Ahn, K. S. Kim, D. Y. Kim, S. B. Noh, N. Aratani, C. Ikeda, A. Osuka, und D. Kim, „Relationship between Two-Photon Absorption and the π-Conjugation Pathway in Porphyrin Arrays through Dihedral Angle Control“, *J. Am. Chem. Soc.*, Bd. 128, Nr. 5, S. 1700–1704, Feb. 2006.

[104] M. Tanaka, S. Hayashi, S. Eu, T. Umeyama, Y. Matano, und H. Imahori, „Novel unsymmetrically π-elongated porphyrin for dye-sensitized TiO2 cells“, *Chem. Commun.*, Nr. 20, S. 2069–2071, Mai 2007.

[105] A. K. Sahoo, Y. Nakamura, N. Aratani, K. S. Kim, S. B. Noh, H. Shinokubo, D. Kim, und A. Osuka, „Synthesis of Brominated Directly Fused Diporphyrins through Gold(III)-Mediated Oxidation“, *Org. Lett.*, Bd. 8, Nr. 18, S. 4141–4144, Aug. 2006.

[106] P. Rempala, J. Kroulík, und B. T. King, „Investigation of the Mechanism of the Intramolecular Scholl Reaction of Contiguous Phenylbenzenes“, *J. Org. Chem.*, Bd. 71, Nr. 14, S. 5067–5081, Juni 2006.

[107] Y. Lu und J. S. Moore, „Semi-fused hexaphenyl hexa-peri-hexabenzocoronene: a novel fluorophore from an intramolecular Scholl reaction“, *Tetrahedron Lett.*, Bd. 50, Nr. 28, S. 4071–4077, Juli 2009.

[108] J. Zhao, S. Ji, und H. Guo, „Triplet–triplet annihilation based upconversion: from triplet sensitizers and triplet acceptors to upconversion quantum yields“, *RSC Adv.*, Bd. 1, Nr. 6, S. 937–950, Okt. 2011.

[109] M. Haase und H. Schäfer, „Upconverting nanoparticles“, *Angew. Chem. Int. Ed Engl.*, Bd. 50, Nr. 26, S. 5808–5829, Juni 2011.

[110] W. Niu, S. Wu, S. Zhang, und L. Li, „Synthesis of colour tunable lanthanide-ion doped NaYF4 upconversion nanoparticles by controlling temperature“, *Chem. Commun. Camb. Engl.*, Bd. 46, Nr. 22, S. 3908–3910, Juni 2010.

[111] A. Monguzzi, J. Mezyk, F. Scotognella, R. Tubino, und F. Meinardi, „Upconversion-induced fluorescence in multicomponent systems: Steady-state excitation power threshold“, *Phys. Rev. B*, Bd. 78, Nr. 19, S. 195112, Nov. 2008.

[112] A. Monguzzi, R. Tubino, und F. Meinardi, „Upconversion-induced delayed fluorescence in multicomponent organic systems: Role of Dexter energy transfer“, *Phys. Rev. B*, Bd. 77, Nr. 15, S. 155122, Apr. 2008.

[113] T. N. Singh-Rachford und F. N. Castellano, „Photon upconversion based on sensitized triplet–triplet annihilation“, *Coord. Chem. Rev.*, Bd. 254, Nr. 21–22, S. 2560–2573, Nov. 2010.

[114] Y. Y. Cheng, T. Khoury, R. G. C. R. Clady, M. J. Y. Tayebjee, N. J. Ekins-Daukes, M. J. Crossley, und T. W. Schmidt, „On the efficiency limit of triplet–triplet annihilation for photochemical upconversion“, *Phys. Chem. Chem. Phys.*, Bd. 12, Nr. 1, S. 66–71, Dez. 2009.

[115] T. N. Singh-Rachford und F. N. Castellano, „Triplet Sensitized Red-to-Blue Photon Upconversion“, *J. Phys. Chem. Lett.*, Bd. 1, Nr. 1, S. 195–200, Jan. 2010.

[116] S. M. Borisov, R. Saf, R. Fischer, und I. Klimant, „Synthesis and properties of new phosphorescent red light-excitable platinum(II) and palladium(II) complexes with Schiff bases for oxygen sensing and triplet-triplet annihilation-based upconversion“, *Inorg. Chem.*, Bd. 52, Nr. 3, S. 1206–1216, Feb. 2013.

[117] M.-E. Ragoussi, G. Katsukis, A. Roth, J. Malig, G. de la Torre, D. M. Guldi, und T. Torres, „Electron-Donating Behavior of Few-Layer Graphene in Covalent Ensembles with Electron-Accepting Phthalocyanines“, *J. Am. Chem. Soc.*, Bd. 136, Nr. 12, S. 4593–4598, März 2014.

[118] A. V. Ivanov, K. V. Kabanova, M. O. Breusova, I. V. Zhukov, L. G. Tomilova, und N. S. Zefirov, „New phosphorus-containing metal phthalocyanine complexes. Synthesis and spectral and electrochemical studies“, *Russ. Chem. Bull.*, Bd. 57, Nr. 8, S. 1665–1670, Aug. 2008.

[119] A. K. Bansal, W. Holzer, A. Penzkofer, und T. Tsuboi, „Absorption and emission spectroscopic characterization of platinum-octaethyl-porphyrin (PtOEP)“, *Chem. Phys.*, Bd. 330, Nr. 1–2, S. 118–129, Nov. 2006.

[120] J. S. Lindsey, I. C. Schreiman, H. C. Hsu, P. C. Kearney, und A. M. Marguerettaz, „Rothemund and Adler-Longo reactions revisited: synthesis of tetraphenylporphyrins under equilibrium conditions“, *J. Org. Chem.*, Bd. 52, Nr. 5, S. 827–836, März 1987.

[121] L. H. Hutter, B. J. Müller, K. Koren, S. M. Borisov, und I. Klimant, „Robust optical oxygen sensors based on polymer-bound NIR-emitting platinum(II)–benzoporphyrins“, *J. Mater. Chem. C*, Bd. 2, Nr. 36, S. 7589–7598, Aug. 2014.

[122] V. V. R. V. A. Vasin, „ChemInform Abstract: Mild and Efficient Method for the Preparation of tertButyl Esters“, *Cheminform*, Bd. 32, Nr. 33, 2010.

[123] K.-W. Poon, W. Liu, P.-K. Chan, Q. Yang, T.-W. D. Chan, T. C. W. Mak, und D. K. P. Ng, „Tetrapyrrole Derivatives Substituted with Ferrocenylethynyl Moieties. Synthesis and Electrochemical Studies†“, *J. Org. Chem.*, Bd. 66, Nr. 5, S. 1553–1559, März 2001.

[124] E. R. Carraway, J. N. Demas, B. A. DeGraff, und J. R. Bacon, „Photophysics and photochemistry of oxygen sensors based on luminescent transition-metal complexes“, *Anal. Chem.*, Bd. 63, Nr. 4, S. 337–342, Feb. 1991.

[125] B. Enko, S. M. Borisov, J. Regensburger, W. Bäumler, G. Gescheidt, und I. Klimant, „Singlet Oxygen-Induced Photodegradation of the Polymers and Dyes in Optical Sensing Materials and the Effect of Stabilizers on These Processes“, *J. Phys. Chem. A*, Bd. 117, Nr. 36, S. 8873–8882, Sep. 2013.

[126] C. J. Medforth, R. E. Haddad, C. M. Muzzi, N. R. Dooley, L. Jaquinod, D. C. Shyr, D. J. Nurco, M. M. Olmstead, K. M. Smith, J.-G. Ma, und J. A. Shelnutt, „Unusual aryl-porphyrin rotational barriers in peripherally crowded porphyrins“, *Inorg. Chem.*, Bd. 42, Nr. 7, S. 2227–2241, Apr. 2003.

[127] I. O. Sang-Kyung Lee, „Photostable Optical Oxygen Sensing Material: Platinum Tetrakis(pentafluorophenyl)porphyrin Immobilized in Polystyrene“, *Anal. Commun.*, Bd. 34, Nr. 6, S. 185–188, 1997.

[128] G. Seybold und G. Wagenblast, „New perylene and violanthrone dyestuffs for fluorescent collectors“, *Dyes Pigments*, Bd. 11, Nr. 4, S. 303–317, 1989.

[129] S. M. Borisov, C. Larndorfer, und I. Klimant, „Triplet–Triplet Annihilation-Based Anti-Stokes Oxygen Sensing Materials with a Very Broad Dynamic Range“, *Adv. Funct. Mater.*, Bd. 22, Nr. 20, S. 4360–4368, Okt. 2012.

11. List of Chemicals and Solvents

Table 3 List of chemicals

Chemical	Company
Tetrahydroisobenzofuran-1,3-dione	Sigma-Aldrich
2-ethylhexylamine	Sigma-Aldrich
N-chlorosuccinimide	Sigma-Aldrich
Thiophenol	Sigma-Aldrich
Meta-Chloroperoxybenzoic acid (m-CPBA)	Acros Organics
1,8-Diaza-7-bicyclo[5.4.0]undecene	Fluka
Potassium t-butoxide	Sigma-Aldrich
Ethyl 2-isocyanoacetate	ABCR
4,5-dichlorophthalonitrile	TCI
2-ethylhexane-1-thiol	Sigma-Aldrich
Fluorophenyl)acetic acid	ABCR
2-(p-tolyl)acetic acid	ABCR
Phthalonitrile	ABCR
Aluminum trichloride	Fluka
Bromine	Sigma-Aldrich
O-xylene	Fluka
Copper(I)cyanide	Fluka
Copper(I) iodide	Sigma-Aldrich
Iron trichloride	Roth
Molybdenumpentachloride	ACR
perylene (94710 fluorescent orange)	Kremer Pigmente
perylene (94720 fluorescent red)	Kremer Pigmente
3,9-perylenedicarboxylate	ABCR
PtTFPP	Frontier Scientific
Pt-OEP	Frontier Scientific

Table 4 List of solvents

Solvent	Abbreviation	Company
Dimethylformamide	DMF	Merck
Dichloromethane	DCM	Fisher
Tetrahydrofuran	THF	Roth
Ethyl acetate	EE	Roth
Cyclohexane	CH	Roth
Toluene	Tol	Fisher
Dimethylacetamide	DMA	Fluka
n-Hexane	Hex	Roth
Methanol	MeOH	Baker
Ethanol	EtOH	Australco
1,2-dichlorobenzene	-	Sigma-Aldrich
Trimethlbenzene	TMB	Acros Organics

13. Appendix

13.1 NMR Spectra

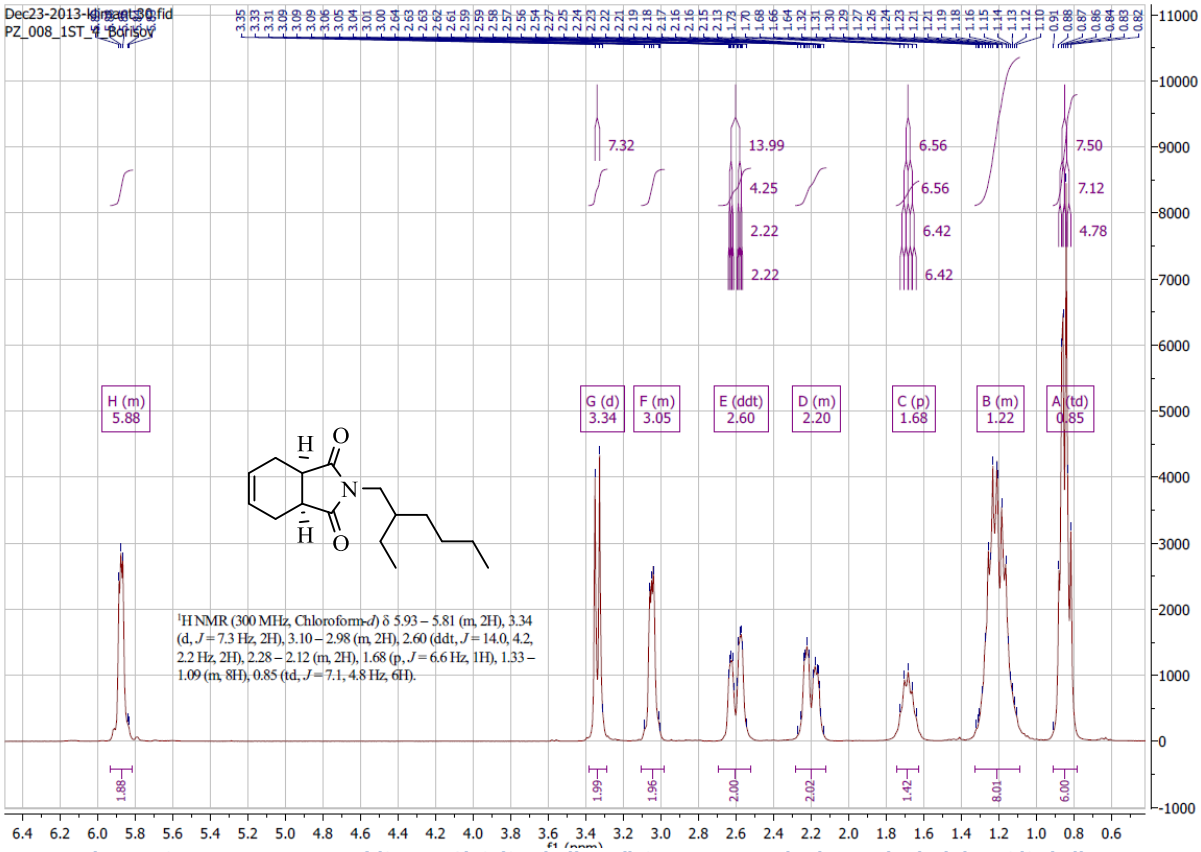

Figure 104 NMR spectrum of (3aR,7aS)-2-(2-ethylhexyl)-3a,4,7,7a-tetrahydro-1H-isoindole-1,3(2H)-dione

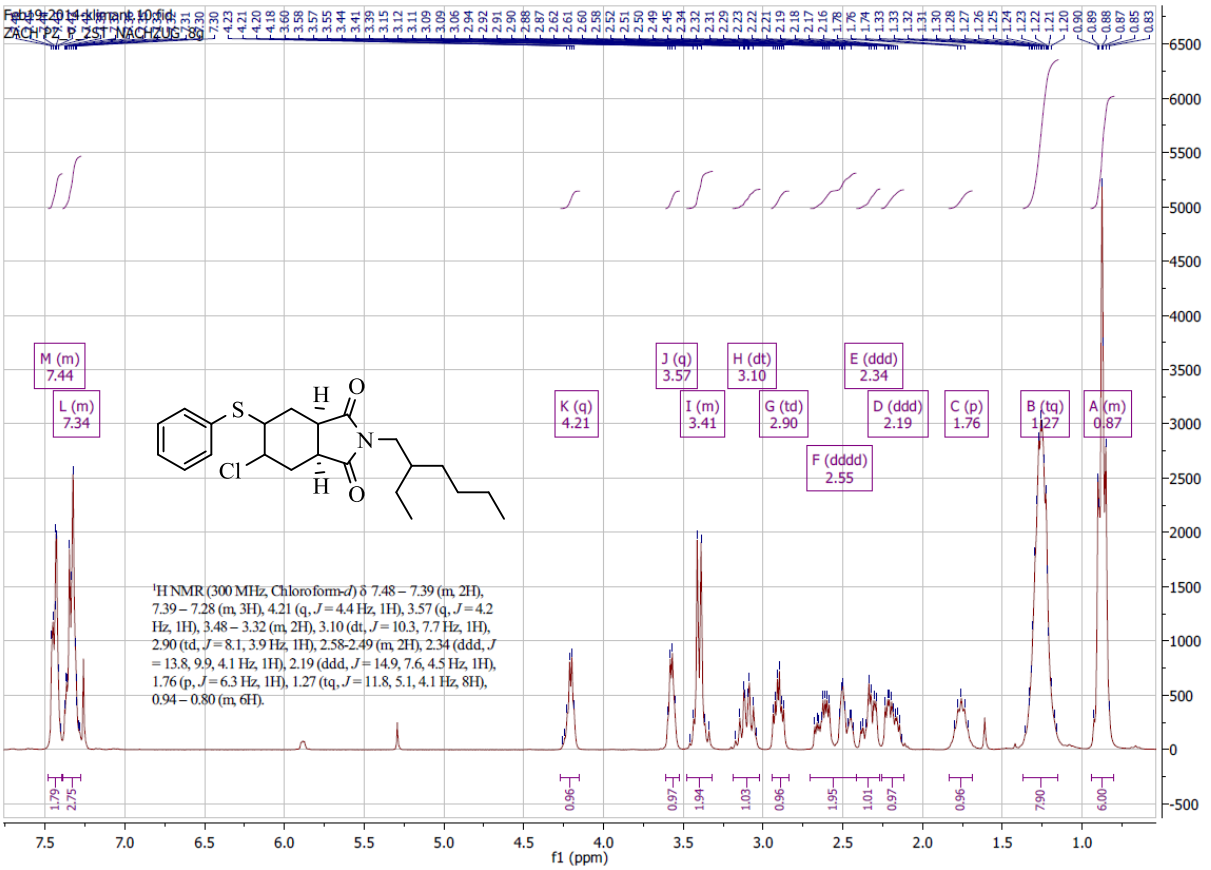

Figure 105 NMR spectrum of (3aS,7aR)-5-chloro-2-(2-ethylhexyl)-6-(phenylthio)hexahydro-1H-isoindole-1,3(2H)-dione

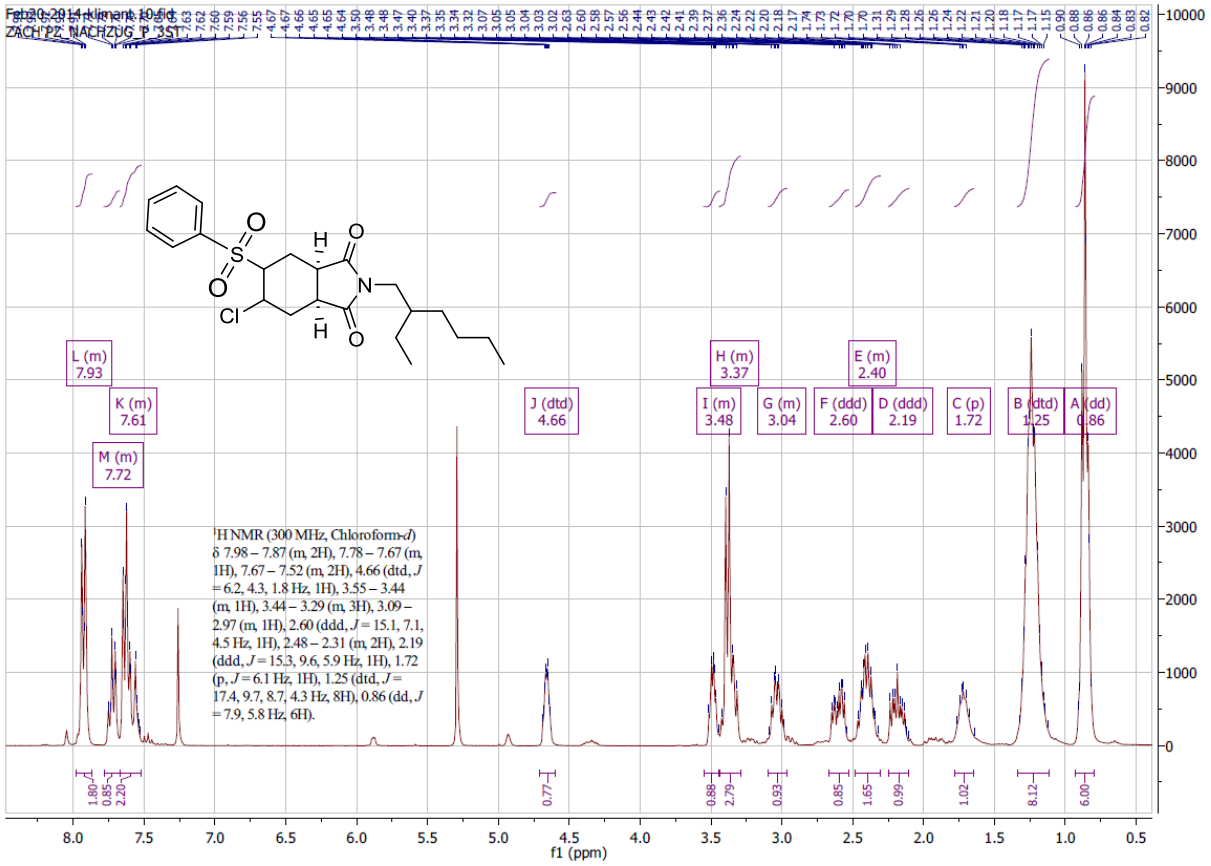

Figure 106 NMR spectrum of (3aS,7aR)-5-chloro-2-(2-ethylhexyl)-6-(phenylsulfonyl)hexahydro-1H-isoindole-1,3(2H)-dione

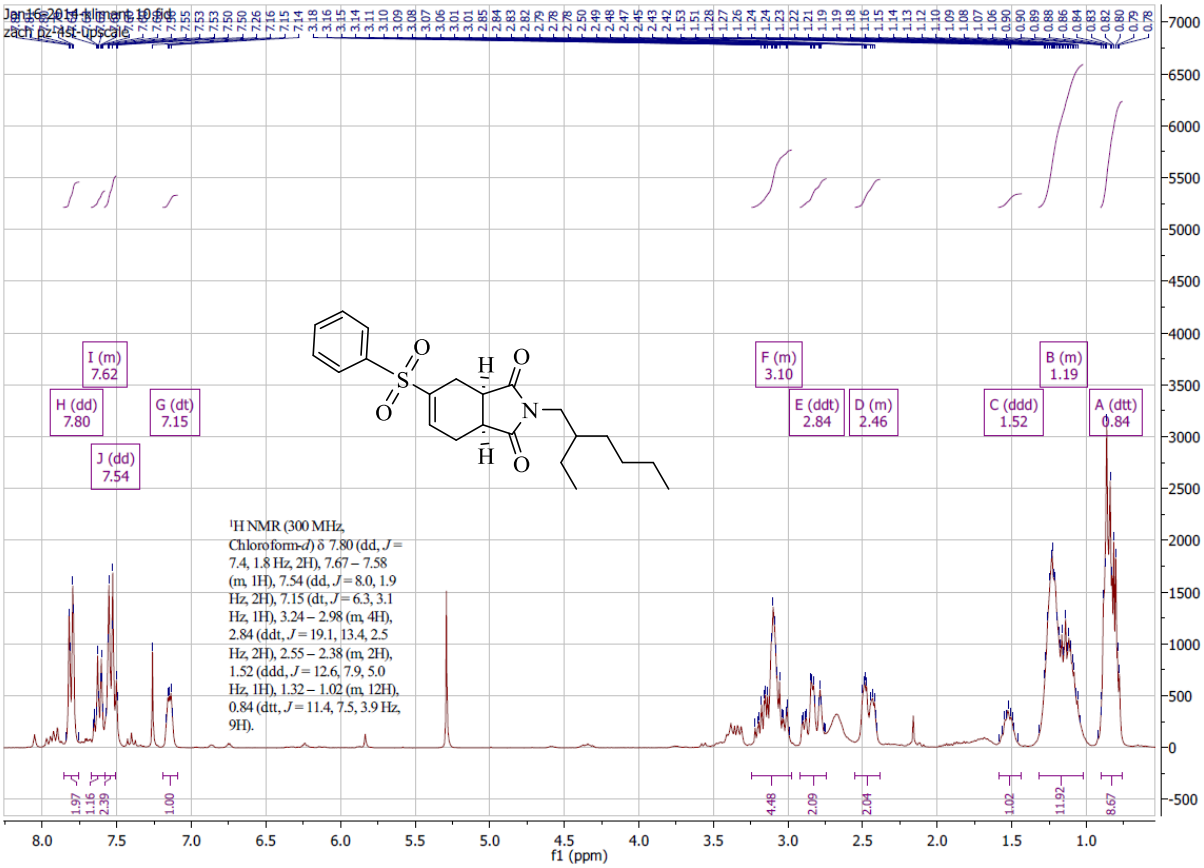

Figure 107 NMR spectrum of (3aR,7aS)-2-(2-ethylhexyl)-5-(phenylsulfonyl)-3a,4,7,7a-tetrahydro-1H-isoindole-1,3(2H)-dione

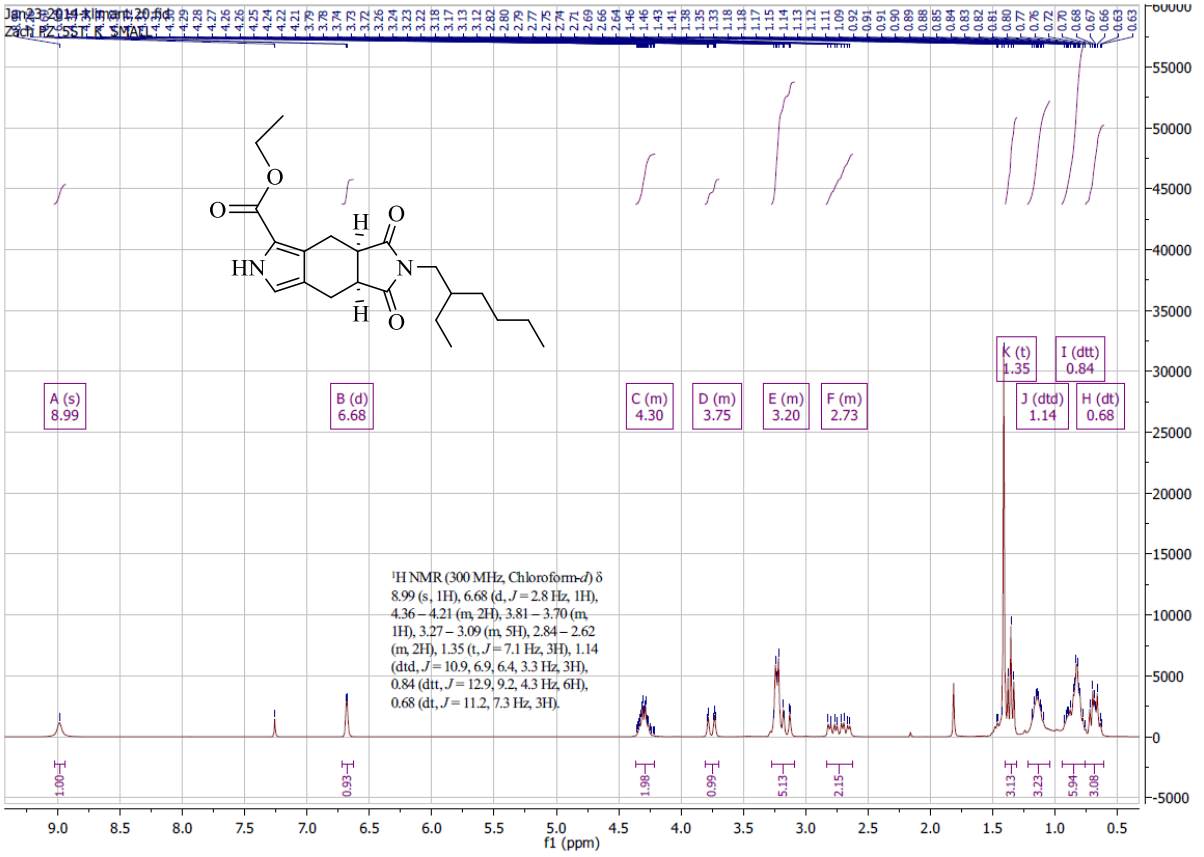

Figure 108 NMR spectrum of (4aS,7aR)-ethyl-6-(2-ethylhexyl)-5,7-dioxo-2,4,4a,5,6,7,7a,8-octahydropyrrolo[3,4-f]isoindole-1-carboxylate

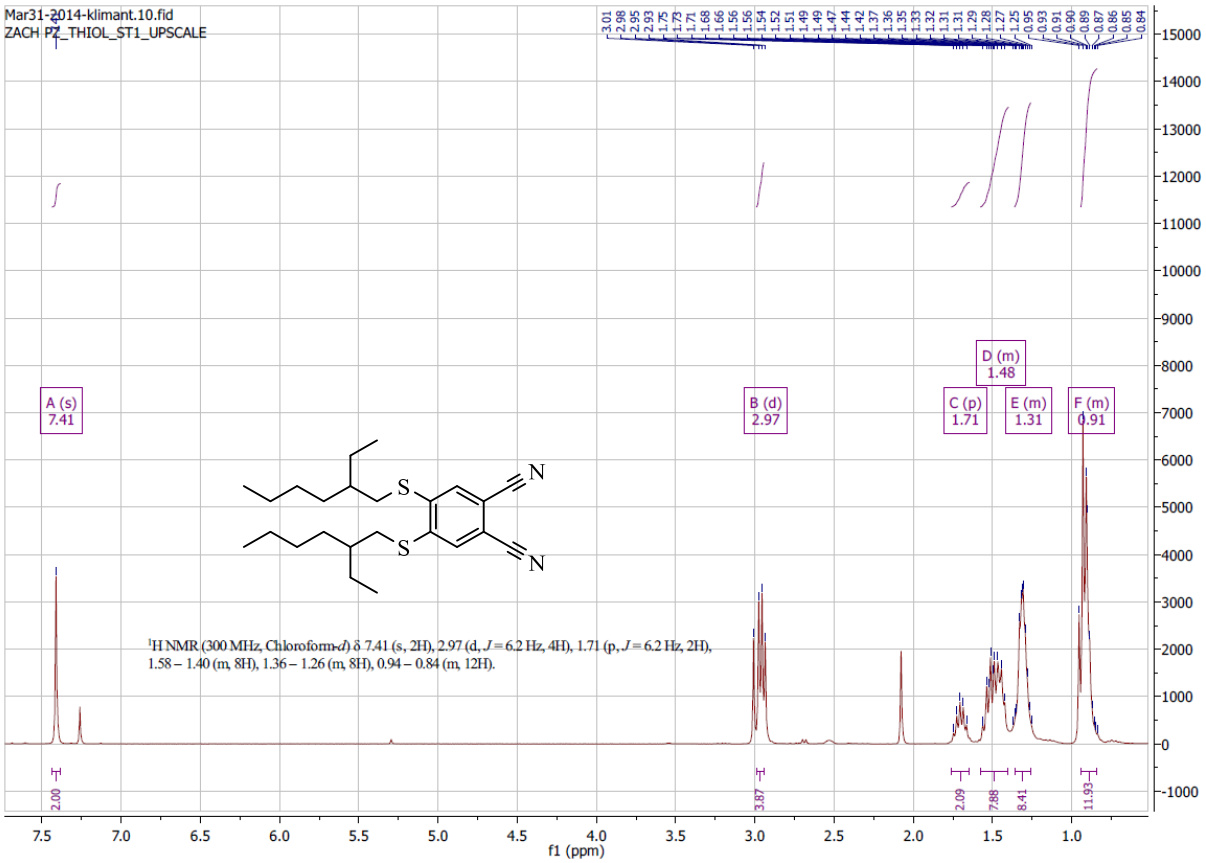

Figure 109 NMR spectrum of 4,5-bis((2-ethylhexyl)thio)phthalonitrile

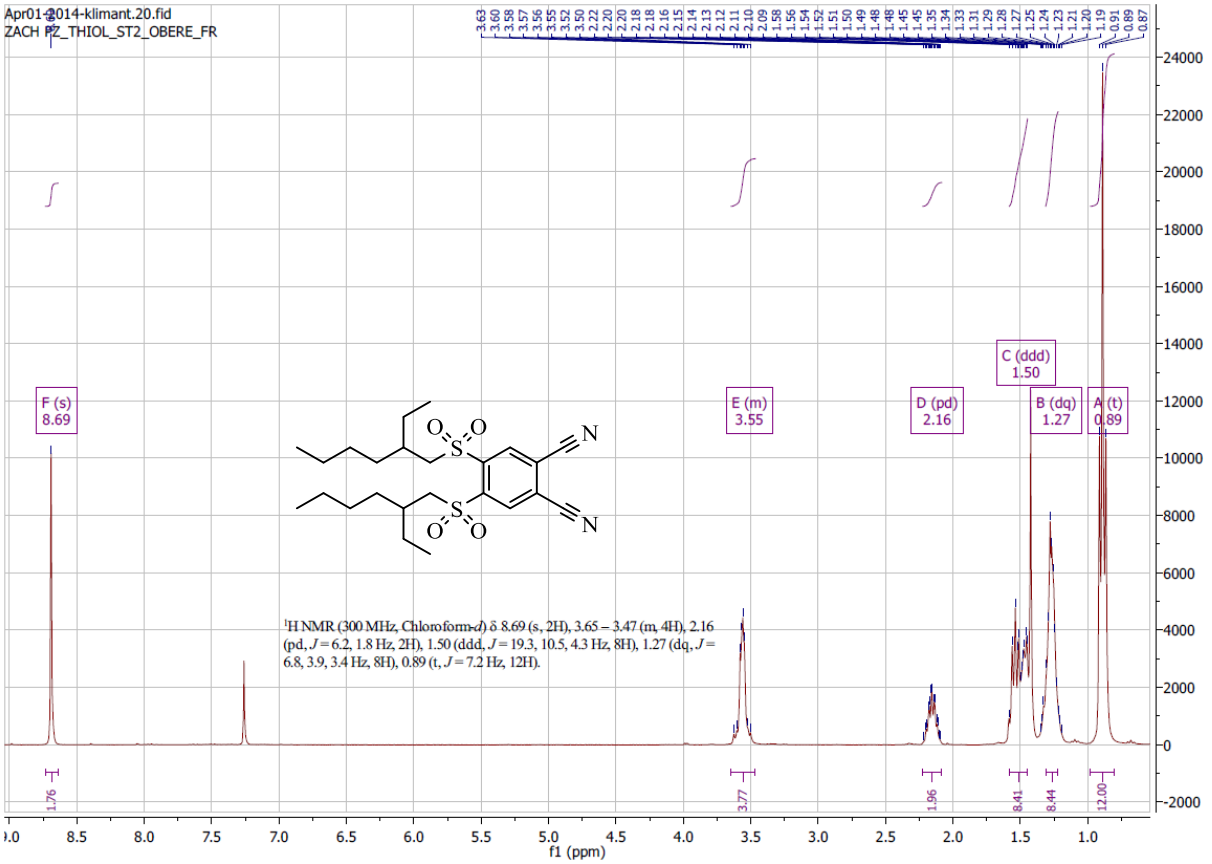

Figure 110 NMR spectrum of 4,5-bis((2-ethylhexyl)sulfonyl)phthalonitrile

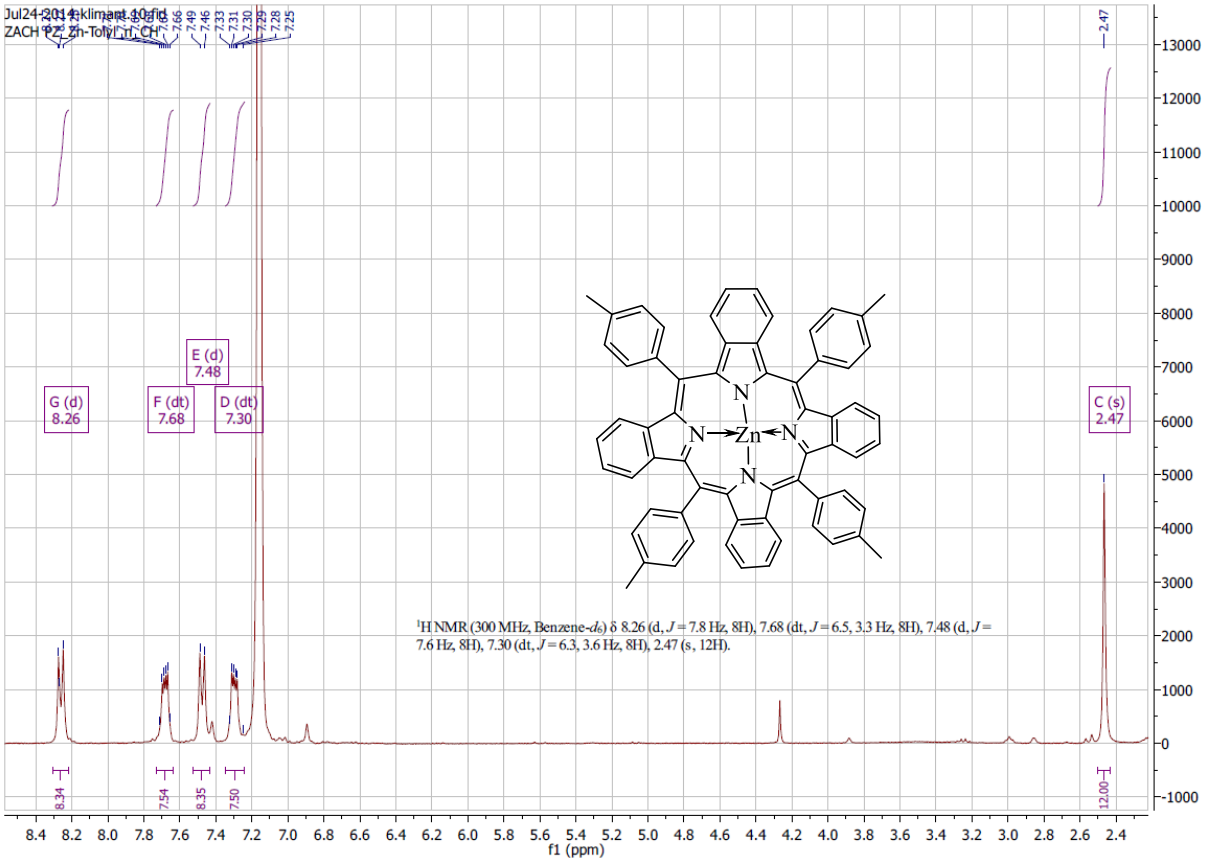

Figure 111 NMR spectrum of Zinc (II) meso-tetra(4-tolyl)tetrabenzoporphyrin (Zn-TTolTBP)

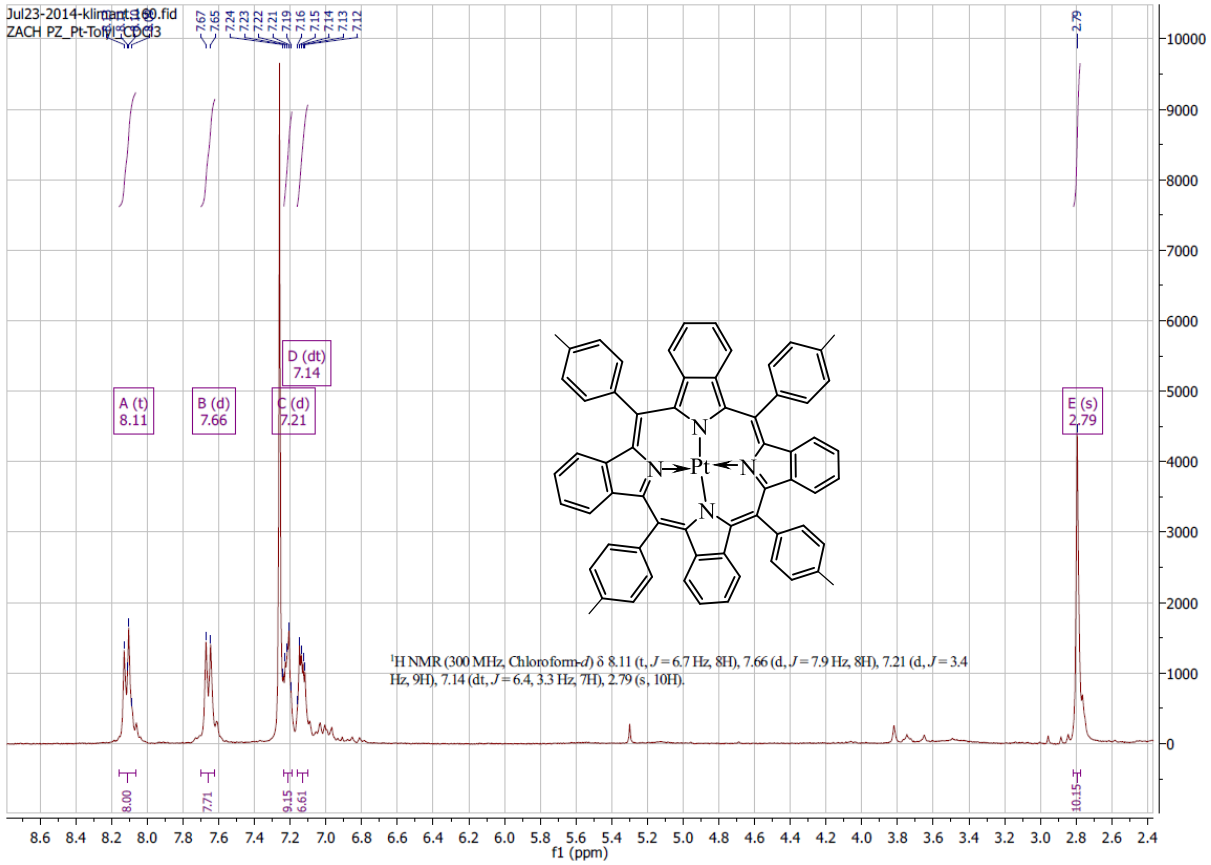

Figure 112 NMR spectrum of Platinum (II) meso-tetra(4-tolyl)tetrabenzoporphyrin (Pt-TTolTBP)

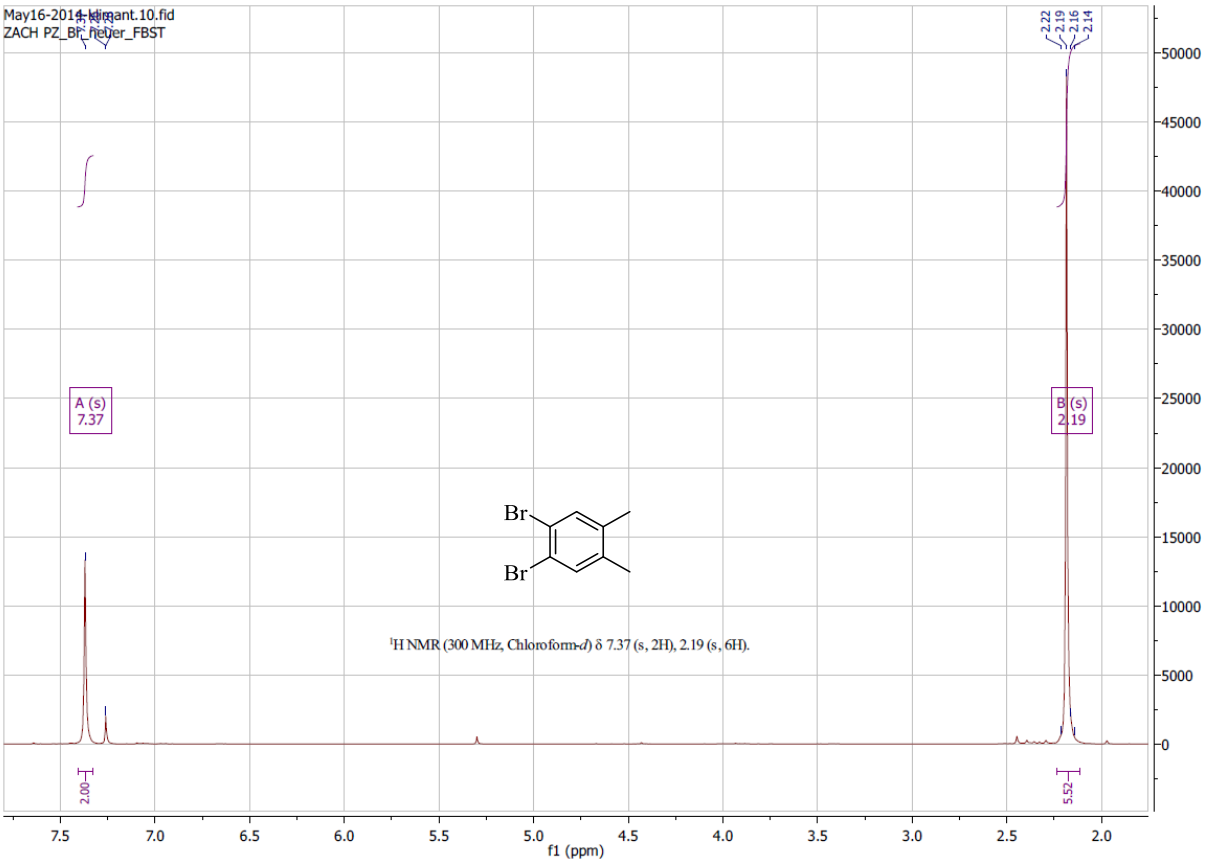

Figure 113 NMR spectrum of 1,2-dibromo-4,5-dimethylbenzene

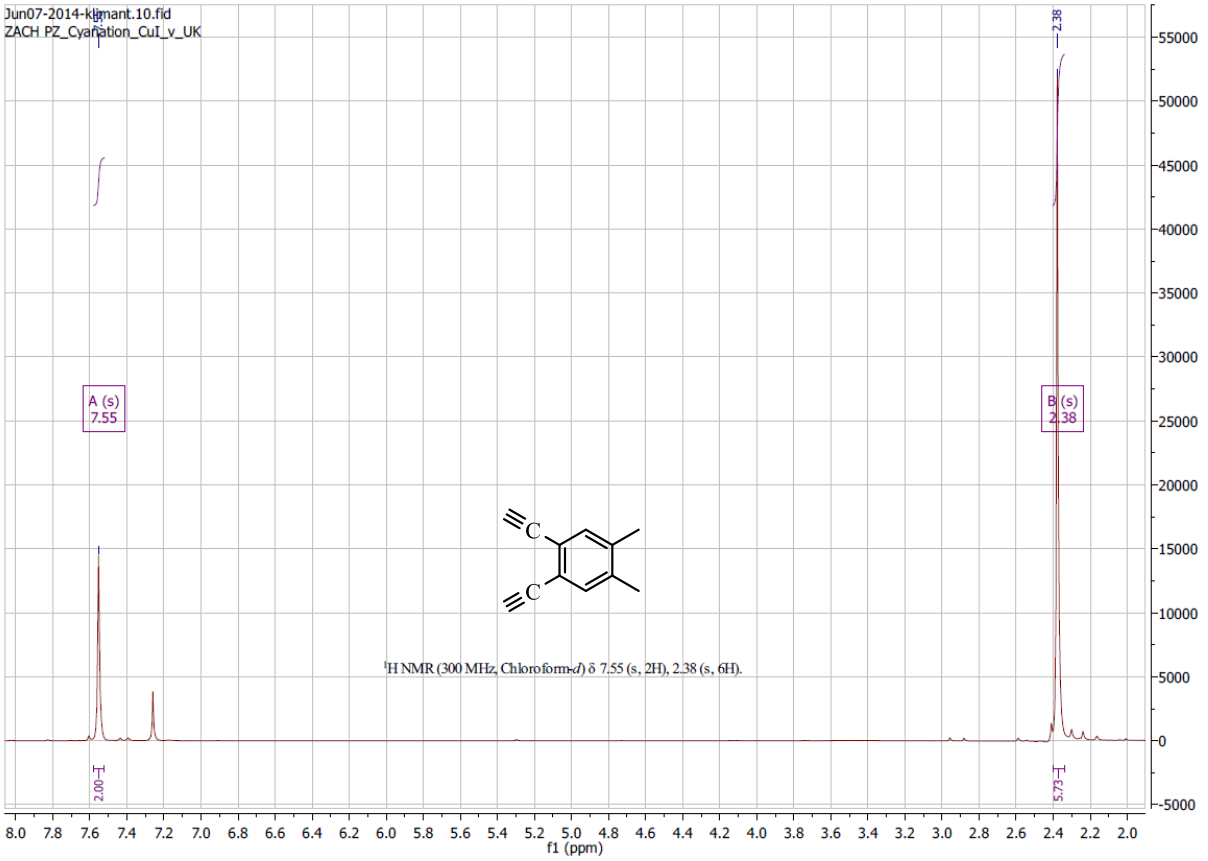

Figure 114 NMR spectrum of 1,2-diethynyl-4,5-dimethylbenzene

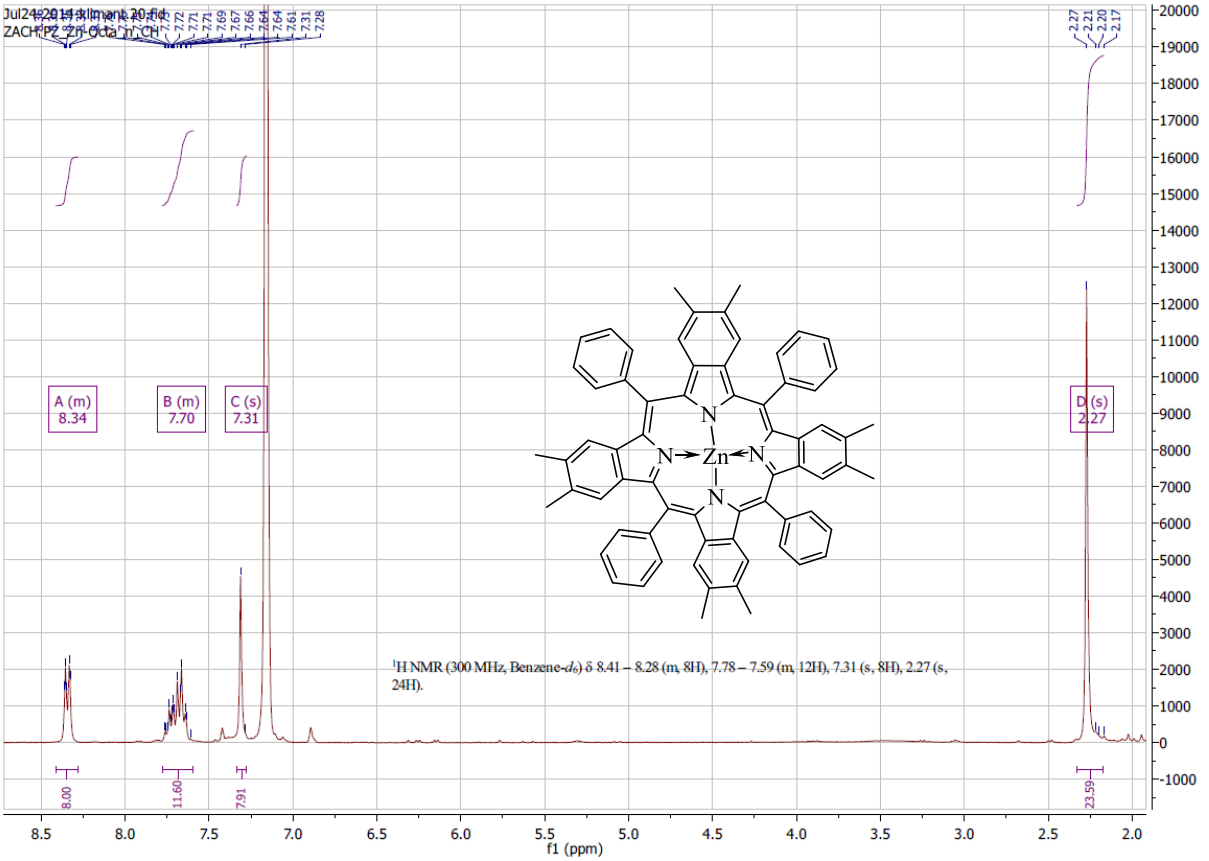

Figure 115 NMR spectrum of Zinc (II) meso-tetraphenyltetra(di-methyl)benzoporphyrin (Zn-TPTBPdM$_4$)

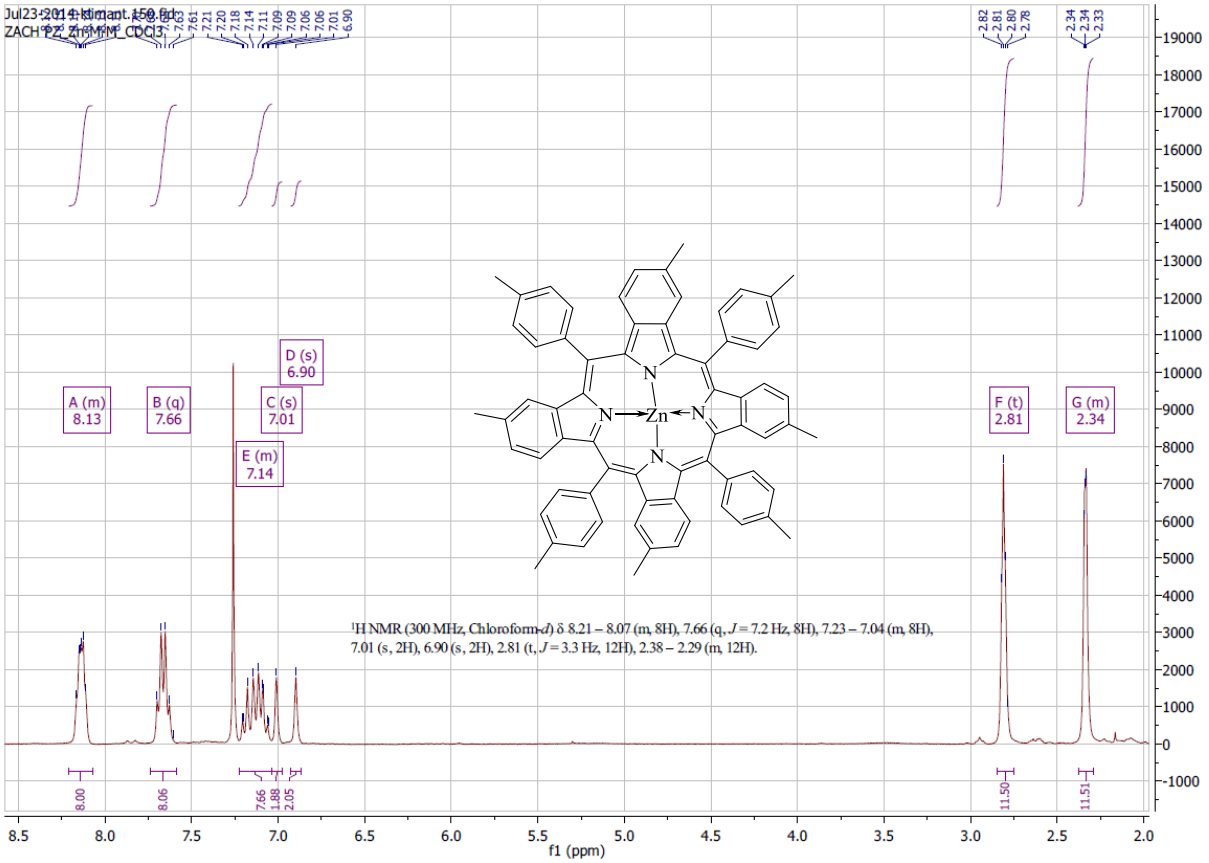

Figure 116 NMR spectrum of Zinc (II) meso-tetratolyltetra(mono-methyl)benzoporphyrin (Zn-TTolTBPmM$_4$)

13.2 Mass spectra

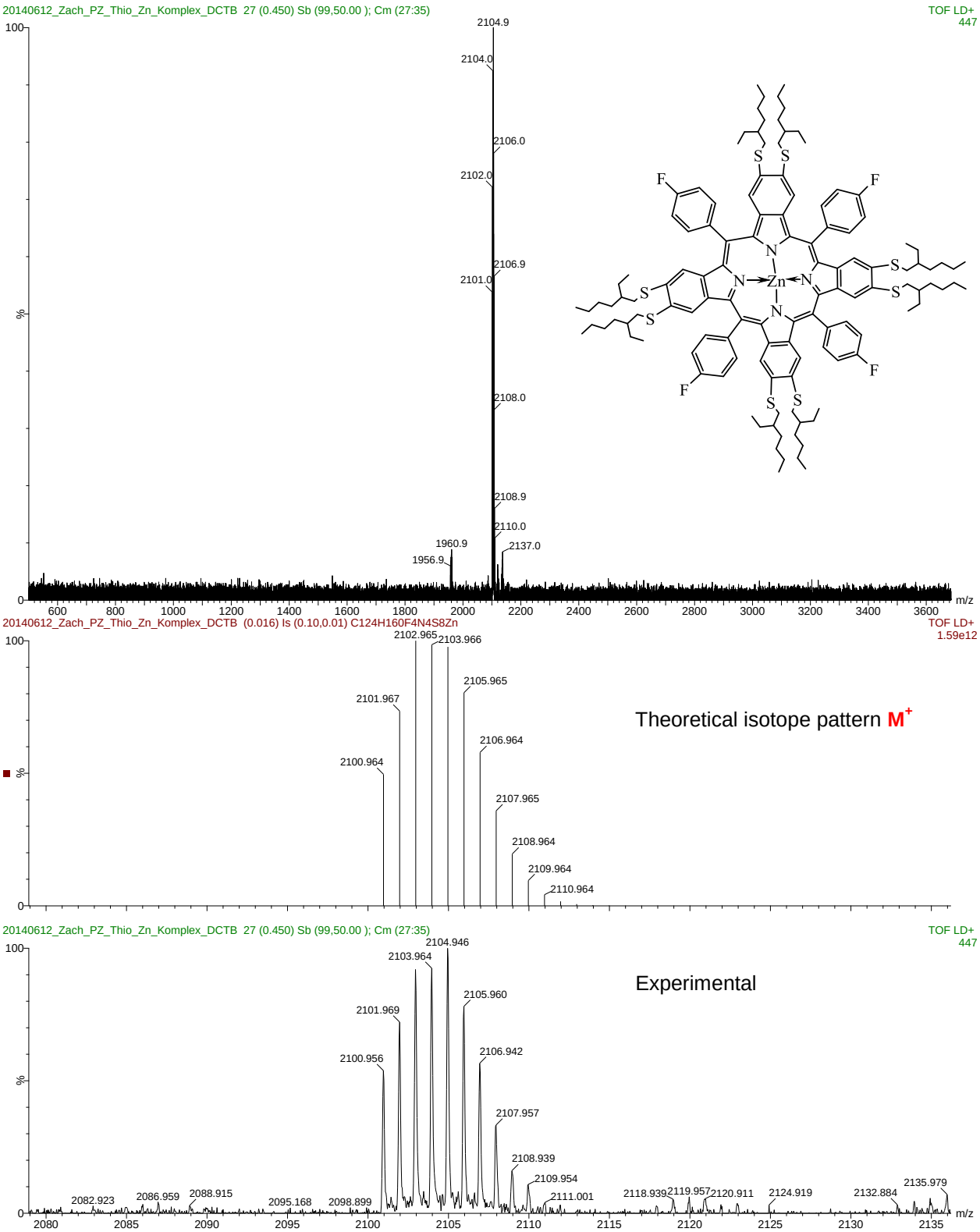

Figure 117 Mass spectrum of Zinc (II) -meso-tetra(4-fluorophenyl)tetra(4,5-bis((2-ethylhexyl)thio)benzoporphyrin(Zn-TPTBPF$_4$bEHT$_4$)

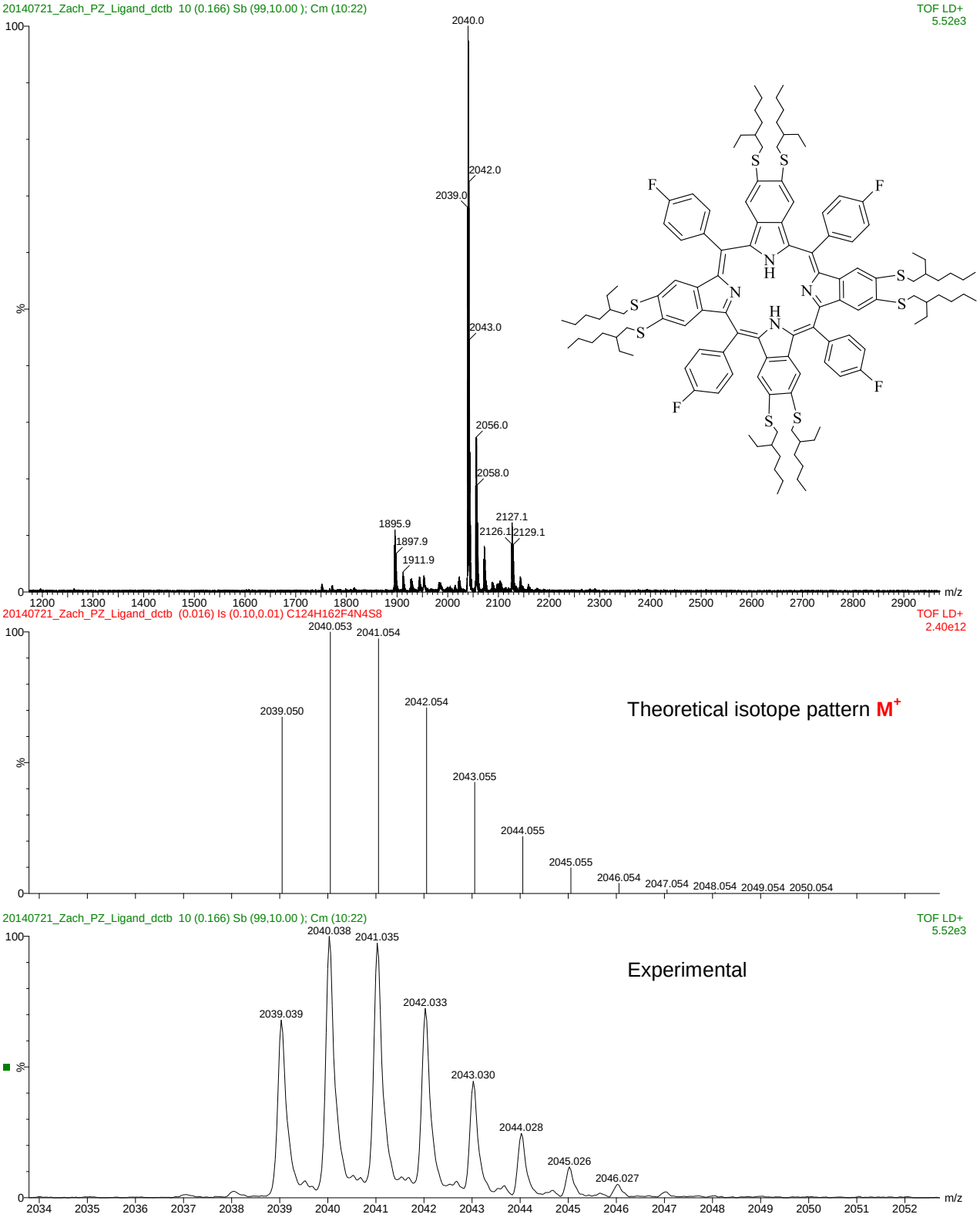

Figure 118 Mass spectrum of Meso-tetra(4-fluorophenyl)tetra(4,5-bis((2-ethylhexyl)thio)benzoporphyrin (H_2-PTBPF$_4$bEHT$_4$)

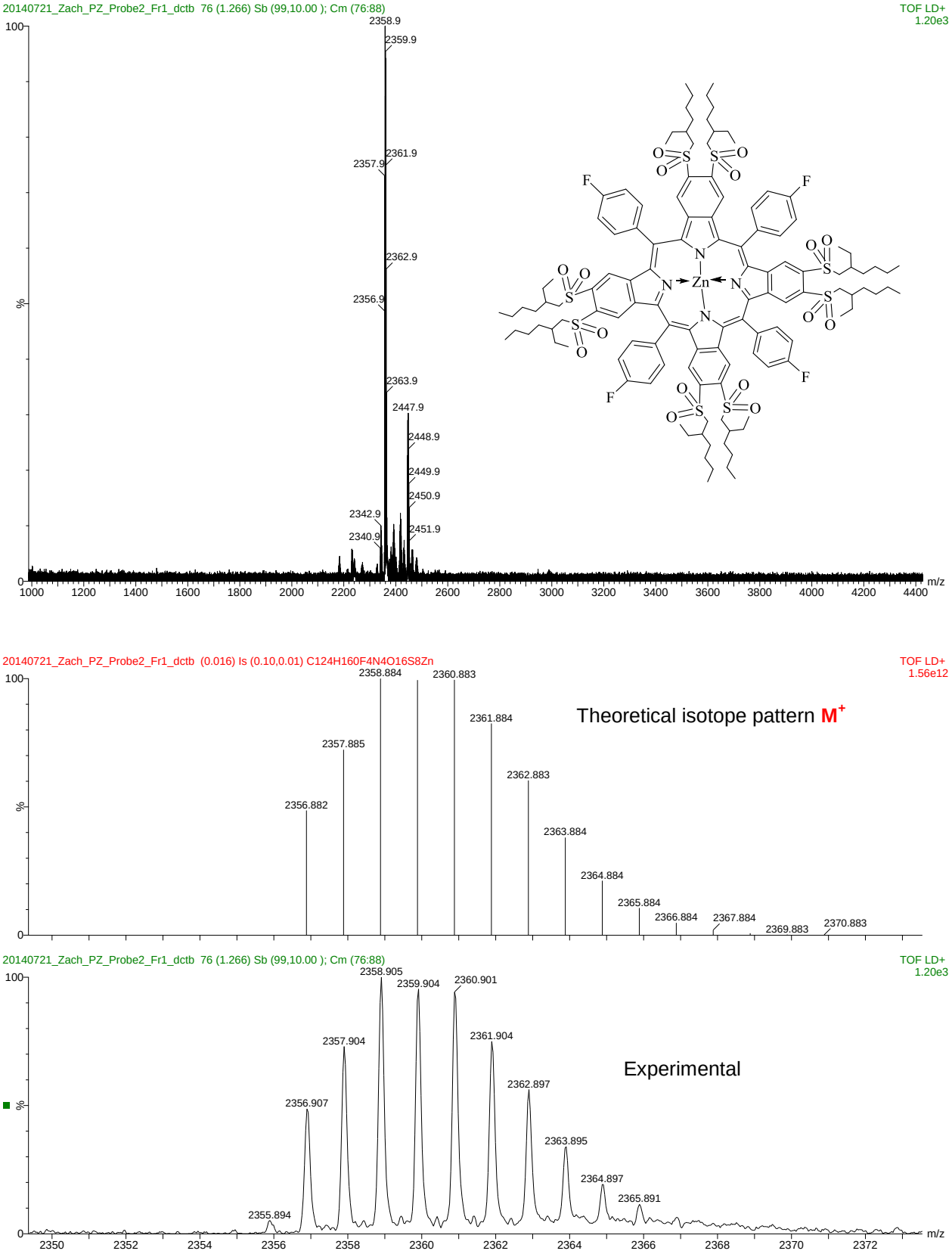

Figure 119 Mass spectrum of Zn (II) -meso-tetra(4-fluorophenyl)tetra(4,5-bis((2-ethylhexyl)sulfonyl)benzoporphyrin (Zn-TPTBPF$_4$bEHS$_4$)

Sample: Tolyl_Zn-Komplex Ionisation: MALDI / DCTB (!)

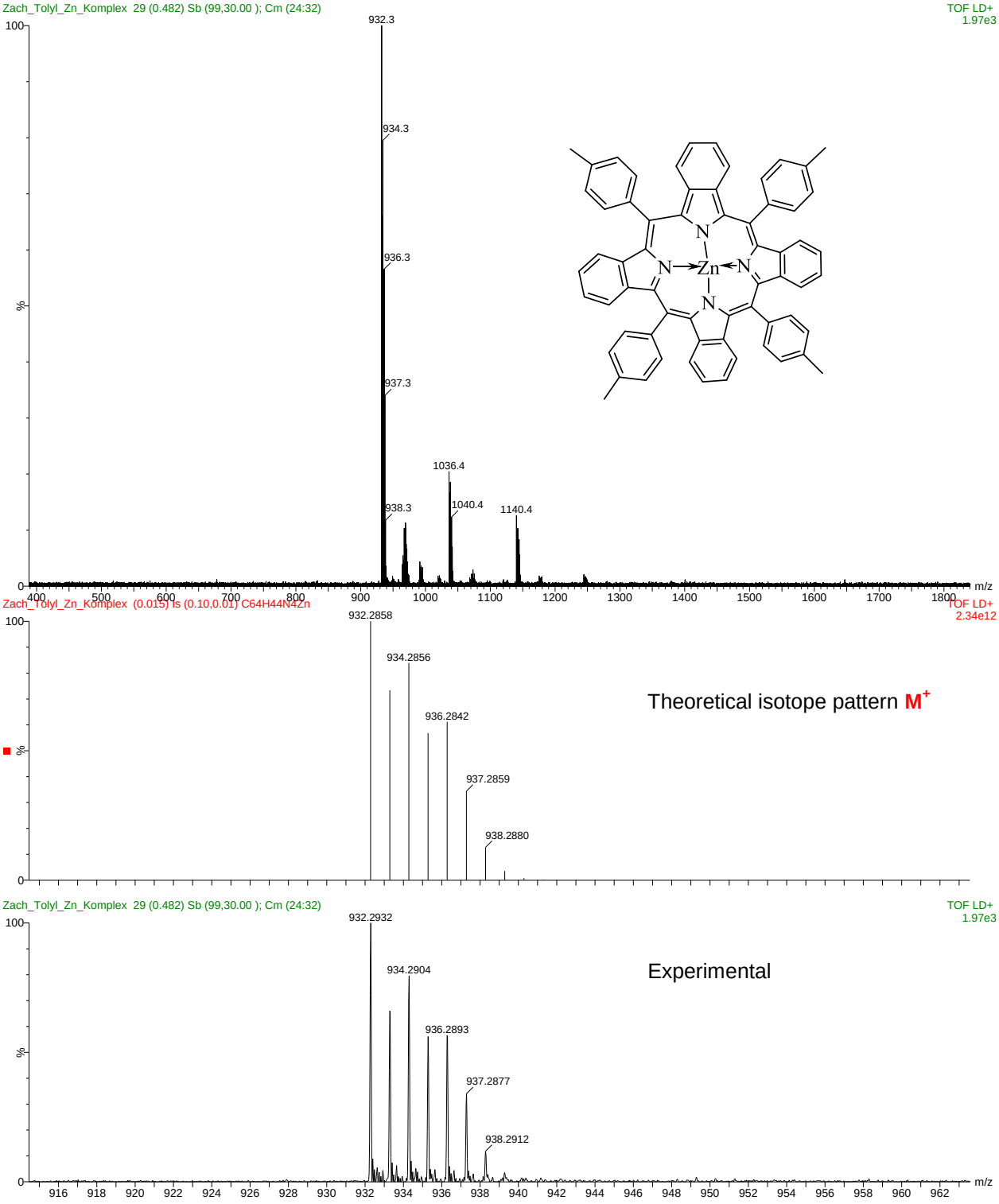

Figure 120 Mass spectrum of Zinc (II) meso-tetra(4-tolyl)tetrabenzoporphyrin (Zn-TTolTBP)

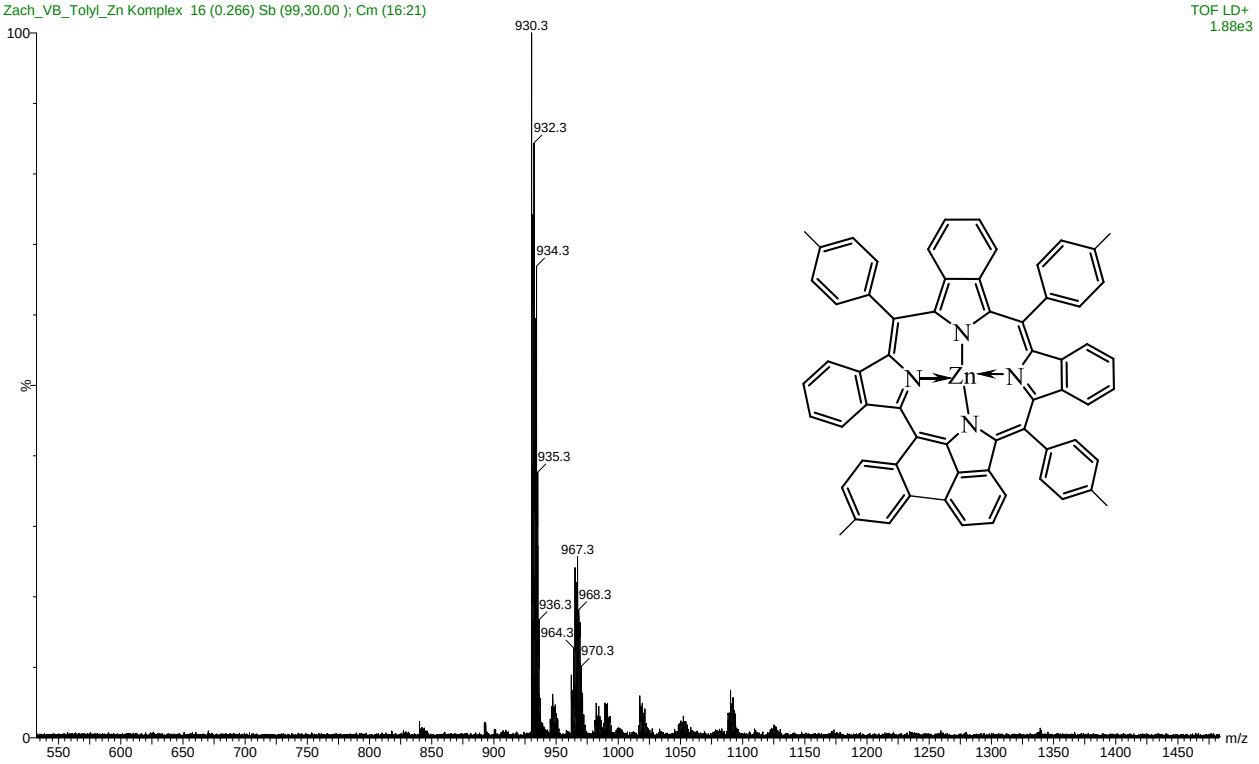

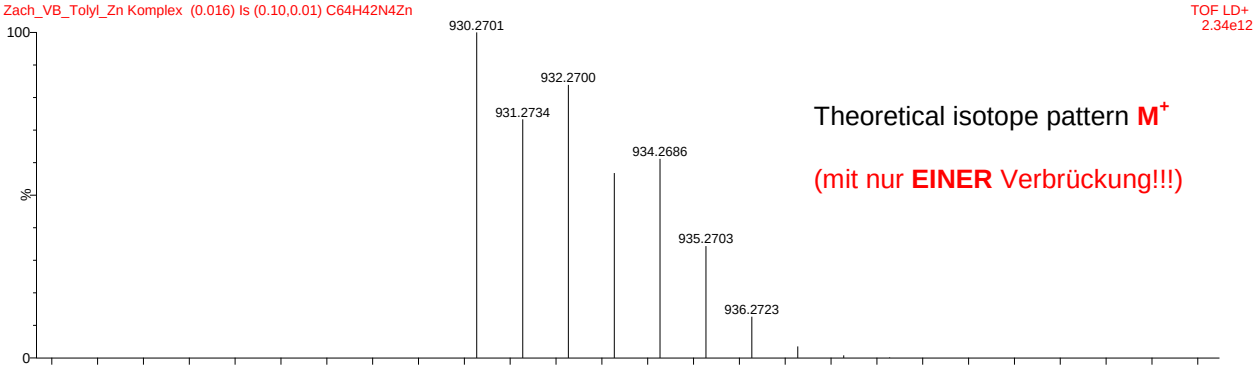

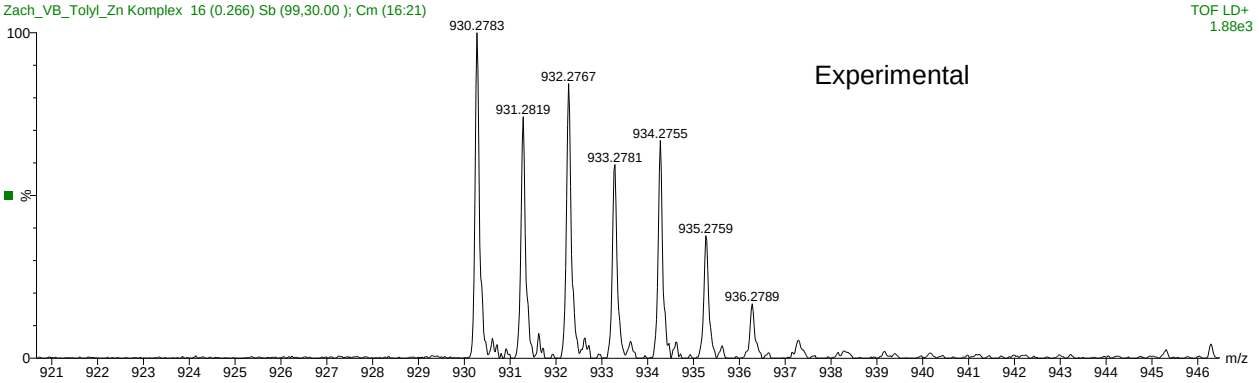

Figure 121 Mass spectrum of Bridged-Zinc (II) meso-tetra(4-tolyl)tetrabenzoporphyrin (bridged-Zn-TTolTBP)

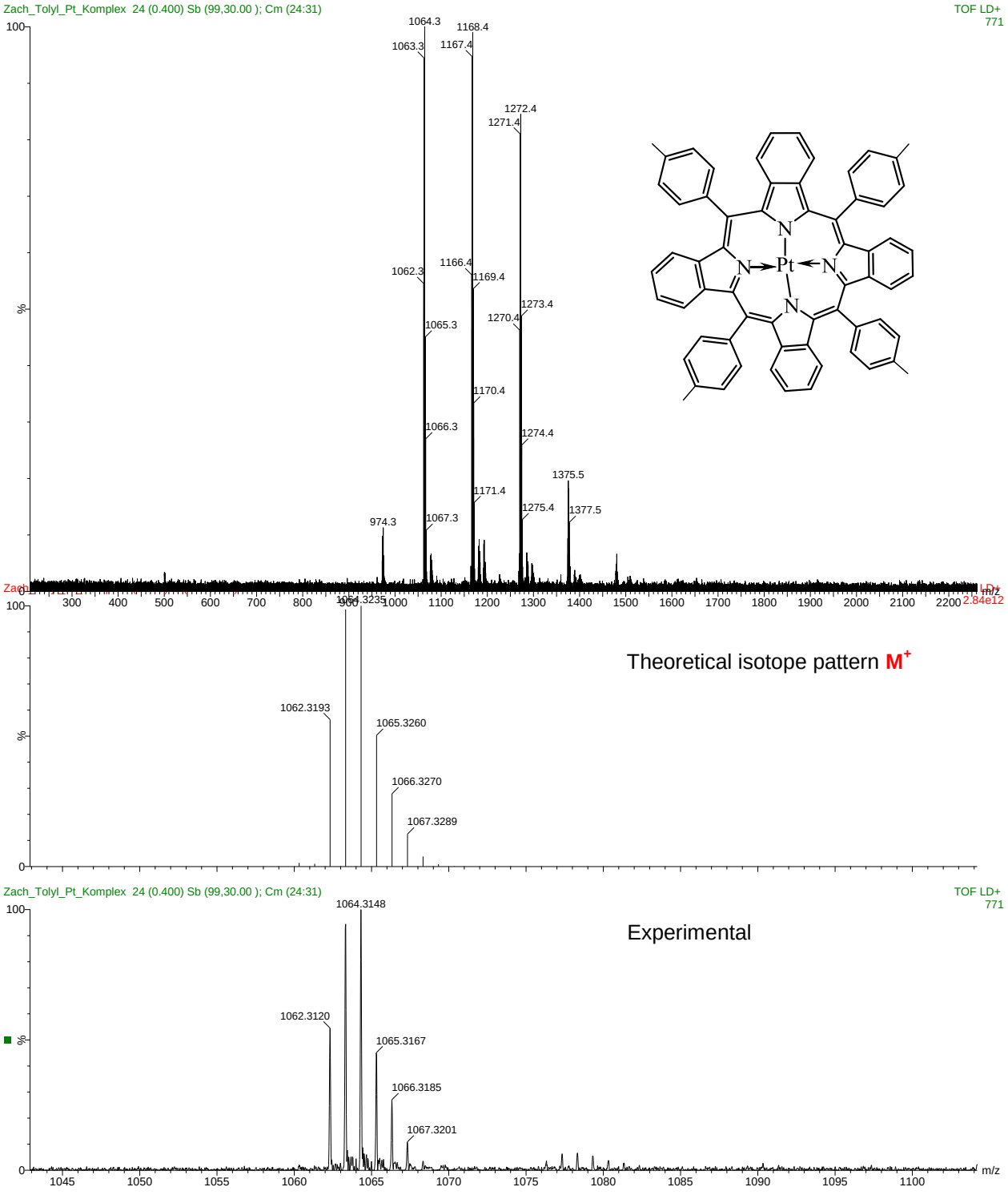

Figure 122 Mass spectrum of Platinum (II) meso-tetra(4-tolyl)tetrabenzoporphyrin (Pt-TTolTBP)

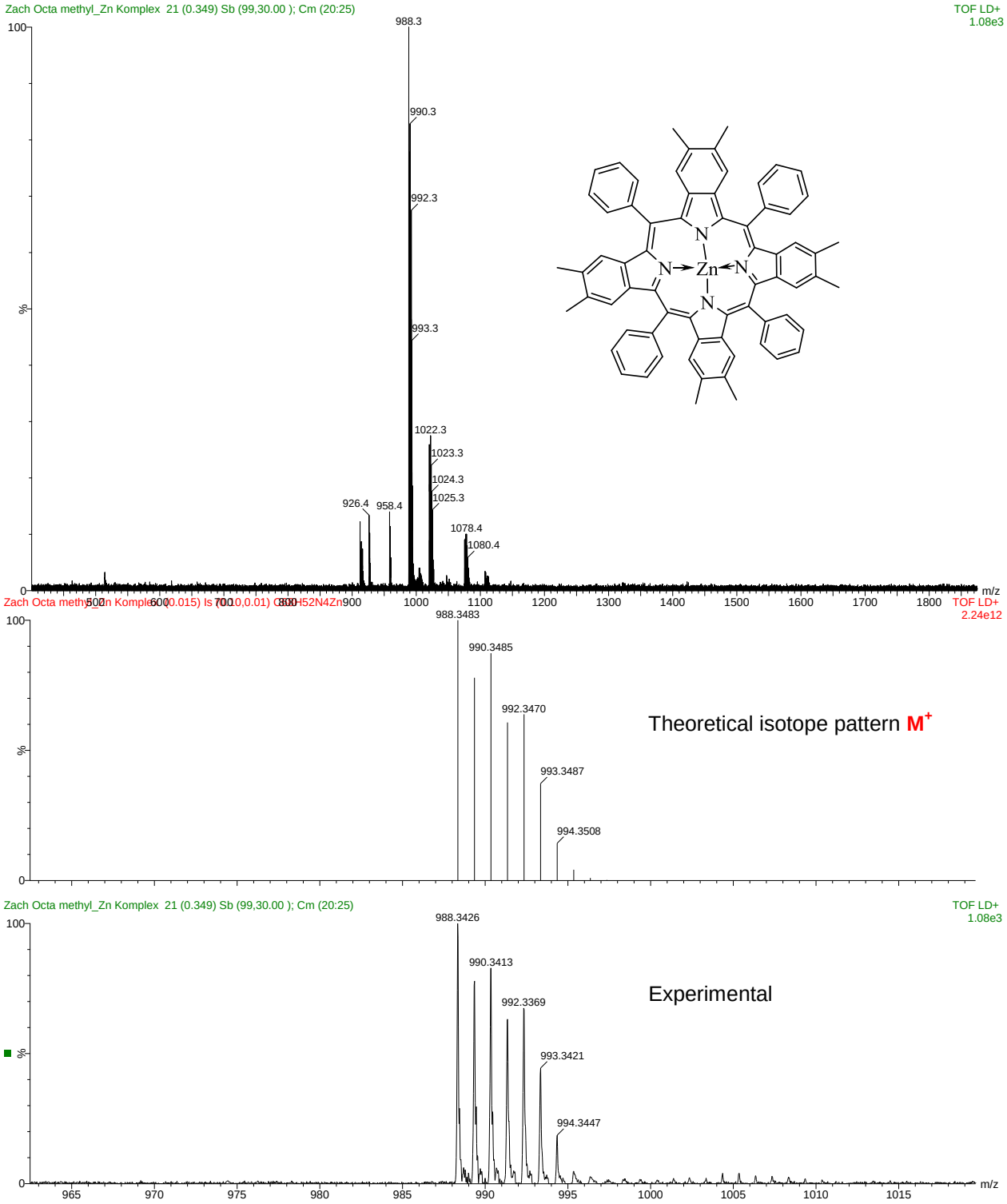

Figure 123 Mass spectrum of Zinc (II) meso-tetraphenyltetra(di-methyl)benzoporphyrin (Zn-TPTBPdM$_4$)

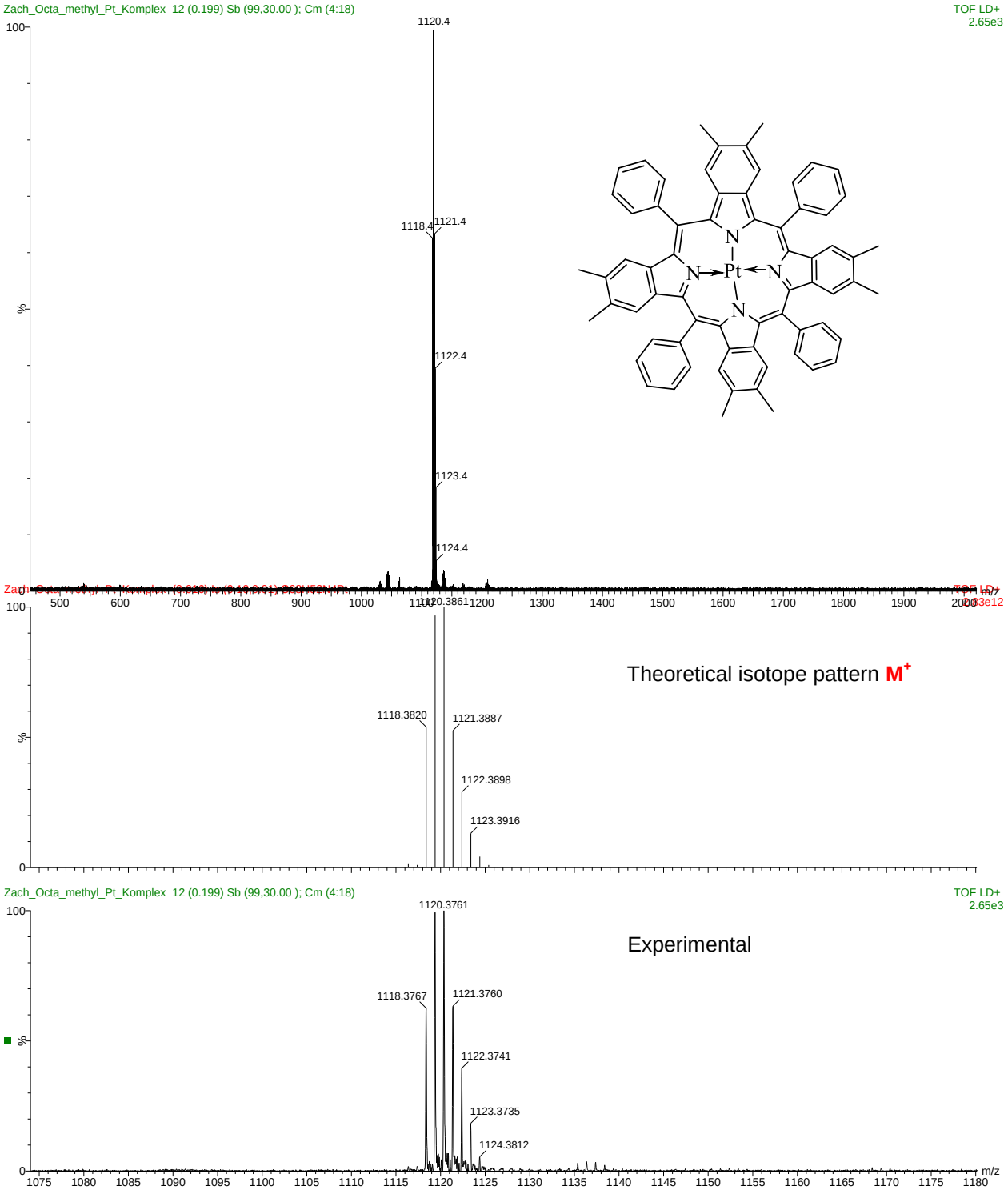

Figure 124 Mass spectrum of Platinum (II) meso-tetraphenyltetra(di-methyl)benzoporphyrin (Pt-TPTBPdM$_4$)

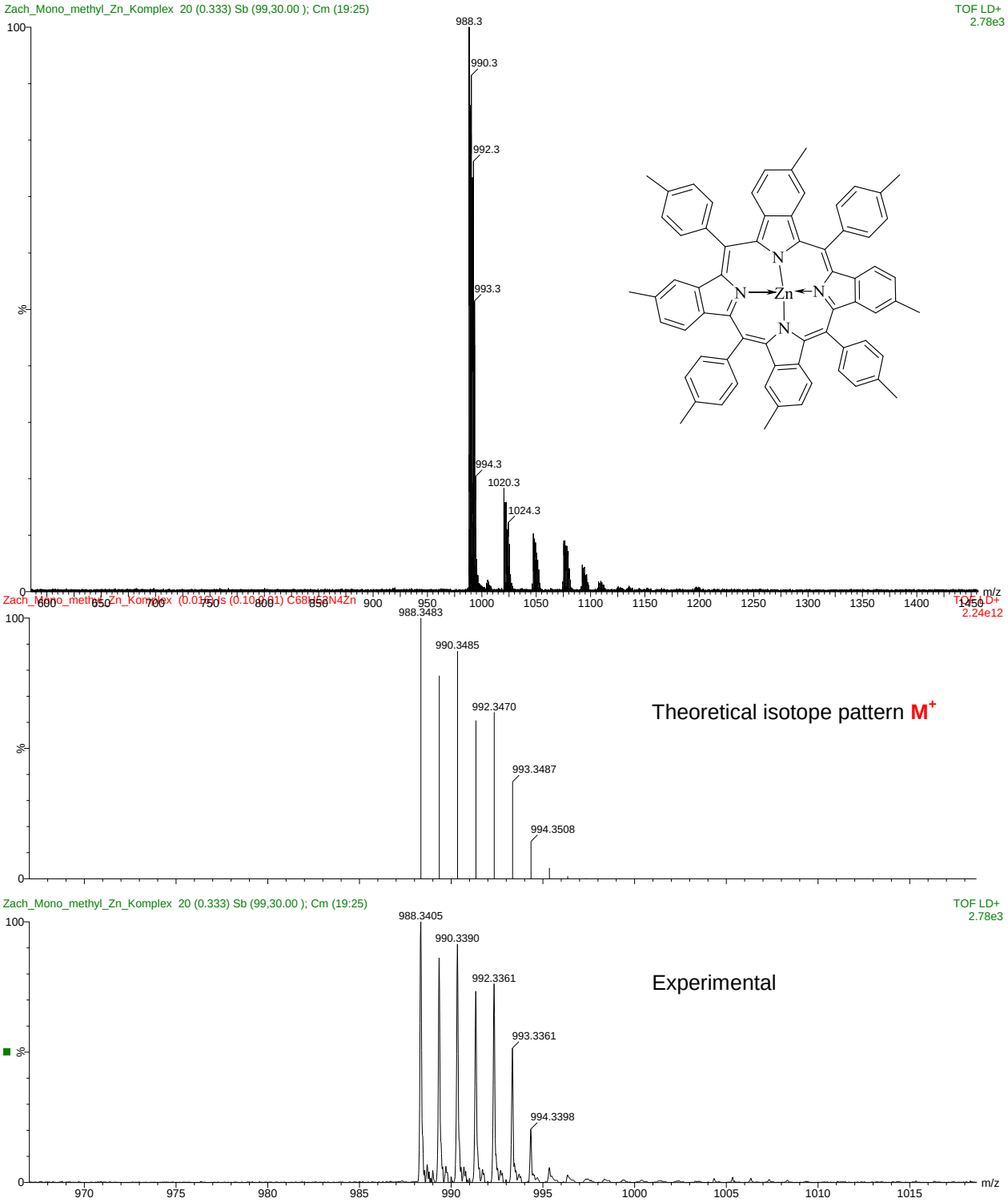

Figure 125 Mass spectrum of Zinc (II) meso-tetratolyltetra(mono-methyl)benzoporphyrin (Zn-TTolTBPmM$_4$)

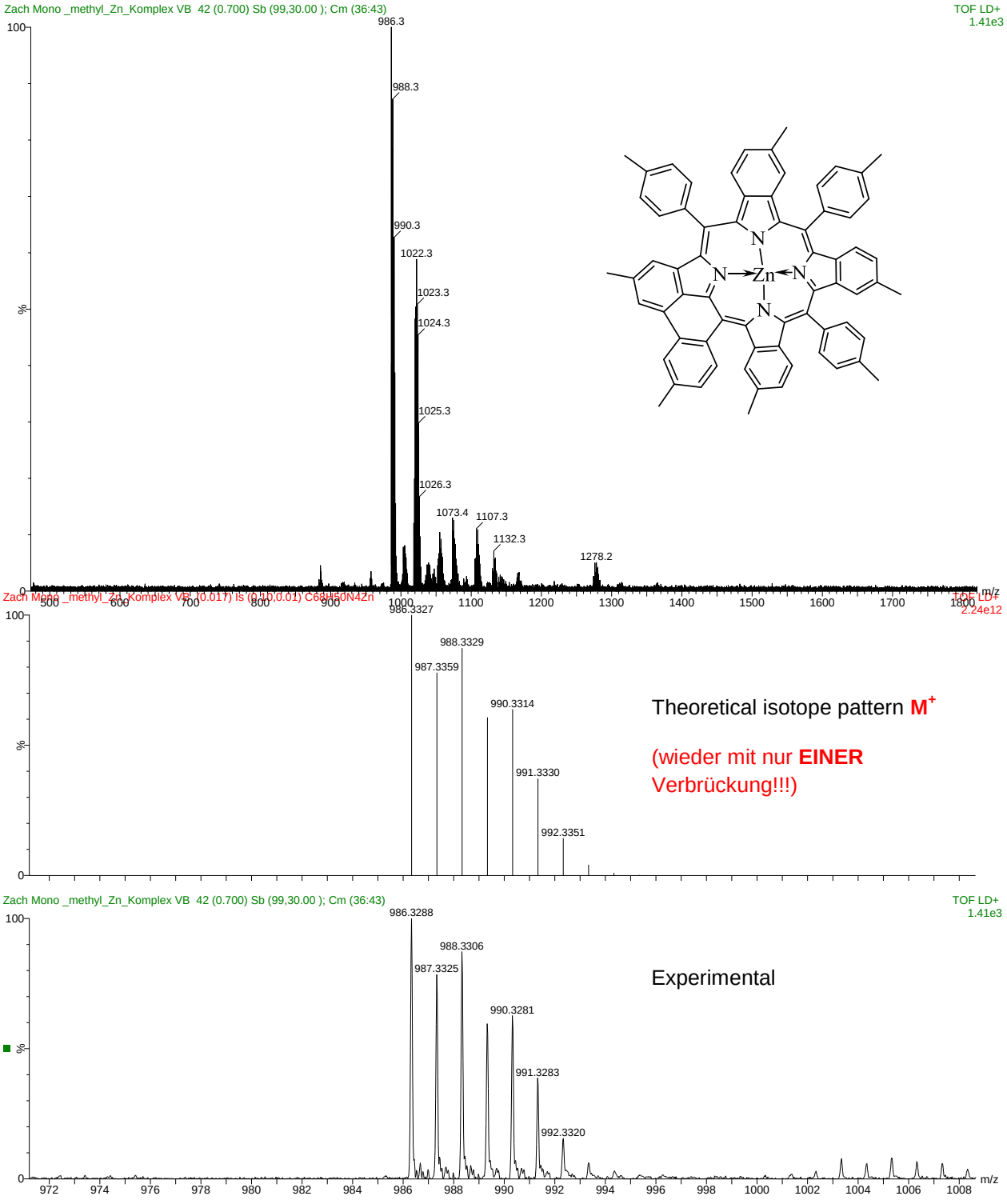

Figure 126 Mass spectrum of Bridged zinc (II) meso-tetratolyltetra(mono-methyl)benzoporphyrin (bridged Zn-TTolTBPmM$_4$)

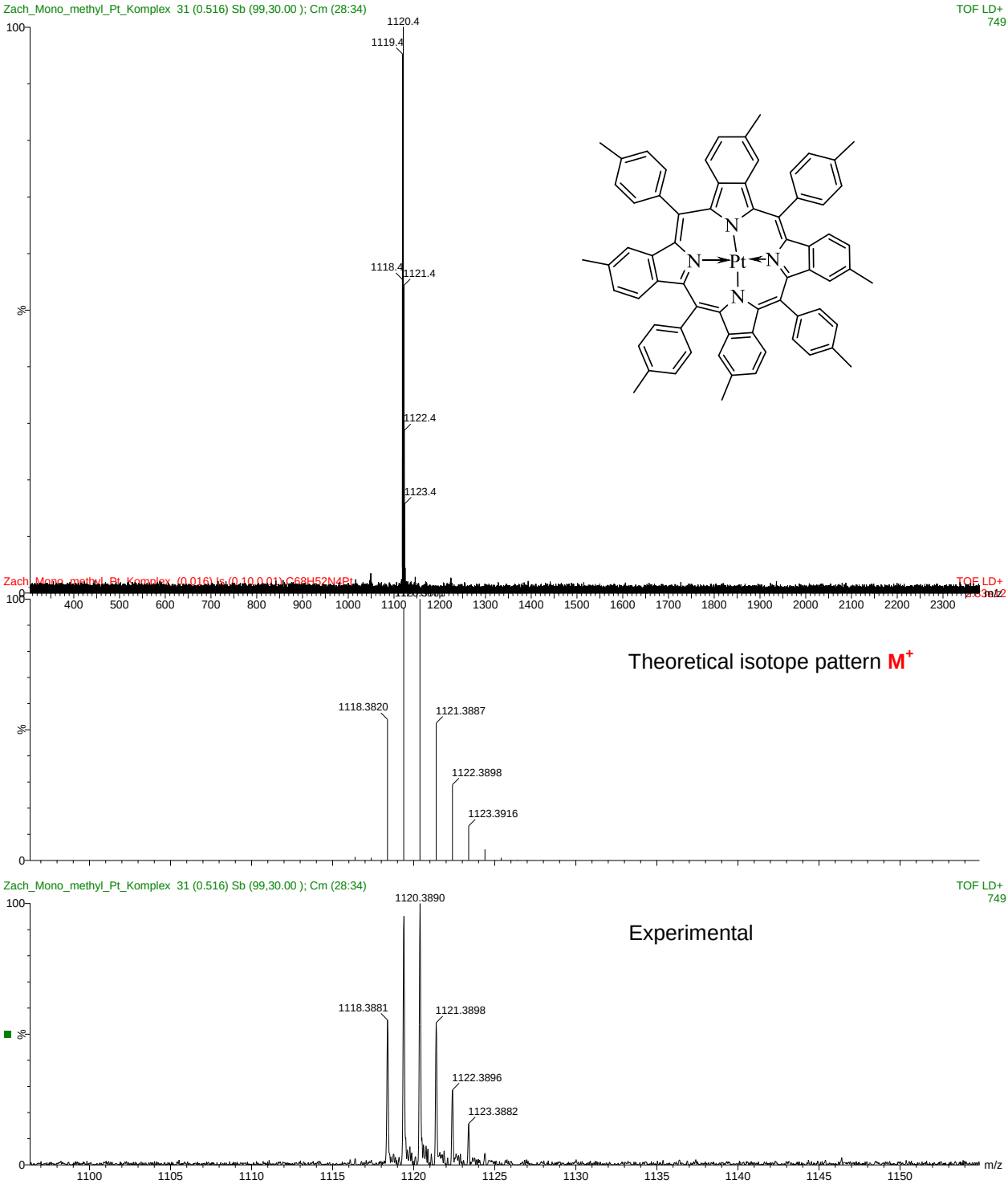

Figure 127 Mass spectrum of Platinum (II) meso-tetratolyltetra(mono-methyl)benzoporphyrin (Pt-TTolTBPmM$_4$)

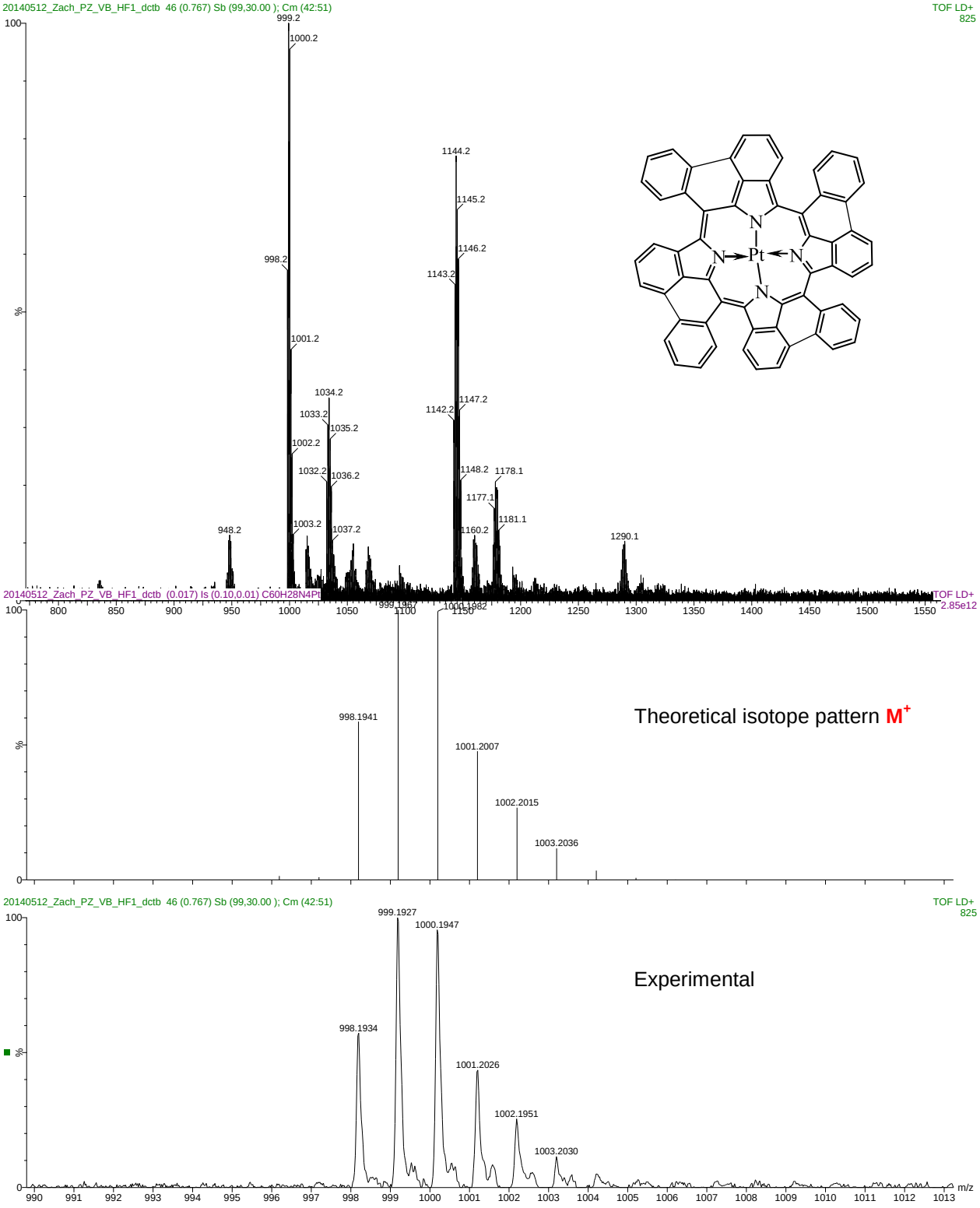

Figure 128 Mass spectrum of Bridged-Platinum (II) meso-tetraphenyltetrabenzoporphyrin (bridged-Pt-TPTBP)

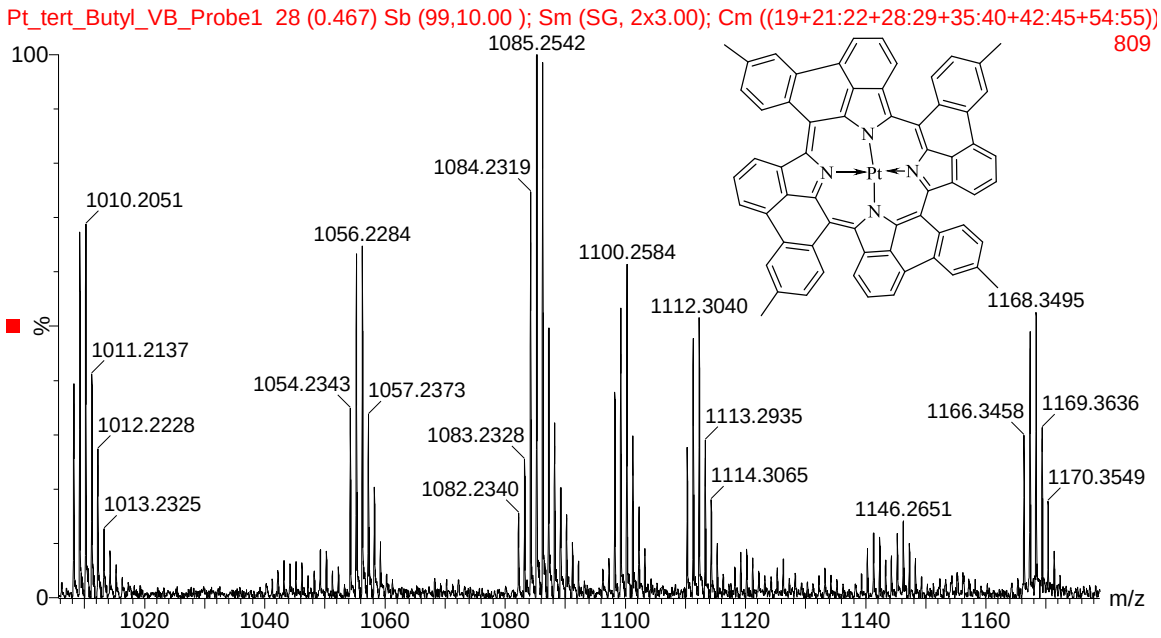

Figure 129 Mass spectrum of Bridged platinum (II) meso-tetra(tolyl)benzoporphyrin (bridged Pt-TTolTBP) Sample1

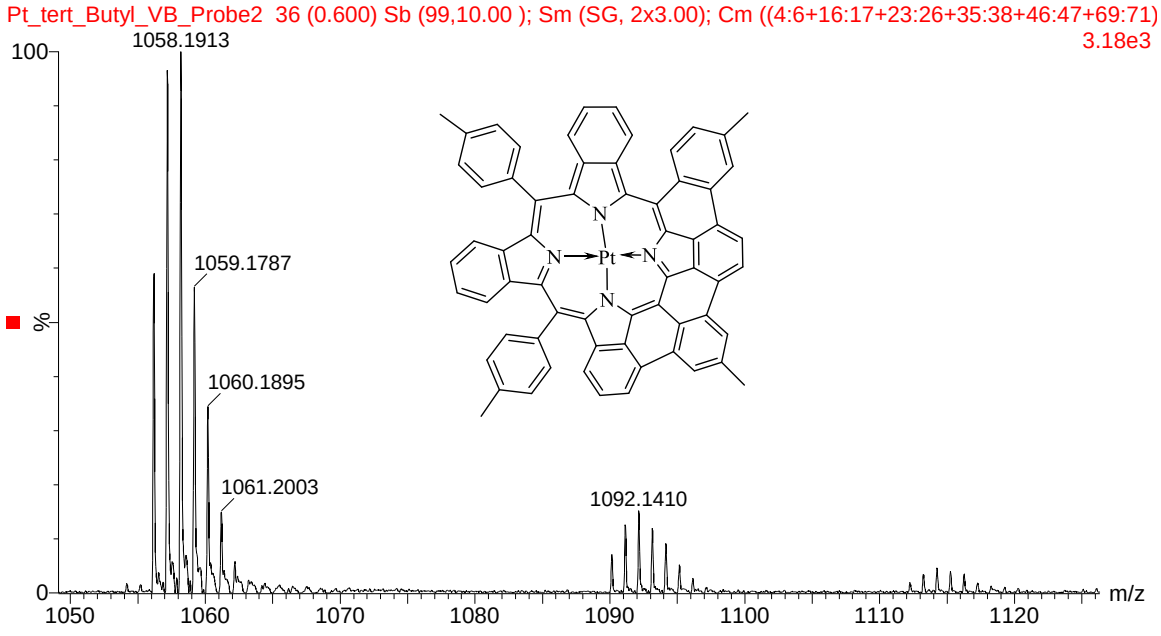

Figure 130 Mass spectrum of Bridged platinum (II) meso-tetra(tolyl)benzoporphyrin (bridged Pt-TTolTBP) Sample 2

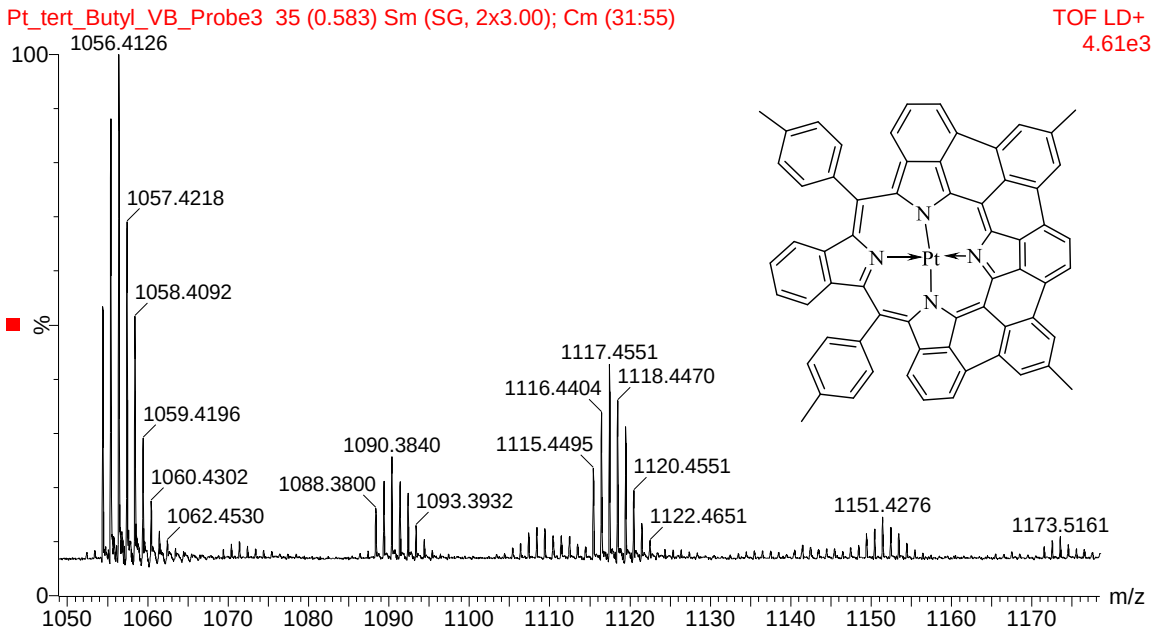

Figure 131 Mass spectrum of Bridged platinum (II) meso-tetra(tolyl)benzoporphyrin (bridged Pt-TTolTBP) Sample 3

EIDESSTATTLICHE ERKLÄRUNG

AFFIDAVIT

Ich erkläre an Eides statt, dass ich die vorliegende Arbeit selbstständig verfasst, andere als die angegebenen Quellen/Hilfsmittel nicht benutzt, und die den benutzten Quellen wörtlich und inhaltlich entnommenen Stellen als solche kenntlich gemacht habe. Das in TUGRAZonline hochgeladene Textdokument ist mit der vorliegenden Masterarbeit identisch.

I declare that I have authored this thesis independently, that I have not used other than the declared sources/resources, and that I have explicitly indicated all material which has been quoted either literally or by content from the sources used. The text document uploaded to TUGRAZonline is identical to the present master's thesis.

Datum / Date	Unterschrift / Signature